

AD-A101 713

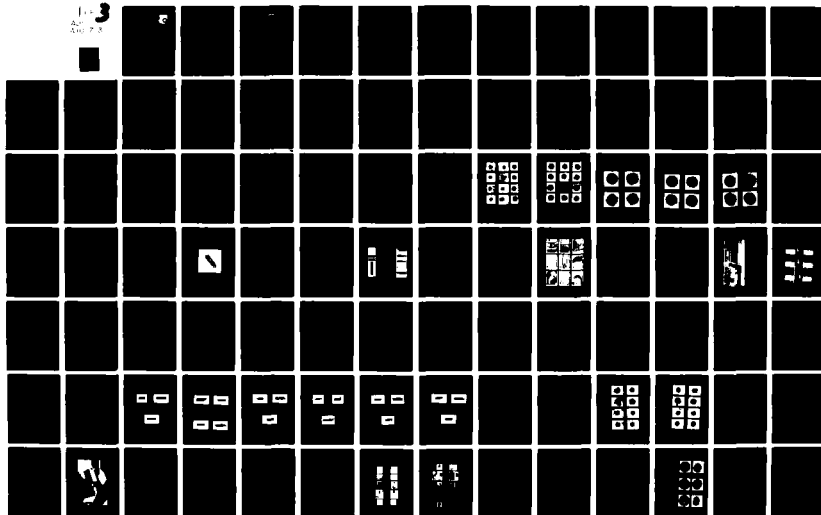
GENERAL ELECTRIC CO CINCINNATI OH AIRCRAFT ENGINE BU--ETC F/G 14/2
HIGH TEMPERATURE STRAIN GAGE SYSTEM FOR APPLICATION TO TURBINE --ETC(U)
JAN 81 R A WEISE, J H FOSTER F33615-76-C-2075
R80AEG388

UNCLASSIFIED

AFWAL-TR-80-2126

NL

3
AD
AND P. 3



AFWAL-TR-80-2126

AD A101713



HIGH TEMPERATURE STRAIN GAGE SYSTEM FOR APPLICATION TO TURBINE ENGINE COMPONENTS

R.A. Weise
J.H. Foster

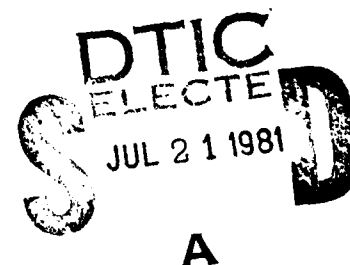
Technology Programs and Performance Technology Department
Aircraft Engine Business Group
General Electric Company
Cincinnati, Ohio 45215

January 1981

Technical Report AFWAL-TR-80-2126
Final Report for Period June 1976 - August 1980

Approved for public release; distribution unlimited.

AERO PROPULSION LABORATORY
AIR FORCE WRIGHT AERONAUTICAL LABORATORIES
AIR FORCE SYSTEMS COMMAND
WRIGHT-PATTERSON AIR FORCE, OHIO 45433



81 7 20 098

NOTICE

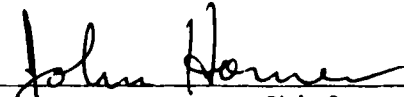
When Government drawings, specifications, or other data are used for any purpose other than in connection with a definitely related Government procurement operation, the United States Government thereby incurs no responsibility nor any obligation whatsoever; and the fact that the government may have formulated, furnished, or in any way supplied the said drawings, specifications, or other data, is not to be regarded by implication or otherwise as in any manner licensing the holder or any other person or corporation, or conveying any rights or permission to manufacture use, or sell any patented invention that may in any way be related thereto.

This report has been reviewed by the Office of Public Affairs (ASD/PA) and is releasable to the National Technical Information Service (NTIS). At NTIS, it will be available to the general public, including foreign nations.

This technical report has been reviewed and is approved for publication.

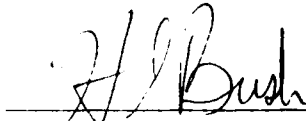


ISAAC G. GERSHON
Technical Area Manager
Components Branch
Turbine Engine Division
Aero Propulsion Laboratory



JOHN E. HORNER, Chief
Turbine Engine & Ramjet Tech Spt Br
Technical Facilities Division
Aero Propulsion Laboratory

FOR THE COMMANDER



H. I. BUSH
Acting Director
Turbine Engine Division


"If your address has changed, if you wish to be removed from our mailing list, or if the addressee is no longer employed by your organization please notify AFWAL/POFA, W-PAFB, OH 45433 to help us maintain a current mailing list".

Copies of this report should not be returned unless return is required by security considerations, contractual obligations, or notice on a specific document.

19 REPORT DOCUMENTATION PAGE		READ INSTRUCTIONS BEFORE COMPLETING FORM 15	
18 1. REPORT NUMBER AFWAL-TR-80-2126	2. GOVT ACCESSION NO. AD-2126	3. RECIPIENT'S CATALOG NUMBER AD-A10172	
4. TITLE (and Subtitle) High Temperature Strain Gage System for Application to Turbine Engine Components, 15		5. TYPE OF REPORT & PERIOD COVERED Final RPT. June 1976 - August 1980	
6. AUTHOR(s) R.A. Weise J.H. Foster		7. PERFORMING ORG. REPORT NUMBER R80AEG388	
9. PERFORMING ORGANIZATION NAME AND ADDRESS Aircraft Engine Business Group, GE Co. Technology Programs & Performance Technology Dept., Cincinnati, Ohio 45215		8. CONTRACT OR GRANT NUMBER(s) F33615-76-C-2075	
11. CONTROLLING OFFICE NAME AND ADDRESS Aero Propulsion Laboratory (AFWAL/POFA) AF Wright Aeronautical Laboratories, AFSC Wright-Patterson AFB, OH 45433		10. PROGRAM ELEMENT, PROJECT, TASK AREA & WORK UNIT NUMBERS 3066/12 32 17 15	
14. MONITORING AGENCY NAME & ADDRESS (if different from Controlling Office) 15, 5541		12. REPORT DATE January 1981	
		13. NUMBER OF PAGES 253	
		15. SECURITY CLASS. (of this report) Unclassified	
		15a. DECLASSIFICATION/DOWNGRADING SCHEDULE	
16. DISTRIBUTION STATEMENT (of this Report) Approved for Public Release: Distribution Unlimited			
17. DISTRIBUTION STATEMENT (of the abstract entered in Block 20, if different from Report)			
18. SUPPLEMENTARY NOTES			
19. KEY WORDS (Continue on reverse side if necessary and identify by block number) Dynamic Strain Gage, Gage Fatigue Strength, Gage Factor, Strain Gage Applications, Compressor Stress, Temperature Stability.			
20. ABSTRACT (Continue on reverse side if necessary and identify by block number) A three-phase program was completed to develop reliable, high temperature dynamic strain gage systems for application to turbine engine components oper- ating to 1500° F. The strain gage element, intermediate leads and gage fabri- cation processes that evolved are used over the full temperature range; however, two different application techniques are required to achieve maximum fatigue strength to 1500° F. A composite-ceramic application design is recommended to 700° F. At higher temperatures, the all-FSA or Rokide design is			

preferred. Gage factor stabilization procedures were established. A strain gage reliability demonstration was conducted on an engine compressor and showed the composite-ceramic gage to have better reliability below 700° F.

The report includes a detailed procedure of gage fabrication and application.



FOREWORD

This report describes the work accomplished under AFWAL Contract Number F33615-76-C-2075 from 15 June 1976 through 15 August 1980. The work was performed by the Measurement Development Engineering Unit, Aircraft Engine Business Group of the General Electric Company. Mr. J. Horner of the Air Force Aero Propulsion Laboratory, Wright-Patterson Air Force Base was the Program Manager.

The report was prepared by R.A. Weise, the General Electric Company Program Technical Manager and J.A. Foster. Other contributors during the fabrication, application, and testing of strain gages were R. St. Clair, and the assistance of D.M. Carlson, Advanced Materials Engineer of the Material and Process Technology Laboratories are recognized.

Accession	
PTIS	1
EDS	1
US	1
Justified	1
By	
Dis	
Avail	
Dist	
A	Special

TABLE OF CONTENTS

<u>Section</u>	<u>Page</u>
1.0 INTRODUCTION	1
1.1 Purpose	1
1.2 Objectives	1
1.3 Background	2
1.4 Plan	2
2.0 TECHNICAL APPROACH AND PROGRESS	4
2.1 Phase I - Selecting Two Candidate Strain Gage Systems	4
2.1.1 Task 1 - Literature Search	4
2.1.2 Task 2 - Alloy Selection and Test	4
2.1.2.1 Alloy Selection	4
2.1.2.2 Alloy Testing	6
2.1.2.3 Selection of Prime Candidate	29
2.1.3 Task 3 - Gage Application Development	30
2.1.3.1 Gage Grid	32
2.1.3.2 Strain Gage Lead Joining	65
2.1.3.3 Application Materials	70
2.1.4 Task 4 - The Two Candidate Systems	76
2.1.5 Candidate Systems - Application Process	83
2.2 Phase II - Laboratory Tests of Two Candidate Strain Gage Systems	85
2.2.1 Task 1 - Fatigue Strength Testing	85
2.2.1.1 Test Equipment and Test Description	85
2.2.1.2 Test Results and Discussion	87
2.2.2 Task 2 - Gage Sensitivity	124
2.2.2.1 Gage Factor and Postheat Treat Stabilization	124
2.2.2.2 Effects of Long Term Exposure	130
2.2.2.3 Conclusions and Recommendations	133
2.2.3 Task 3 - Effect of Applications on Small Blades	134
2.2.3.1 Testing and Test Results	134
2.2.3.2 Discussion of Results	147
2.2.3.3 Conclusions	155
2.2.4 Task 4 - Effect of High Rotational Speed on Application Integrity	155
2.2.4.1 Application Integrity Testing - F101 Engine Applications	156
2.2.4.2 Application Integrity Test - J85 Engine Applications	161
2.2.4.3 Conclusions From Integrity Tests	170

TABLE OF CONTENTS (Concluded)

<u>Section</u>		<u>Page</u>
2.3	Phase III - Demonstrating the Reliability of the Two Candidate Systems	171
2.3.1	Reliability Demonstration Engine	172
2.3.1.1	Instrumenting the Engine	172
2.3.1.2	Engine Testing	177
2.3.1.3	Test Results	177
2.3.1.4	Posttest Inspection	184
2.3.1.5	Discussion of Engine Testing	189
2.3.2	Selecting the Most Promising Candidate	193
3.0	GAGE FABRICATION AND APPLICATION DETAILS	194
3.1	Strain Gage Fabrication	194
3.1.1	Material	194
3.1.2	Strain Gage Details	194
3.1.3	Gage Annealing	198
3.2	Gage Application Instructions	199
3.2.1	Preparing for the Gage Application	200
3.2.2	Composite-Ceramic Application	202
3.2.3	All-FSA Application	206
3.2.4	Postapplication Heat Treat	208
3.2.5	Splice to Primary Leads	208
3.3	Lead Routing Design	209
3.3.1	Design Philosophy	209
3.3.2	Typical Application and Routing Designs	210
3.4	Summary	214
4.0	TEST EQUIPMENT	216
4.1	High Temperature Strain Gage Evaluation Facility	216
4.1.1	General Description	216
4.1.2	High Temperature Gage Factor Facility	216
4.1.3	Strain Gage Fatigue Test Facility	224
4.2	Erosion Test Facility	226
4.3	Hot Shake Facility	226
	REFERENCES	233

LIST OF ILLUSTRATIONS

<u>Figure</u>		<u>Page</u>
1.	Alloy Selection Based on Physical Properties Data.	5
2.	Karma Strain Gage.	8
3.	Sensitivity Test Temperature Cycle.	10
4.	Sensitivity Versus Temperature - Karma.	11
5.	Sensitivity Versus Temperature - Nichrome V.	12
6.	Sensitivity Versus Temperature - Tophet C.	13
7.	Sensitivity Versus Temperature - Tophet 30.	14
8.	Sensitivity Versus Temperature - FeCrAl.	15
9.	Sensitivity Versus Temperature - Pt8W.	16
10.	Oxidation - Karma, Nichrome V, and Pt8W.	19
11.	Oxidation - Tophet C, Tophet 30, and FeCrAl.	20
12.	Oxidation - 90Pt8Ni2W.	21
13.	Oxidation - 90Pt8Ni2Cr.	22
14.	Oxidation - 90Pt10Ni.	23
15.	Fatigue Tests at Room Temperature.	25
16.	Sensitivity Versus Temperature - Pt-Coated FeCrAl.	27
17.	Oxidation of Platinum-Coated Gage.	38
18.	Standard and Composite Applications.	31
19.	Gage Factor Versus Temperature of Heat Treated Karma.	33
20.	Gage Defects Shown by SEM.	34
21.	Modified Gage Flattening Fixtures.	35
22.	Fine Wire Test Machine.	37
23.	Pull Test Specimens.	38
24.	Effect of Coldwork on Load and Elongation of Karma with No Heat Treatment.	39
25.	Effect of Coldwork on Load and Elongation of Moleculoy with No Heat Treatment.	40
26.	0.2% Yield and Elongation Versus Conditioning - Karma.	42
27.	0.2% Yield and Elongation Versus Conditioning - Moleculoy.	43
28.	0.2% Yield and Elongation Versus Conditioning - FeCrAl.	44

LIST OF ILLUSTRATIONS (Continued)

<u>Figure</u>		<u>Page</u>
29.	0.2% Yield and Elongation Versus Conditioning - Pt8W.	45
30.	Gage Factor Versus Temperature - Moleculoy.	49
31.	Typical Order-Disorder Phenomenon of Nichel-Chromium Alloys.	51
32.	Oxidation Test Coupons - Coated Alloys.	54
33.	Coated Gage Oxidation.	55
34.	Coated Gage Oxidation.	56
35.	Coated Gage Oxidation.	57
36.	Coated Gage Oxidation.	58
37.	Coated Gage Oxidation.	59
38.	Coated Gage Oxidation.	60
39.	Oxidation of Fine Wires Covered with Denex 2 Cement.	63
40.	Oxidation of Fine Wires Covered with Al ₂ O ₃ - 1/8 Inch Rokide Gun - Cement.	64
41.	Sonobond Welded.	68
42.	Schematic of Weld Specimen Test.	69
43.	Adhesion Shock Test.	73
44.	Adhesion Shock Test.	74
45.	Erosion Test Facility.	77
46.	Erosion of Flame-Sprayed Al ₂ O ₃ .	78
47.	Goodman Diagram Showing Relative Endurance Limits of Moleculoy and Pt8W on Common Blade Alloys from Thermal Expansion Differences.	81
48.	Application Designs.	84
49.	1/8-Inch Long Moleculoy Gage, Flattened to 0.6 Mil from 0.8 Mil Diameter Wire (Typical).	89
50.	Moleculoy Gage in RTC Epoxy Cement.	92
51.	Comparison of Particle Size Distribution Between H Cement and Denex Cement.	94
52.	Typical Outer Filament Failures (40X).	96
53.	Gage 2 Installed Too Close to Edge of FSA Base Coat (10X).	96
54.	Failure Site of Gage 2.	97
55.	1/8-Inch Long Moleculoy Gage Flattened to 0.4 Mil - Typical.	98

LIST OF ILLUSTRATIONS (Continued)

<u>Figure</u>		<u>Page</u>
56.	Defects in Chromel P Convolute Leads (70X) - Not Caused by the Convoluting Fixture.	98
57.	Differences Between First Coats of a Properly and Improperly Applied Gage.	100
58.	Particle Size Comparison of Fine Ground Denex 2 and H Cement.	103
59.	Gage Failures Resulting from Fatigue Testing at A-Ratio = ∞ .	105
60.	Pt-10Ni Lead Failure Near Splice, Gage 2, TN 13-78.	107
61.	Gage Failures Resulting from Fatigue Testing at A-Ratio = 2.	108
62.	Moleculoy Gage Applications to F101 Rotor Blading After First Coat (Failure Sites Marked with "X").	111
63.	Typical Splice of Convolute Leads to Primary Leads.	112
64.	Gage 1 After First Coat Spray. Notice Failure Site of Three Gages, TN 29-78.	113
65.	Fatigue Strength at 10^6 Cycles of Candidate Strain Gage Systems on Beams 30 Hz Test Frequency - A-Ratio = ∞ .	115
66.	Fatigue Strength at 10^6 Cycles of Candidate Strain Gage Systems on Beams 30 Hz Test Frequency - A-Ratio = 2.	116
67.	Gage Failures Resulting From all Fatigue Testing.	117
68.	Tape Adhesive Residue After 15 Minutes at 650° to 700° F.	118
69.	Tape Adhesive Residue After 15 Minutes at 500° to 550° F.	119
70.	Adhesive Residue After Reexposure to 900° F for 10 Minutes.	119
71.	Longitudinal Cut of the Interface Between the First and Top Spray Coats Showing Gage Filament (250X).	121
72.	Typical Radial in Outer Filament.	123
73.	Average Gage Factor and Resistance Versus Temperature 840° F Postheat Treat Candidates 1 and 2.	126
74.	Average Gage Factor and Resistance Versus Temperature 1050° F Heat Treat Candidates 1 and 2.	127
75.	Comparison of Average Gage Factor for Two Candidate Gages.	128
76.	Long Term Stability at 1200° F and 1500° F for Candidates 1 and 2.	132
77.	Typical Dovetail Rework Prior to Brazing.	136
78.	System for Obtaining Resonance Diagram of Blades Electro-magnetic Drive.	137

LIST OF ILLUSTRATIONS (Continued)

<u>Figure</u>		<u>Page</u>
79.	Typical Resonance Diagram for an Uninstrumented Blade.	139
80.	Blocks Contain Blades and Gage Applications for Damping Studies.	140
81.	J85 Stage 6 Blade Mounted on Blocks for Damping Tests.	141
82.	Resonance Diagrams - J85 Stage 6 Titanium Blade, Block 6, Before and After Instrumenting Candidate 1 - Composite-Ceramic.	143
83.	Resonance Diagrams - F101 Stage 6 Titanium Blade, Block 3, Before and After Instrumenting Candidate 2 - All-FSA.	144
84.	Strain Gage Map, Typical Stage 6 Rotor Blade.	146
85.	Test Data - Effect of Candidate Gages on Strain Distribution, F101 Stage 6 Titanium Blades.	148
86.	Test Data - Effect of Candidate Gages on Strain Distribution, F101 Stage 9 Inconel 718 Blades.	149
87.	Test Data - Effect of Candidate Gages on Strain Distribution, CF6-50L Stage 8 A 286 Blades.	150
88.	Relative Damping of Candidate Applications with Airfoil Size.	151
89.	Resonance Diagrams on Increasing and Decreasing Frequency Sweeps, F101 Stage 9 Inconel 718 Blade, Block 1 With Candidate 2, All-FSA.	153
90.	F101 Stage 3 Blade Instrumentation Location and Routing Instructions (Part of GE Drawing 4013246-884).	157
91.	F101 Stage 8 and 9 Blade Instrumentation Location and Routing (Part of GE Drawing 4013246-677).	158
92.	Instrumentation for Compressor Rotor F101 Engine 470-021 and Routing.	159
93.	Stage 3 Blade Composite-Ceramic Applications - After Test on F101 Engine 470-021/4.	162
94.	Gage Routing Instructions.	163
95.	Stage 9 Candidate Gages After Test and Before Removal of Nichrome.	165
96.	Stage 9 Blades After Removal From Rotor.	166
97.	Stage 8 Blades After Removal From Engine.	167
98.	Stage 8 Blades After Removal From Engine.	168
99.	Typical Splice on Dovetail Post of Stage 8 Rotor Blades.	169
100.	Basic Polyscientific Slip Ring.	173
101.	100 Point Slip Ring Assembly.	174

LIST OF ILLUSTRATIONS (Continued)

<u>Figure</u>		<u>Page</u>
102.	Stage 7 and 9 Blade Gage Locations.	176
103.	Strain Gage Instrumentation, Lead Routing, and Assembly Procedures.	179
104.	Stage 1 and 7 Strain Gage Signals Before, During, and After Stall.	181
105.	Stage 9 Strain Gage Signals Before, During and After Stall.	182
106.	Stage 9 Strain Gage Signals Before, During, and After Stall.	183
107.	Candidate Strain Gage Reliability Chart, CF6-6 Core Engine 451-000/1.	185
108.	Stage 7 Blades After 54:40 Hours of Testing.	186
109.	Gage A04 (A11-FSA) After 36 Hours in Hot Caustic Soda.	187
110.	Stage 7 Blades After 28 Hours of Testing.	188
111.	Stage 9 Blades Containing Composite-Ceramic Applications (Except for S/N 16, the Blades Containing Calibration Gages Were Operating at the End of the Test).	190
112.	Stage 9 Blades Containing A11-FSA Gage Applications (S/N K and S/N 17 Gage Applications Were Operating at the End of the Test).	191
113.	Failure Sites of Stage 9 Applications (S/N 13 and S/N 14).	192
114.	Application Designs.	195
115.	Fabrication Details.	197
116.	Gage Flattening Block.	198
117.	F101 Stage 3 Blade Instrumentation.	211
118.	F101 Stage 4-9 Compressor Rotor Instrumentation.	212
119.	CF6 Compressor Rotor Instrumentation.	213
120.	Routing Across Pressure Face.	215
121.	High Temperature Strain Gage Evaluation Facility.	217
122.	Sensitivity Beam.	218
123.	High Temperature Gage Factor Test Fixture.	219
124.	Temperature Profile with Suppressor Plates in Position.	221
125.	Schematic of Test Wiring Diagram.	222

LIST OF ILLUSTRATIONS (Concluded)

<u>Figure</u>		<u>Page</u>
126.	Fatigue Test Fixture.	225
127.	Strain Gage Fatigue Test Beam.	227
128.	Strain Gage Locations and Temperature Profile for 850° F Fatigue Tests.	228
129.	Erosion Test Facility - Grit Blast Nozzle.	229
130.	Hot Shake Facility Schematic.	230

LIST OF TABLES

<u>Table</u>		<u>Page</u>
1.	Selection of Prime Candidates.	17
2.	Depth (% Radius) to Which Deterioration Proceeded After 150 Hour, 1500° F Exposure Having Been Coated Prior to Embedding in Cements.	61
3.	Depth (% Radius) to Which Deterioration Proceeded After 150 Hour, 1200° F Exposure After Embedding in Cement With No Prior Coating.	62
4.	Depth (% Radius) to Which Deterioration Proceeded After 150 Hour, 1500° F Exposure After Embedding in Cement With No Prior Coating.	62
5.	Breaking Loads of Ultrasonic Welds.	71
6.	Quench Test.	75
7.	Two Candidate Gage Systems.	79
8.	Fatigue Test Matrix.	86
9.	Early Fatigue Testing to Develop/Improve Gage Application Procedures and Materials.	90
10.	Fatigue Test Results.	102
11.	Fatigue Test Results.	106
12.	Fatigue Test of Gages on Compressor Rotor Blades in the Hot Shake Facility (See Paragraph 5.3).	109
13.	Average Gage Factor and Standard Deviations From 10 Gages Tested.	109
14.	Gage Normalizing and Cycle Correction Based on Starting Resistances.	131
15.	Summary of Before and After Instrumenting on Damping and Frequency of Blades.	145
16.	Relative Strain Normalized with the Indicated Calibration Gage.	154
17.	Maximum Conditions of Blade Response and Temperature During Testing of F101 Engine 470-021/4.	160
18.	Postmortem Results of Stage 8 and 9 Rotor Blades After 38:31 Hours on J85-21 Engine 221-010/11A.	170
19.	Instrumentation Requirements for CF6-6 Engine 451-000/1.	175
20.	Gage Application Materials and Processes.	196

SUMMARY AND CONCLUSIONS

SUMMARY

A three-phase program was completed to develop a reliable, high-temperature dynamic strain gage system for application to turbine engine components to 1500° F.

Two candidate gage systems were selected in Phase I and developed in early Phase II to meet a fatigue strength goal of 4000 microinches/inch double-amplitude at 10^7 cycles. Table 20 (Page 196) describes the salient materials and processes of the developed systems. The developed gages were tested for fatigue strength at R-ratios of infinity and two to a temperature of 1500° F. Fatigue diagrams of the two candidates are compared in Figures 65 and 66. Gage factor at temperature was defined for the gages and are shown in Figures 73, 74, and 75.

Also qualitatively determined in Phase II was the effects of the applied sensors on fundamental frequency, strain distribution, and damping of small engine blades. Rotational tests of the gage systems were conducted on J85 and F101 engines at a centrifugal force in excess of 50,000 gravitational units. There was no application loss from the 20 gages tested.

In Phase III, a piggyback demonstration of reliability was conducted on a CF6 engine. Stages 1, 7, and 9 were instrumented with a total of 22 strain gages. Despite a hard-stall in early testing, the reliabilities of the gages were 60% for Candidate 1 and 43% for Candidate 2 after 54:40 hours of testing. Most failures occurred at stall or shortly thereafter. Figure 107 (Page 185) compares the reliability of the gage systems on the demonstration engine.

Included in this report is Section 4.0, Gage Application and Fabrication Details. There are a number of changes to the Candidate 1 gage system from those described in the Phase I Interim Report. These are summarized at the conclusion of Section 3.2, Gage System Improvements. The routing designs described have evolved over the past 11 years. They are currently used on all AEG-Evendale development engine tests. They have been proven reliable, although much engine rework is required.

The Candidate 2 gage system has been adopted as standard at AEBC-Evendale because the process and material used to apply this gage system (flame-sprayed alumina) have been used exclusively for high temperature strain gage applications for over 15 years. They, therefore, are well-known by our Instrumentation Application Mechanics. The gages have been used at temperatures beyond those investigated in this program with dramatic results. Thirty-one of the gages were applied to Stages 1 and 2 of a low pressure turbine of an advanced F101-type engine. The maximum temperature of Stage 1 was 1625° F and 1400° F at Stage 2. Maximum stress observed was 15,000 psi double-amplitude. At the end of 33 hours of rotation, the reliability based on the number of gages was over 93%; 29 gages were still returning data.

CONCLUSIONS

- Either gage is a marked improvement over gages previously used at Evendale. A comparison of the fatigue strengths obtained on beams at room temperature and 10^7 cycles is shown in the following tabulation:

<u>Application</u>	<u>Improvement, %</u>	<u>μ in./in.-DA</u>
1. <u>Composite</u>		
a. Karma + H Cement (Old)	67	{ 2400 4000
b. Moleculoy + Denex 2 (New)		
2. <u>FSA or Rokide</u>		
a. Karma (Old)	68	{ 1900 3200
b. Moleculoy (New)		

Similar gains in reliability are to be expected.

- Based on fatigue strength data, the composite-ceramic gage system is preferred at compressor stage temperatures below about 700° F. This was verified by the demonstration of application integrity on the CF6 engine. The all-FSA gage system is preferred at higher temperatures.
- The application time for the composite gage is substantially longer than for the FSA gage. This is because of the lengthy cure schedule of the Denex 2 cement.

1.0 INTRODUCTION

1.1 PURPOSE

The purpose of this program is to develop and demonstrate a strain gage system that will improve the reliability, survivability, and accuracy for measuring alternating strain levels with an imposed mean load on rotating turbine engine components.

Emphasis is placed on providing reliable strain information associated with the aerodynamical response of blading during compressor testing. The strain gage system shall have a high survivability rate with application in the higher operating temperatures of advanced compressors and at higher levels of alternating and mean strain. The application of the strain gage to the compressor blade surface shall not significantly alter the mechanical response of the blade.

1.2 OBJECTIVES

The objective of this program is to advance strain measurement technology as applied to compressor rig and full-scale engine test programs. The strain gage system is defined as the strain sensing element, insulating substrates, protective overcoats, and associated lead wires running from the sensing element through the main shaft, and terminating at a point which will interface with either a slip ring or telemetry.

The strain gage system shall have a high degree of reliability and survivability. The strain gage system will be used to monitor the aeromechanical response of compressor blading exposed to erosive conditions, high thermal fatigue, and flutter test program. Design goals are 80% strain gage reliability for 150 hours of testing at a maximum gas temperature of 1500° F. The room temperature fatigue strength is targeted to be greater than ± 2000 microinches per inch at 10^7 cycles with a maximum mean strain of +1000 microinches per inch.

1.3 BACKGROUND

Recent low cycle fatigue and flutter programs associated with the development of lightweight efficient compressors have been seriously hampered due to the high mortality rate of dynamic strain sensors. These gages, located on the critical stages of the compressor, fail prematurely due to the oxidation and erosion of the protective overcoats. Also, the high vibratory strains imposed on the blades during the above types of test cause unacceptable fatigue damage to the strain sensing element and the associated lead wires resulting in premature failures. During full-scale engine tests, extended and costly delays have been experienced while attempting to decide whether to continue the program jeopardizing the hardware or reinstrument the critical stages. Typically, 6-month delays have occurred in test programs resulting from gage failures on critical compressor stages. A high risk exists in continuing these programs without proper reinstrumentation because of possible catastrophic engine failure. The availability of a reliable and durable strain gage system would have prevented these unnecessary and costly delays.

By developing an improved strain gage system, the significant Air Force payoff shall be a major cost savings associated with elimination of test delays due to premature instrumentation failures. Utilization of the developed technique by Aero Propulsion Laboratory personnel should greatly enhance the capability to perform in-house strain gage instrumentation. Additionally, the procedures used to apply the selected strain gage systems shall be disseminated throughout industry for possible adaptation in future compressor rig and full-scale engine development programs.

1.4 PLAN

The program is organized into three phases which are subdivided into tasks. Phase I consists of defining the problem and establishing, through preliminary screening tests, the most promising metallurgical systems and application procedures for the strain gage substrates, strain sensing element, and lead wire joining techniques. Factors governing the selection of these systems and procedures will include fatigue strength, gage size, oxidation protection, erosion protection, and gage sensitivity stability to 1500° F. The most promising systems will be subjected to detailed testing and analysis.

Phase II is the detailed laboratory evaluation of the two candidate systems selected in Phase I. Bench tests will be conducted to define the fatigue strengths, gage factors, and stabilities from room temperature to 1500° F. The effects of the strain gage application on blade mechanical response will be determined. In addition, techniques will be developed for applying gages to typical high pressure compressor blades made of a titanium alloy and of a high nickel alloy, such as Inconel 718.

Phase III will be the demonstration of the integrity of the two selected gage systems on a piggyback compressor test. The tests at engine operating conditions will establish gage life reliability and performance.

2.0 TECHNICAL APPROACH AND PROGRESS

2.1 PHASE I - SELECTING TWO CANDIDATE STRAIN GAGE SYSTEMS

2.1.1 Task 1 - Literature Search

A search of scientific and technical literature of the libraries of DDC, NASA, and the General Electric Company retrieved over 2500 document titles that had subject matter related to the key words: strain gage, dynamic, sensitivity, temperature stability, applications, and fatigue strength. The search was conducted to aid in selecting candidate strain gage alloys, processes, application materials, and techniques.

Only 25 reports (Section 6.0) were considered pertinent to the program. They provided information on the performance and stability of common and new strain gage alloys and application materials but mostly for the measurement of high temperature steady-state (static) strains rather than for rotating, dynamic strain measurements. However, the physical, thermal, and electrical properties data of common and new alloys published in these reports were considered in the selection of primary candidate strain gage alloys.

2.1.2 Task 2 - Alloy Selection and Test

2.1.2.1 Alloy Selection

Since the literature search failed to identify any specific alloy that had good potential as a high temperature dynamic strain gage, other methods of selection were pursued. The basic approach to alloy selection was by materials properties as reported by the wire manufacturers and knowledgeable strain gage experimentors. Even though the literature did not specifically identify any dynamic strain gage candidate, it did define relative material capabilities of various alloys at elevated temperature, e.g., Reference 14 states that FeCrAl alloys have 4 to 10 times the oxidation resistance of nickel-chrome, which is considered excellent. This along with the fact that FeCrAl also has a very high specific resistance (1128 Ω/cmf) and a known gage factor of approximately 2.0 made it one of the candidate alloys chosen for evaluation. Other nickel-chrome and platinum base alloys shown in Figure 1 were selected

Alloy	Composition	Resistivity $\rho/\Omega\text{cm}$	TMR ρ/ρ_0 $\times 10^{-6}$	Tensile Strength $\times 10^6 \text{ psi}$		Elongation		Melting Point $^{\circ}\text{C}$ $^{\circ}\text{F}$	Thermal Expansion $10^{-6}/^{\circ}\text{C}$ $\times 10^{-6}$	Large Factor RT	Resistance 1.6 in. Gage 0.001 mil wires $\times 10^{-6}$	Sensitivity of ρ to $\times 10^{-6}$
				PSI	MPa	Hard	Ann.					
*1 Karna Driver Harris	76Ni, 20Cr+ Fe + Al	800	0 25	180	130		14 0.001 wire	1400	13.5	2.3	170	391
2 Mich. V Driver Harris	79Ni, 20Cr 1Si	650	+80 20	200	100		17 0.001 wire	1400	12.5	2.1	138	290
3 Tophet C W.B. Driver	60Ni, 16Cr 24Fe	675	+150	175	95			1350	13.7	2.6	143	372
4 Tophet 30 W.B. Driver	70Ni, 30Cr	710	+90	200	120		30 0.001 wire	1377 2510	12.2	1.9	151	302
5 Iron Chrome Aluminum Driver Harris	70Fe, 20Cr 10Al	1128	91		120				17.2	2.2	240	528
*6 479 Sigmund Cohn	90Pt, 8W	400	240	280	130	2	24	1870	8.0	4.4	85	374
7 3 Bill Bean	90Pt, 8Ni 2W	188								4.2	40	168
8 4 Bill Bean	90Pt, 8Ni 2Cr	228								4.1	48	197
9 14 Bill Bean	90Pt, 10Ni	180	140	230	118	2	28	1650		4.2	38	160
*Alloys with past history at Evendale												

Figure 1. Alloy Selection Based on Physical Properties Data.

as proven strain gage alloys with the physical properties required for a good high temperature dynamic strain gage. The properties considered as most significant are (1) tensile strength, (2) elongation, (3) resistivity, (4) gage factor, and (5) coefficient of thermal expansion.

Tensile strength was one of the primary properties considered and elongation was used when available. Tensile strength is one of the best measures of fatigue resistance of an alloy assuming the material has reasonable ductility. Most of the alloys selected had tensile strengths from 100 to 200 kpsi. It should be recognized, however, that specific strengths of fine wires can vary significantly due to size only. Driver-Harris reports in Reference 2 that the tensile strength of 0.008-inch diameter Karma wire is 145,000 psi while it is 130,000 psi for wire having a diameter of 0.004 inch. For this reason, values reported were used as guides and the specific wires planned for use would be tested for relative fatigue strength.

The gage sensitivity, which is the product of gage factor and resistance, was another factor of consideration. The value listed in Figure 1 under column entitled "Sensitivity" is based on calculated values for a gage wound from 0.0008-inch diameter wire with a 0.125-inch grid length. The gage factor listed is either from literature or from tests conducted by General Electric. Figure 1 lists the final selection of alloy candidates. The nine alloys selected and the materials properties that were available are listed.

2.1.2.2 Alloy Testing

The objective of this portion of the program was to determine (by screening tests) the alloys having the best potential for satisfying the program objective. The broad temperature range required (RT to 1500° F) could demand that more than one alloy be used to accomplish the program requirement. The screening tests would include gage sensitivity, oxidation, and fatigue.

Gage Fabrication

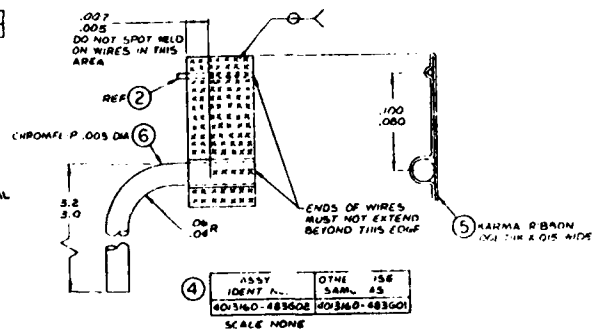
Gages were fabricated from fine wire of Alloys 1 through 6. Alloys 7, 8, and 9 were not fabricated into strain gages because of the low gage sensitivities shown in Figure 1. A typical gage with general fabrication requirements

is shown in Figure 2. The grid is wound on a hand fixture with 12 longitudinal grid wires. The gage is flattened as defined in Section A-A to maintain its form and improve handling. The 0.001 x 0.015-inch Karma foil is joined to the grid, View B, by capacitance discharge resistance welding. Special care is required when welding at the grid wire to foil interface. This has been identified as a predominate failure point. Item 8 of the drawings is the General Electric designed, convoluted lead. This concept was incorporated as the primary airfoil mounted lead system in the early 1970's and has since proven to be a very dependable design. Its use has not only eliminated lead failures on the airfoil but also has reduced failures at the critical interface of the grid wire to ribbon. The leads are formed between two gears, the spacing of which can be adjusted to allow the convoluting of different wire sizes. The gears are manually rotated and the wire is fed into the meshing teeth where it is formed into the shape illustrated in Figure 2. In addition to the gains in mechanical reliability, the convoluted leads introduce negligible errors into the strain gage signal. Laboratory tests of the leads applied to a beam that is strained to 1000 microinches/inch in bending have shown, for a 1-inch length of convoluted lead, that the signal output is 25 microinches/inch (2.5%) with the strain field longitudinal to the convoluted lead axis. With the strain field transverse to the lead axis, the signal output is 1 microinch/inch or 0.1%.

Gage Sensitivity Tests

Sensitivity test beams, shown in Section 5, were instrumented with four gages, two on each side, using GA100 ceramic cement. The gage includes two convoluted leads on each gage tab, a total of four leads on each gage. The four leads permit the determination of gage resistance (R_g) and resistance change (ΔR) due to strain (ϵ) while completely eliminating the effects of lead resistance. Thus, the gage factor is determined for the grid only and does not include erroneous values that could be caused by the lead system. A precision epoxy calibration gage and a thermocouple were applied to the measuring section adjacent to the test gages.

The sensitivity tests were conducted in the General Electric High Temperature Gage Factor Test Facility. Section 5.0 describes the facility, test setup, and data recording. The test beam is fixed in the facility and is run



as a cantilever beam. The system is calibrated at room temperature, using the precision foil strain gage, before elevated temperature testing is initiated. A typical test cycle is shown in Figure 3. Data are taken at temperatures to 1200° F and then the higher temperature (1500° F) testing is completed. This was done first to establish the characteristics of the alloy to 1200° F and also to reduce the possibility of gage failure at higher temperatures before adequate data were obtained at the lower temperatures of interest.

Test Results and Discussion

The results of the sensitivity testing are shown for Alloys 1 through 6, Figures 4 through 9. Generally speaking, the sensitivity screening tests indicated that all six alloys have relatively good characteristics over the RT to 1500° F operating range. Since this is a qualification test to determine whether or not the alloy should be considered for further testing, the results are considered positive for all of the six alloys tested.

The alloys of nickel-chromium (Alloys 1 through 4) exhibit shifts in gage factor which is caused by order-disorder transformations of the alloy. This inherent characteristic has been thoroughly investigated by Willis and Easterlin in References 4 and 8, Section 6. The iron-chrome-aluminum (FeCrAl) showed excellent repeatability with little cycle-to-cycle variation as shown in Figure 8. The resistance stability is very good to 1500° F and, on the basis of these screening tests, FeCrAl exhibits the best sensitivity characteristics over the temperature range RT to 1500° F. Platinum-8% tungsten has the highest gage factor of all alloys tested. The first two cycles to 1200° F show excellent agreement with very little variation. The resistance also demonstrated outstanding characteristics. On a sensitivity basis, this alloy exceeds all others in the RT to 1200° F range. Temperatures exceeding 1200° F cause significant shifts in gage factor and resistance. This is thought to be associated with oxidation of the tungsten.

Average rating of relative gage sensitivities is listed in Table 1 (Page 19). The rating method is discussed in Paragraph 3.1.2.3.

Oxidation Study

The determination of the basic oxidation resistance of the nine selected alloys was completed at the maximum operating temperature of 1500° F. Four wire samples of each alloy were cut from the spool of wire designated for

Sensitivity Test Beams

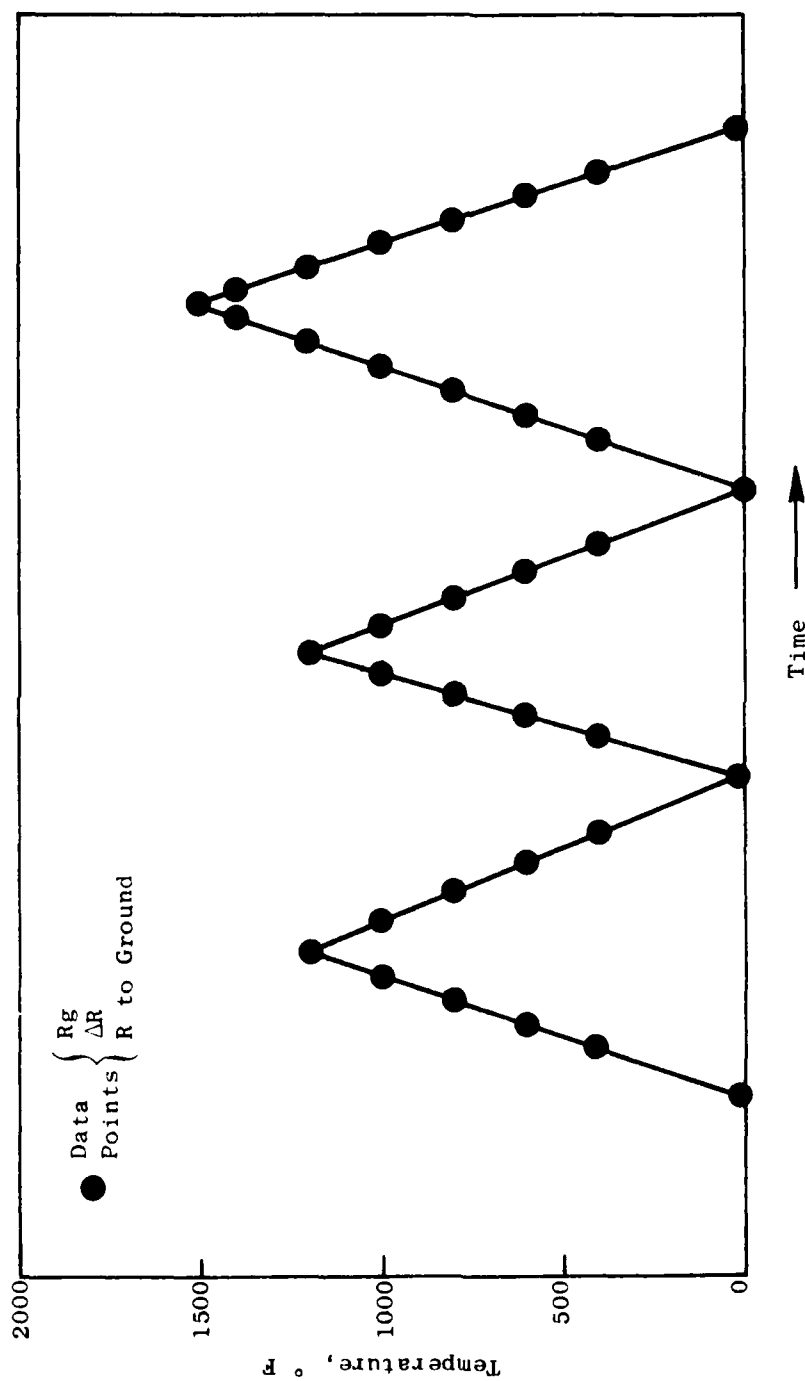


Figure 3. Sensitivity Test Temperature Cycle.

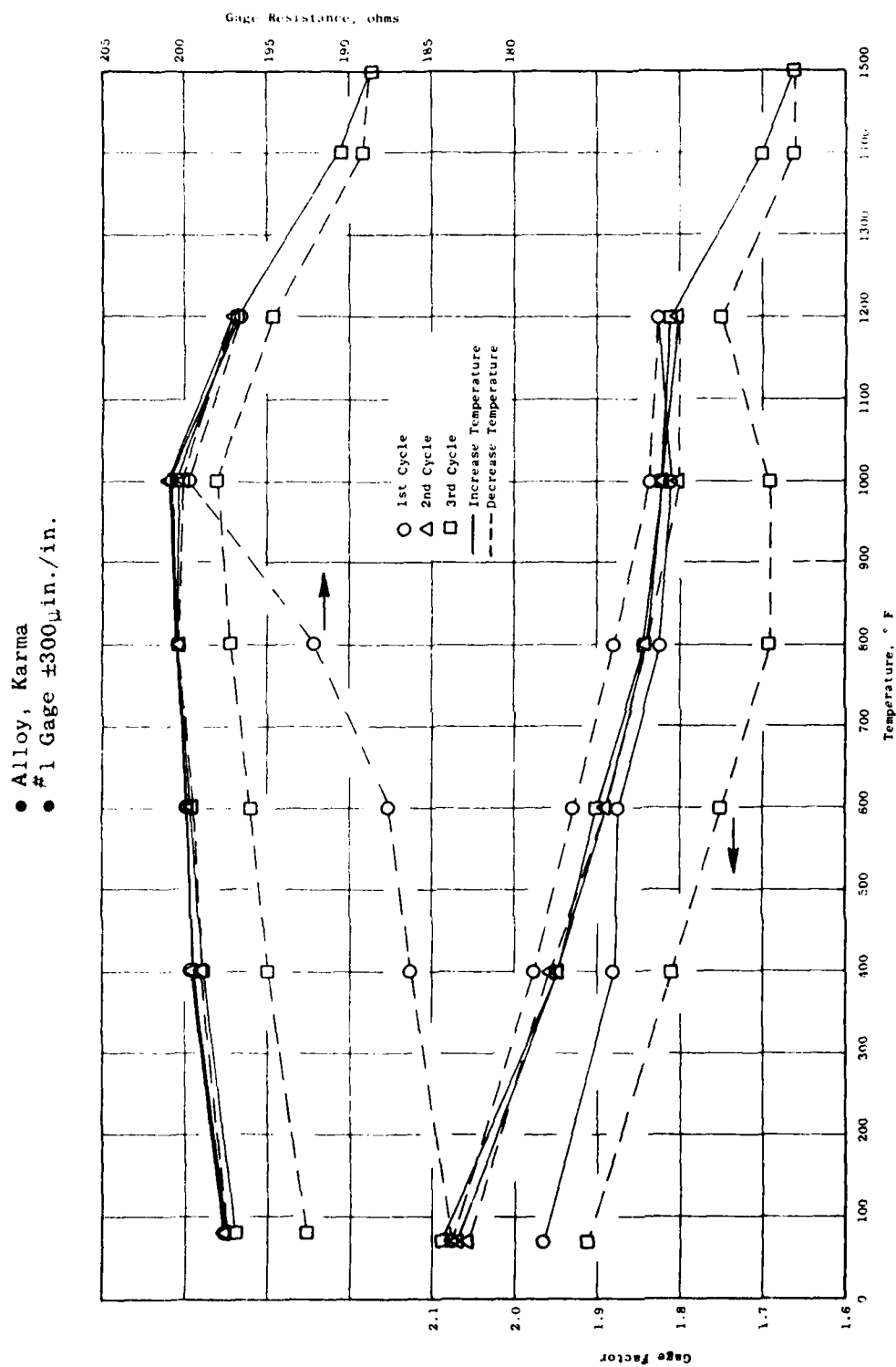


Figure 4. Sensitivity Versus Temperature - Karma.

- Alloy, Ni V
- #1 Gage $\pm 300 \mu\text{in./in.}$

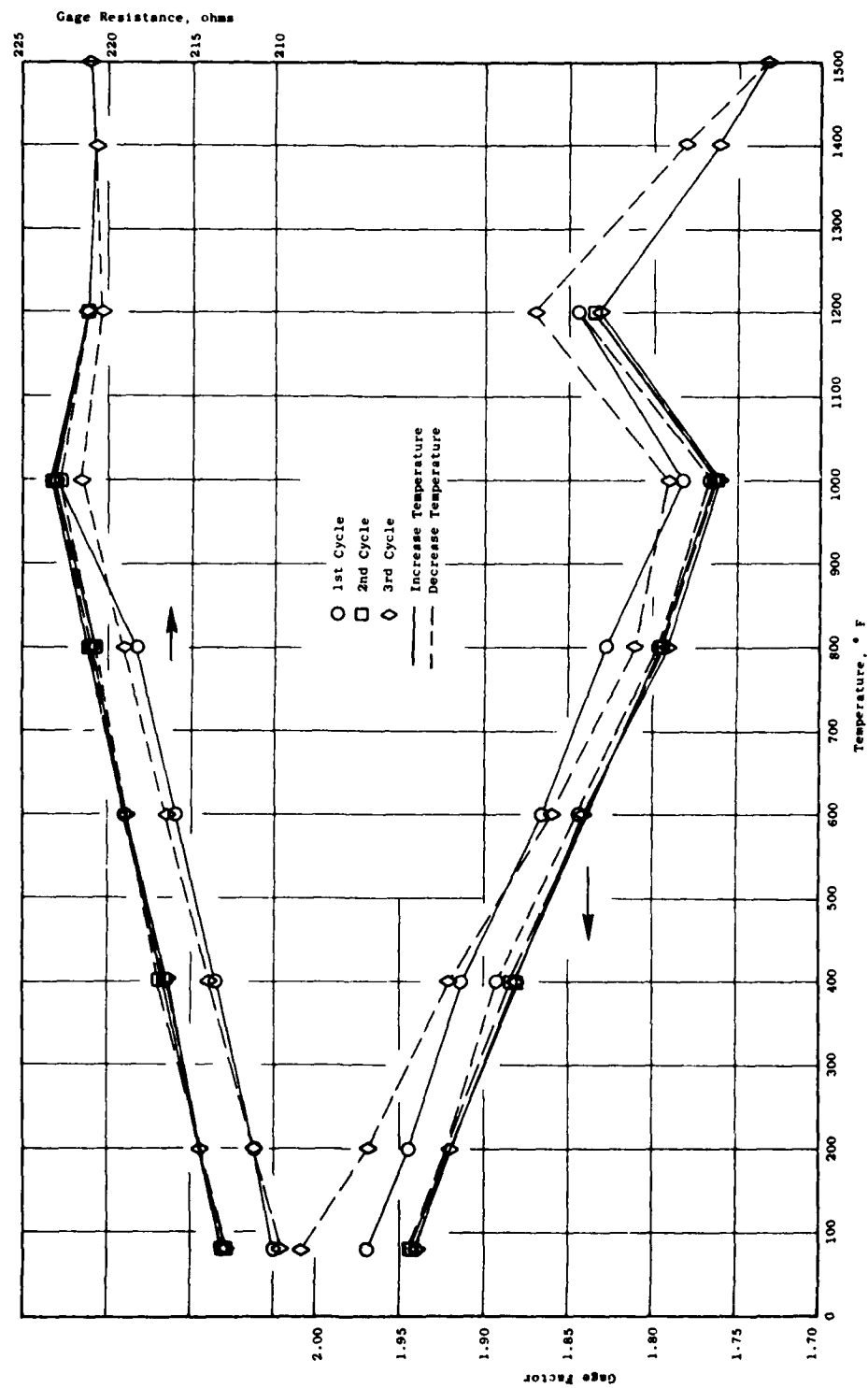


Figure 5. Sensitivity Versus Temperature - Nichrome V.

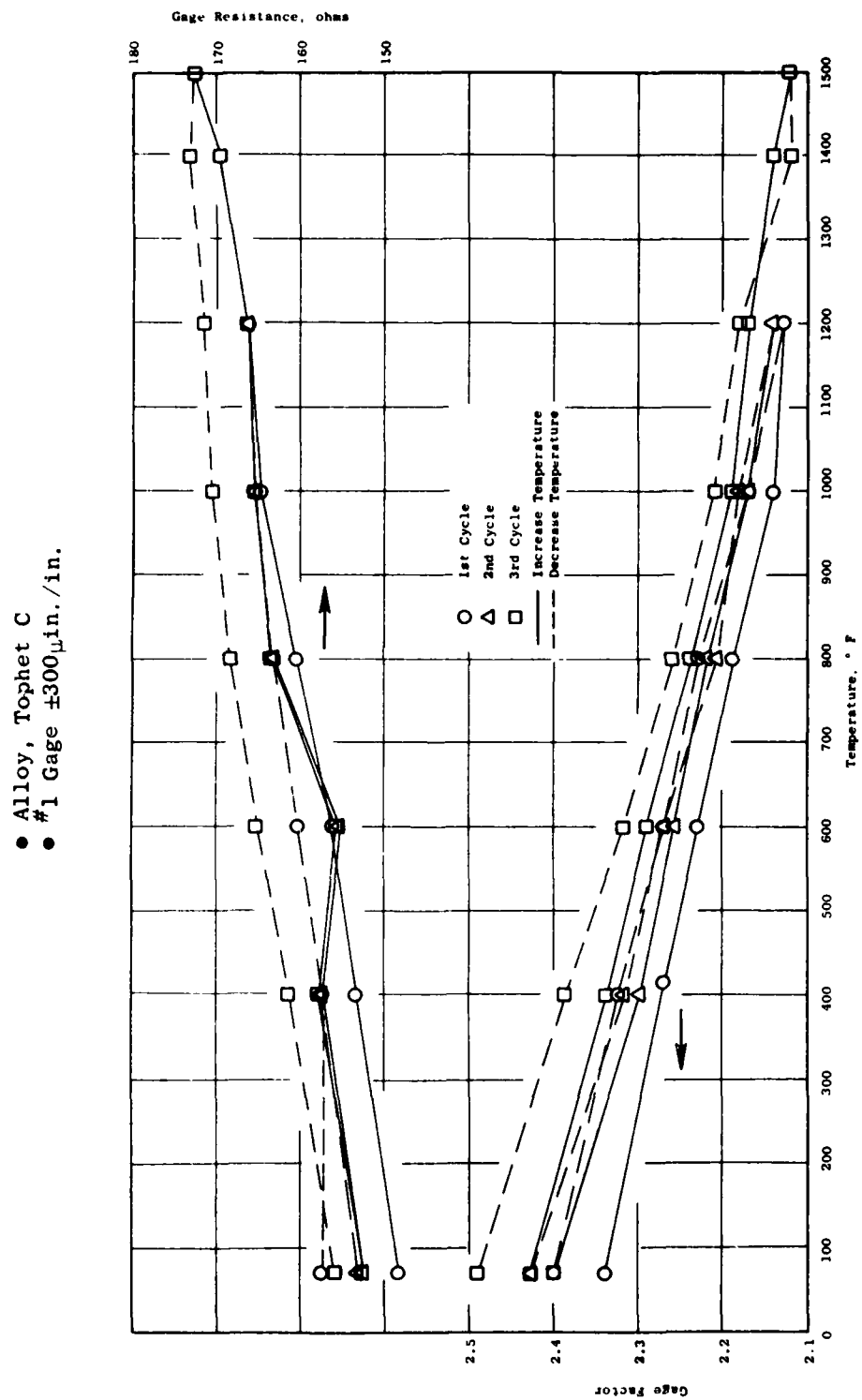


Figure 6. Sensitivity Versus Temperature - Tophet C.

- Alloy, Tophet 30
- #1 Gage $\pm 300 \mu\text{in./in.}$

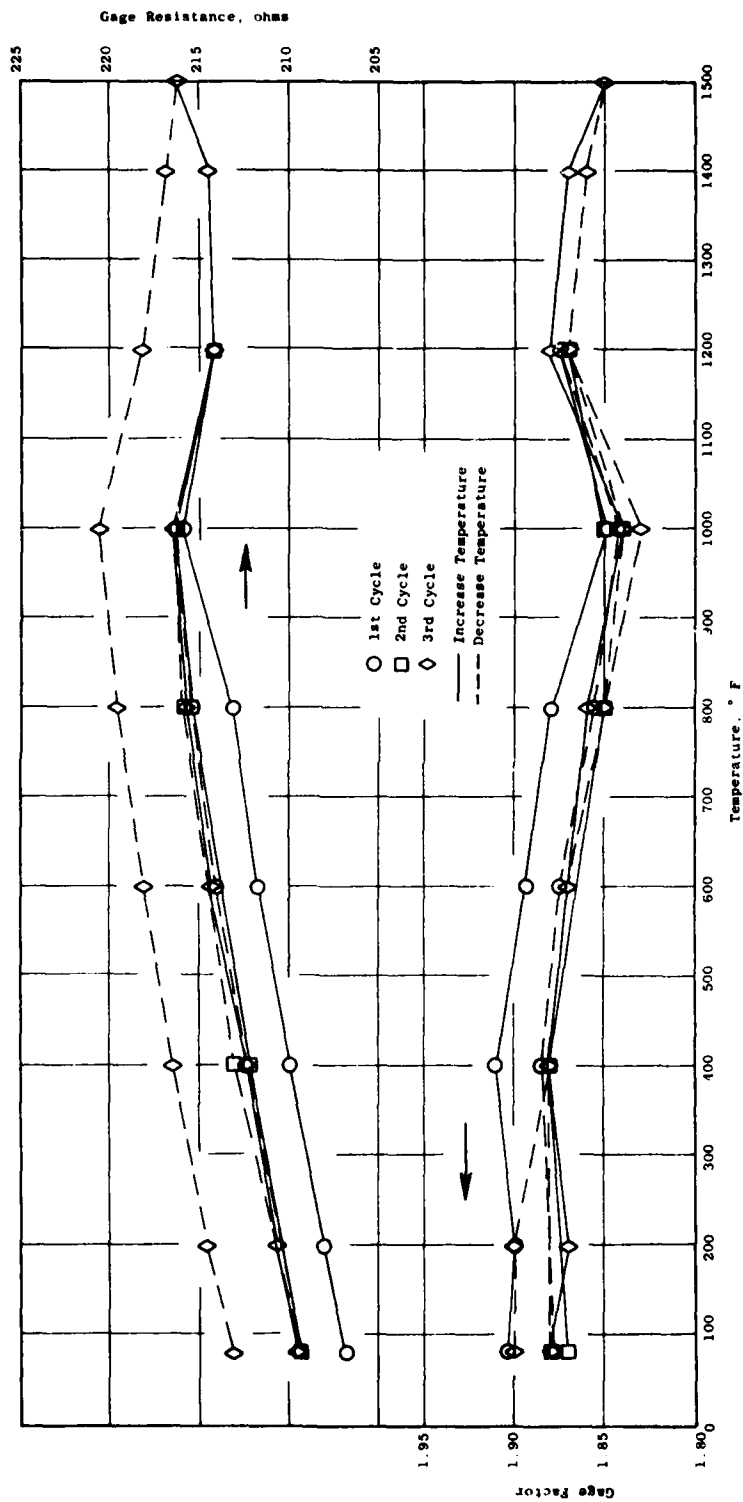


Figure 7. Sensitivity Versus Temperature - Tophet 30.

- Alloy, FeCrAl
- #1 Gage $\pm 300 \mu\text{in./in.}$

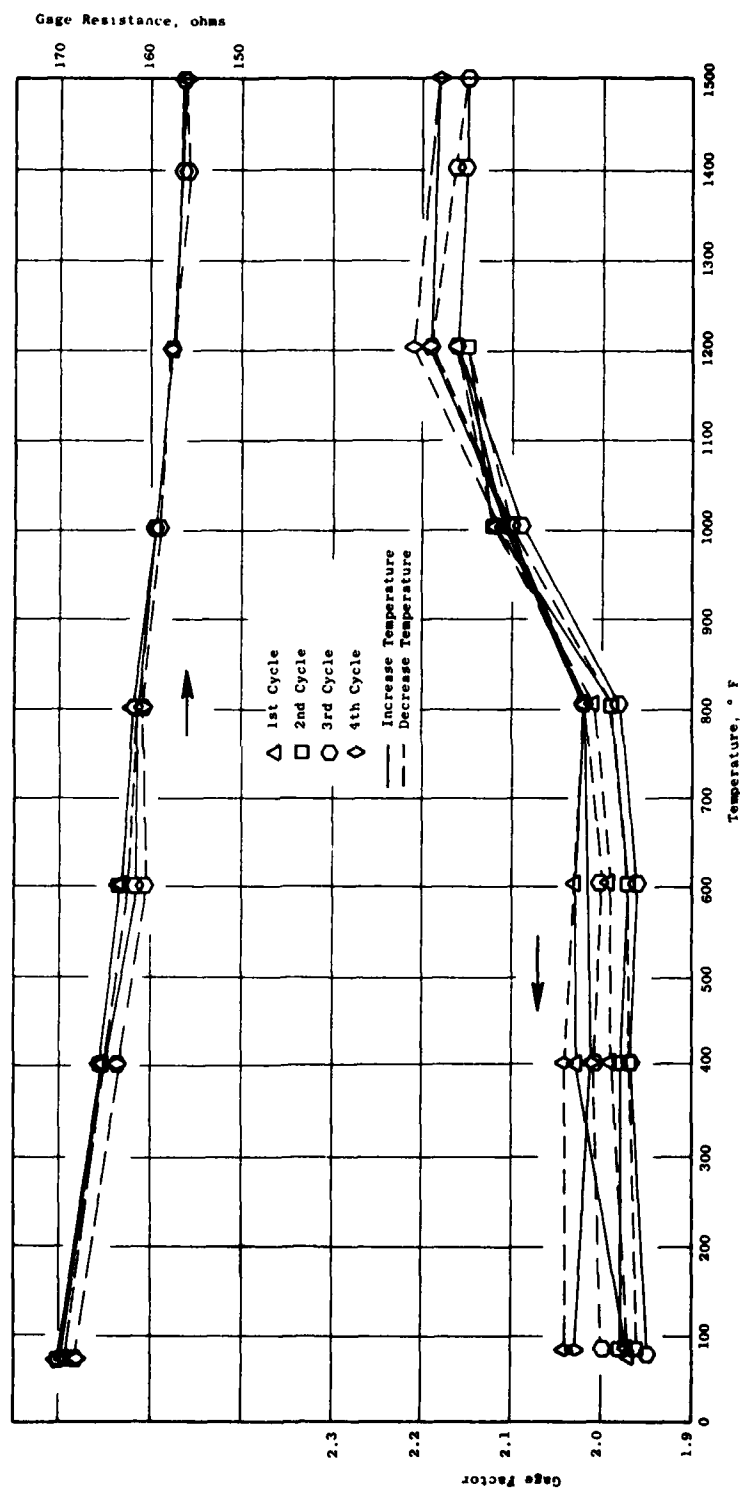


Figure 8. Sensitivity Versus Temperature - FeCrAl.

- Alloy 479, Pt8W
- #1 Gage $\pm 300 \mu\text{in./in.}$

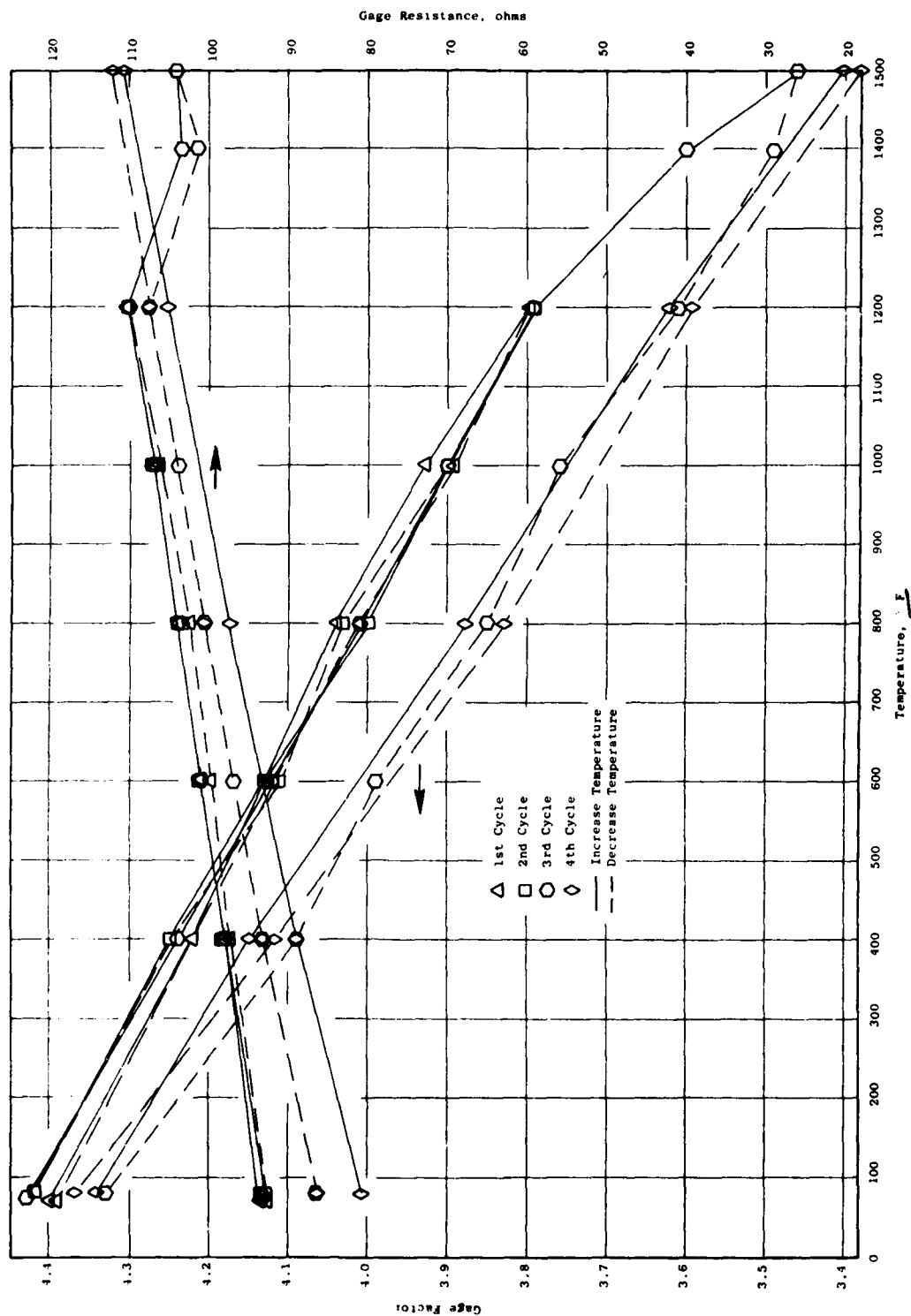


Figure 9. Sensitivity Versus Temperature - Pt8W.

Table 1. Selection of Prime Candidates.

Weight - 15%		10%		25%	20%	30%
Alloy	Alloy No.	Physical Properties		Gage Sensitivity Stability to 1500° F	Oxidation 1500° F 150 Hr	Fatigue Total
		Rg X G.F.	Therm Exp.			
Karma	1	83 - 12	82 - 8	80 - 20	78 - 16	75 - 23
Nich V	2	73 - 11	80 - 8	85 - 21	95 - 19	30 - 9
Tophet C	3	80 - 12	84 - 8	80 - 20	90 - 18	35 - 11
Tophet 30	4	74 - 11	78 - 8	85 - 21	80 - 16	40 - 12
FeCrAl	5	95 - 14	95 - 10	85 - 21	60 - 12	87 - 26
Pt8W	6	80 - 12	60 - 6	83 - 21	80 - 16	60 - 18
Pt8Ni2W	7	61 - 9			60 - 12	
Pt8Ni2Cr	8	63 - 9			65 - 18	
Pt10Ni	9	60 - 9			60 - 12	

program testing. Three samples were inserted into small alumina oxide tubes to prevent possible loss of identification and to aid in handling the fine wire and then placed in a furnace. One sample of each wire was removed from the furnace at 100, 150, and 200 hours. The samples were tagged and sent to the metallographic laboratory where they were mounted for microscopic examination and photographs. Figures 10 through 14 show the as-received wire as well as those exposed to 1500° F for 100, 150, and 200 hours. The wire diameters are listed; and, even though they range from 0.0007 inch to 0.002 inch, a good relative measure of oxidation resistance was obtained. The photographs were considered the best measure of relative oxidation from alloy-to-alloy and were used for the rating listed in Table 1 (Page 19).

The FeCrAl alloy, one of the prime candidates at this time, proved to be one of the least resistant to oxidation, which is contrary to Reference 14. The photographs show fissure-like oxide lines that are relatively consistent from specimen-to-specimen. The increased time shows progressive damage of similar fissure defects. Various coating techniques are planned in Task 3 of this phase to enhance oxidation resistance, and FeCrAl will be a prime alloy for the coatings work. In general, all of the alloys exhibit severe oxidation after the 100-hour time period. Nichrome V and Tophet C show the best resistance to oxidation. Alloys 7, 8, and 9 were eliminated from the program because of low oxidation resistances coupled with low gage sensitivities. Table 1 summarizes the appraisals of the oxidation resistance of the nine alloy tests. The weighted percentage relative to a maximum of 20% is shown for each alloy.

Fatigue Testing

Gage Fabrication/Application

Special gages were fabricated for fatigue testing of Alloys 1 through 6. The gages were terminated with constantan foil instead of Karma foil shown in Figure 2. The purpose of this was to permit soft soldering of small 36-gage copper leads to the foil. The intent of this testing was to evaluate the grid alloy only and to exclude the failures that might occur in the junctions or any point other than the grid wire. To eliminate the possibility of

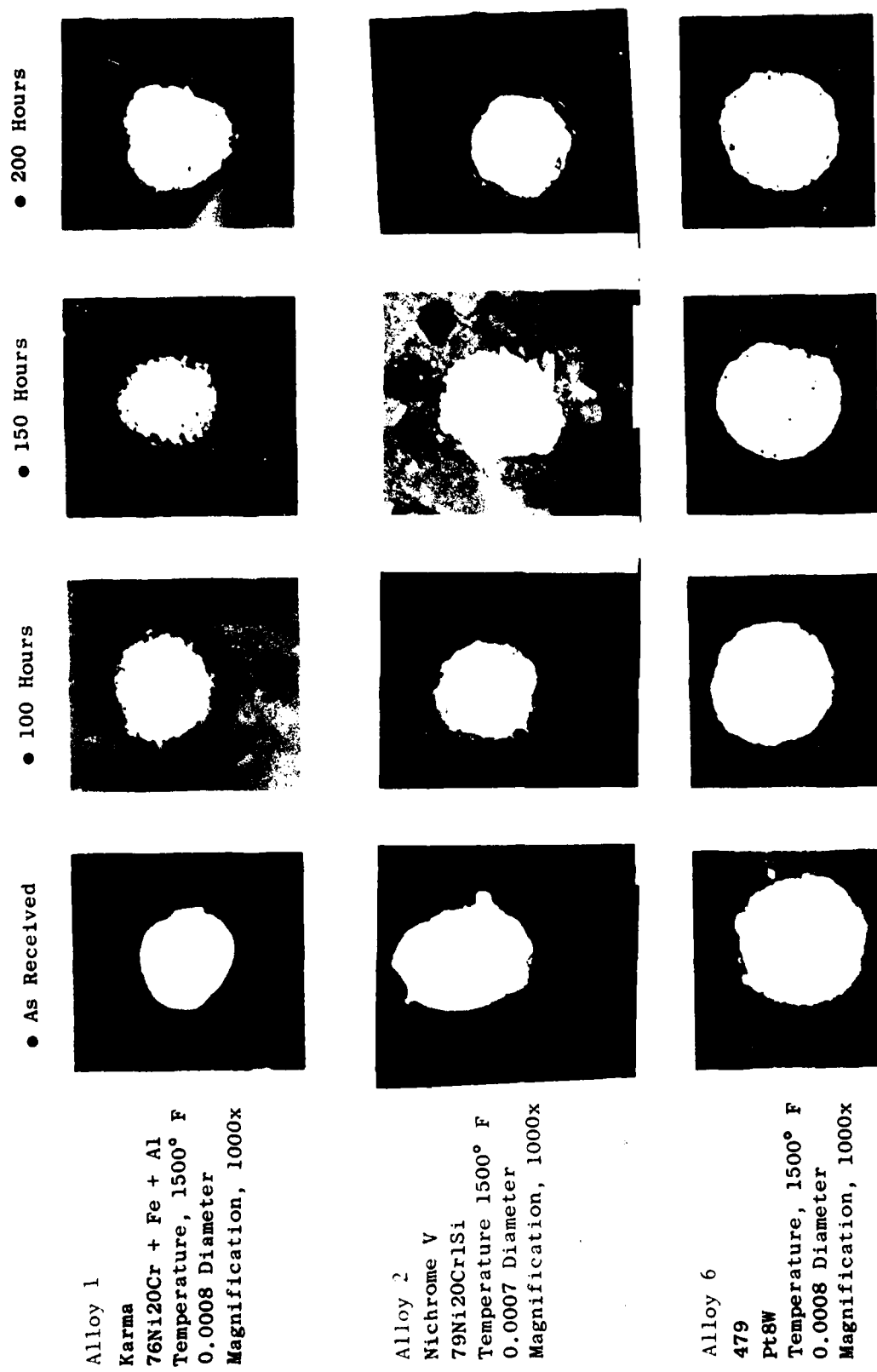


Figure 10. Oxidation - Karma, Nichrome V, and Pt8W.

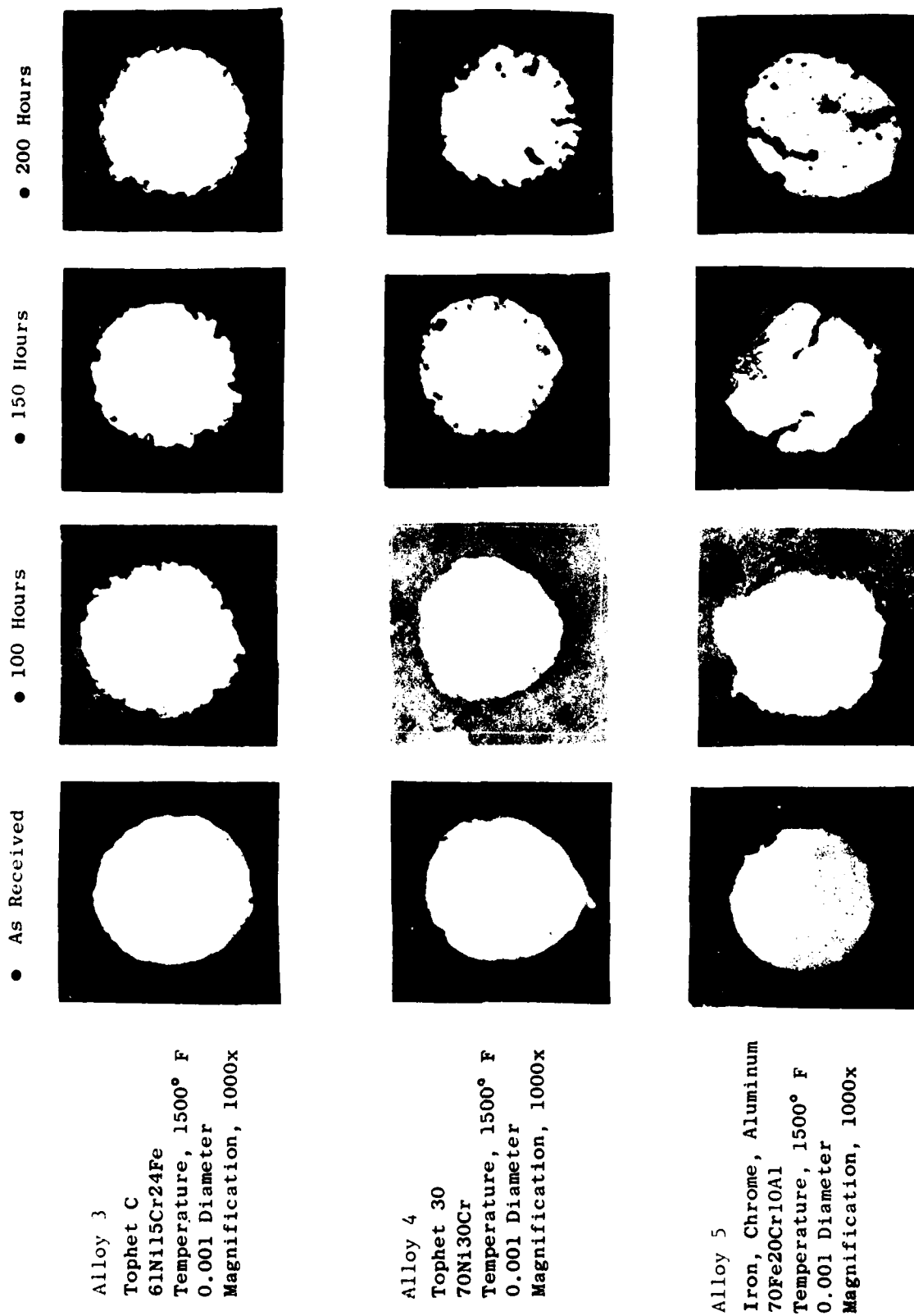
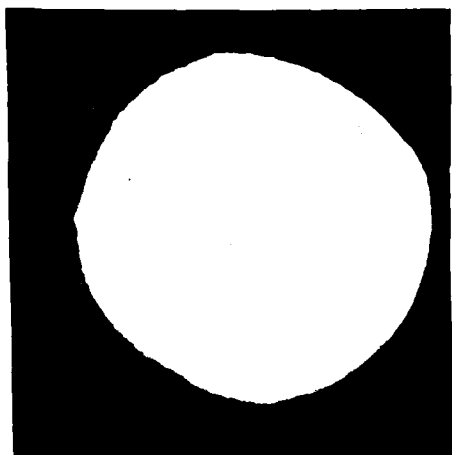


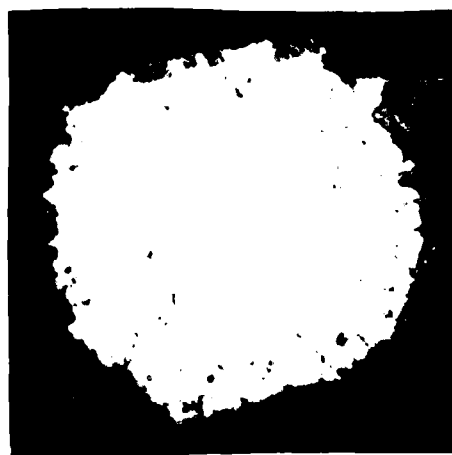
Figure 11. Oxidation - Tophet C, Tophet 30, and FeCrAl.

Alloy 7
90Pt8Ni2W
Temperature, 1500° F
0.002 Diameter
Magnification, 1000x

● As Received



● 100 Hours



● 150 Hours



● 200 Hours

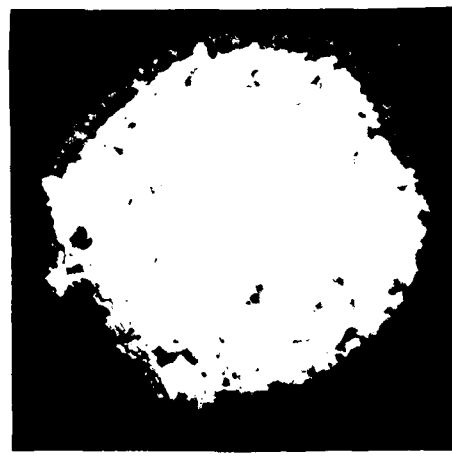
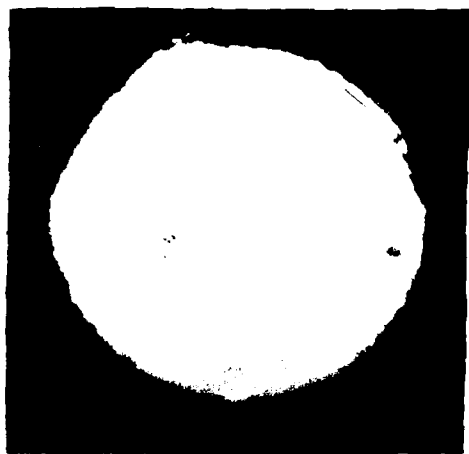


Figure 12. Oxidation - 90Pt8Ni2W.

Alloy 8
90Pt8Ni2Cr
Temperature, 1500° F
0.002 Diameter
Magnification, 1000x

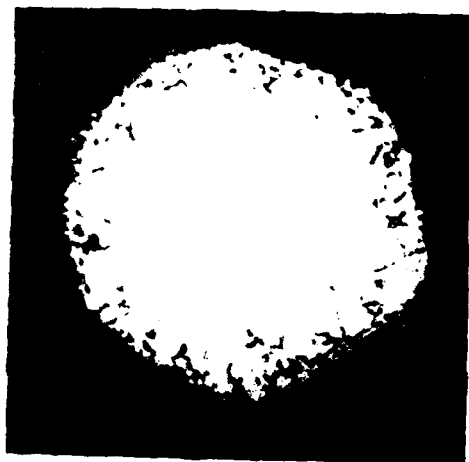
• As Received



• 100 Hours



• 150 Hours



• 200 Hours

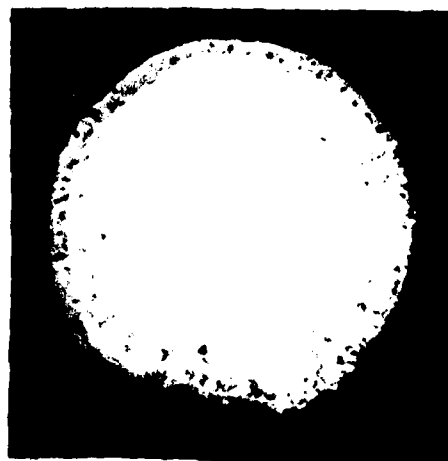


Figure 13. Oxidation - 90Pt8Ni2Cr.

Alloy 9

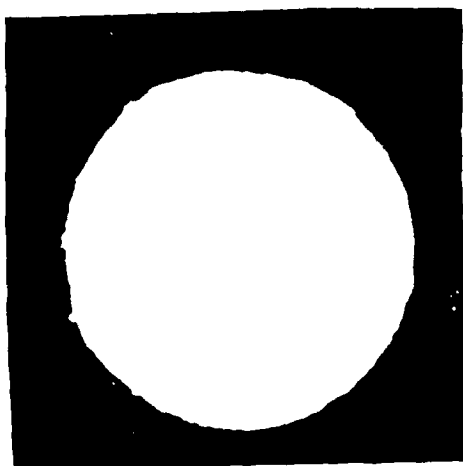
90Pt10Ni

Temperature, 1500° F

0.002 Diameter

Magnification, 1000x

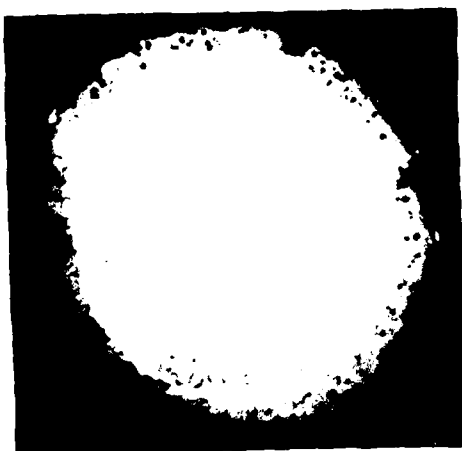
• As Received



• 100 Hours



• 150 Hours



• 200 Hours

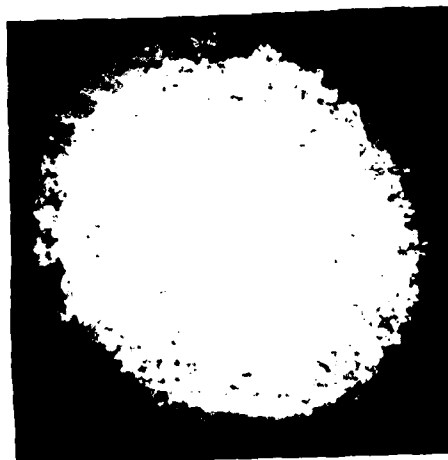


Figure 14. Oxidation - 90Pt10Ni.

junction failure, the grid only was cemented to the test beam with GA100 ceramic cement. The constantan foil and 36 gage lead were encapsulated in silicone rubber to reduce the strain transmission from the beam to the foil/lead wire. The 0.25-inch thick titanium test beam has a rectangular test section that will accommodate three test gages on each side of the beam. The test beam is fixed at one end and driven by a mechanical cam at 30 Hz. A calibration gage is used to set the strain initially by adjusting the amount of tip deflection. The tip deflection is then maintained constant for the duration of the test (see Section 5.0 for equipment description).

Test Results

A presentation of the fatigue results, Figure 15, shows gages tested and the number of cycles accumulated at the time of failure. All beams were set at ± 1000 microinches/inch and run until gage failure was detected; $\pm 15\%$ deviation from signal level of the test gage at the start of test shuts down the system. When shutdown occurs, the number of cycles is logged and the gage is checked by resistance measurements to assure that failure caused shutdown. A grid that has opened will normally measure infinite resistance with the gage at maximum tension and will measure resistance with the gage at the maximum compression point. After confirming by resistance measurement that the gage has failed, the machine is restarted, put in automatic shutdown position, and the remaining good gages are tested to failure. Gages that survive 1×10^7 cycles at ± 1000 microinches/inch are raised in level to ± 1500 microinches/inch, and the test is continued until a gage failure is incurred.

Alloy 1, Karma, and Alloy 6, Pt8W, were tested on the same beam. Testing of these alloys was discontinued after 10 million cycles were accumulated because the alloys are commonly used at General Electric and, therefore, machine time could be better utilized investigating materials that are new to GE. None of the gages of Nichrome V or Tophet 30 accumulated 10 million cycles at the first level and testing was discontinued on these materials. Of the first three gages tested of Tophet C, one ran out and accumulated some cycles at the 1500 microinches/inch level. The other two failed in the grid very early in the first level. A second beam containing six Tophet C gages was prepared and tested. The results of the first beam tests were confirmed - two ran out at

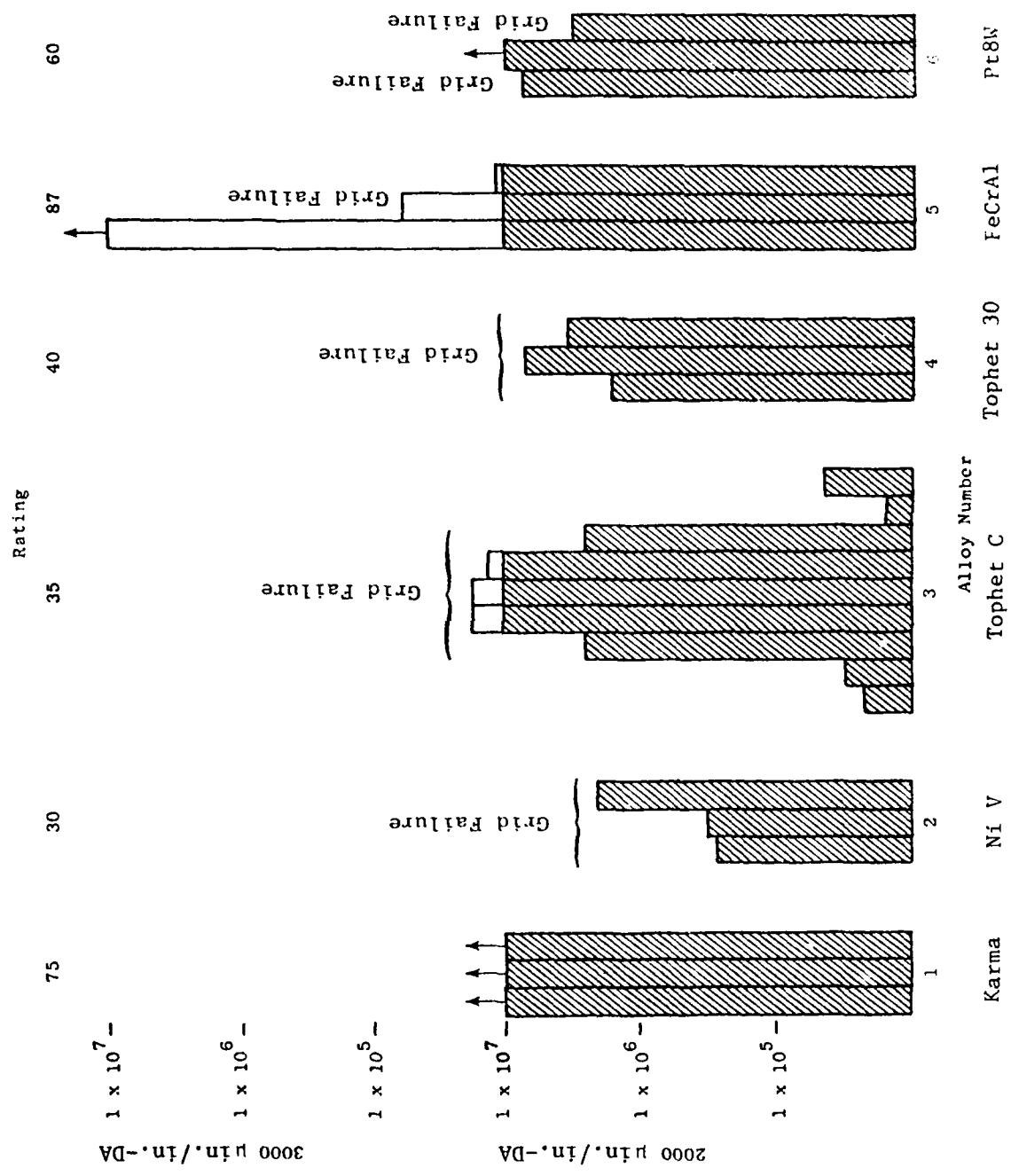


Figure 15. Fatigue Tests at Room Temperature.

the first level and four failed early. The performance of Alloy 5, FeCrAl, was excellent. All gages survived the first strain level and one ran out 10 million cycles at ± 1500 microinches/inch. Again, the alloy loomed large as a prime candidate, especially if the intolerable oxidation discussed previously could be retarded by a coating of metal or metallic oxide.

The ratings shown in Table 1 are the assessments of the relative fatigue strengths of the alloys based on the tests conducted.

Metal-Coated FeCrAl Gage Grids

An early attempt to evaluate the potential of coating gage grids to enhance their high temperature characteristics was to platinum-coat FeCrAl gages. This was accomplished by (1) fabricating gages by conventional wire gage winding methods, (2) gage cleaning and mounting in a special fixture, and (3) depositing ≈ 100 microinches of platinum on the grid by sputter deposition. The resistance of the gages as fabricated was ≈ 160 ohms and, after coating, the resistance was ≈ 93 ohms. This was expected when considering the resistivity of the platinum coating.

The gages were applied to a test beam for sensitivity testing and were heat treated (20 hours at 1050° F) to stabilize them for elevated temperature testing. The result of this was that Gage 1, Figure 16, increased to 134 ohms and Gage 2 increased to 113 ohms. Some explanation of this variation is possible but additional data on other gages would be required to resolve it completely.

Figure 16 shows the results of sensitivity tests that followed. It is apparent that the two gages have different characteristics. The only similarity between the performance of the two gages is the shape of the gage factor curve versus temperature.

A platinum-coated FeCrAl gage was also exposed to 1500° F for 200 hours to determine if the coating would retard oxidation. As shown in Figure 17, the coating afforded no protection of the material; the fissures are still present although there may be some oxidation reduction at the surface of the wire.

● FeCrAl; Pt. Coated Gages, Gage Factor Vs. Temperature

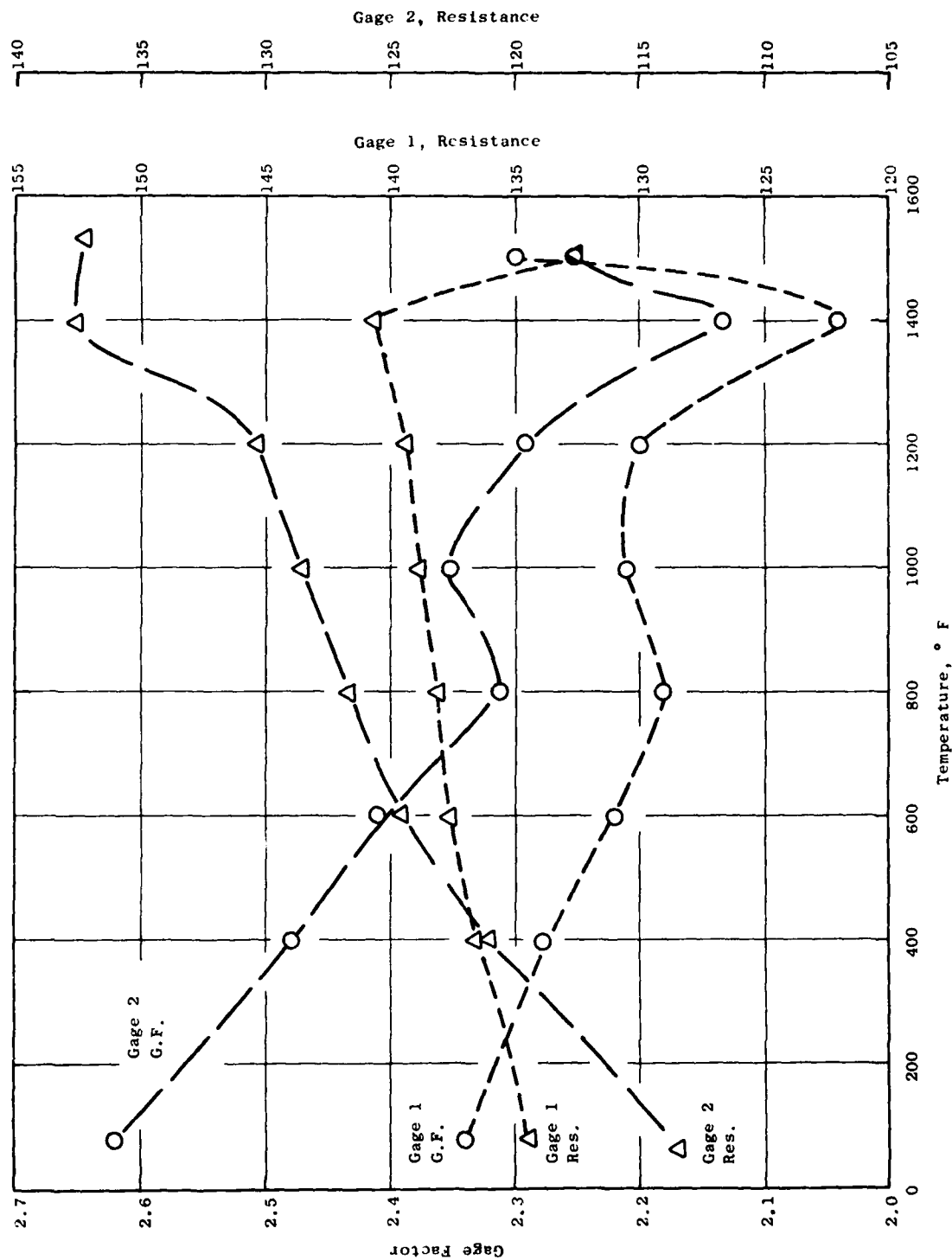


Figure 16. Sensitivity Versus Temperature - Pt-Coated FeCrAl.

70% Fe, 20% Cr, and 10% Al Gage Coated
with Platinum, Soaked at 1500° F for
200 hr



Figure 17. Oxidation of Platinum-Coated Gage.

It must be concluded, based on these tests, that the thin coating of platinum did not provide the desired results. Further attempts to provide protection of candidate alloys by sputter coating with oxides will be conducted in Task 3 of Phase I.

2.1.2.3 Selection of Prime Candidate

The rating method used in selecting the primary alloys to be studied further in Task 3 testing is shown in Table 1. The rating is based on the following characteristics:

The Physical Properties of the alloys from Figure 1 included (1) gage factor, (2) resistance of a fabricated gage having a grid length of 0.125 inch, and (3) the overall thermal expansion over the operating range (RT to 1500° F). Physical properties comprise 25% of the total rating.

Gage Sensitivity Stability is the characteristics of the alloy observed during gage factor/sensitivity testing. This is the estimate of the alloy's ability to return valid data based on test results, Figures 4 through 9. Stability also is 25% of the total rating.

Oxidation is based on the test results and photomicrographs of wire sections after exposure to 1500° F, Figures 10 through 14. This appraisal does not include the possibility of coating; it only considers bare wire as tested and is 20% of the total rating.

Fatigue is based entirely on the results of fatigue testing, Figure 15. Although it was apparent that a minimum number of samples were tested, Task 3 work would include testing to confirm the selection of materials used for the Phase II Program. Fatigue comprises 30% of the total rating.

The weight percent is the estimated value assigned to the categories of investigation that will yield an alloy capable of satisfying the program objectives.

The overall rating listed in the Total column represents a numerical value of the candidate for evaluation in Task 3.

Three alloys will be carried into Task 3 and tested in various strain gage systems. The alloys in order of preference are:

Alloy 5, FeCrAl

Alloy 1, NiCrAl (Karma)

Alloy 6, Pt8W

2.1.3 Task 3 - Gage Application Development

The specific objective of this task is to establish two candidate strain gage systems that would come closest to meeting the program requirements of temperature, strain, blade effects, life, and reliability. Two different applications methods would be considered (Figure 18). One is the Rokide or flame-spray alumina technique. This method is fairly standard throughout industry, varying only in the composition of alumina used and in the method of deposition. The other is the composite-ceramic design that was developed at GE to protect the gage from the effects of the direct bombardment of molten alumina during the application process thus improving the fatigue strength. In that design, H ceramic cement was used. A different cement may be better in the composite structure, and this will be determined later in this task. Where appropriate, the areas of investigation in this task must include the effects of candidate ceramics on the gage grid performance.

Areas of Investigation

A. Gage Grid

1. Fatigue - effects of manufacturing, coldwork, heat treatment
2. Sensitivity Stability - effects of temperature
3. Oxidation/Corrosion with candidate ceramics

B. Lead Attachment - current methods of attaching leads are a potential source of failure

C. Application Materials - adhesion, shrinkage, and outer coat erosion.

• Strain Gage Application Development

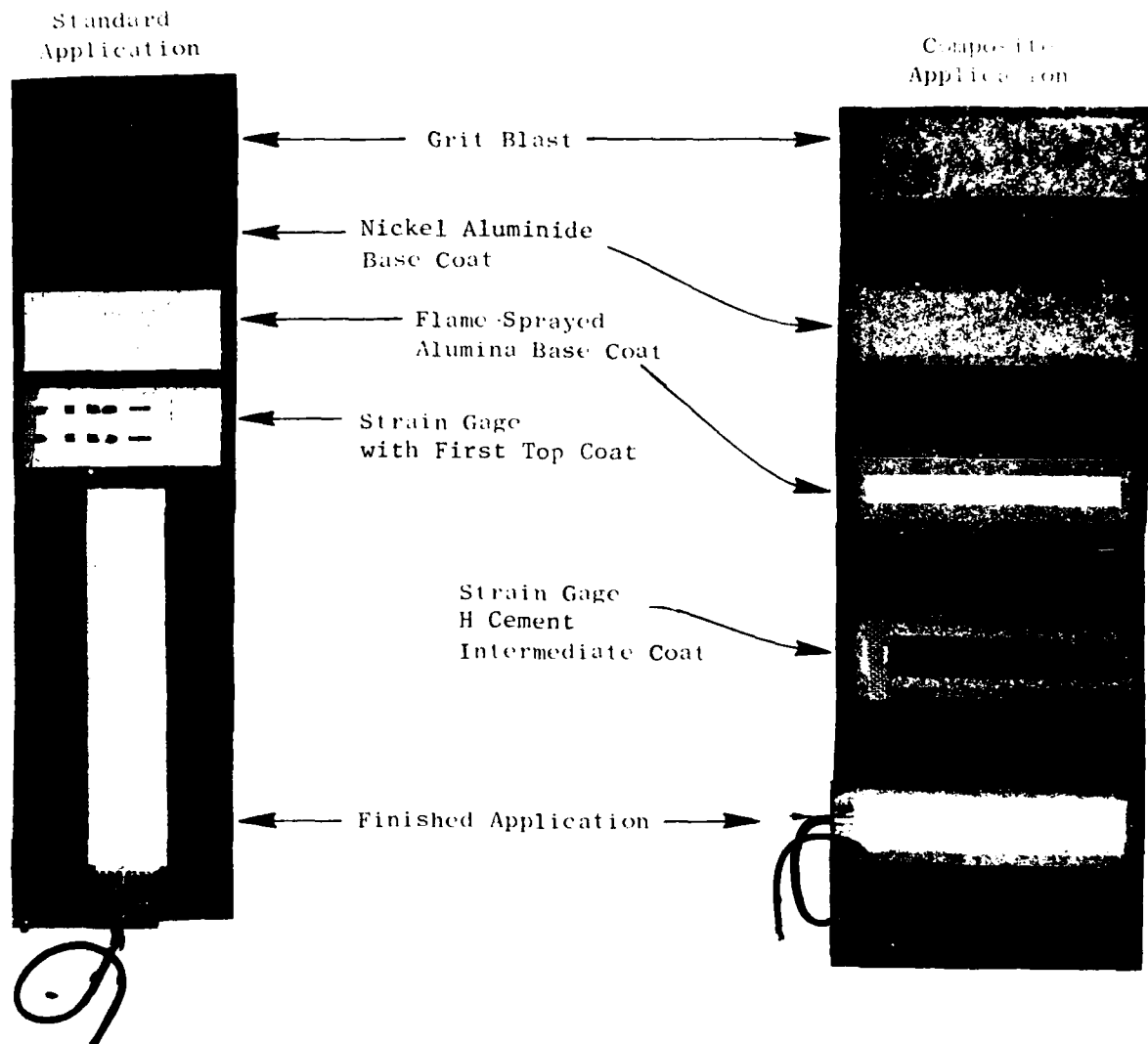


Figure 18. Standard and Composite Applications.

2.1.3.1 Gage Grid

Fatigue

Wire strain gages made by GE are flattened at about 25% coldwork to improve handling of the gages during lead attachment and application. It was shown, Reference 26 and Figure 19, that Karma strain gage performance could be stabilized for use between room temperature and 1000° F by heat treating at 1050° F. It was also shown during testing in a GE Strain Gage Improvement Program that the heat treatment improved the fatigue strength of the gage. Since gage fatigue strength is a very important factor in a highly reliable dynamic strain gage system, it was believed that the established conditions of coldwork and heat treatment temperature might be varied to produce a higher fatigue strength in Karma.

To verify this, fatigue tests were conducted with gages that were conditioned with different amounts of coldwork and heat treatments. Of the 18 gages tested, only one survived the first level of dynamic strain and most failed before 10^5 cycles. These premature failures were unexpected. Post-test inspection showed all gages failed in the grids and grid thicknesses among the gages tested varied from 0.25 mil to 0.4 mil. By specification in Figure 2, the thickness of the flattened gage grid should be 0.5 mil to 0.65 mil.

Because of this, gages stored in the crib that were fabricated by shop personnel were inspected for thickness and found to vary from 50% to 60% of the original diameter (0.0008 in.) for one mechanic, to 25% to 40% for the other. Scanning electron microscope pictures of a "good" gage (Figure 20) revealed surface defects that could significantly reduce the gage fatigue strength. Gage flattening procedures, which are unique to GE, and equipment were reviewed. They did not provide adequate gage thickness, finish, or flatness control. The equipment and procedures were redefined. Figure 21 shows the new concept. Gage blocks are hardened jo-blocks having parallelism and flatness controlled to ± 2 microinches with a surface finish of 0 to 0.4 microinch. The center block can be changed in 0.1-mil increments to provide control of gage thickness. Gage thicknesses obtained using these blocks were verified by a measurement gage capable of resolving 0.05 mil. This technique will be refined and used in the fabrication of gages for Phase II testing.

- G.E. Karma Strain Gage for Dynamic Use to 800° F and 1000° F
- Fabricated per 4013160-483004-6
- Post Application - H.T. at 1050° F for 2 hours

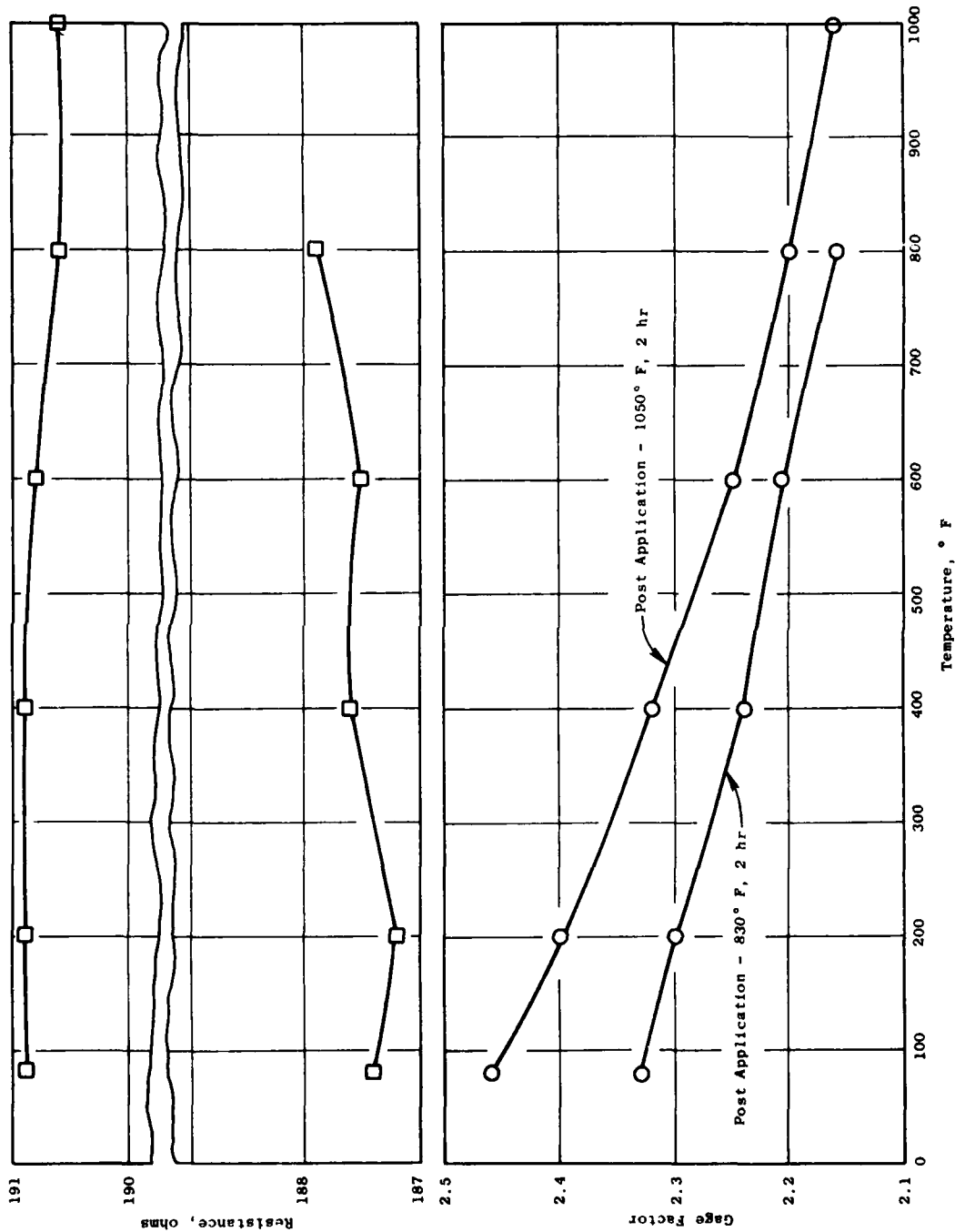


Figure 19. Gage Factor Versus Temperature of Heat Treated Karma.

- Karma Gage Flattened to 0.0003 in.; Inspected with Electron Microscope, Reveals Grooves, Cracks, and Damage from Too Much Work Hardening.

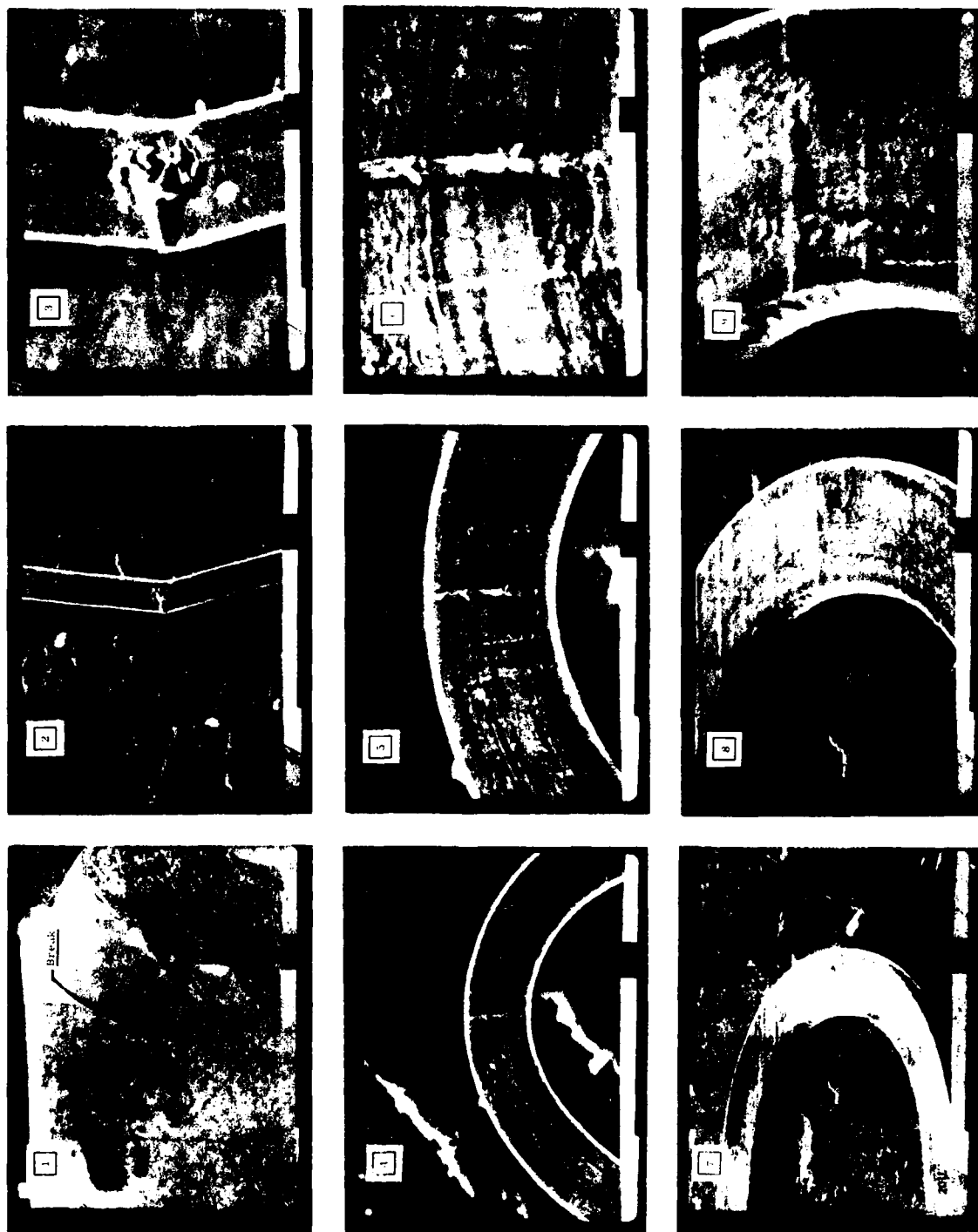
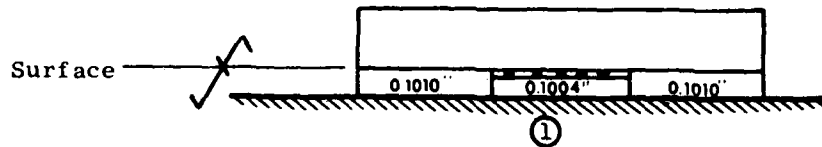


Figure 20. Gage Defects Shown by SEM.

- a) Controlled Thickness and Finish with Polished Gage Blocks



- λ = 0-0.4 Microinch
- Flatness = ± 2 μ inches Over Gage Length

① Variable in 0.1 mil Increments

- b) Thickness Gage to Monitor Gage Flattening
Accurate to 0.05 mil

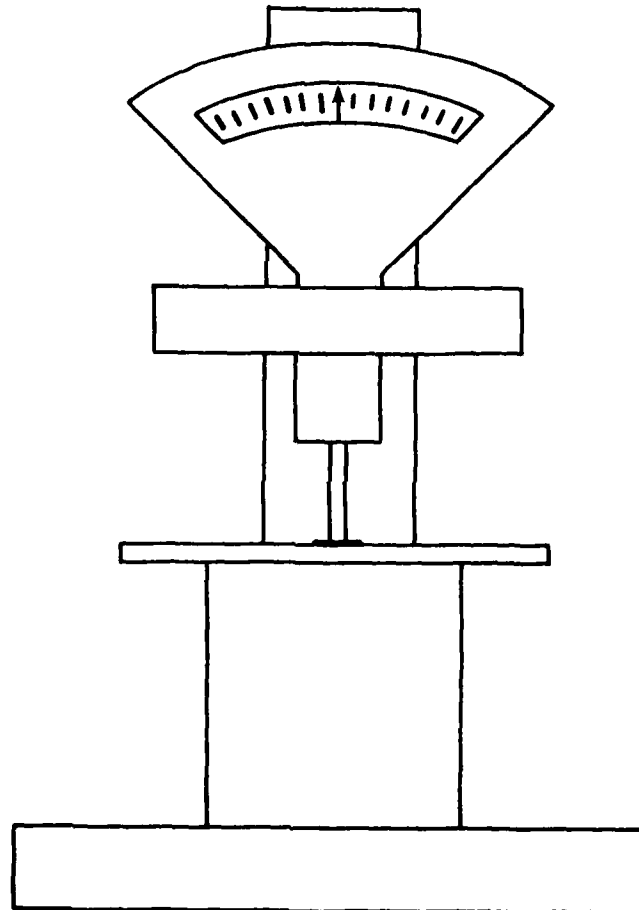


Figure 21. Modified Gage Flattening Fixtures.

It was recognized, during early testing, that optimizing fatigue strength through cold work/heat treatment conditioning by fatigue testing applied gages would require time-consuming matrices of conditioning variables for the three candidate alloys. An alternate technique was required to determine the degree of high cycle fatigue improvement provided by various conditioning for each alloy and, then, to rank the alloys with regard to fatigue strength. Gages fabricated to the conditioning that would provide maximum fatigue strength could then be tested on fatigue beams.

According to the GE Advanced Metallurgist, without regard to surface defects of a material, high cycle fatigue primarily is a function of grain size, yield strength, and ductility. It is believed grain size should not be altered by the processes involved in strain gage manufacture; therefore, a pull test to determine stress versus elongation of the wire under different conditions would provide the required information. It was decided to use load (P) versus elongation because of (1) the difficulty in measuring the area changes of the very fine wire to obtain stress (P/A), and (2) the requirement to later establish system fatigue with applied strain gages.

A test was designed that involved pulling a 1/2-inch length of wire and recording the load in grams versus the elongation in mils on an X-Y recorder. Each end of the wire undergoing test was cemented to a Kapton tab. One tab was pinned to a small strain gaged cantilever beam that provided a calibrated signal of load to the recorder. The other Kapton tab was pinned to the carriage of a 4-inch lathe that traveled 2.4 mils/second. The motion of the carriage (elongation) was measured by a spring-loaded displacement transducer (LVDT) that provided X-axis input to the recorder. Elongation data must be corrected for load cell deflection versus load. This fine-wire test facility is shown in Figure 22. Typical failed test specimens are shown in Figure 23.

Initial testing was conducted on the as-received wire to establish a baseline for comparison with conditioned specimens. Conditioned specimens were tested to obtain the average and range of ultimate tensile and yield load and elongation. Figures 24 and 25 show typical average load versus elongation curves for Karma, and a new candidate, Moleculoy, which is a modified Karma alloy of 75Ni 20Cr 4.5Al. Moleculoy was introduced to the

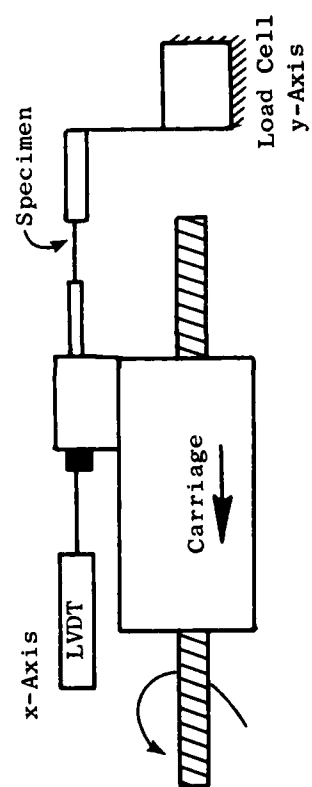


Figure 22. Fine Wire Test Machine.

- Typical Wire Pull Test Specimen, ↓ Wire Failure Point

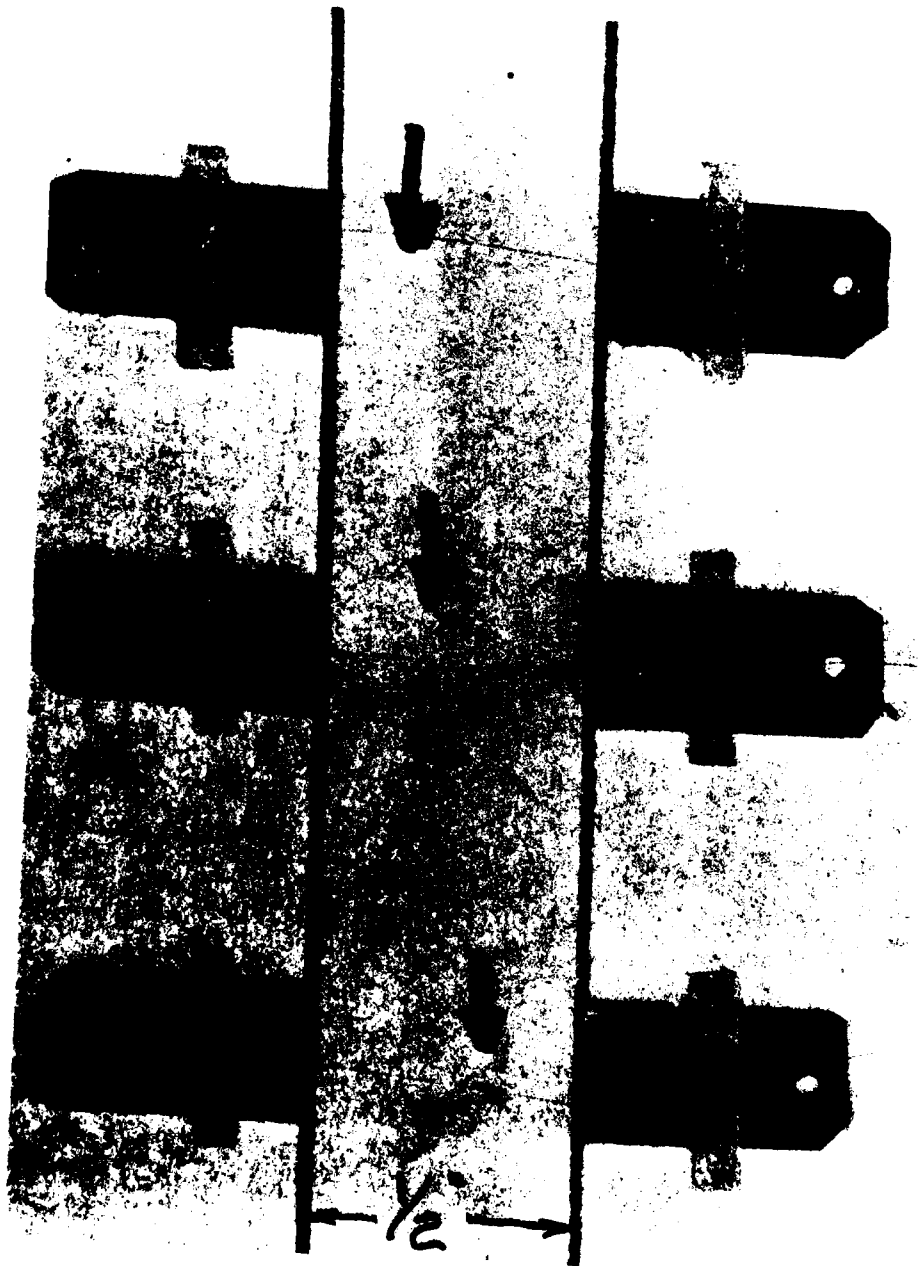


Figure 23. Pull Test Specimens.

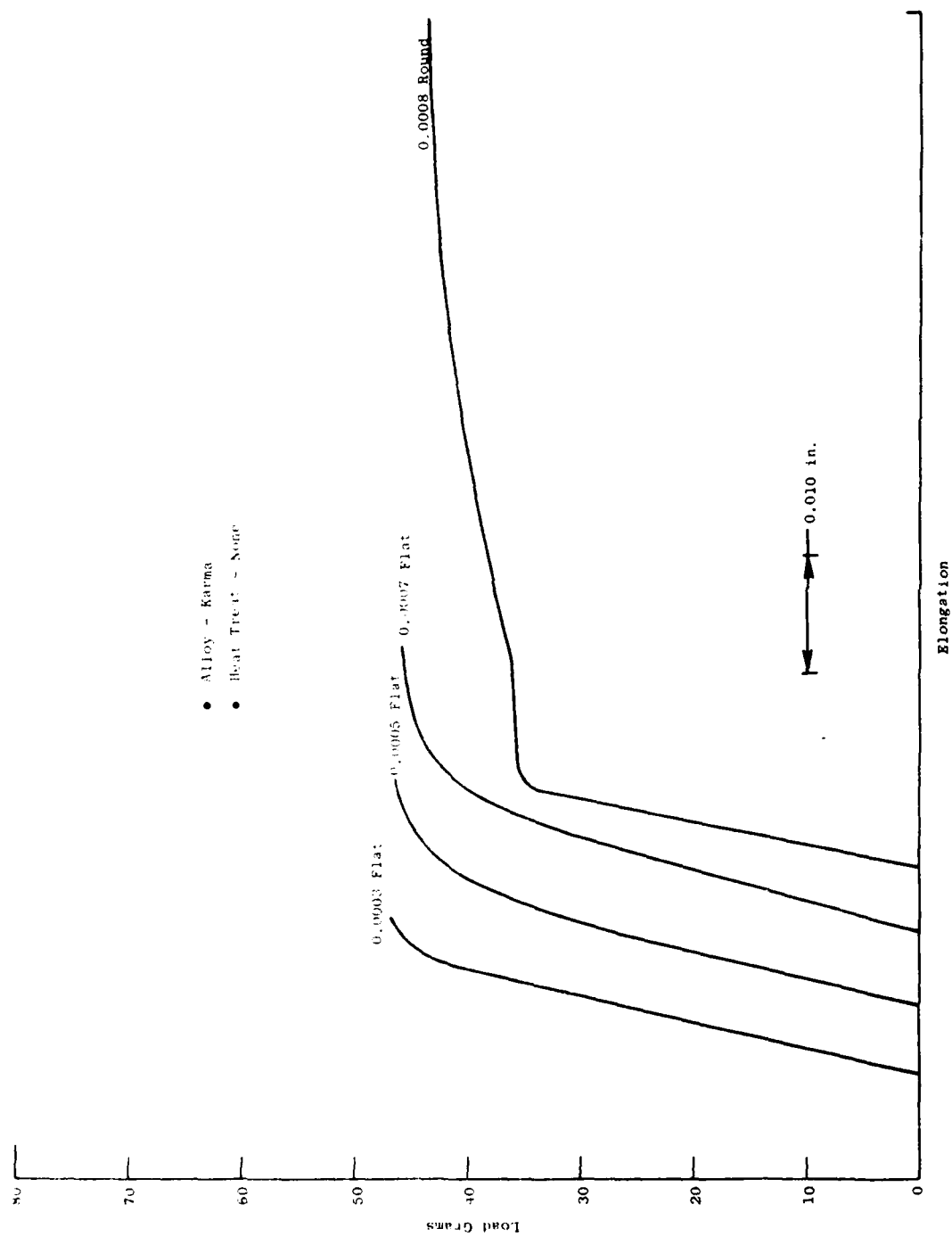


Figure 24. Effect of Coldwork on Load and Elongation of Karma with No Heat Treatment.

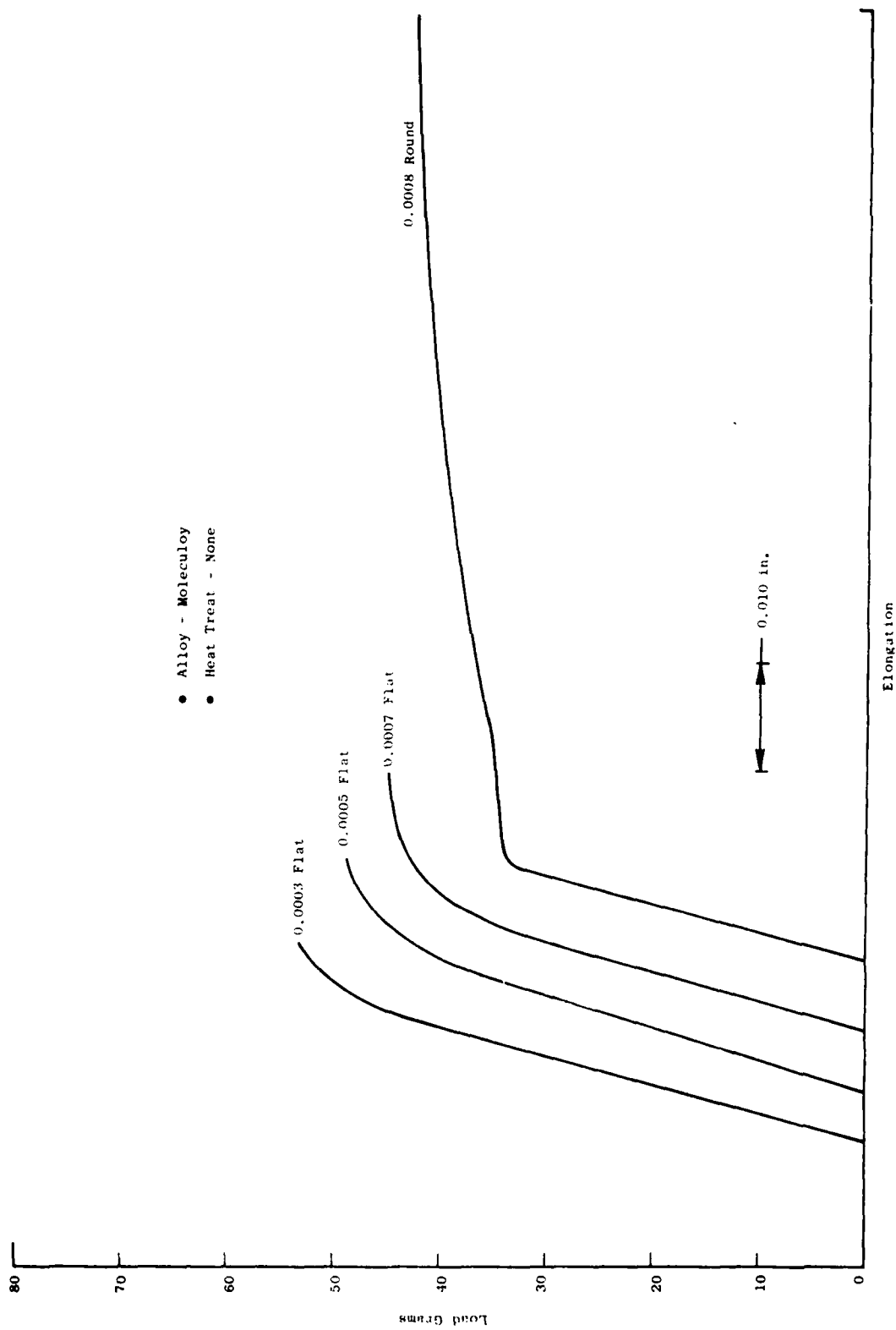


Figure 25. Effect of Coldwork on Load and Elongation of Molecule with No Heat Treatment.

program because the GE Karma alloy was not readily available and the modified alloy that came closest to it was obtained from Molecu-Wire Corp., Wall Township, New Jersey.

All data were analyzed by the Advanced Metallurgist. The criteria used to select the combination of coldwork and heat treatment that would provide maximum fatigue strength are maximum 0.2% yield strength with an elongation of about 3%. Figures 26 through 29 are plots of 0.2% yield load and elongation versus coldwork and heat treatment. Elongation data have been corrected for load cell deflection.

Following is a brief discussion of each wire by the metallurgist:

Karma (76Ni, 20Cr, FeAl) - Karma wire improved its strength very little when simply flattened; however, when the flattened wire was heat treated, a 30% strength increase was realized. Higher strength but lower ductility is realized by increasing the degree of coldwork. The wire, even when flattened to 0.0003 inch, gave fairly repeatable results. The current 1050° F heat treatment is as good as 850° or 1300° F for strength and ductility.

Moleculoy (75Ni, 20Cr, 4.5Al) - The Moleculoy wire responded slightly to coldwork. But when heat treated after working, the strength increased nearly 40%. The best combination appears to be coldworking to 0.0005 inch followed by 1300° F heat treatment. Lower temperature heat treatments and increased coldwork resulted in lower ductility. Increased time at 1300° F could result in even better strength.

FeCrAl (70Fe, 20Cr, 10Al) - The FeCrAl wire was weakened by the heat treatments investigated. It responded well to coldwork; however, its strength and ductility fell short of that demonstrated by Karma or Moleculoy. In addition, the FeCrAl data were less repeatable. The above factors indicate FeCrAl would be weaker in HCF compared to Karma or Moleculoy.

Alloy 479 (92PT, 8W) - Alloy 479 has the best as-received strength of the alloys studied. Coldwork, heat treatment, or combinations thereof failed to increase the strength or ductility. The property reduction resulting from the 1050° and 1300° F heat treatment may be due to oxidation. Apparently, the alloy has a very low work hardening coefficient since it did not respond to coldwork.

Karma - 76Ni20Cr + Al - Fe

○ As Received

□ 850° F Heat Treat, 2 hr

◇ 1050° F Heat Treat, 2 hr

△ 1300° F Heat Treat, 2 hr

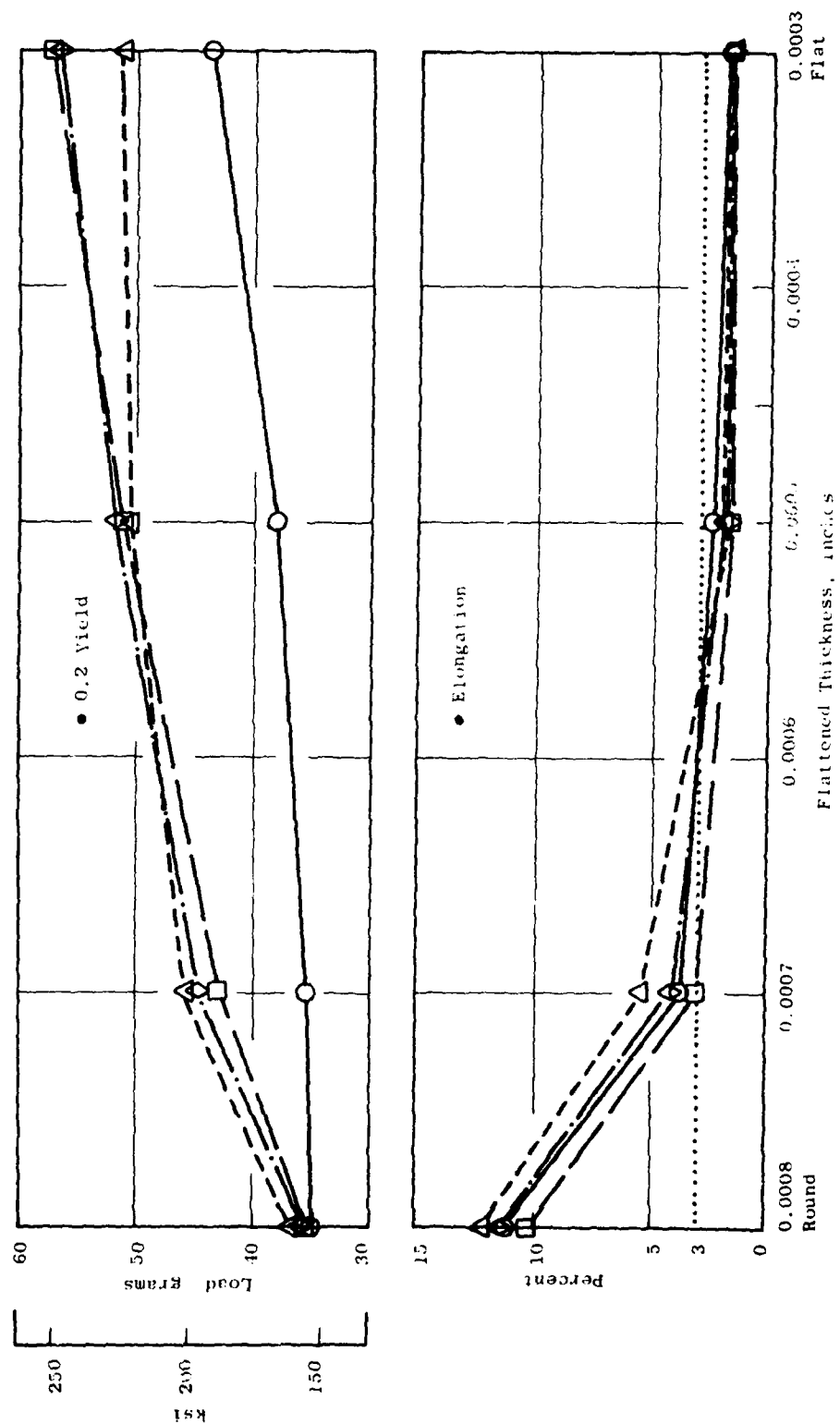


Figure 26. 0.2% Yield and Elongation Versus Conditioning - Karma.

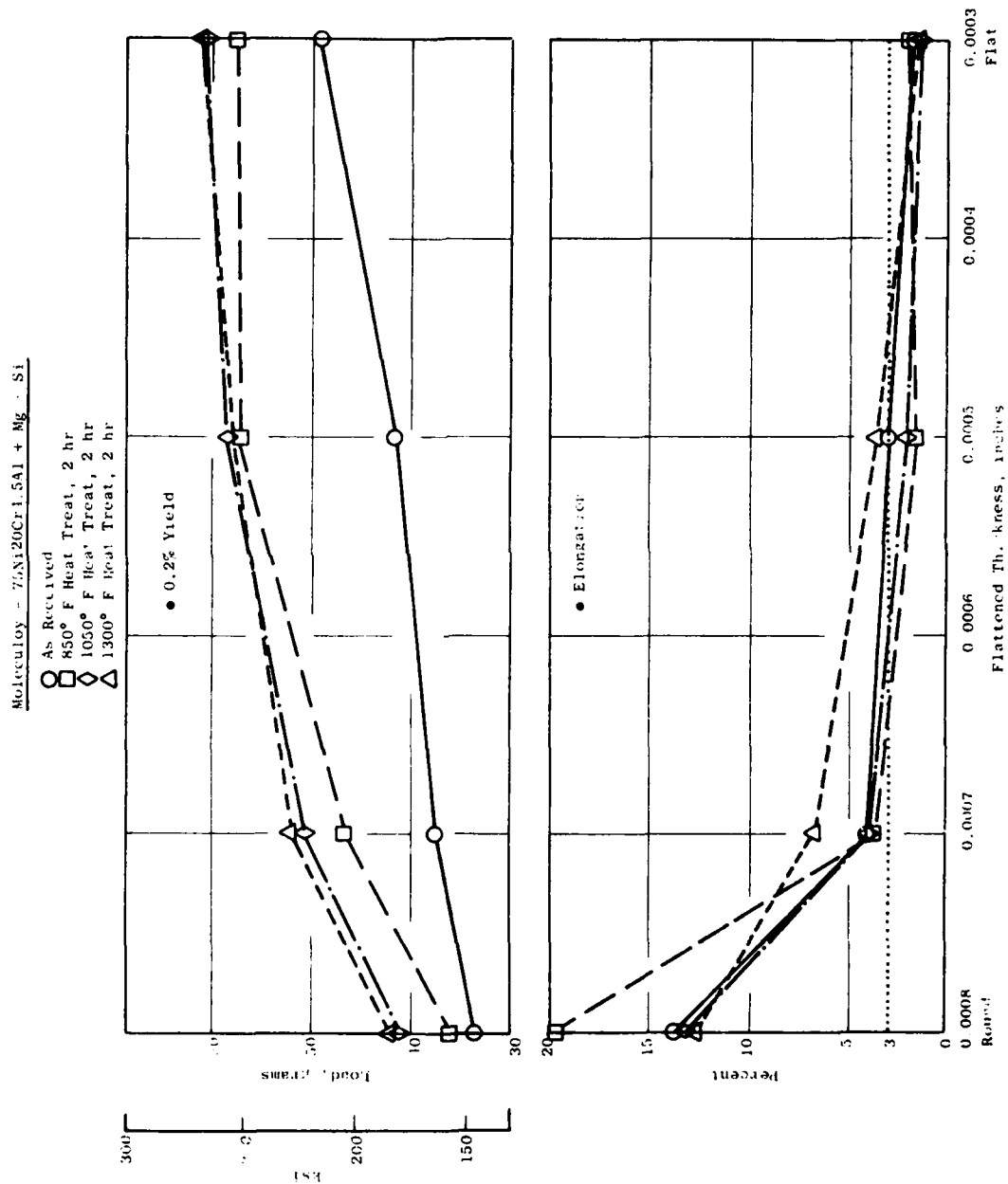


Figure 27. 0.2% Yield and Elongation Versus Conditioning - Moleculey.

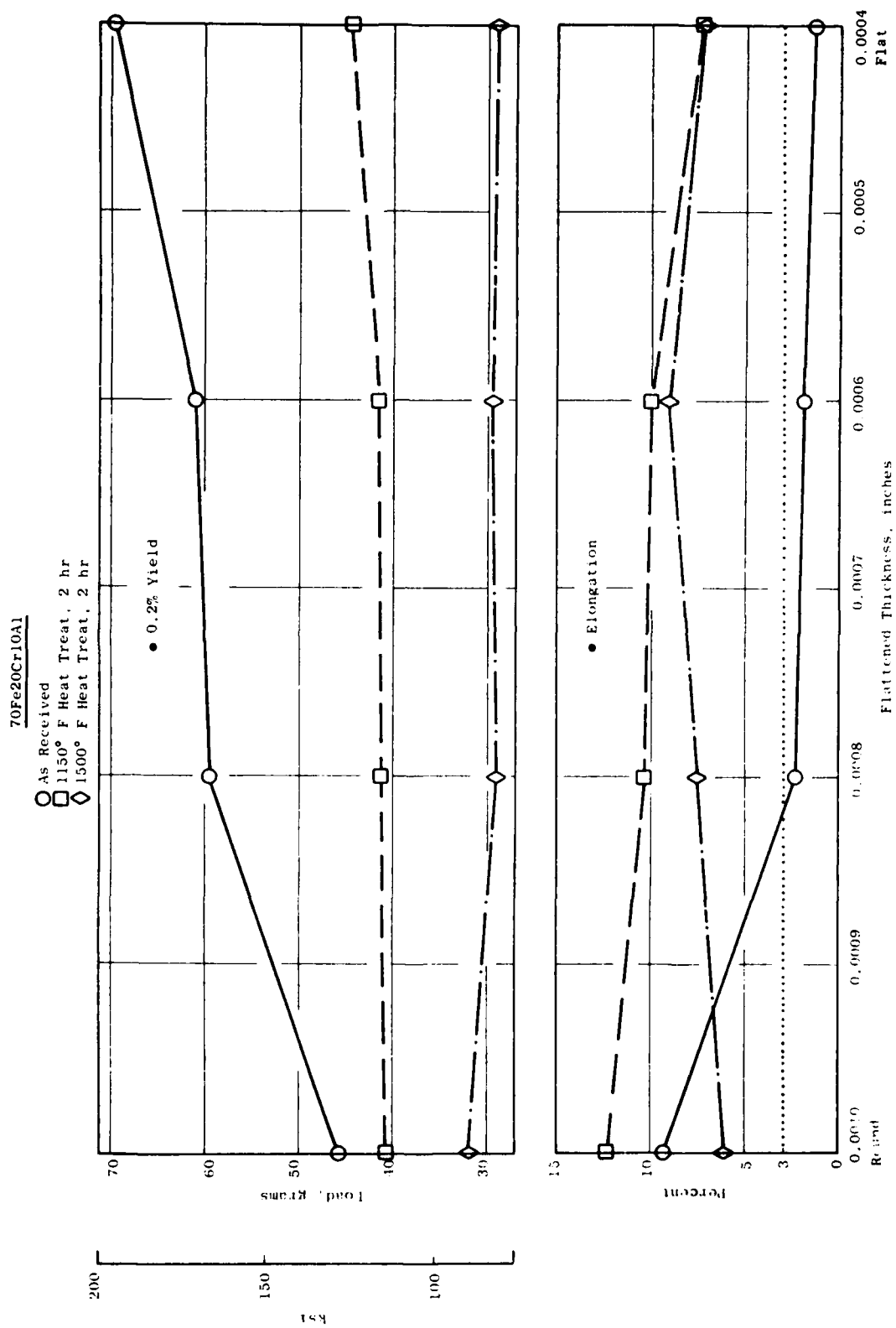


Figure 28. 0.2% Yield and Elongation Versus Conditioning - FeCrAl.

92F15W

○ AS Received
 □ 1050° F Heat Treat, 2 hr
 ◇ 1300° F Heat Treat, 2 hr

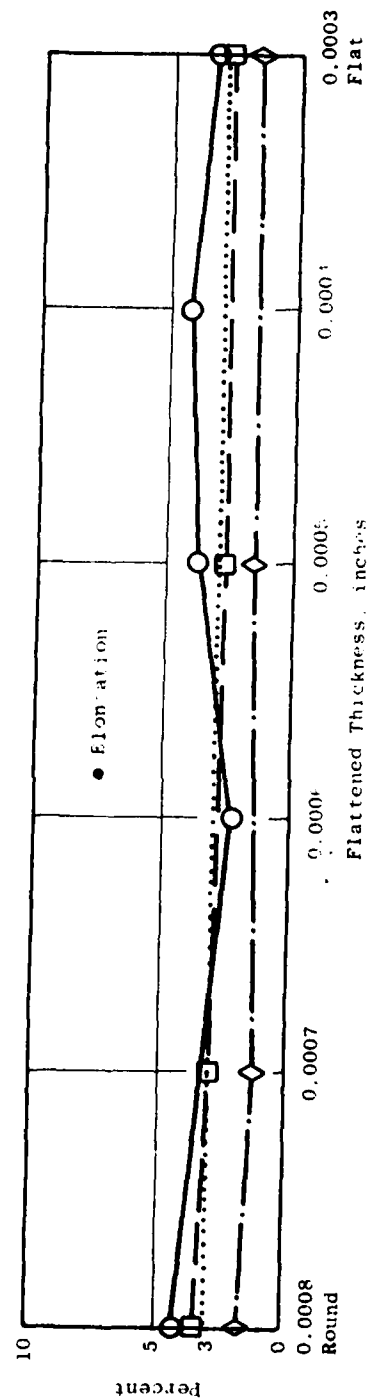
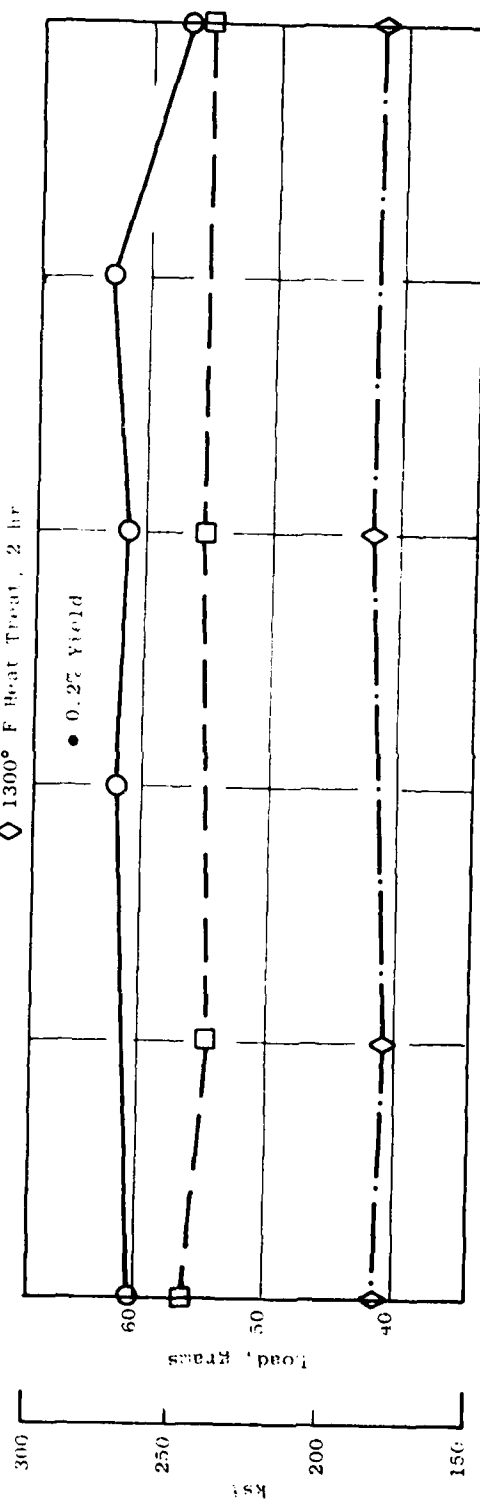


Figure 29. 0.2% Yield and Elongation Versus Conditioning - Pt8W.

The summary of 0.2% yield strength and elongation for different conditioning schedules shown in Figures 26 through 29 should be useful in ranking the alloys and processes with regard to HCF strengths. The degree of improvement in HCF offered by a particular process might be estimated using the ratio of the 0.2% yield strengths. An estimate of yield stress can be calculated assuming the original cross sectional area of the wire remains unchanged (there is a small reduction in area which occurs during flattening). For many high-yield-strength alloys, the endurance limit is generally greater than 0.5 times the tensile strength. With the conservative assumption that it is only 50% of the 0.2 yield strength, the estimated room temperature endurance limits for the various alloys, when flattened and heat treated to the recommended conditions, are:

<u>Material</u>	<u>Condition</u>	<u>Single Amplitude Endurance Limit, microinches/inch</u>
Karma	25% CW-1050° HT	3470
Moleculoy	37% CW-1300° HT	4160
FeCrAl	20% CW-None	2910
Pt8W	25% CW-None	5430

Obviously, without regard to other factors such as oxidation, thermal expansion, etc., platinum-tungsten is the best fatigue resistant alloy. But the data show a loss in room temperature fatigue strength of the Pt8W and FeCrAl that is probably related to oxidation. In the case of platinum-tungsten, the loss would be from the selective oxidation of tungsten. A test to confirm this was conducted on Pt8W that was heat treated at 1300° F for 2 hours in an argon atmosphere. The yield strength was not reduced as it was when heated in air. Reference 6 states, "Above about 800° F, the effect of oxidation of small diameter Pt-W wire is appreciable because of the selective oxidation of tungsten."

The comparison of room temperature fatigue strength of the candidate alloys after exposure to temperature indicated for only 2 hours is shown in the following tabulation:

<u>Material</u>	<u>Cold- work, %</u>	<u>No Heat Treat</u>	<u>Endurance Limit Single Amplitude After 2 Hours at Temperature In- dicated (° F)</u>				
			<u>850</u>	<u>1050</u>	<u>1150</u>	<u>1300</u>	<u>1500</u>
Karma	25	2670	2990	3470	---	3470	---
Moleculoy	37	3010	4090	4090	---	4160	---
FeCrAl	20	2910	---	---	2050	---	1430
Pt8W	25	5430	---	4820	---	3630	---

The estimates of endurance limits are for the wire alone when conditioned as noted. It does not include distress or stress risers that could occur during gage fabrication, lead attachment, and application processes.

Based on this testing, the conservative estimates of endurance limit determined from the data and without regard to other factors such as loads from other sources (e.g., thermal expansion, centrifugal strains, etc.), it is concluded:

1. Pt8W has the highest endurance limit; but to avoid selective oxidation of tungsten that would reduce strength, it should be used below 800° F.
2. Moleculoy is more fatigue resistant than the GE-Karma and appears the best single candidate alloy for meeting long life requirements over the required temperature range to 1500° F.
3. FeCrAl should be dropped as a candidate strain gage alloy.

Sensitivity Stability

The gage factor-at-temperature testing conducted in Task 2 provided no additional information about the performance of Karma and platinum 8% tungsten. Both alloys are commonly used at GE and their advantages and shortcomings were thought to be well known. FeCrAl was new, and it appeared to be the best single candidate because of its stability over the temperature range to 1500° F and its room temperature fatigue strength. However, the strength testing in this task indicates it is weaker in high cycle fatigue than the other candidates. For this reason, no additional sensitivity tests were conducted.

Platinum-tungsten suffers the selective oxidation of tungsten, Reference 6, above 800° F that causes changes in strain sensitivity as well as strength. It was believed that the stability of the alloy could be improved with suitable protective coatings that would retard if not prevent oxidation. Attempts to provide this protection with sputtered oxide coatings were unsuccessful and are discussed later. In any event, it seems advisable to limit the application of platinum 8% tungsten to 800° F to obtain maximum sensitivity stability pending the development of suitable coatings.

In a GE-funded program to establish the accuracy of Karma strain gages for compressor rotor use, it was found that gages heat-treated after being applied, using standard Rokide techniques, had very stable resistance and gage factors at temperature. Two different heat-treatment temperatures were investigated - one at 830° F because some of the early-stage blades in the rotor have dovetails containing an antifret material that cannot be exposed to temperatures above 860° F and the other at 1050° F. Heat treatment time for both temperatures to stabilize resistance was determined to be 2 hours. Figure 19 from Reference 26 shows the gage factor and resistance of gages when tested to 800° F and 1000° F for stabilization heat treats of 830° F and 1050° F, respectively.

Since Karma and Moleculoy are similar nickel-chromium alloys and Moleculoy has the higher estimated endurance limit, a high temperature sensitivity test was conducted with two gages made from Moleculoy mounted to a high-temperature gage factor beam using Denex 2 cement. The test was to determine (1) if the alloy when heat treated at 1050° F would have stable gage factor and resistance at temperatures below 1000° F, and (2) if heat treatment above 1500° F would produce stable gage characteristics between 1000° F and 1500° F. The tests were conducted at 640 microinches/inch double amplitude.

Figure 30 shows the gage factors and gage resistances at temperature for Moleculoy when subjected to the thermal cycles as shown in the figure. The data points are the average of the two gages. Moleculoy responds very similar to Karma when heat treated at 1050° F. The gage factors for the two cycles to 1000° F were repeatable for each gage to better than 1%. Moleculoy gage resistance exhibited a steady decrease with temperature while the Karma gage resistance change is essentially zero from room temperature to 1000° F.

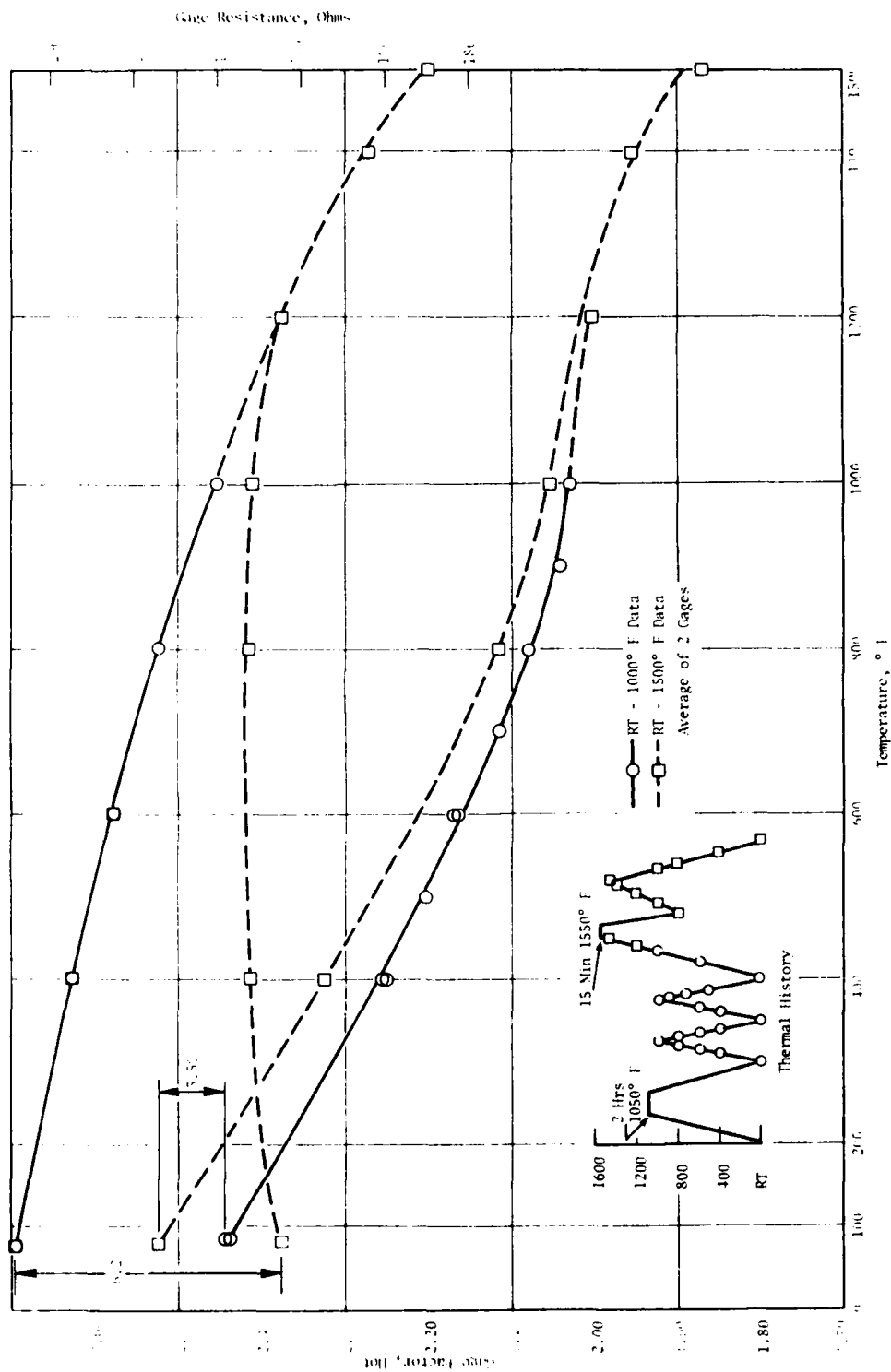


Figure 30. Gage Factor Versus Temperature - Molecule.

After exposure to 1550° F, the gage factor is greater than that of the 1050° F heat treated gage in the range from room temperature to 1000° F, and its repeatability on the two high temperature cycles was 1%. The resistance curve on cooling underwent a permanent change at room temperature of 6.2%. The resistances to 1500° F were also repeatable on the two successive cycles.

Below 1200° F, the gage factor and resistance of the 1050° F heat-treated gage are different from the gage exposed to 1550° F. At or near that temperature there exists a critical temperature where alloys high in nickel-chromium undergo a metallurgical phase change or order-disorder transformation. The order-disorder phenomenon of nickel-chromium alloys makes them unsuitable for steady-state strain measurements above 650° to 700° F. Easterling, Bertodo, Taylor, et al., in References 8, 12, 16, and 23, discuss the effects of this transformation and cooling rate on the resistances of nickel-chromium alloys. The resistance change characteristics of these alloys are generally similar to those shown in Figure 31 (Reference 12). The relationship between these resistance changes and dynamic gage factor or strain sensitivity is not discussed by the investigators. The data show it is an inverse one for Moleculoy.

It is concluded that Moleculoy can be stabilized by heat treatment at 1050° F for use below 1000° F. Gage factors above the critical temperature are repeatable. Long term drift should be less than either FeCrAl or Pt8%W because of its lower oxidation rate when applied with Denex 2 cement which is discussed in the following paragraphs.

Oxidation/Corrosion

Oxide Coated Gages - Investigations were conducted to protect gage alloys that showed good potential from a fatigue and sensitivity standpoint but were heavily oxidized at higher test temperatures. Previous work completed by GE Corporate Research and Development Center (CR&D) showed that Forsterite (2 MgO - SiO₂) was best suited for wire coating. This oxide coating provides excellent insulation resistance (over 10⁷ ohms at 1500° F for

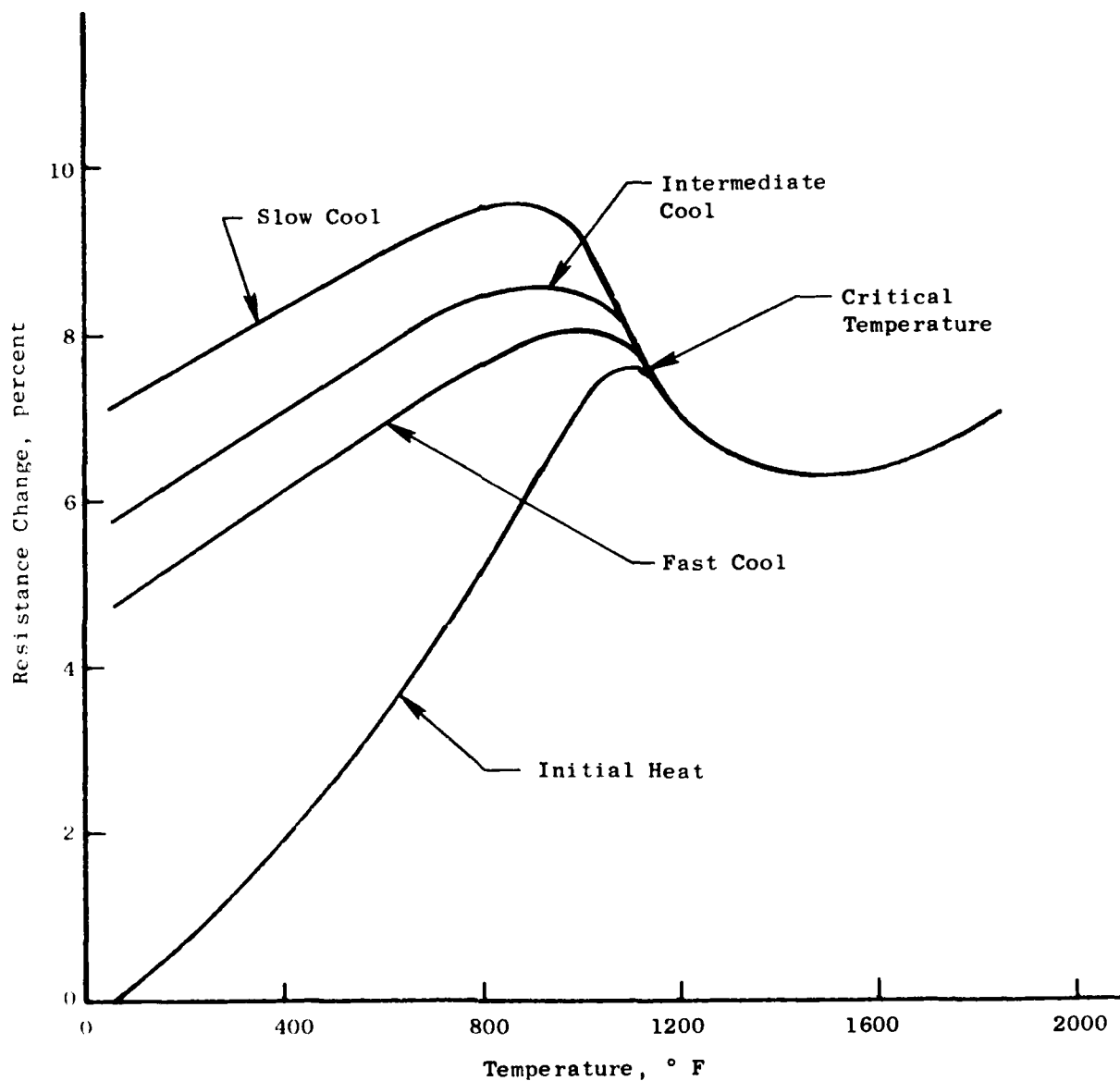


Figure 31. Typical Order-Disorder Phenomenon of Nickel-Chromium Alloys.

0.1-mil coating) and good bond strengths at the oxide-wire interface. However, in early 1976, it was shown that the material totally decomposed after a few hours in a weak solution of carbon dioxide in water at room temperature. It was reported by CR&D that this acid sensitivity is characteristic of a number of silicates that do not contain crystalline ring structures which promote chemical stability (such as is found in quartz). Most common ceramic cements used in strain gage work use aluminum phosphate as the bonding agent. Forsterite-coated gages cannot be applied with these cements, but this is required for coated gages applied by composite-ceramic techniques which is a major thrust of this program.

It was decided to investigate alternate coating materials applied by RF-sputtering. Aluminum oxide (Al_2O_3) had been investigated as a sputter coating for Karma strain gages in 1974 by Corporate Research and Development in our "Calrod" strain gage program. Although it gave good pinhole-free vitreous layers on the wires, the Al_2O_3 would ruin the preformed shape of the gage because of thermal expansion differences between the two materials (7.4 ppm/ $^{\circ}\text{F}$ for Karma and about 4 ppm/ $^{\circ}\text{F}$ for alumina). Materials having higher coefficients of thermal expansion (TCE) than Al_2O_3 were selected from available targets; the thermal expansion of chromium oxide (CrO) is 5×10^{-6} in./in./ $^{\circ}\text{F}$ and for magnesium oxide (MgO), it is 7.4×10^{-6} in./in./ $^{\circ}\text{F}$. The TCE for platinum-tungsten is 4.4×10^{-6} in./in./ $^{\circ}\text{F}$ and FeCrAl is 9.6×10^{-6} in./in./ $^{\circ}\text{F}$.

Five strain gages of each candidate alloy were resistance welded by the gage legs to the sides of a sputtering fixture so that the free grids extended above the top surface of the fixture. Two fixtures containing the 15 gages each were prepared, one for MgO , the other for CrO coating. The first fixture was installed in the sputtering chamber. A sputter-etch cycle was employed to clean the surfaces of the gages. Five microns (0.2 mil) of MgO were then RF sputtered onto the gages using standard process parameters for applying the material onto flat substrates. Upon removal from the chamber, all gages were heavily distorted and could not be used for sensitivity or fatigue testing. It was thought that the bias voltage used during the sputter-etch cycle was too great and the gages had been overheated. The second fixture was installed with the CrO target and the bias voltage during the sputter-etch cycle was reduced to about 20% of the original voltage used. But again,

the gages were found to be distorted after coating with 5 microns of the material either from overheating and/or insulating film stresses that were too great for the free gage grids. Coating fine wires with CrO and MgO is not within the current state of the art. No further investigations into alternate coating materials or process parameter adjustment were attempted.

While all the gages that were sputter coated with CrO and MgO were distorted, most of them were sufficiently flat that they could be covered with cements or flame-sprayed alumina to test the combinations for oxidation protection. This test might provide some direction for future coated strain gage development. The best gages were applied to 1/2 x 1 x 0.040 inch thick Hastelloy X test coupons. Three coated gages (Karma, FeCrAl, and Pt8W) were applied to each coupon and covered with coatings of candidate cements or flame-sprayed alumina applied with the Rokide gun or the Hitec minigun.

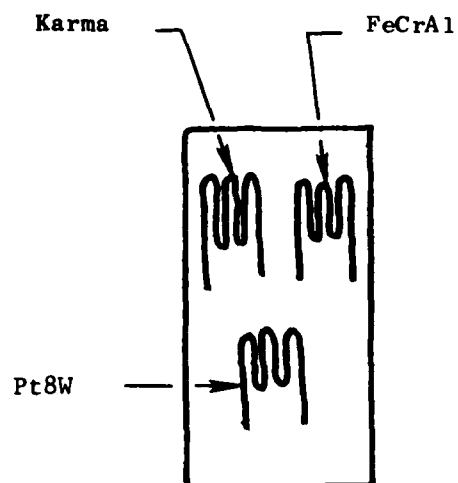
Sufficient gages were obtained to fabricate four coupons with MgO-coated gages using H, P₁ and Denex 2 cements. Chromium-oxide-coated gages were applied with GA100, PBX, and alumina flame sprayed with the 1/8-inch rod gun and the Hitec minigun. Figure 32 shows the combinations of coated gages and application materials possible with the limited number of acceptable gages.

After soaking the coupons 150 hours at 1500° F, they were mounted, sliced, and polished for examination by the Materials Engineer. Figures 33 through 38 are photomicrographs of the coated wires after exposure.

Materials Engineers Appraisal

Evaluation of Wires Having Been Coated Prior to Embedding in the Cements and Heated at 1500° F for 150 Hours

Wires embedded in H, P₂, and Denex 2 were coated with MgO prior to embedding them in their respective cements while wires embedded in other cements were coated with chrome oxide prior to the embedding. Moleculoy was not evaluated in this test. The results of this test are presented in Table 2, Page 63.



Test Coupon
1/2 x 1 x 040
Hastelloy X

Application: Base Coat and Top Coat of
Candidate Application
Materials.

Use Standard Cure Cycle Recommended by
Vendor.

Heat at 1500° F for 100 Hours.

Cement	Karma	FeCrAl	PT8W
H	MgO	MgO	MgO
P1	MgO	MgO	MgO
Denex 2	MgO	MgO	MgO
GA100	CrO	CrO	CrO
PBX	CrO	CrO	CrO
FSA-ROD	CrO	CrO	CrO
FSA-MG	CrO	CrO	CrO

Figure 32. Oxidation Test Coupons - Coated Alloys.

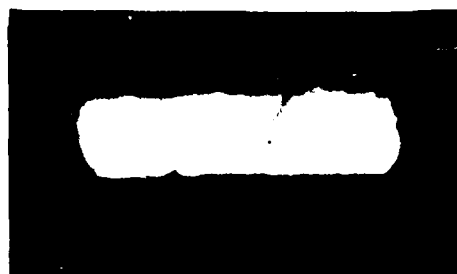
Oxidation of Fine Wires Covered and Coated with
Cement - PBX Coating - CrO

Karma



1000X

FeCrAl



1000X

479

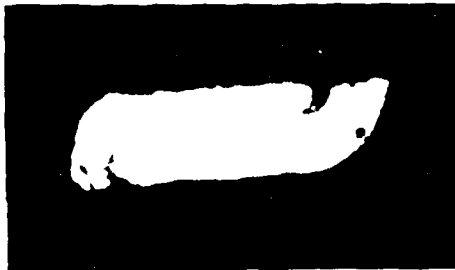


1000X

Figure 33. Coated Gage Oxidation.

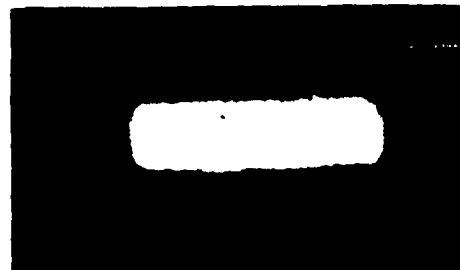
Oxidation of Fine Wires Covered and Coated with
Cement - GA100 Coating - CrO

FeCrAl



1000X

479



1000X

Oxidation of Fine Wires Covered and Coated with
Cement - P₁ Coating - MgO

Karma



1000X

FeCrAl



1000X

Figure 34. Coated Gage Oxidation.

Oxidation of Fine Wires Covered and Coated with
Cement - H Coating - MgO

Karma



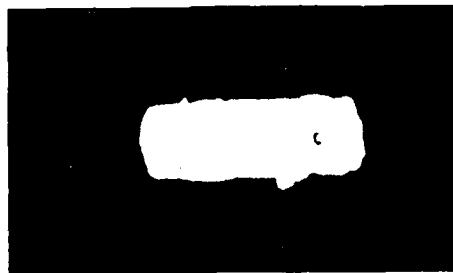
1000X

FeCrAl



1000X

479

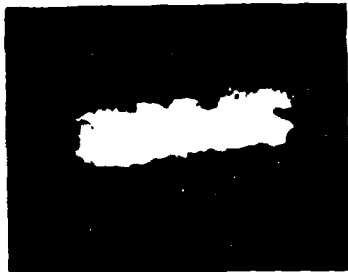


1000X

Figure 35. Coated Gage Oxidation.

Oxidation of Fine Wires Covered and Coated with
Cement - Denex 2 Coating - MgO

Karma



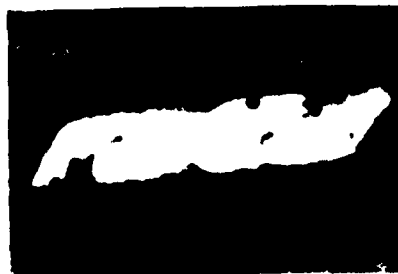
1000X

479



1000X

FeCrAl

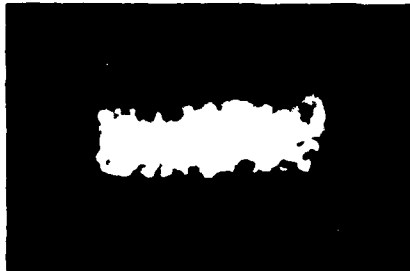


1000X

Figure 36. Coated Gage Oxidation.

Oxidation of Fine Wires Covered and Coated with
Cement - Al_2O_3 Hitec Coating - CrO

Karma



1000X

FeCrAl



1000X

479



1000X

Figure 37. Coated Gage Oxidation.

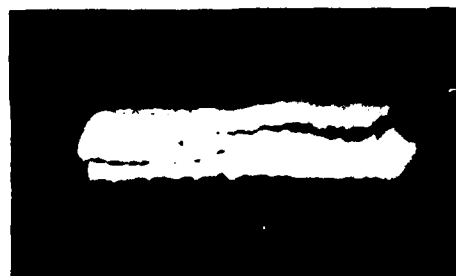
Oxidation of Fine Wires Covered and Coated with
Cement - Al_2O_3 Rokide 1/8 in.. Coating - CrO

Karma



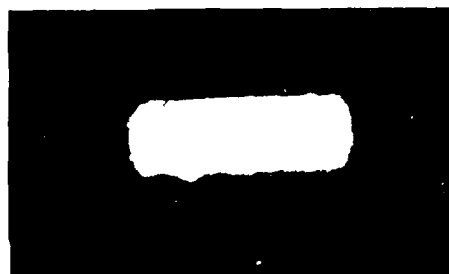
1000X

FeCrAl



1000X

479



1000X

Figure 38. Coated Gage Oxidation.

Table 2. Depth (% Radius) to Which Deterioration Proceeded After 150 Hour, 1500° F Exposure Having Been Coated Prior to Embedding in Cements.

<u>Cement</u>	<u>Karma Wire</u>	<u>FeCrAl Wire</u>	<u>Pt8W Wire</u>	
Denex 2	20	Cracked	0	
GA100	No	Cracked	25	
H	40	40	100	
PBX	5	Cracked	20	
P ₁	15	Cracked	No	Not Obtained
Al ₂ O ₃ (Mini)	25	Cracked	90	
Al ₂ O ₃ (Rod)	5	Cracked	25	

In general, coating the wires prior to embedding seemed to postpone deterioration until the coating was destroyed or penetrated. With but two exceptions after 150 hour exposure at 1500° F, deterioration was proceeding as if no coating were present.

Pt8W wire coated with MgO prior to embedding in Denex 2 showed no deterioration. Karma coated with chrome oxide prior to embedding in PBX also showed good results. FeCrAl again had a propensity to crack when coated prior to the embedding. These results suggest that with the proper coating deterioration resistance can be improved.

Uncoated Wires

The purpose of this test was to determine the oxidation and/or corrosion of the candidate wires when covered with candidate application materials and exposed to high temperatures for 150 hours. The objective was to identify those combinations of cements and wires that will exhibit the least deterioration of the wires. Two exposure temperatures were selected: 1500° F, the maximum use temperature for the gages, and 1200° F because it satisfies near-future compressors.

Each test coupon was prepared with 1-inch lengths of the four candidate wires and base coats and top coats of a candidate application material. Two coupons were prepared with the same application material - one for the 1200° F exposure and the other for 1500° F. After the coupons were exposed, they were mounted, polished, and photographed. Figures 39 and 40 are typical photomicrographs of the exposed wires.

Evaluation of Wires After Being Embedded in Cements

Wires were exposed either at 1200° F or at 1500° F for 150 hours. The results of the evaluation from these wires are presented in Tables 3 and 4.

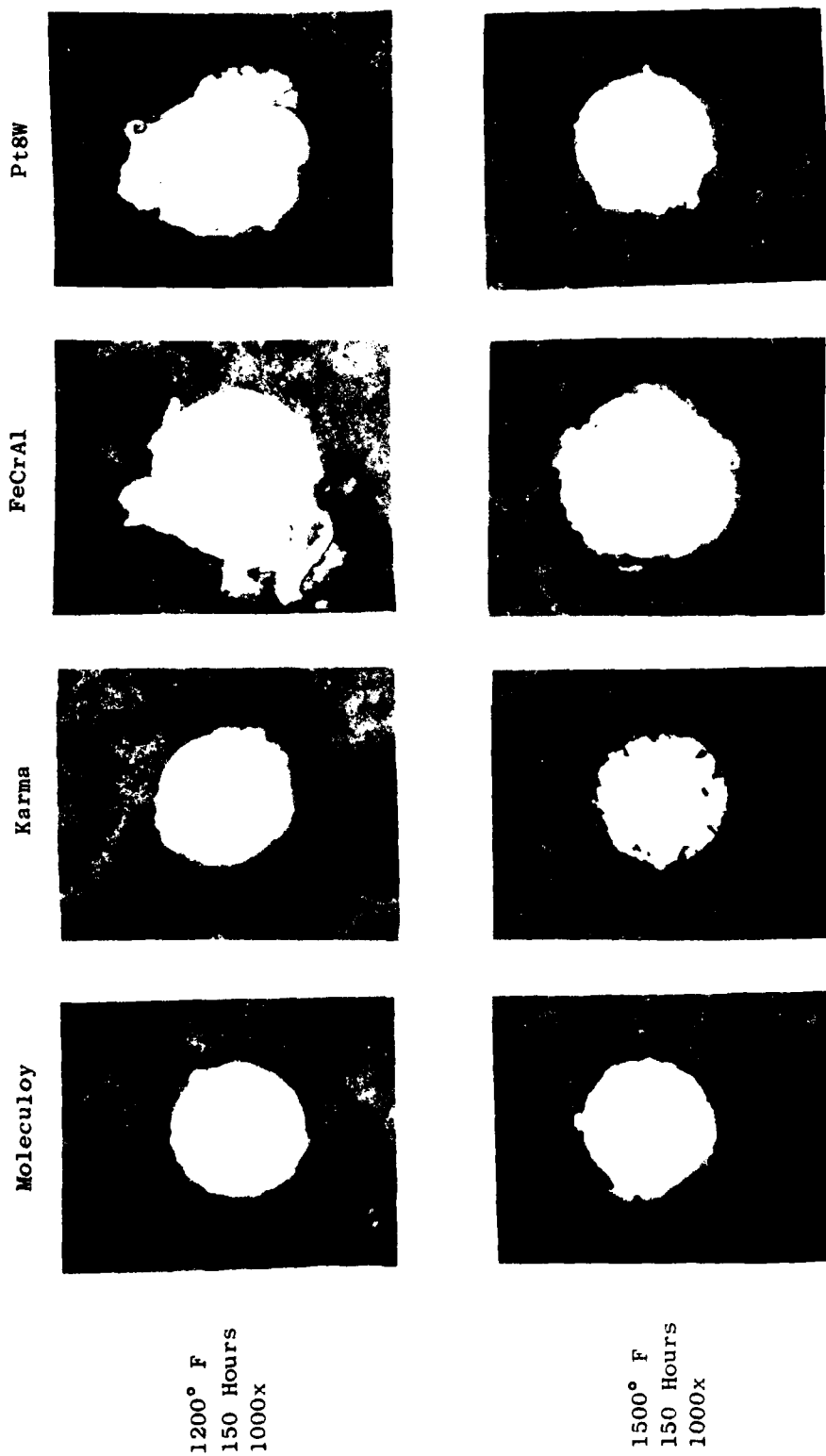
Table 3. Depth (% Radius) to Which Deterioration Proceeded After 150 Hour, 1200° F Exposure After Embedding in Cement With No Prior Coating.

<u>Cement</u>	<u>Moleculoy Wire</u>	<u>Karma Wire</u>	<u>FeCrAl Wire</u>	<u>Pt8W Wire</u>
Denex 2	0	0	<5	10
GA 100	<5	5	10	15
H	10	30	10	20
PBX	5	5	10	15
P ₁	5	10	0	25
Al ₂ O ₃ (Mini)	5	20	15	25
Al ₂ O ₃ (Rod)	15	75	10	90

Table 4. Depth (% Radius) to Which Deterioration Proceeded After 150 Hour, 1500° F Exposure After Embedding in Cement With No Prior Coating.

<u>Cement</u>	<u>Moleculoy Wire</u>	<u>Karma Wire</u>	<u>FeCrAl Wire</u>	<u>Pt8W Wire</u>
Denex 2	5	40	10	10
GA 100	5	5	10	25
H	10	15	15	20
PBX	0	40	90	30
P ₁	10	10	10	60
Al ₂ O ₃ (Mini)	40	100	10	25
Al ₂ O ₃ (Rod)	10	5	0	25

Cement - Denex 2



1200° F
150 Hours
1000x

1500° F
150 Hours
1000x

Figure 39. Oxidation of Fine Wires Covered with Denex 2 Cement.

Cement - Al_2O_3 Rokhide 1/8 in.

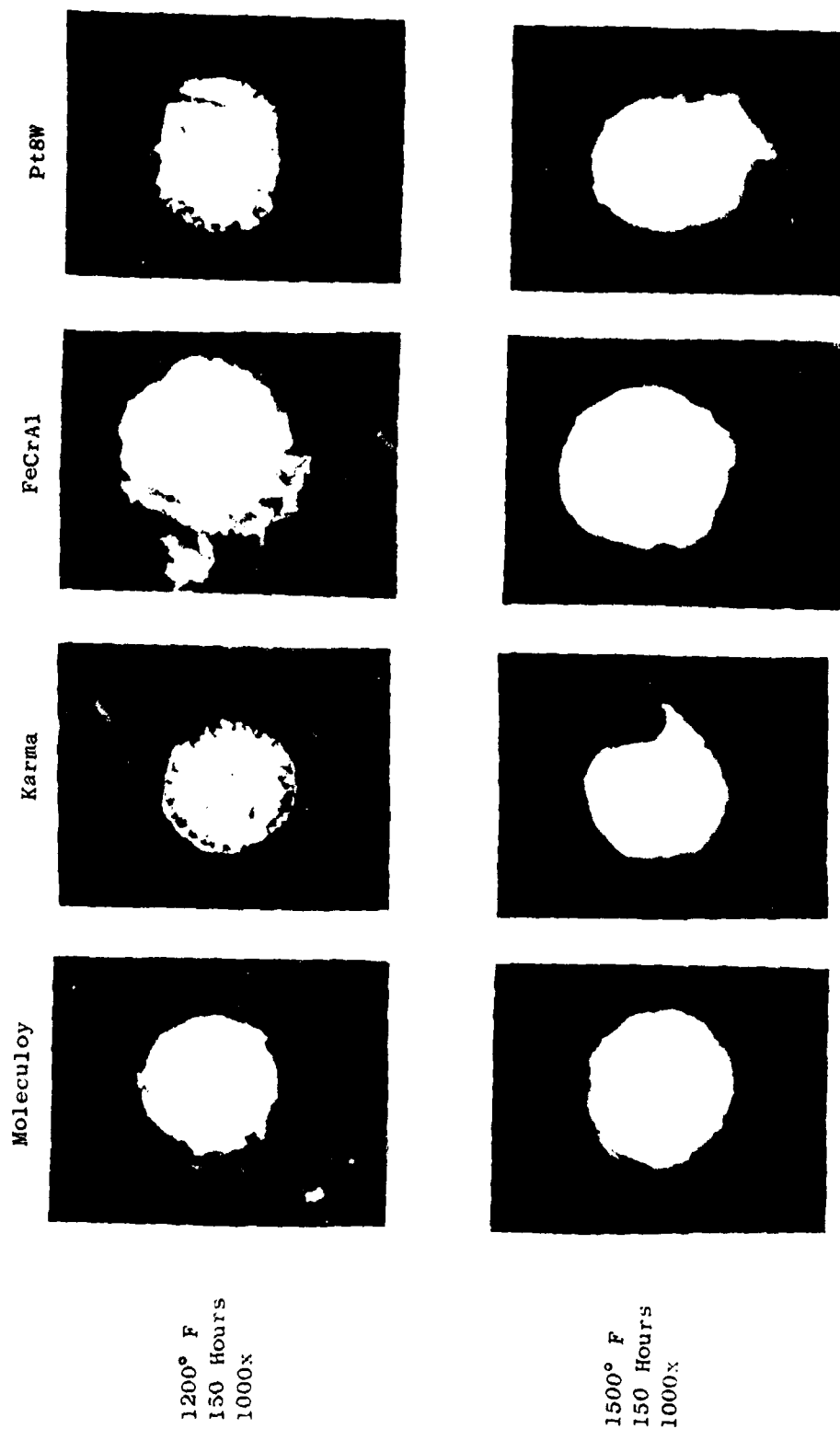


Figure 40. Oxidation of Fine Wires Covered with Al_2O_3 - 1/8 in. Rokide Gun - Cement.

Moleculoy exhibited a superior ability to retard deterioration over the entire range of cements.

Moleculoy in combination with Denex 2 cement was very impressive in reducing deterioration as was Moleculoy in combination with PBX cement. Embedding Pt8W wire in any cement failed to improve deterioration appreciably and worsened deterioration in some cases. The Karma and FeCrAl wires exhibited selective deterioration resistance depending on the cement in which they were respectively embedded. Embedding Karma in GA100 cement best reduced deterioration, while embedding it in P₁ was seen to also be beneficial. Embedding FeCrAl in Denex 2, P₁, and Al₂O₃ (Rod) produced good deterioration resistance. FeCrAl when embedded in the cements seemed to lose its propensity to form radial cracks.

Denex 2 was superior to all other cements in reducing deterioration. There was no other cement which limited deterioration in combination with all wires.

Summary of Oxidation Protection

It appears that of the materials selected for evaluation at this time the Moleculoy wire and Denex 2 cement are best qualified to reduce deterioration. Coating the wires prior to embedding did not appreciably improve results; however, results suggest more research in this area might be beneficial.

2.1.3.2 Strain Gage Lead Joining

The strain gage grid joining technique that is currently used in fabricating GE strain gages is shown in Figure 2. The technique is to capacitance discharge weld the grid wire between folded Karma ribbon 0.001-inch thick by 0.015-inch wide. The joint has always been suspected of being the major cause of gage loss because of the deformation of the wire at the weld from the combination of pressure applied to the electrode and the heat generated during discharge. The deformation is a stress concentration that seriously degrades the tensile and fatigue strengths of the wire. Moreover, since no fixturing is used in the process, the strength of the joints would be fairly random exhibiting a wide range of scatter. It was thought significant reliability improvements could be achieved by improving the lead joining technique.

Lead Joining Program

A lead joining development program was initiated in the Weld Development Laboratory to improve the strength of the joint between the gage grid wire and the lead wire of 0.003-inch diameter Chromel P. Several important goals and considerations to be established were:

1. Effects of the specific joining processes on candidate wires strength and fatigue resistance with a goal of 80% of the ultimate tensile load of the wire
2. Reliable operation to 1500° F
3. Heat treatment procedures
4. Existing manufacturing geometries with a goal to remove the intermediate attachment ribbon
5. Realistic gage handling capabilities.

Processes that were considered by the laboratory were (1) brazing, (2) low pressure diffusion bonding, (3) capacitor discharge resistance welding, and (4) ultrasonic welding.

The techniques were reviewed with the following resulting conclusions:

1. Brazing with special eutectic and activated alloys suitable for brazing nickel base materials was investigated. Brazing was considered because the fillets which result with this process are excellent for distributing stress and therefore increasing fatigue life. Very refined and detailed techniques would be required of this process. The grid wires, being small, have little mass to absorb the diffusion of the eutectic and activated alloys, and it is very probable that with continued exposure at high temperature the resulting grid wire strength, local to the joint, would be lower than the unbrazed grid wire. Moreover, ordinary silver- or gold-base braze alloys do not have sufficient strength at 1500° F and are unacceptable for this application.
2. Low pressure diffusion bonding was investigated. Previous work done in this area showed promising results. Attempts similar to the initial work met with little success. Further serious work was abandoned because of the high heat input and the resulting large heat affected zone.

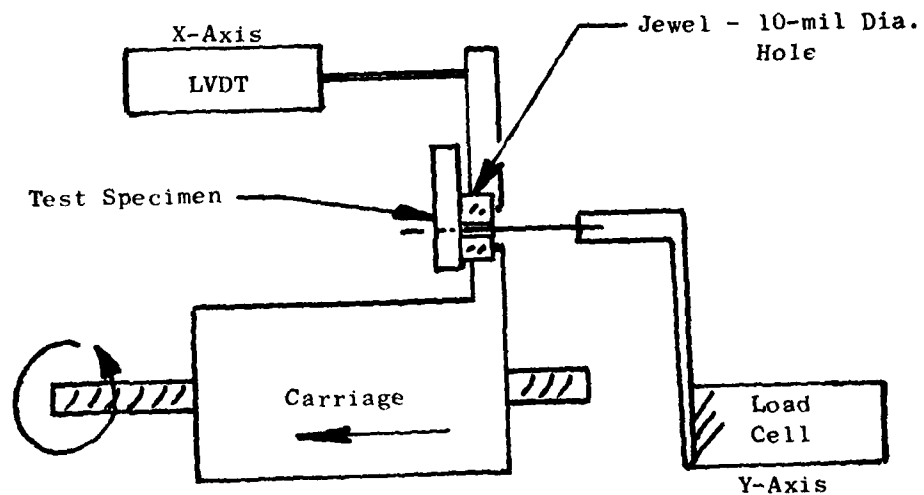
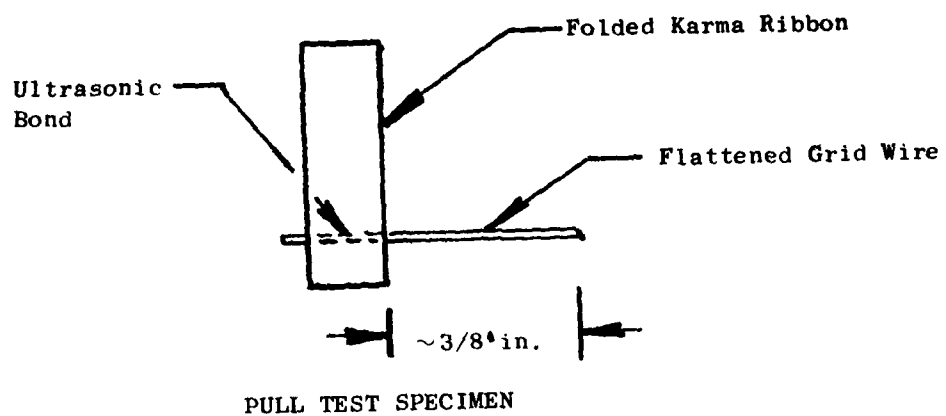
3. The existing method of capacitor discharge resistance welding was evaluated. Pull tests were made on several resistance-welded joints and failures occurred at or near the bond area with less force than the tensile strength of the wire. The pull specimens were fabricated using standard techniques by the Instrumentation Mechanic who now makes all Karma strain gages for application to engine components. All specimens failed in the joints (four tested) at 37.5, 33, 31, and 14 grams. Breaking load for Karma, as determined by load versus elongation tests discussed earlier, is 45 grams. Attempts to increase the strength of the wire at the joint by varying probe shape and welder power settings resulted in some improvement.
4. Ultrasonic welding, a solid-state process, seemed to be the most suitable course for continued development by the GE Weld Development Lab. Minimum changes in wire properties in the weld area are expected because of the low temperatures generally involved. A search of technical literature for information on the process indicates that it has been used to join metals such as nickel, nichromes, and ferrous-based alloys among others. References 27 and 28 provide discussion of metal joining using ultrasonic welding. These also indicate that ultrasonically-made bonds have higher endurance limits with some materials than resistance or fusion welding.

Ultrasonic Welding

An ultrasonic welding system, Sonobond Model W-1040, Figure 41, was available for evaluation and process development. Original work, because it was a goal to remove the short piece of ribbon used to join the grid to the 0.003-inch diameter Chromel P lead, included bonding flattened grid wire to round and flattened specimens of Chromel P. Handling problems were encountered, however, because of inadequate fixturing. The process development continued using 0.015 inch x 0.001 inch Karma ribbon, as in the existing gage fabrication process. The Fine Wire Test Facility shown in Figure 22 was used to determine the strengths of the specimen bonds. Figure 42 shows the specimen design and the method of installation in the facility. By varying the force of the ultrasonic welder transducer arm, the power setting and time setting, and the number of discharges of the welder, bonds of the flattened wires to the ribbon were obtained that approached 80% of ultimate tensile loads of flattened wire. Cleaning the wire and ribbon surfaces with an acid solution of $\text{HNO}_3 + 5\text{HF} + 70\text{H}_2\text{O}$, which was neutralized before the weld was made, resulted in joints that nearly always exceeded the 80% UTL goal. All failures occurred in the wire next to the bond. Heat-treated Karma and Moleculoy weld



Figure 41. Sonobond Welder.



FINE WIRE TEST MACHINE

Figure 42. Schematic of Weld Specimen Test.

specimens were also tested. Improvements in strengths were obtained, as expected, although Moleculoy specimen strengths did not increase proportionally to increases in wire strength as determined in the wire pull tests.

Table 5 (Page 73) shows the results of testing specimen bonds using the developed parameters of force, power, and time settings.

Even though the goal to eliminate the intermediate attachment ribbon has not been accomplished from a tensile strength viewpoint, the ultrasonic bonding technique provides more consistent, higher strength joints than the standard capacitance discharge welding procedures now used. The ultrasonic bonding technique will be used with ribbon intermediate leads on future gages for this program until procedures of flattening and joining the 3-mil, Chromel P lead are developed.

2.1.3.3 Application Materials

As mentioned early in this task, two candidate applications would be considered: (1) the Rokide or flame-spray alumina (FSA) technique, and (2) the composite-ceramic technique. For the composite-ceramic technique, Denex 2 appears superior to all other cements tested in preventing or retarding high-temperature oxidation and corrosion. Since it was new to GE, there was little known of its electrical resistance, shrinkage (that might cause loss of the top coat of flame-spray alumina), and adhesion. Its resistance to erosion was not considered important because the top coat of FSA would be selected to provide that capability for the structure.

In the literature, a BLH Technical Bulletin 4310-9 compared the electrical properties of seven ceramic cements. It states, "Brimor U-529 (which is Denex 2 cement) appears to afford the best combination of handling characteristics and high temperature insulating properties. This cement was significantly superior to all others tested..... Six cements maintained a resistance to ground of approximately 1 to 3 megohms at 1200° F and only Brimor U-529 retained a resistance value in excess of 1 megohm at 1400° F." The cements tested were P1 Dry Mix, PBX, H, Brimor U-527 and U-529, Transonics 64CP, and

Table 5. Breaking Loads of Ultrasonic Welds.

Material	Condition	Weld Setting			Break Load Range	Wire UTS	
		Power	Load	Time			Number of Discharges
Karma	Flat	1.6	1.0	4	2	(46) 43 - 51	45
	HT	1.6	1.0	4	2	(50) 50	50
Moleculoy	Flat	1.6	1.0	3	1	(43) 42 - 45	48
	HT	1.6	1.0	3	1	(47) 44 - 49	58
FeCrAl	Flat	2.0	1.25	4	1	(59) 55 - 62	65
Pt8W	Flat	1.7	1.0	5	1	(56) 51 - 58	68
Karma	Flat	Standard Capacitance Discharge Welds				(29) 14 - 37.5	45
Note: () Average Value							

NBSX-142A. Denex 2 when used in the composite-ceramic structure on top of a base coat of FSA, as shown in Figure 18, would provide more than adequate insulation properties at 1500° F, one of the goals of this program. Resistance tests were not considered necessary at this time.

The problem of shrinkage was also thought to be unimportant provided the cement is cured properly. The manufacturer's instructions state, "A final curing should be done for 1 hour at a temperature at 100° F above the operating temperature of the gage being mounted." Therefore, detailed shrinkage tests were not conducted.

Although it was believed that the surface provided by the FSA base coat in the composite-ceramic structure would provide excellent adhesion for the cement, a test of Denex 2, along with 9 other common ceramic cements, was conducted to assure it had adequate bond strength.

Quench Test - The bond strength of ceramics can be determined a number of different ways. A quick test is to subject applications of the cement to thermal shock to obtain bond strength relative to those of cements that, by experience, have proved adequate. The test was to water quench from 1400° F a coupon containing strain gages applied with the cement. The coupons were Inconel 718. Half the surface of the coupon was blasted with coarse 36 grit, the other half with either 120 or 220 grit to determine the effect of surface finish on adhesion. A strain gage was applied to each roughened surface using recommended application and cure techniques for the cement under investigation.

Of the 10 cements subjected to this test, 6 had no losses as shown in Table 6 (Page 77). Figures 43 and 44 are photographs of the quenched samples.

The surface finish of flame-spray alumina when applied as a base coat is about the same as a surface treated with 60 to 80 grit. Without regard to the belief that the solvent system used in ceramic cements etches the surface of alumina base coat creating much better adhesion than on steel, it is concluded that the adhesion of Denex 2 is as good as H cement which has been used in previous composite applications without adhesion problems. It therefore is acceptable for the candidate strain gage system.

Water Quench from 1400° F
Ceramic Cements on Inconel 718

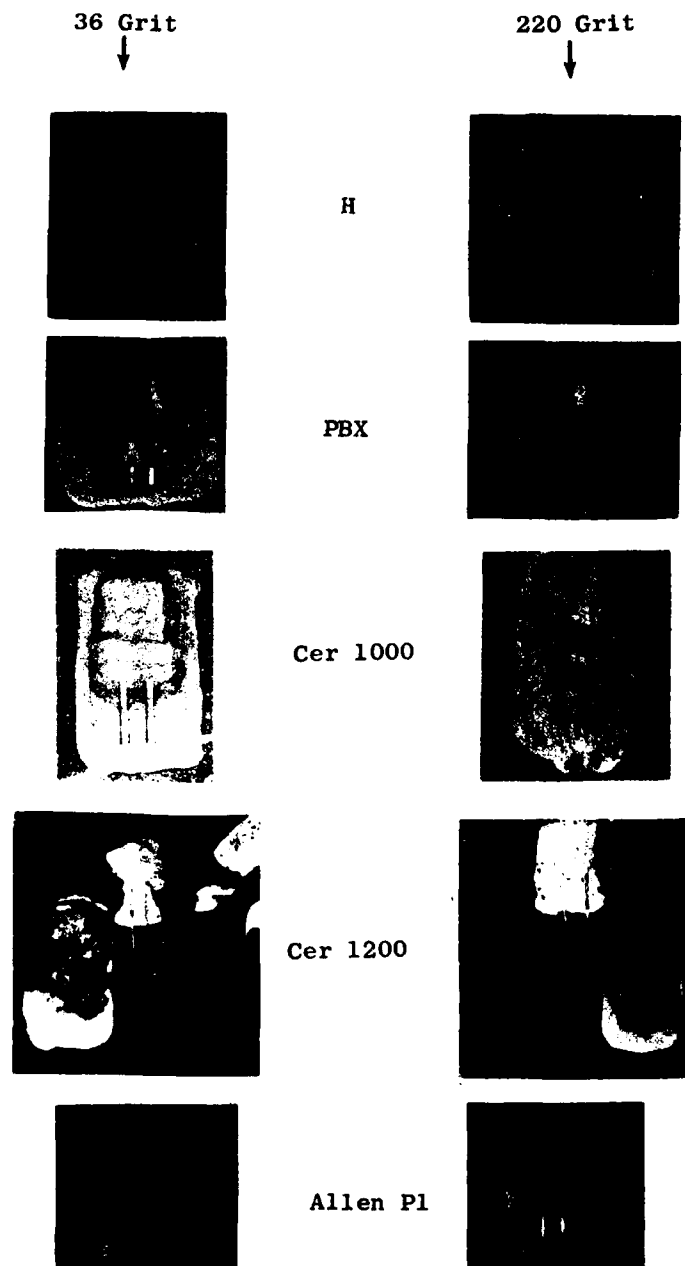


Figure 43. Adhesion Shock Test.

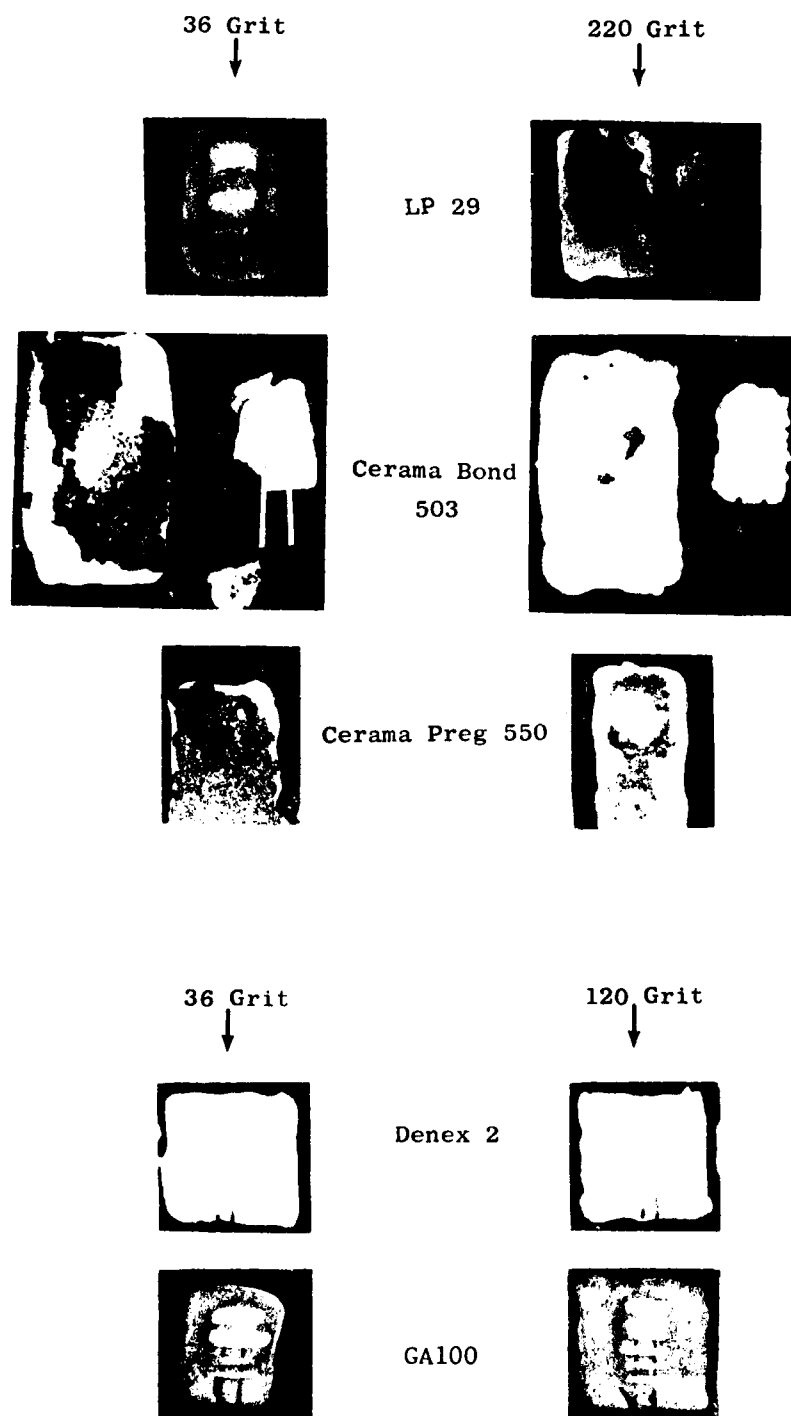


Figure 44. Adhesion Shock Test.

Table 6. Quench Test.

O-Passed	X-Debond		
	Surface		
Cement	36 grit	120 grit	220 grit
H	0	---	0
PBX	0	---	0
Cer. 1000 (PBX)	0	---	0
Cer. 1200	X	---	X
P ₁	0	---	0
LP29	0	---	X
Cerama Bond 503	X	---	X
Cerama Preg 550	X	---	X
GA100	0	0	---
Denex 2	0	0	---

Erosion Tests - In the composite-ceramic or straight flame-spray strain gage applications, only the outer coat of aluminum oxide is subjected to erosion from the airstream. Therefore, only alumina applied by the three different application systems were tested for erosion resistance. The three systems are:

1. 1/4 in. Al₂O₃ rod gun
2. 1/8 in. Al₂O₃ rod gun
3. Hitec miniature powder gun.

The first two are generally used throughout industry for the applications of high temperature strain gages. The processes are noisy and the spray guns generally unwieldy. The Hitec minigun has the advantages of light weight, adjustable powder feed, and very low noise output.

Three flame-spray alumina (FSA) coupons of steel were prepared with a strip of Al₂O₃ 1/2 inch wide and 6 inches long by 0.015 inch thick. Half of each FSA strip was scrubbed with H ceramic cement, because it was observed that the process seemed to improve the erosion resistance of the Al₂O₃ spray

coat. After curing the cement, the specimens were alternately placed in the erosion fixture, Figure 45, and blasted with SS White No. 3 grit at 80 psi. The time was measured to erode away the alumina and expose about the same size area of steel coupon underneath on the three specimens. Time is the figure-of-merit for relating erosion resistance of the coatings if all exposed areas are the same.

As seen in Figure 46, the area of alumina removed is nearly the same for applications with the 1/8-inch rod gun and the low-noise Hitec minigun. The time measured to expose each area was 50 seconds. For the 1/4-inch rod gun, the area is slightly smaller but the time was 200 seconds. Therefore, it is concluded that Al_2O_3 applied with the 1/4-inch rod gun is greater than four times as erosion resistant as the other two techniques.

The H cement improved the erosion resistance of sprayed coatings provided by the 1/8-inch gun and minigun. The eroded area of these treated specimens is 25% to 30% smaller than the untreated surfaces for a 50-second exposure, indicating a slight improvement in resistance to erosion. A slight reduction in area was noted between the treated and untreated applications for the 1/4-inch gun.

The compositions of these alumina rods and powder mixtures were obtained from vendor literature. They are:

1/8-inch rod: BLH-S; $98.5 \text{ Al}_2\text{O}_3 + 0.5 \text{ SiO}_2 + \text{Ti} + \text{Na}$

1/4-inch rod: BLH-H; $97.5 \text{ Al}_2\text{O}_3 + 2.5 \text{ SiO}_2$

Powder: $99.52 \text{ Al}_2\text{O}_3 + 0.33 \text{ NaO}_2 + 0.10 \text{ FeO}_2 + 0.04 \text{ SiO}_2$

The superior erosion properties of the 1/4-inch rod are apparently from the high percentage of quartz (silica) that might cause the formation of an alumina-filled silica glass. The resistance to erosion is one of the properties desired in the candidate gage systems; therefore, top coat applications will be made using the 1/4-inch rod gun.

2.1.4 Task 4 - The Two Candidate Systems

Combining the results of Phase I, the candidate systems can now be selected. Table 7 (Page 81) is a summary of the proposed candidate systems.

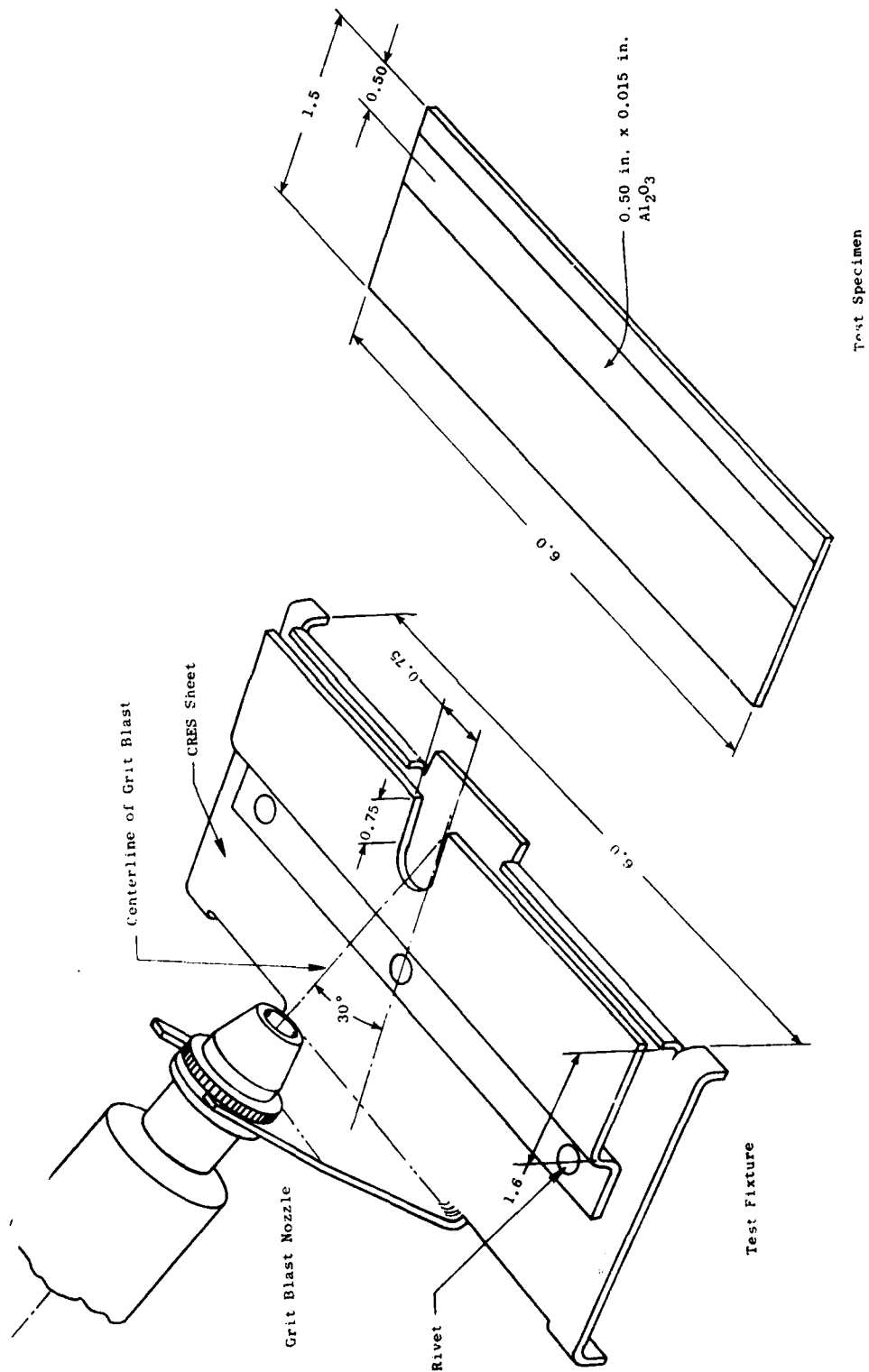


Figure 45. Erosion Test Facility.

• Typical Samples Grit Blasted with SS White No. 3 Powder at 80 psi

BLH-H High Purity
Alumina Applied with
1/4 in. Gun



200 sec



200 sec H Cement
Treatment

BLH-S Alumina Applied
with 1/8 in. Gun



50 sec



50 sec H Cement
Treatment

High Purity Alumina
Applied with Hitec
Powder Gun



50 sec



50 sec H Cement
Treatment

Figure 46. Erosion of Flame-Sprayed Al_2O_3 .

Table 7. Two Candidate Gage Systems.

<u>Gage System Element</u>	<u>Candidate 1 Composite-Ceramic</u>	<u>Candidate 2 All-FSA</u>
• Surface Prep	Norton Dynablast 120 grit	Norton Dynablast 120 grit
• Adhesion Layer	Plasma-Sprayed Metco 450 to 1300° F and Metco 443 to 1500° F	Plasma-Sprayed Metco 450 to 1300° F and Metco 443 to 1500° F
• Insulating Layer Base Coat	Al ₂ O ₃ - 1/4-inch rod gun	Al ₂ O ₃ - 1/4-inch rod gun
• Gage	Molecularoy, 0.8 mil dia.; Flat to 0.6 mil, heat treat 1050° F, 2 hours	Molecularoy, 0.8 mil dia.; Flat to 0.6 mil, heat treat 1050° F, 2 hours
• Lead Attachment	Grid-to-Ribbon; Ultrasonic Weld Ribbon-to-3 mil convoluted lead; Capacitance discharge weld	Grid-to-Ribbon, Ultrasonic Weld Ribbon-to-3 mil convoluted lead; Capacitance discharge weld
• Gage Attachment	Denex 2	Al ₂ O ₃ 1/4-inch rod gun
• Top Coat	Al ₂ O ₃ 1/4-inch rod gun	Al ₂ O ₃ 1/4-inch rod gun

Application Selection

It has already been shown that a Karma gage applied with composite-ceramic techniques has a higher fatigue strength at room temperature than the same gage applied with an all flame-spray structure (2400 microinches/inch versus 1900 microinches/inch). Both tests were conducted with unheat-treated gages. The composite-ceramic technique is, therefore, selected as a candidate. The all-FSA or Rokide technique is selected as the second candidate.

Gage Material Selection

When considering all properties of the candidate strain gage alloys - fatigue, sensitivity stability, oxidation, and/or corrosion - combined with materials of application, Moleculoy appears to be the only alloy that is suitable for the whole temperature range to 1500° F. One might be tempted to select Pt8W for use to 800° F because of its high fatigue strength and sensitivity stability, and Moleculoy to cover the rest of the temperature range to 1500° F. However, Pt8W has a very low thermal coefficient of expansion and, when applied to a blade of high thermal expansion, would be subject to large static strains that reduce the fatigue strength of the gage. In the absence of fatigue limit (stress range) data for the two candidate alloys, an estimate of the effect of mean strain on endurance limits can be obtained from Goodman diagrams.

In Figure 47, Goodman diagrams have been constructed for the two alloys using 0.2% yield strain obtained from the pull tests and the estimated endurance limits of the gage after two hour exposure at about 800° F. Plotted on diagrams is the sum of the strain on the gage caused by thermal expansion difference limits of the gage after 2-hour exposure at about 800° F. Plotted on diagrams is the sum of the strain on the gage caused by thermal expansion differences, with the gage applied to typical engine blade materials at 800° F, and the mechanical strain of 1000 microinches/inch, which is a program requirement. Based on these comparisons, Pt8W does not afford an improvement over Moleculoy at a blade temperature of 800° F. The temperature at which the estimated endurance limits of the alloys would be equal on a blade of A 286 is 630° F. Below that, Pt8W has the higher estimated endurance.

AD-A101 713

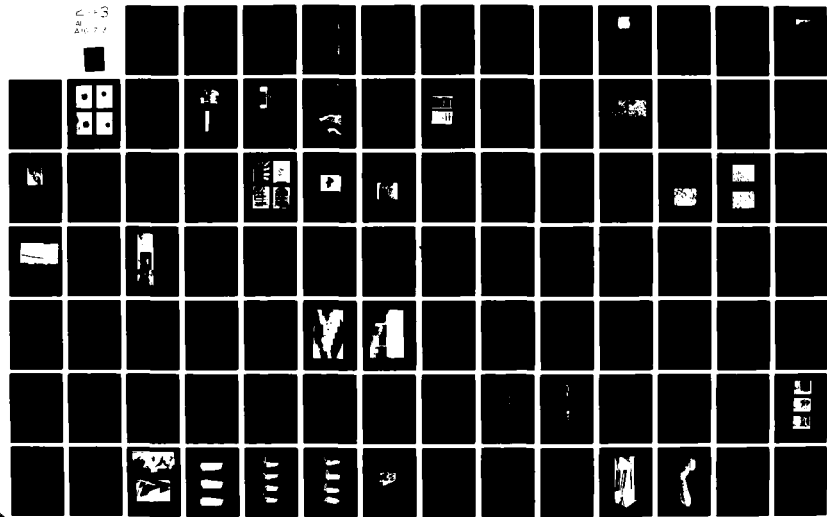
GENERAL ELECTRIC CO CINCINNATI OH AIRCRAFT ENGINE BU--ETC F/G 14/2
HIGH TEMPERATURE STRAIN GAGE SYSTEM FOR APPLICATION TO TURBINE --ETC(U)
JAN 81 R A WEISE, J H FOSTER F33615-76-C-2075
R80AEG388

UNCLASSIFIED

AFWAL-TR-80-2126

NL

6-1-3
R
AUG 7 1



Thermal Coefficients
of Expansion

Blade Mtl.	TCE $\times 10^{-6} \mu\epsilon/^{\circ} F$
Ti	5.2
Inco 718	7.8
A 286	9.6
Gage Matl.	TCE $\times 10^{-6} \mu\epsilon/^{\circ} F$
PT8W	4.4
Moleculoy (Karma)	7.4

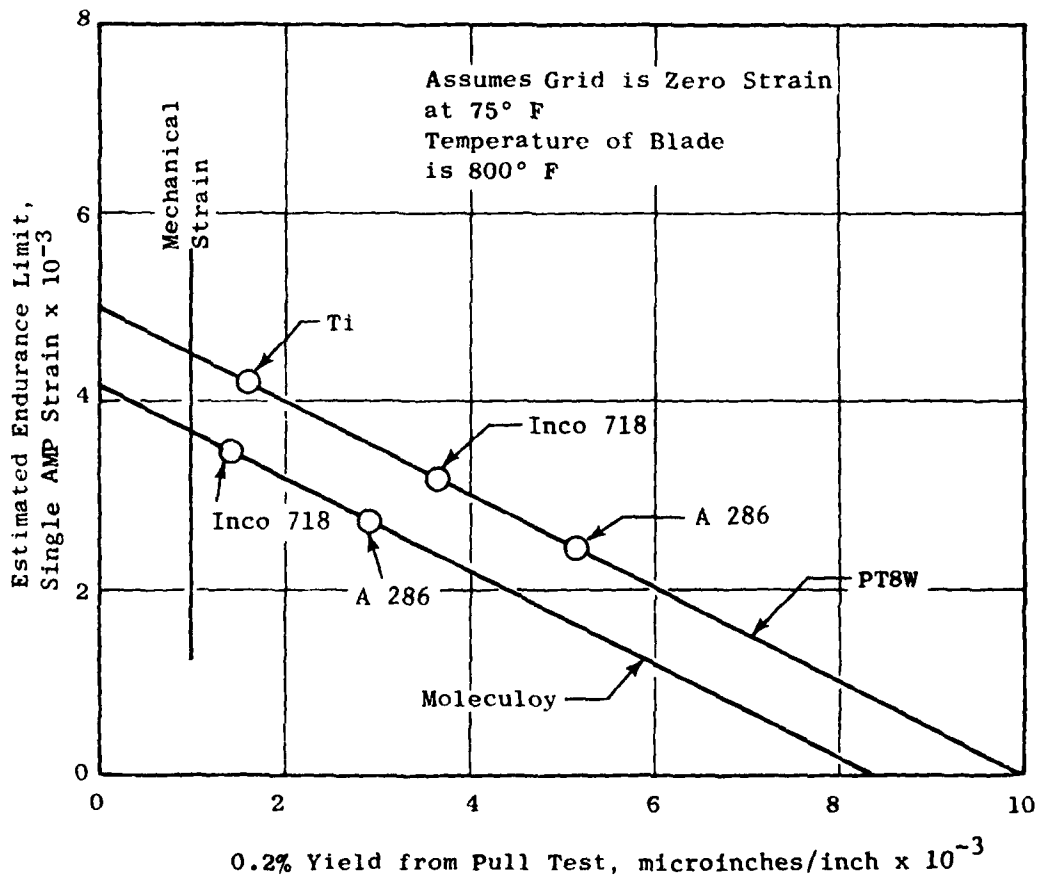


Figure 47. Goodman Diagram Showing Relative Endurance Limits of Moleculoy and Pt8W on Common Blade Alloys from Thermal Expansion Differences.

Moleculoy is selected as the single candidate alloy that will cover the complete temperature range requirements of this program.

Ceramic Cement

Based on the results presented under Oxidation/Corrosion and the results of Task 3, Denex 2 (fine-ground Brimor U-529) is selected for the composite-ceramic system.

Flame-Spray Application

A four-to-one erosion resistance is afforded by flame spray applied by the 1/4-inch rod gun over 1/8-inch rod and the Hitec minigun. The 1/4-inch rod gun will be used throughout the remainder of this program.

Lead Joining

The ultrasonic welder used in the development of the technique will be used with the short Karma ribbon, as defined in the present gage, until the development of direct attachment of the grid to 3-mil, Chromel P leads.

Blade Surface Preparation

The blade surface in the area that will be equipped with the strain gage and leads will be grit-blasted to remove all scale and surface contamination. The grit-blast material is 120-grit, 90% pure virgin aluminum oxide, called Dynablast, from Norton Co.

An adhesion coat 2 to 3 mils thick of Metco 443 will be applied by plasma spray. Metco 443 has superior oxidation resistance to Metco 450 presently being used.

Primary Lead Wire

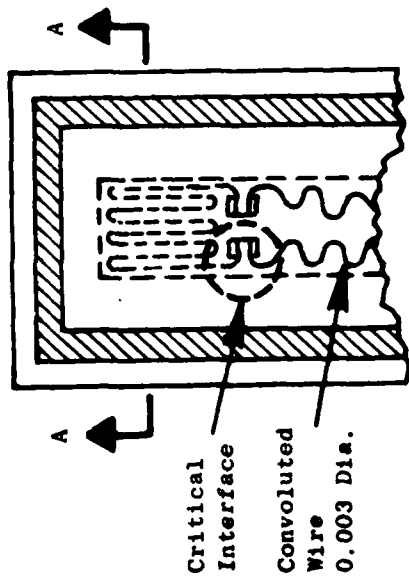
The wire that has been adopted as standard at GE is 30-gage chromel-alumel wire in a duplex insulation of carded asbestos with a tightly woven glass cover overall. The wire is normally spliced to the strain gage leads of 3-mil Chromel P under the blade platform.

2.1.5 Candidate Systems - Application Process

The process steps that will be used for the application of the candidate main gage systems in Phase II are those currently considered "standard" at Evendale. Modifications of these processes may be introduced to improve application performance.

Whether the gage application is to be composite-ceramic or all-flame spray, the process is the same up to and including the applicaiton of the flame-sprayed Al_2O_3 base coat. The process steps applying the gage involve either the use of ceramic-cement or strips of Scotch 64 tape. Obviously, the final top coat spray is the same for both systems.

The gage applications that should result from careful application procedures are shown in Figure 48. The salient difference between the two structures is that the ceramic cement replaces the flame-spray tie-down coat of the FSA application in the composite-ceramic application.



Typical Structure

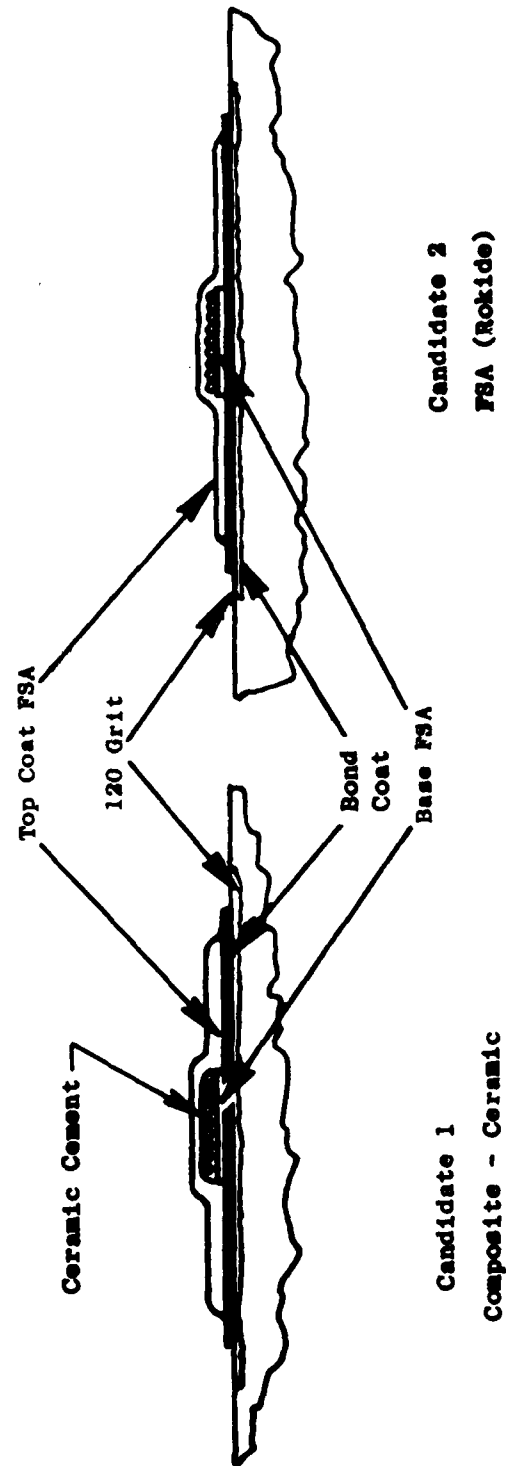


Figure 48. Application Designs.

2.2 PHASE II - LABORATORY TESTS OF TWO CANDIDATE STRAIN GAGE SYSTEMS

The purposes of this phase of the program were to develop/improve the techniques and materials of applications and to establish the electrical and mechanical performance of the two candidate gage systems. The performance characteristics that were determined during this phase were:

- Task 1 - Fatigue Strength
- Task 2 - Sensitivity
- Task 3 - Effect of Applications on Small Blades
- Task 4 - Effect of High Rotational Speeds on Application Integrity.

2.2.1 Task 1 - Fatigue Strength Testing

The objectives of this testing were to (1) identify system faults and correct them by design or technique modifications during the room temperature tests phase, and (2) establish the fatigue strength of each system at room temperature, 850° F, 1200° F and 1500° F. The technical objective was to achieve a room temperature fatigue strength greater than ± 2000 microinches/inch at 10^7 cycles with a tensile mean strain of 1000 microinches/inch.

2.2.1.1 Test Equipment and Test Description

Most fatigue testing was conducted in the High Temperature Strain Gage Evaluation Facility described in Section 5.0 and shown in Figure 121. The fatigue test beam design, Figure 127, was used for room temperature (Ti6-4) and 850° F (Inconel 718) tests. The sensitivity beam design, Figure 122, was used for high temperature testing - Inconel 718 at 1200° F and Udimet 700 at 1500° F. The fatigue tests were conducted at mean strain levels of zero (A-ratio = 0) and at one-half the single-amplitude alternating strain (A-ratio = 0.5). (A-ratio is the ratio of the single-amplitude alternating strain to the mean strain.) In early testing, 10 million cycles (10^7) were used to define

gage fatigue strength. This was later changed to 10^6 cycles because of the extremely long time required to accumulate 10^7 cycles on the 30-Hz Krouse fatigue test machines.

Test Matrix

The test matrix that was used in the fatigue testing is shown in Table 8:

Table 8. Fatigue Test Matrix.

Temperature, ° F	Beam Type	Candidate Design*	A-Ratio = ∞		A-Ratio = 2	
			Number		Number	
			Beams	Gages	Beams	Gages
RT	Figure 127	1	1	3	1	3
	Ti-6Al-4V	2		3	1	3
850	Figure 127	1	1	2	1	2
	Inco 718	2		2	1	2
1200	Figure 122	1	1	2	1	2
	Inco 718	2		2	1	2
1500	Figure 122	1	1	2	1	2
	U700	2		2	1	2

*Candidate 1 is the Composite-Ceramic Application
Candidate 2 is the all-FSA (Rokide) Application

Test Sequence

In all fatigue testing, it was assumed that no damage to the gage structure results from testing at vibratory strain levels lower than the fatigue strength of the gage system. Therefore, the test sequence used was to accumulate 10^7 (later 10^6) cycles at a low strain level, increase the strain level by 400 to 600 microinches/inch peak-to-peak (for A-ratio = 2 testing,

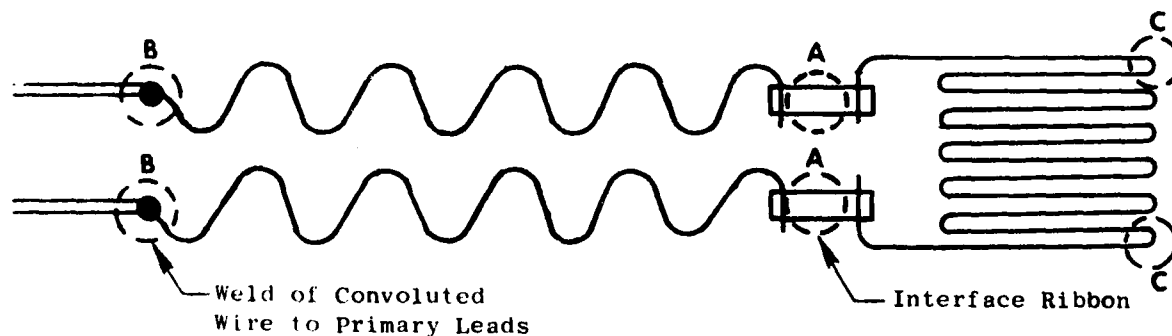
mean strain was increased 1/2 the increase in vibratory strain), and again accumulate 10^7 cycles. This sequence was continued until all gages failed. Obviously, since damage is incurred at strain levels lower than, but very near the fatigue strength, the fatigue strength defined in these tests is a conservative one. All failure modes were recorded with a view toward improving the candidate system fatigue strength by either design or technique/material changes.

Data Handling Considerations

The application of strain gages by either composite-ceramic or all flame-spray ceramic techniques results in a very complex structure that has many potential failure sources. It was, therefore, expected that cycles-to-failure and strain level at failure could be very random among the gages tested. Because of this and because of the small number of gages that would be used at each test condition, a statistical approach of determining average fatigue strength and standard deviation would not provide a meaningful measure of the fatigue strength capability of properly applied gage systems. All fatigue diagrams were obtained using the gage that survived the highest strain level and therefore represents the highest strength of the gages tested.

Postmortem Techniques

Failure locations were identified by nondestructive and destructive post-mortem techniques. Nondestructive postmortems were conducted to locate the failure that caused the signal conditioning circuit to automatically turn off the Krouse fatigue test machine. In this technique, the application material is removed carefully from Locations A and B in the following sketch:



Resistance measurements are made between points A-A, B-B and A-B. If it is determined that the open circuit is in the strain gage element, the end loops C are exposed by abrading the top coat away with a stick of alumina. Resistance is metered from A to C. If it indicates open, the failure(s) is in the outer filament or the weld. If the open exists between C and C, no attempt to locate it is made at this time. Similarly, if it is in a lead, the postmortem is discontinued and the Krouse machine restarted. This process is continued until all gage systems fail. During this first inspection, the gage system is disrupted as little as possible.

All circuits are then thoroughly postmortemed. Failures generally are located by abrading the top coat with the alumina rod. If the abrading does not cause further damage to the wire, a photograph is taken through the microscope. These photographs are compared with photographs taken during the application cycle in an attempt to determine the need for process changes.

2.2.1.2 Test Results and Discussion

Gage Systems Improvements

As mentioned before, initial fatigue testing at room temperature was used to improve the techniques and materials of the selected gage structures. Most of the effort was directed toward the composite-ceramic structure, because it was new to GE and had not been used for strain gage applications on engines.

Twenty-five Moleculoy strain gages were fabricated and flattened to 0.6 mil using the modified gage flattening fixture. Inspection of the gages under the microscope (at 70X) did not reveal any major defects introduced by the flattening between the jo-blocks. Measured gage thickness ranged between 0.55 mil and 0.65 mil. The gage shape was not uniform, tending to spread at the lead attachment end (Figure 49). This indicates that there was insufficient flattening and coldwork to set the form. Additional gage flattening would be required to improve the gage shape, but these gages would be used during the improvement phase.



Figure 49. 1/8-Inch Long
Moleculoy Gage,
Flattened to 0.6
Mil from 0.8 Mil
Diameter Wire
(Typical).

Table 9 (Page 92), Early Fatigue Testing to Develop/Improve Gage Application Procedures and Materials, is a chronological compilation of the results of early fatigue testing. The following discussion (by Test Number) presents the purpose of the test, application difficulties, conclusions and changes, if any, to application process, materials, and structure design.

Test Number 38-77. The purpose of the first test was to determine the fatigue strength of Moleculoy gages when applied with Denex 2 cement. During the application of the gages, difficulty was experienced in wetting the cured base coat of Denex with the top coat that encapsulates the gage, interface ribbon, and the Chromel P convoluted leads. Attempts to apply the gages without tape strips to hold the gage grid to the base coat proved unsuccessful because the gage grid became distorted when touched by the brush used to apply the cement. Two tapes 0.025 to 0.030 inch wide were used to hold the grid to the base coat. The applications were thick.

Initial beam strain was set at 2000 microinches/inch peak-to-peak. All systems failed between 50,000 and 600,000 cycles. Four failures were in the gage grid and two were interface ribbon failures. The ribbon failures were caused by inadequate support of the Chromel-P leads and were discounted. (These failures were not encountered again throughout the test program.)

GE experience with composite-ceramic applications when using Karma gages with H-cement showed a system fatigue of 2400 microinches/inch p-p at 10^7 cycles.

It was concluded that either the fatigue strength of Karma was greater than Moleculoy (in which event, the pull-tests and/or assumptions used in Phase I to determine the fatigue strengths of candidate alloys did not produce valid results) or the Denex 2 cement was the major contributor to early failure. Tests Number 44-77 and 45-77 were conducted to identify which of the above caused the low fatigue strength obtained on the beam.

Test Number 44-77. This test was conducted to determine the relative fatigue strengths of Moleculoy and Karma gages. There were two major considerations in the test design. First, the application technique should not damage the gages. Second, only the grid was to be tested for fatigue strength - the interface ribbon and weld were not to be tested. Room temperature curing (RTC) epoxy cement was selected to apply the gage grid. This is a clear epoxy cement that is used for the application of foil gages. Figure 50 shows a typical gage application on the test beam.

Three Karma gages were fabricated using standard techniques and heat treated with three Moleculoy gages at 1050° F for 2 hours. These were applied to opposite sides of the test beams. The test sequence was the same as described earlier except periodic manual shutdown was required so that gage resistance could be measured. Resistance measurements were made across the gage legs at the end of the RTC near the interface ribbon.

All three Moleculoy gages and one Karma gage survived the test sequence through 4000 microinches/inch p-p and 10^7 cycles as shown in Table 9 (Page 92). The failures occurred in the grids of the Karma gages.

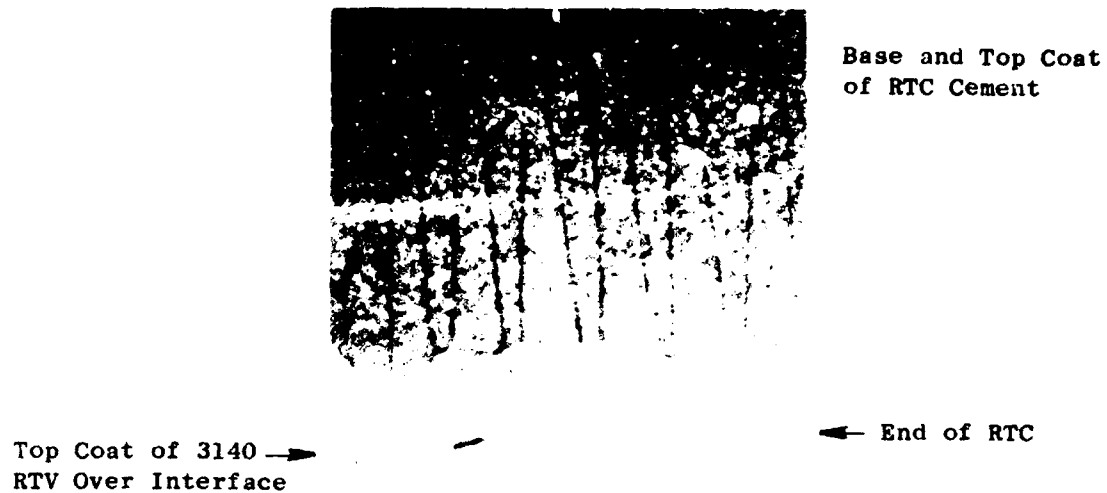


Figure 50. Moleculoy Gage in RTC Epoxy Cement.

It appears that the estimates of fatigue strength from pull-test data of Phase I are valid. Moleculoy has a higher endurance limit than Karma. It also appears that the "infant mortality" in TN 38-77 was Denex 2 oriented.

Test Number 45-77. This test was conducted to compare the fatigue life of Moleculoy gages when applied with Denex cement and H cement. Three Moleculoy gages were applied with each of the cements. The Denex 2 application procedure was modified slightly to ensure better wetting of the FSA base coat when the tip coat is applied. The technique used was to etch the base coat surface with aluminum phosphate prior to the application of the gage and the first top coat of cement. The first top coat appeared to flow better onto the base. Application thickness was reduced from that of TN 38-77.

The test results (Table 9, Page 92) indicate an improvement in fatigue strength by the slight change in application procedures. Nevertheless, the performance of H cement applied systems appeared superior to the Denex systems.

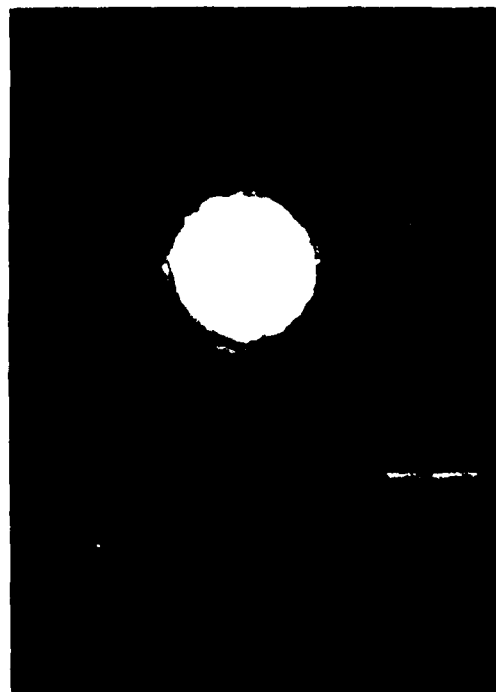
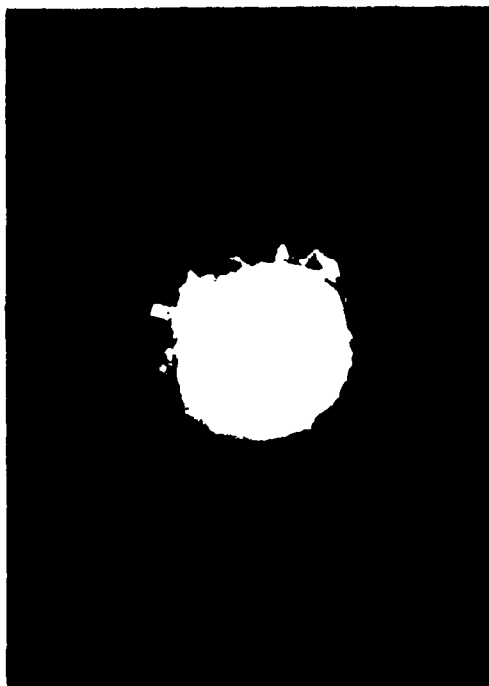
Postmortem of the H cement application showed one grid failure and two Chromel P lead failures that occurred at the 3000 microinches/inch level. The Denex applications at the 2400 microinches/inch level had one grid and one lead failure. After the 3000 microinches/inch level and 5×10^5 cycles, one more grid failure and one more Chromel P lead failure were revealed by the postmortem.

It had been suggested that a large number of large particles could increase the probability of damage to the fine strain gage wires and create a failure site, especially at high dynamic strains. A review of photomicrographs of the two cements obtained for oxidation protection studies in Phase I, showed a significant difference in particle size distribution. With few exceptions, Figure 51 shows that, while the size of the large "rocks" in the two cements was about the same, there were significantly more "rocks" in the Denex cement. Fine ground cement was ordered from the vendor, Dentronics, to test in future composite-ceramic applications.

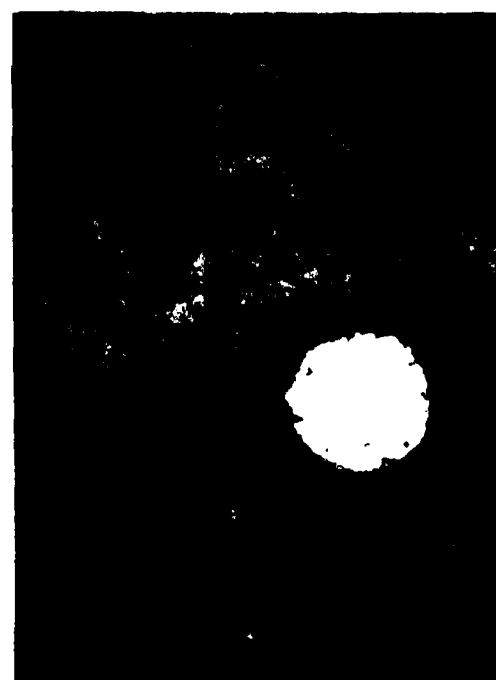
While it was thought possible that the large "rocks" could also damage the 3-mil diameter Chromel P leads, the most probable source of stress risers was the convoluting fixture gears. Inspection of the gear teeth did not show any major defects. However, an inspection cycle of convoluted leads was initiated for future applications.

Test Number 48-77. There were two investigations conducted during the application of gages for this test. First, because only moderate changes in Denex application improved the fatigue characteristics in TN 45-77, it was thought that additional changes might produce even better results. Second, all convoluted leads would be inspected for defects that would reduce the fatigue strength of the Chromel P leads.

According to Dentronics, Denex 2 cement could be thinned with distilled water in the ratio of 4 parts cement to 1 part water by weight. Using this thinned cement with the aluminum phosphate etch improved the application



H Cement



Denex Cement

Figure 51. Comparison of Particle Size Distribution Between H Cement and Denex Cement.

characteristics, providing better control of thickness. It was also found that the tape holding the gage to the base coat had to be removed while the part is still warm after the partial cure of the first top coat at 170° F. If the tape is removed at room temperature, there is noticeable motion of the grid wires and leads that probably cause damage.

Photographs were made of all gage applications and lead wires after the first top coat of cement was cured. Any defect observed in the wire was photographed at 70X with the intent of correlating lead failures with the defects. Application difficulties were also noted.

The performance of these composite-ceramic applications was better than those previously tested, as can be seen in the table. The failures shown in the table were identified by postmortem techniques after the Krouse machine was automatically shut down by the open circuit and before the test was restarted. The application was damaged as little as possible during the postmortem so that additional failures could be accumulated. These might aid in identifying poor application procedures or design faults by correlations with problems observed during the application phase.

The postmortem at the end of the test showed two additional lead failures for a total of five and six additional grid filament failures for a total of nine. Grid filament failures mostly occurred in the outer filament near the interface ribbon. Two of these were believed to be related to the first postmortem to identify the first failure.

Failures of Gages 1, 3, and 6 were in the outer filaments as shown in Figure 52. These were associated with an application problem that involved the removal of gages after the first taping and retaping to the base coat.

Gage 2 was applied with the outer filament very near the edge of the flame-sprayed alumina base coat because of the gage shape. Figure 53 shows the installed gage held in place with the first top coat. The postmortem showed that the gage failed in this filament. Figure 54 shows the failure site. It failed at 2×10^4 cycles at 2400 microinches/inch peak-to-peak.

Failures

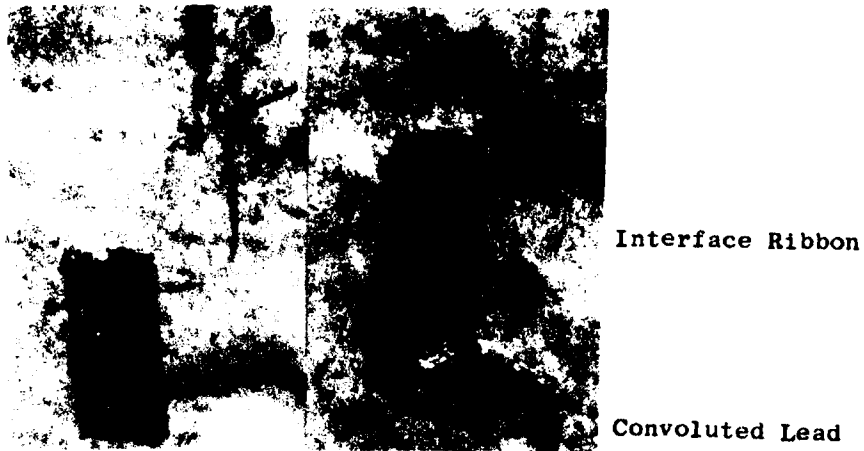


Figure 52. Typical Outer Filament Failures (40X).

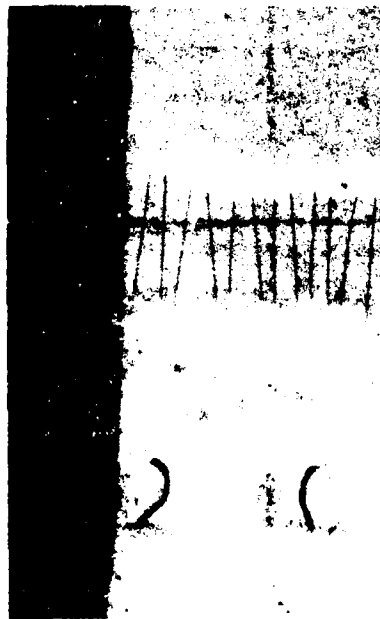


Figure 53. Gage 2 Installed Too Close to Edge of FSA Base Coat (10X).



Figure 54. Failure Site of Gage 2.

Because of this failure, gages were flattened to 0.4 mil instead of the original 0.6 mil. Figure 27 from Phase I, 0.2% yield and elongation versus conditioning for Molecule, shows that the estimated fatigue strength would be increased about 5% but the elongation would decrease from 3% to 1.5% to 2%. This decrease in elongation was not considered a serious problem at this stage of the fatigue test program.

Using the new flattened thickness, gages were much more uniform and could be better aligned with the stress field (Figure 55).

There was little correlation between observed Chromel P leadwire defects, strain level, and failures. For instance, both Gages 4 and 5 had defects in the lead as shown in Figure 56. These were the only lead wire defects, among all gages, observed during the application inspection. While the defect in the Gage 4 lead appeared small, lead failure did occur at that site but at

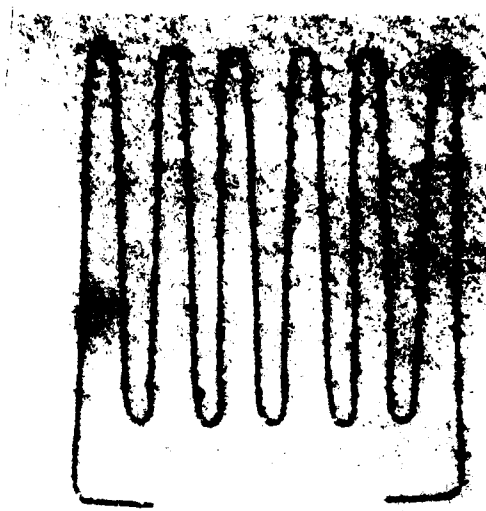


Figure 55. 1/8-Inch Long
Moleculoy Gage
Flattened to
0.4 Mil - Typical.



Figure 56. Defects in Chromel P Convoluted Leads
(70X) - Not Caused by the Convoluting
Fixture.

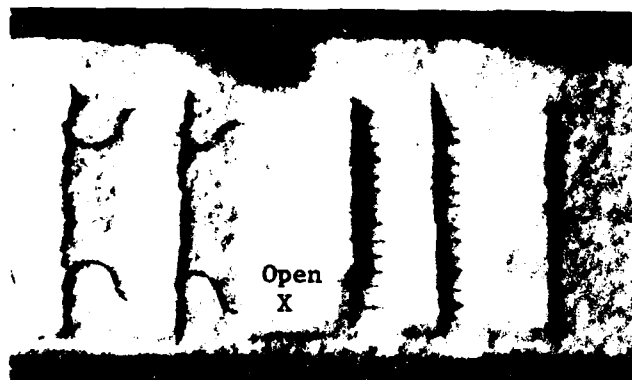
the 3400 microinches/inch level. The defect in Gage 5 appeared much more serious, but the lead never did fail although it was subjected to the same stress level. Other lead failures occurred at 2400 microinches/inch. The fatigue strength of the alloy became suspect.

Chromel P (Ni-10Cr) was the prime candidate for airfoil leads in these strain gage systems because it was routinely used at GE in all high temperature, dynamic strain gage applications. Failures of these leads had never been observed in such applications. Because of the GE design approach of routing these intermediate leads on the airfoil through low dynamic strain areas (determined from strain distribution tests), it was likely the alloy had never been subjected to strain levels used in these beam tests. Vendor literature contained no fatigue strength data, only the ultimate tensile stress (UTS) which is 95,000 lb/in.². Pull-tests of the wire in the Fine Wire Test Machine showed the UTS ranged between 94,000 and 97,000 lb/in.². The 0.2% yield strength is about 84,000 lb/in.². The modulus of elasticity, calculated from the weighted moduli of the alloy constituents, is 30.6 million lb/in.². As in estimating the single amplitude endurance limits of candidate strain gage alloys from the 0.2% yield strength (Phase I), the endurance limit of Chromel P was estimated to be ± 1370 microinches/inch or 2740 microinches/inch peak-to-peak. While this value probably is low, it nevertheless indicates the need for a higher strength intermediate lead.

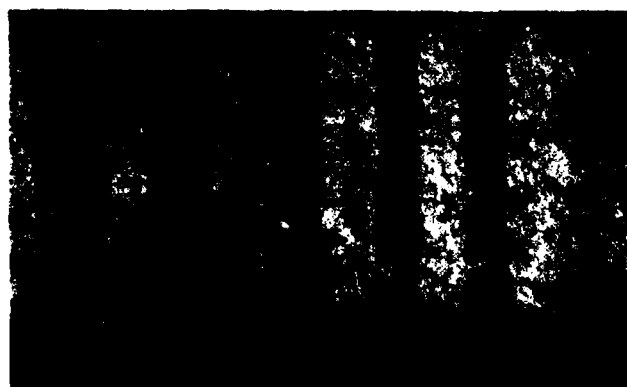
Platinum-10% nickel having a diameter of 2 mils was available and was subjected to the same tests. The UTS is 270,000 to 274,000 lb/in.². Vendor data show 230,000 lb/in.². The 0.2% yield strength is about 260,000 lb/in.². The modulus of elasticity, again calculated from the weighted moduli of platinum and nickel, is 24.6 million lb/in.². The estimated endurance limit is 5300 microinches/inch. The Pt-10Ni replaced the Chromel P and will be used throughout the program.

Test Number 57-77. The purpose of this test was to determine the fatigue life of the Moleculoy gages when applied with all flame-spray alumina techniques (Candidate 2). The new platinum-10% nickel leads along with the gages flattened to 0.4 mil. Three of the gages being applied to one side of the beam failed during the application of the first coat of flame-spray alumina. The interface ribbons had not been properly secured to the base coat with tape.

The ribbons fluttered during spraying causing the outer filaments to fail. The taping procedures were redefined and the applications of gages to the opposite side of the beam were completed. The failed gages were not reapplied. Figures 57(a) and (b) show the differences between the first coats of improperly and properly taped gages.



(a) Improperly Applied Gage.
Notice the Wide First
Coat Over the Ribbon.
Tapes too Narrow.
1st Coat Thick.



(b) Properly Applied Gage.
Interface Ribbon Held
by Tape.
Tape Width Increased.

Figure 57. Differences Between First Coats of a Properly and Improperly Applied Gage.

The test results of the three gages shown in Table 9 (Page 92) were very encouraging. The strain level of 3000 microinches/inch and 10^7 cycles is

58% higher than Karma gages applied using similar techniques and tested in the same manner. The highest strain level that the Karma gages survived 10^7 cycles was only 1900 microinches/inch p-p. There were no failures of the Pt-10Ni convoluted leads.

Postmortems showed the failures were in grid filaments at locations corresponding to the interfaces of the first and second coats (top coat). It is currently thought that these failures are inherent to the Rokide process. It is one of the reasons the composite structure was developed.

Summary of Improvements From Table 9

As a result of these early fatigue tests, there were a number of changes/improvements in the candidate strain gage systems. It was still to be proved that all changes enhanced fatigue performance.

1. Modified application techniques of the composite-ceramic structure improved the fatigue strength of the gages. The impact of finer ground Denex 2 still is to be determined.
2. Increased flattening of the gage from 0.6 mil to 0.4 mil was introduced to improve gage shape and, thereby reduce application problems.
3. The convoluted lead material was changed from Chromel P to Pt-10Ni. This appears to be an improvement.
4. Gage grid and interface taping techniques were redefined to reduce gage loss during the application of gages using the flame-spray process.

These changes were used in all gage systems applied for the fatigue testing at temperature and at A ratios of infinity and 2.

Fatigue Testing at A-Ratio = ∞

The results of fatigue testing of the modified gage systems are shown in Table 10 (Page 104). In these tests after TN 2-78, it was necessary to redefine fatigue strength from 10^7 cycles to 10^6 cycles. This was because over 92 hours were required to accumulate 10^7 cycles. In the event a gage failed, i.e., at night or over the weekend, the machine was shut down until a post-mortem of the failed gage was made and the testing of survivors was restarted. This caused serious delays in the program schedule.

Table 10. Fatigue Test Results.

Beam Type and Material (See Table 8)

A-Ratio = $\frac{a}{W}$

1/8-inch Long Molecule Grid Flattened to 0.0004-inch

Test Number	Test Temperature ° F	Cand.	Dynamic Strain Level Peak-to-Peak $\epsilon \times 10^{-2}$										Symbols Used:		Comments
			10	14	18	22	26	30	34	38	42		▲	●	
2-78	RT	1						●	▲	▲	●		▲	●	Survived 10 ⁶ Cycles.
		2						●	▲	▲	●		▲	●	Survived 10 ⁷ Cycles 6 × 10 ⁵ = Failed at 6 × 10 ⁵ Cycles
5-78	850	1						▲	▲	▲	▲		▲	●	Beamed failed; gages okay
		2						▲	▲	▲	▲		▲	●	Fine ground Denex 2 cement used. Failures in grid.
19-78	850	1						▲	▲	▲	▲		▲	●	Grid failures at tape hold-down.
		2						▲	▲	▲	▲		▲	●	Gage failed in 1st filament of grid. Beam failed. Gage okay at failure.
12-78	1200	1						▲	▲	▲	▲		▲	●	Beam failed. Gages okay at failure. Redo this test.
		2						▲	▲	▲	▲		▲	●	Failed in grid. Considered failed because of GF decay.
25-78	1500	1						▲	▲	▲	▲		▲	●	Failed in grid at tape hold-down. Failed at edge of ribbon interface.
		2						▲	▲	▲	▲		▲	●	Loose weld. Exhibits supersensitivity grid. Outer filament.
		1						▲	▲	▲	▲		▲	●	Pt-10Ni lead failure near splice to primary lead. Grid.
		2						▲	▲	▲	▲		▲	●	Grid failure in outer filament. Splice Pt-10Ni lead to primary lead. Gage okay.
		1						▲	▲	▲	▲		▲	●	Grid failure. Outer filament at tape hold-down. Splice Pt-10Ni lead to primary lead. Gage okay.
		2						▲	▲	▲	▲		▲	●	

Fine-ground and thinned Denex 2 cement was used in the composite structures. The grind that was used was 65 hours (nominal) of additional pulverizing. The large particles in this cement were about one-half the size of large particles in H cement as shown by the photomicrographs in Figure 58.

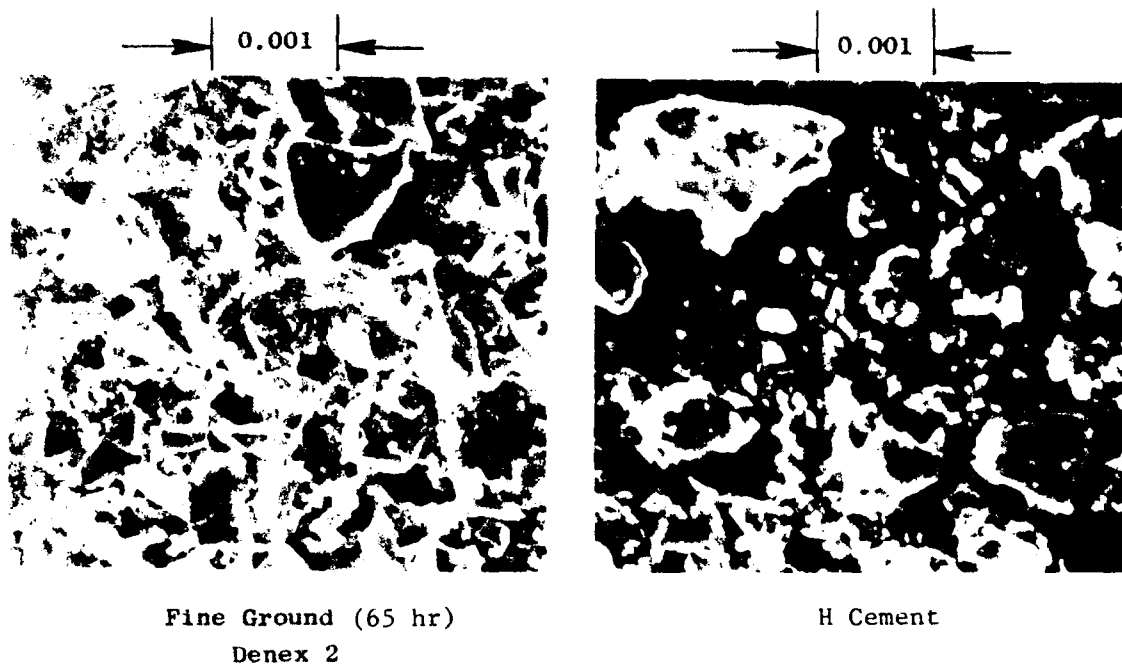


Figure 58. Particle Size Comparison of Fine Ground Denex 2 and H Cement.

The cement application procedures that were developed in TN 48-77 were used with the fine-ground cement.

The results of Test Number 2-78 shown in the table indicate a remarkable improvement in fatigue strength of gages applied with composite-ceramic techniques. The Pt-10Ni leads did not fail. The composite-ceramic gage that

survived 10^7 cycles at 4000 microinches/inch p-p was tested at A-ratio of 2 (3000 microinches/inch tension and 1000 microinches/inch compression). It accumulated 220,000 cycles before failure in the grid occurred.

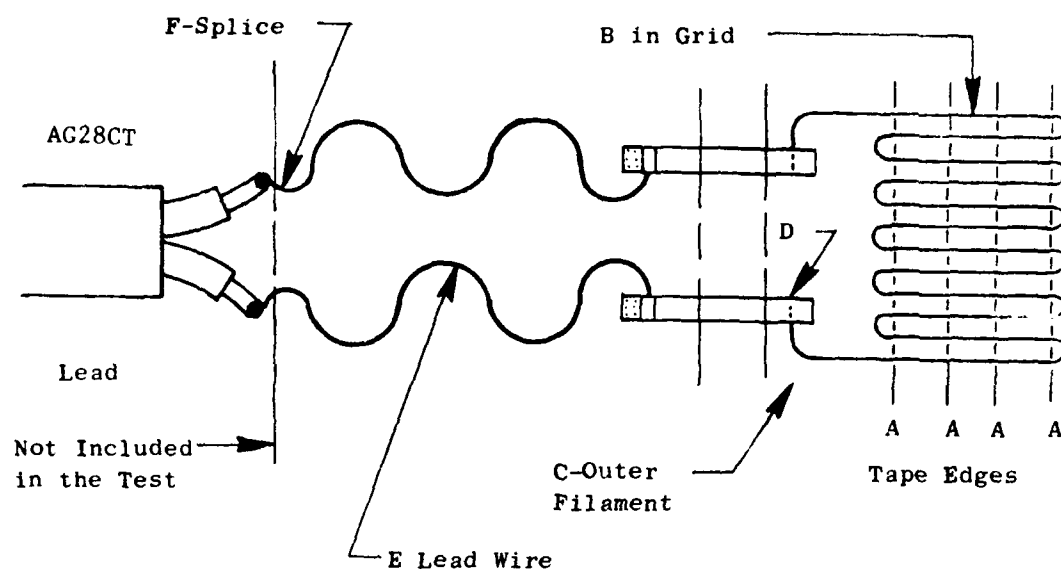
One of the composite applications in Test Number 19-78 (a repeat of TN 5-78 because of beam failure) exhibited a downward shift in gage factor and was considered failed when the decay was observed. During the postmortem, the ceramic cement in this structure was found to be loose and grainy, the result of insufficient mixing of the cement before application. The other gage did not exhibit this gage factor shift.

The postmortem results of the testing at A-ratio of infinity (Table 10) are shown in Figure 59. All failures that were observed are included. The letters indicate failure site and correspond to those shown by the sketch included with the table. As shown, failures in the composite-ceramic gage system tend toward the gage grid and outer filament while those in the all-FSA structure are at the edge of the tape hold-down.

Fatigue Testing at A-Ratio = 2

Fatigue test results of gages tested at A-ratio of 2 are shown in Table 11 (Page 108). Gage fabrication, application materials, and techniques were the same as used in A-ratio = ∞ testing.

Some of the test beams were started at strain levels that caused failures before 1 million cycles could be accumulated. In Test Number 13-78 at 1200° F, both gages exhibited supersensitivity or increasing gage output prior to failure. The 2-mil Pt-10Ni leads failed near the junction of the 10-mil chromel-alumel primary leads shown in Figure 60. Similar failures at 1500° F and A-ratio = ∞ (TN 25-78) led to moving the splice to a lower stress area on the beam for TN 30-78 and 31-78. There were no lead failures of the gage systems in these test numbers.



Candidate Gage System	Failure Site							Total
	A	B	C	D	E	F	Other	
1 (Composite)	---	3	3	1	---	1	2(2)	10 ⁽¹⁾
2 (FSA)	5	---	2	---	---	2	2(2)	11

(1) Surviving Candidate 1 from TN 2-78 not included.
 (2) TN 5-78 beam failed; 3 gages still operating.
 TN 19-78 Candidate 1 gage factor shift.

Figure 59. Gage Failures Resulting From Fatigue Testing at A-Ratio = ∞ .

Table 11. Fatigue Test Results.

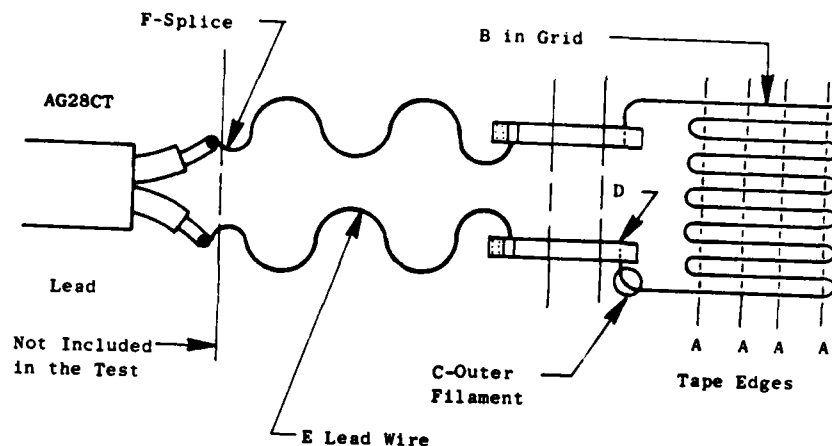
Beam Type and Material (See Table 8)
 A-Ratio = 2
 1/8-inch Long Molecule Grid Flattened to 0.0004-inch

Test Number	Test Temperature	Cand.	± Single Amplitude Dynamic Strain + Mean Tensile Strain $\epsilon \times 10^{-2}/\epsilon \times 10^{-2}$										Symbols Used:	Comments
58-77	RT	1	±5 +2.5	±7 +3.5	±9 +4.5	±11 +5.5	±13 +6.5	±15 +7.5	±17 +8.5	±19 +9.5	±22 +10.5		▲ = Survived 10 ⁶ Cycle ✕ 6 × 10 ⁵ = Failed at 6 × 10 ⁵ Cycles △ Beam Failed: Gages okay.	
4-78	RT	2												Failed in outside filament as did Gage 2. Gage 3 did not fail. The failure was in the 30 ga. flex lead used to route signal off beam.
9-78	850	1												All failures in grid at tape locations.
10-78	850	2												Outer filament failures.
14-78	1200	1												Beam failed near clamp. Gages still operating at failure.
13-78	1200	2												Grid outer filament failure. Ultrasonic weld failure.
31-78	1500	1												Pt-10 Ni leads at splice to flexible leads. Both gages exhibited supersensitivity when failing.
30-78	1500	2												Failures in outer filament.
														Failure in outer filament. Failure in outer filament at tape location.



Figure 60. Pt-10Ni Lead Failure
Near Splice, Gage 2,
TN 13-78.

The results of the postmortem inspections are summarized in Figure 61. As can be seen from this figure and Figure 59, a pattern of failures is beginning to evolve. Composite-ceramic gages are prone to fail in the outer filaments between the interface ribbon and the bottom of the gage grid. The all-FSA failures occur primarily in the grid at the edge of the first FSA coat.



Candidate Gage System	Failure Site							Total
	A	B	C	D	E	F	Other	
1 (Composite)	---	---	7	1	---	---	1(1)	9
2 (FSA)	4	---	1	---	---	2	2(2)	9
(1) Gage did not fail; 30-gage lead failure. (2) Beam failed near clamp. Gages still operating satisfactorily - TN 10-78								

Figure 61. Gage Failures Resulting from Fatigue Testing at A-Ratio = 2.

Fatigue Testing on Blades

All the fatigue testing discussed above was conducted on constant-stress beams. Tests were also conducted on engine blading in the Hot Shake Facility which is described in Section 5.0, Test Equipment. It was thought testing on blades would provide a more realistic fatigue strength, because it factors into the gage application the complexities of curved surfaces, lead routing through fillets, and stress riser.

Table 12 (Page 111) shows the results of this testing.

Table 12. Fatigue Test of Gages on Compressor Rotor Blades in the Hot Shake Facility (See Paragraph 5.3).

Test Number	Test Temperature ° F	Candidate	Blade Type	Blade Material	Dynamic Strain Peak-to-Peak $\epsilon \times 10^{-2}$										Comments
					10	14	18	22	26	30	34	38	42		
1-78	660	1	F101 Stage 3	Ti		●	●	●	●	●	●	●	●	●	Failure in Chromel P lead. Failure in grid wire on Hi-C line near fillet. (Center of gage 0.120" above platform on Hi-C). Same failure mode as Stage 9.
	1020	1	F101 Stage 9	Inco 718		●	×	Failed during setup							
	1075	2	F101 Stage 8	Inco 718		●	×	6.5×10^6	Actual temp. ~ 1050°						
29-78	1100	2	F101 Stage 9	Inco 718	No. 1	●	●	●	●	●	●	×	10^6	Center of gage moved to 0.150" above platform to avoid high strain gradient. 1. Splice failure on platform. 2. Failure not identified. 3. Grid at tape strip. 4. Grid at tape strip. 5. Grid at tape strip.	
					No. 2	●	●	●	×	1.3×10^6					
					No. 3	●	●	×	10^4						
					No. 4	●	●	●	●	×	$> 10^4$				
					No. 5	●	●	●	●	×	On Setup				

Test Number 1-78. These blades were prepared in conjunction with Task 4, Effect of High Rotational Speeds on Application Integrity. Twelve blades were instrumented - 4 Stage 3, and 4 Stage 9 received composite-ceramic applications, and 4 Stage 8 were equipped with all-FSA applications. One of each stage was to be fatigue tested in the Hot Shake Facility.

Stage 3 and 8 blades were completed before it was determined that Pt-10Ni leads were superior to Chromel P (Test Number 57-77). These blades used the Chromel P leads on the airfoil. The Stage 9 blades were completed with Pt-10Ni leads. Figure 62 shows photographs of the gage applications after the first coats of alumina or Denex 2 cement have been applied. This figure identifies the failure sites determined by postmortem inspections. Figure 63 shows a typical completed splice of the convoluted leads to the Chromel Alumel leads that are routed through the spool of the compressor rotor to the slip ring or telemetry.

The failure of the Chromel P lead in the Stage 3 application was not surprising in light of previous experience. Stage 8 and 9 failures were in a grid filament that was either on or very near the Hi-C line. In Figure 62 the end loops of the gages appear to be in the fillet radius where the strain could be significantly higher than the average strain indicated by the gage.

Test Number 29-78. Near the end of the fatigue test program on beams, the performance of the gage was shown to be superior to the standard Karma gage used for all engine dynamic strain investigations at GE-Evendale. It was decided to implement the Moleculoy gage, ultrasonic welding and Pt-10Ni leads into the Instrument Shop where flame-spray alumina techniques would be used for gage application. A demonstration was conducted of the gage capability on blades using the all-FSA application technique.

F101 Stage 9 Inconel 718 blades were selected for this demonstration. Because of the failure of the gages on the same blade design in Test Number 1-78, a review was conducted to assure the end loops of the gage would not fall in the fillet. Considering the tolerances of fillet radius and gage location, the dimension was 0.148 inch from the top of the platform to the gage centerline (0.120 inch was used in TN 1-78). Five blades were instrumented on

Stage 3 - S/N 08751
Composite-Ceramic



Stage 3 Complete



Stage 8 - S/N 14540
All-FSA



Stage 9 - S/N 11509
Composite-Ceramic



Figure 62. Molecule Gage Applications to F101 Rotor Blading After First Coat (Failure Sites Marked With "X").

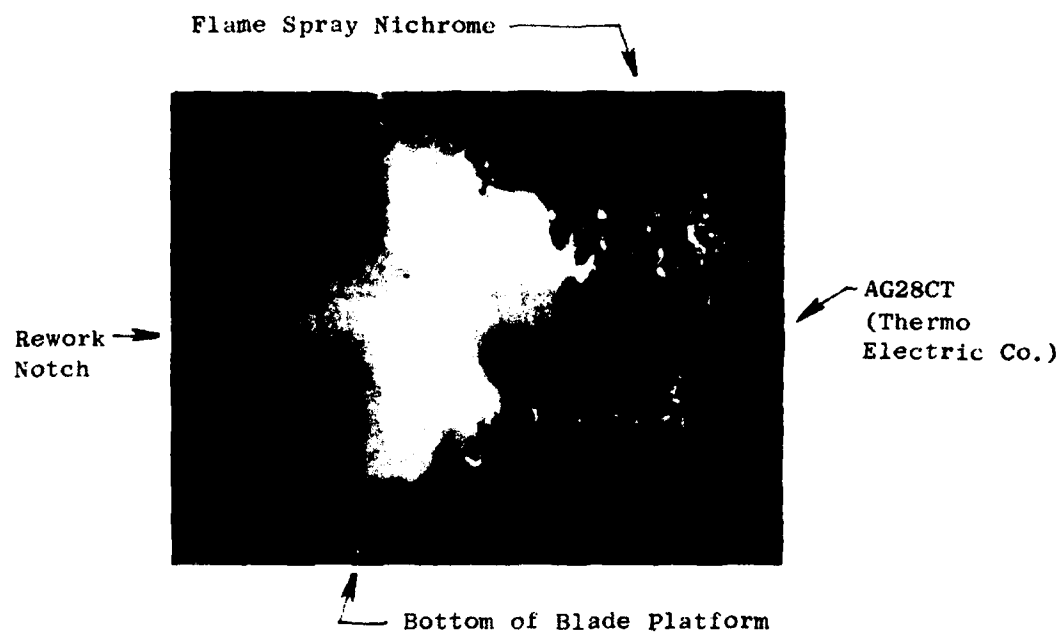


Figure 63. Typical Splice of Convoluted Leads to Primary Leads.

TN 29-78 using this new dimension. The splice to primary lead was completed on top of the platform to prevent interference of the under-the-platform splice with the clamp used in the Hot Shake Facility.

The results show even higher fatigue strength than obtained from the beam tests. The highest strain that Karma gages had survived in the Hot Shake Facility was 2500 microinches/inch p-p but at 850° F, not 1100° F.

The postmortem inspection showed three gages failed near the grid center on either side of the center first coat of alumina. The failures are shown in Figure 64 which is a photograph of Gage 1 failed in the splice on top of



Figure 64. Gage 1 After First Coat Spray.
Notice Failure Site of Three
Gages, TN 29-78.

the blade platform - a splice location not used on blades for engine test. The failure site of Gage 2 could not be identified except that it was in the gage grid.

Summary of Fatigue Test Results

A comparison of the estimated fatigue strengths of the candidate strain gage systems is shown in Figures 65 and 66 for A-ratios of infinity and 2, respectively. Beam test data from Tables 10 and 11 (Pages 104 and 108) were used in estimating the fatigue strengths for 10^6 cycles. Fatigue data from blades, Table 12 (Page 111), are included on the diagram for A-ratio = ∞ .

Figure 67 summarizes the failure sites of all gages tested in fatigue after the development/improvement program. Failures in that program are not included. Composite-ceramic failures occur more frequently in the outer filament near the interface ribbon. The failures in the all flame-spray alumina structure are predominantly at the interface between the first spraycoat and the top spraycoat of alumina.

Discussion of Failure Sites

Because very nearly 50% of all failures in the candidate structures occur at specific sites as shown in Figure 67, it was thought if the reason for these failures could be identified it might be possible to modify procedures/designs to improve the fatigue strength of the systems. This would be especially desirable for the low-temperature end of the Candidate 2 gage system because of its superiority above about 700° F.

In both fatigue diagrams, the fatigue strength of the all-FSA strain gage system is greater at 850° F than at room temperature. This suggests that either the gage applications tested at room temperature were not of the same quality as those tested at 850° F, or the difference is real and the failure mechanism involves a stress riser at the failure site that becomes less severe at higher temperatures.

It is possible that the quality of the applications was different since all the room temperature applications were completed earlier in the fatigue

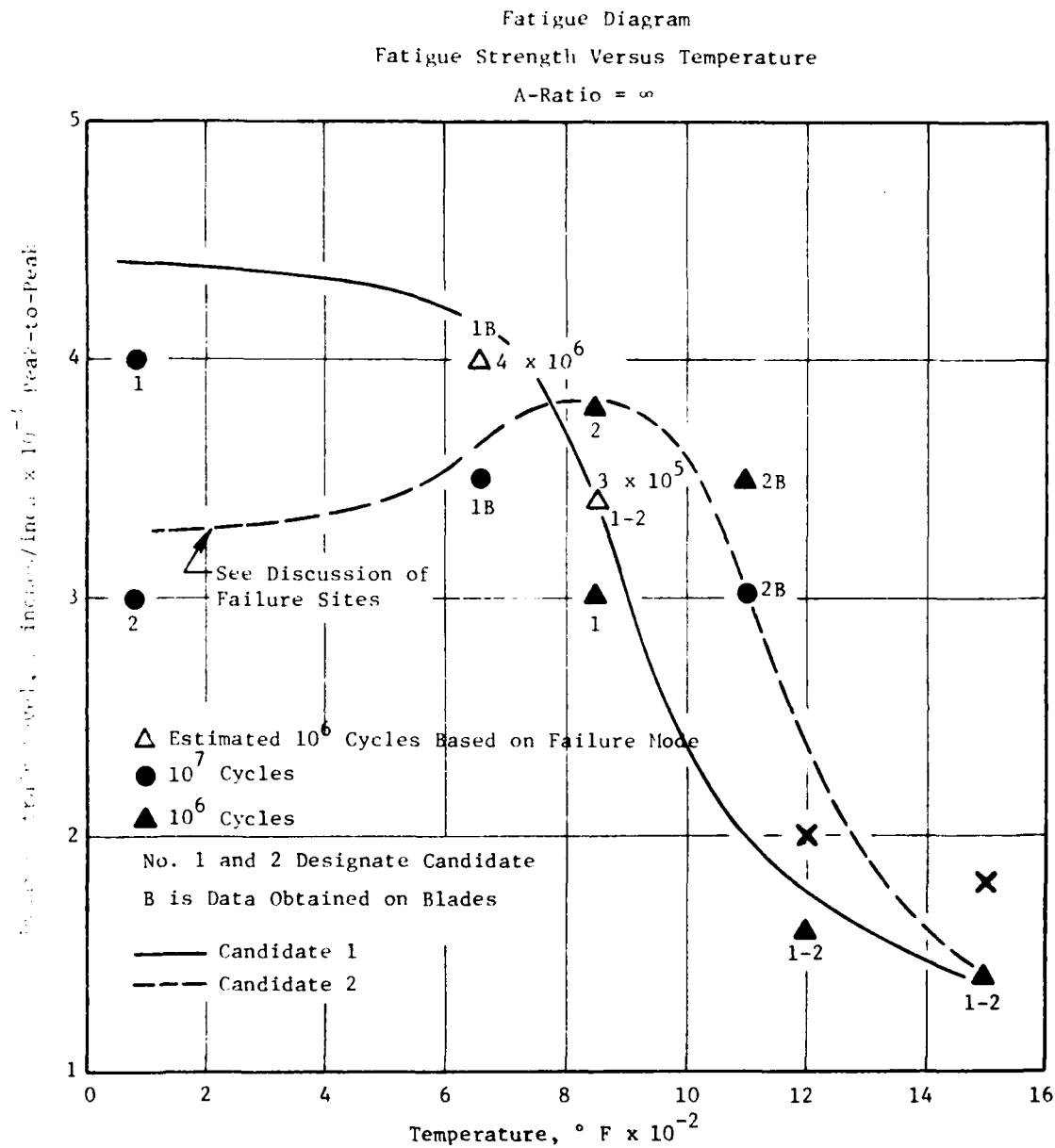


Figure 65. Fatigue Strength at 10^6 Cycles of Candidate Strain Gage Systems on Beams 30 Hz Test Frequency - A-Ratio = ∞ .

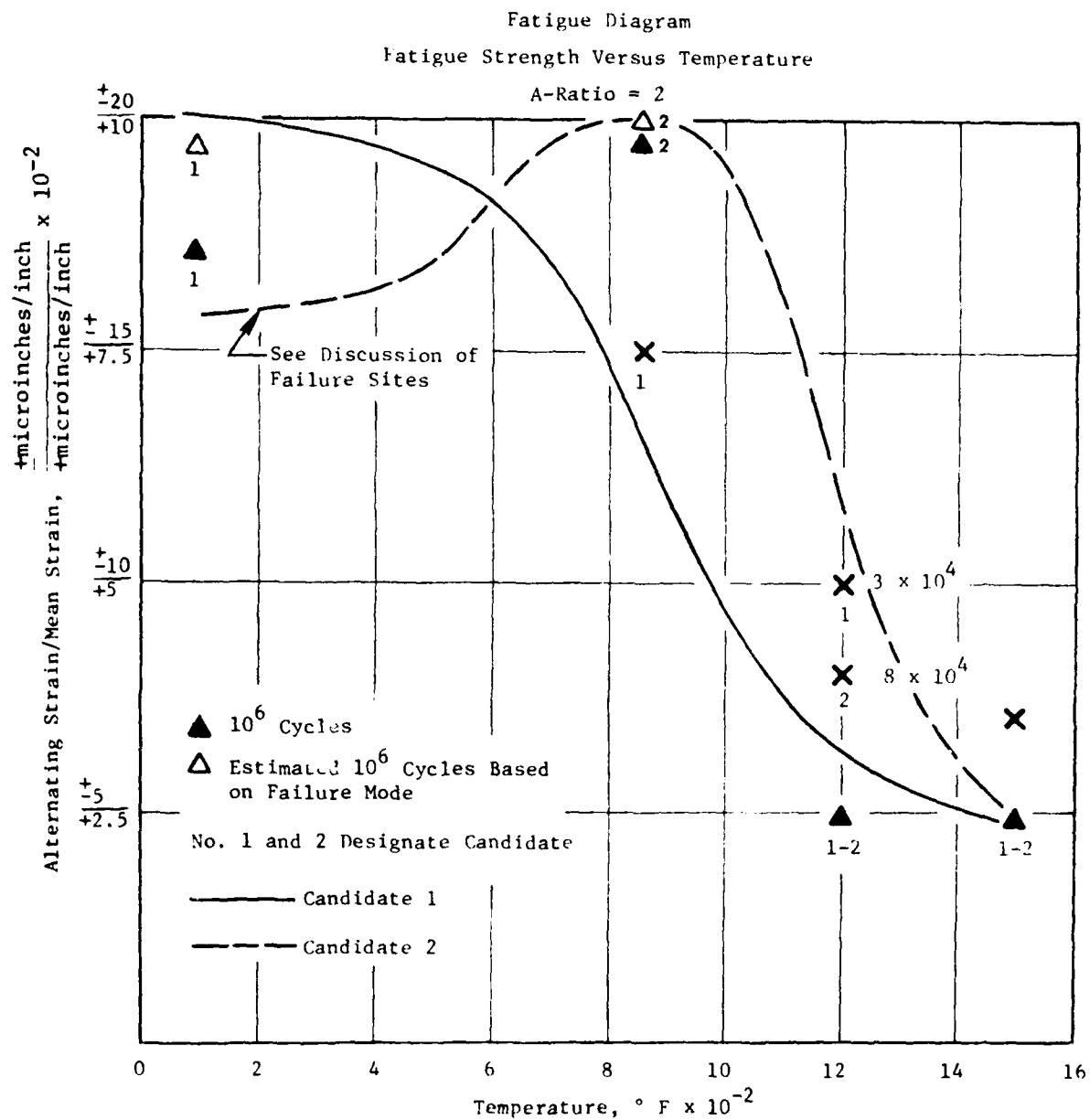
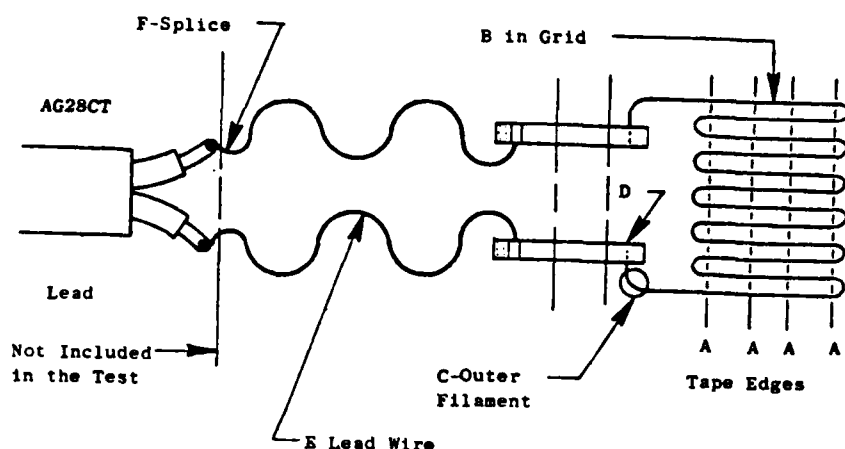


Figure 66. Fatigue Strength at 10^6 Cycles of Candidate Strain Gage Systems of Beams 30 Hz Test Frequency - A-Ratio = 2.

test program than those tested at 850° F. However, this seemed unlikely because of the skill of the Application Technician and his familiarity with the process. The reason for the strength differences lies elsewhere - apparently, in the materials of application.



Candidate Gage System	Failure Site							Total
	A	B	C	D	E	F	Other	
1 (Composite)	---	4	10	2	1	1	3	21
2 (FSA)	13	---	3	1	---	4	6	27

Figure 67. Gage Failures Resulting From all Fatigue Testing.

Location F failures are included to account for all gage systems tested. However, they are not considered system failures.

If the stress risers that are believed to exist near the edge of the first spraycoat are from the alumina alone, it is doubtful that severity of the concentration would become less at 850° F; the softening temperature of Al_2O_3 is much higher. The only reasonable explanation is that some material from the tape adhesive is contaminating the alumina. It must be hard at room temperature and soften at some higher temperature.

The tape strips used in gage applications is TFE teflon-coated glass cloth. It contains a thermosetting silicone pressure-sensitive adhesive. The manufacturer was reluctant to divulge the filler material used in the adhesive, but he did say the adhesive softens at 250° to 300° F and hardens or sets at 500° F in 3 hours. Accelerated hardening may be achieved in shorter times at higher temperature. "Breakdown" of the set material would occur at higher temperature with time.

Pieces of tape were applied to test coupons. One was heated to 650° to 700° F, the other to about 500° to 550° F for about 15 minutes. Figures 68 and 69 are photographs of adhesive residue on the metal coupons after tape removal at magnification of 20. The material exposed to the high temperature was clear and glassy but shattered when touched. On the other hand, the material on the lower temperature coupon was also clear but very soft. Reexposure of this coupon to 900° F for about 10 minutes resulted in the hard, glassy film shown in Figure 70.

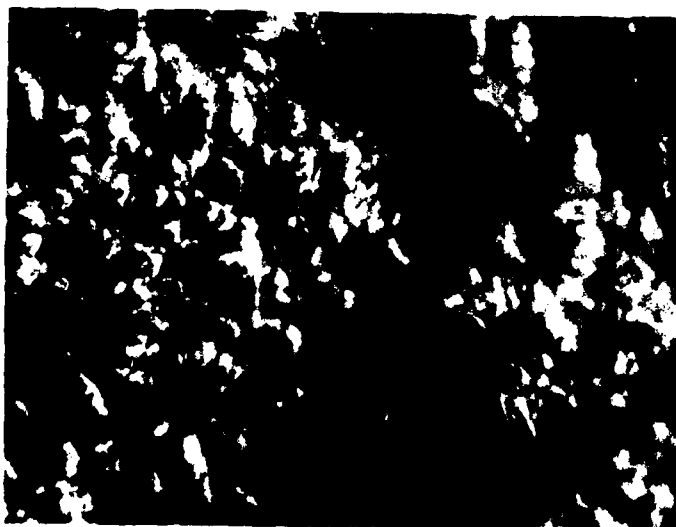


Figure 68. Tape Adhesive Residue After
15 Minutes at 650° to 700° F.

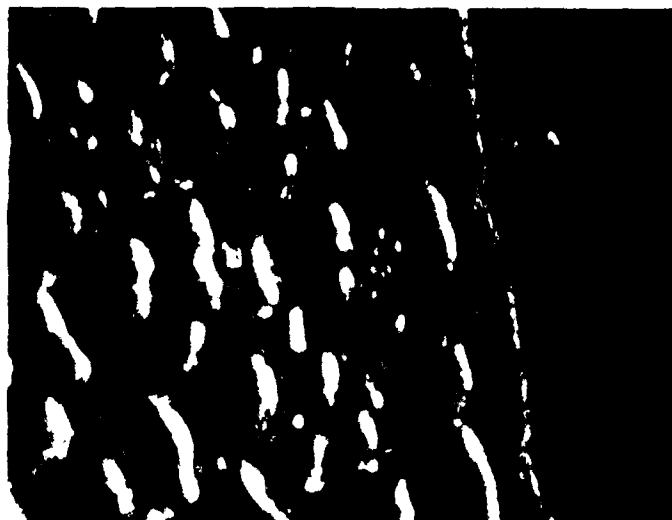


Figure 69. Tape Adhesive Residue After
15 Minutes at 500° to 550° F.



Figure 70. Adhesive Residue After
Reexposure to 900° F
for 10 Minutes.

It is possible that the adhesive filler is silica, and it combines with the silicone at high temperature to form a kind of soda glass. The presence of glass in the alumina structure would explain the increased fatigue strength at 850° F because glass gradually softens when heated.

A photomicrograph at the interface of the alumina coats is shown in Figure 71. The black areas are voids where poorly adherent pieces of alumina were pulled from the structure by the grinding operation used to prepare the specimen. The inner surface of these voids are coarse and irregular. If they were left during the application, the surfaces would be smooth and glassy. The "soft" alumina of the top coat (shown by the arrow) has been observed in the past. These particles are probably encased by the glass from the tape which shatters readily under pressure. The diagonal path of the soft-alumina is from shadowing as the top coat builds up and out over the valley left by the tape.

Locations of the base coat and first coat are approximate. They are based on coating thicknesses specified for the application process.

The following is an attempt to explain how the tape adhesive contaminates the structure and causes a reduction of stress concentrations with increasing temperature:

1. Temperatures during the first spray operation are sufficient to melt the adhesive, especially at locations where the wire is held by the tape. As the wire gets hot and expands, it lifts the edge of the tape and the adhesive melts, moving along the wire and into the alumina being deposited. This lifting of the tape edge probably explains why the top coat alumina at the edge of the first coat appears fairly dense; the adhesive had not melted by the time it lifted, and little or no adhesive was deposited in the corner. After cooling, the material hardens or sets, especially in the first coat. Away from the edge of the tape, toward the center, temperatures were sufficient to melt the adhesives but not set it. When the tape is removed, the set or nearly hard adhesive would remain on the wire. Toward the cooler area, it pulls loose from the wire but some remains on the base coat, soft and clear. During the second operation, the deposited material near the wall of the first coat mixes into the sprayed structure, moves upward as the spray is applied, and sets upon cooling.

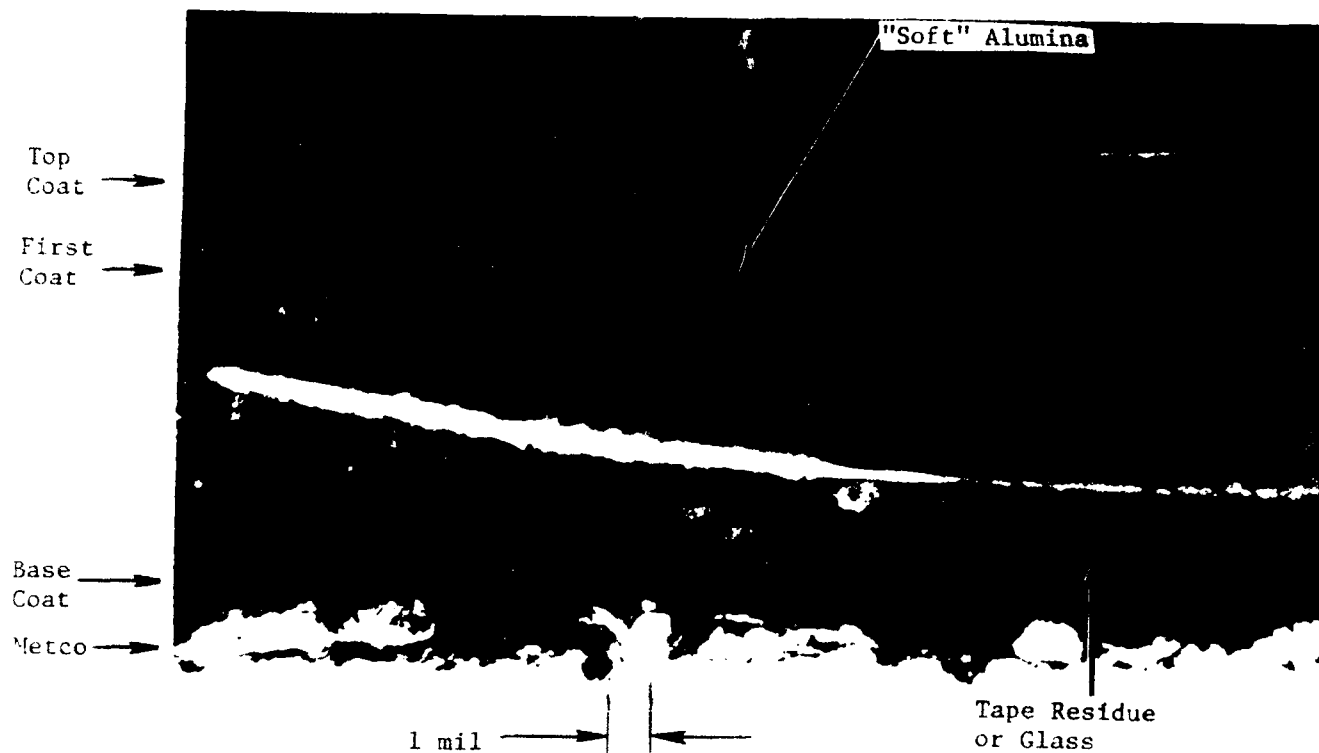


Figure 71. Longitudinal Cut of the Interface Between the First and Top Spray Coats Showing Gage Filament (250X).

2. When such a glass-filled structure is dynamically strained at room temperature, the glass shatters, allowing motion of the alumina particles and wire. However, where there is no glass surrounding the alumina pieces, there would be little or no loose alumina and even the glass encasing the wire would remain solid and a stress riser or concentration would be created. In Figure 71, the concentration may be at the edge of the void immediately behind the wall of the first coat. At high temperature, the glass would become soft (not melt) and would not shatter when exposed to dynamic forces. The glass on the wire at the stress riser also softens. This, in combination with the softly restrained particles, reduces the magnitude of the concentration and the filaments would survive higher strain levels.

This is the model that explains the fatigue strength difference between room temperature and 850° F. The estimated fatigue strengths of the Candidate 2 gage systems shown in the fatigue diagrams were drawn to reflect the softening of the glass-filled alumina structure.

There appears no way to improve the low-temperature fatigue strength of this gage system short of eliminating the tape. Metal straps in place of the tape were tried but they expand too fast to hold the gage against flutter during the first-coat application.

The fatigue strength of the composite-ceramic gage system (Candidate 1) decays rapidly above 750° F. The wire becomes softer and is more easily abraded by the hard ceramic particles. The predominant failure site in the outer filament near the ribbon is from stress concentrations introduced during fabrication of the gage. Figure 72 compares a well-made gage and interface ribbon with gages that failed because of fabrication defects. These failures could be reduced by incorporating pins in the gage winding fixture that would control the radius size and shape. However, this would not appreciably increase the fatigue strength of the gage system because failure is primarily from wear-out from abrasion; but it would increase the average life of all gages.

Conclusion

Testing in this Task has shown that both candidate gage systems would be required for maximum gage life over the temperature range from room temperature to 1500° F. Obviously, the composite-ceramic system should be used to about 700° to 750° F, while the all-FSA structure is clearly superior for high temperature work. Although there were no failures of the top coat in the composite-ceramic structure in all this testing, it is still to be determined that it will survive stress and centrifugal loads on a test compressor.



A. Gage 3, TN 58-77.
Radius correct. No failure
results. Stress concentra-
tion low.
35 Magnification

B. Gage 2, TN 14-78.
Interface ribbon too close
to gage filament. Stress
concentration at edge of
ribbon is high.

C. Gage 2, TN 58-77.
Radius sharp. Stress
concentration high.
70 Magnification

Figure 72. Typical Radif in Outer Filament.

2.2.2 Task 2 Gage Sensitivity

The intent of the sensitivity testing was to evaluate the gage performance under conditions of temperature and strain that would be encountered during engine test. The primary areas of investigation were selected based on experience in evaluating the performance of Karma and other nickel-chromium alloys. They are: 3.2.2.1 - Gage Factor and Postheat Treat Stabilization, and 3.2.2.2 - Effects of Long Term Exposure.

Gage fabrication and application techniques used in these tests were those that were developed in Task 1 during early fatigue testing. The details of these techniques are provided in Section 4.0. Test equipment (such as test beams, test machines, signal conditioning and indicators) and test methods as well as data handling techniques are discussed in Section 5.0.

2.2.2.1 Gage Factor and Postheat Treat Stabilization

As with Karma, it was believed that Moleculoy gages after application would require a heat treat to stabilize their performance characteristics, especially the Candidate 2 applied gage because of the changes in gage resistance that are caused by bombardment of alumina. In general, during the fabrication of the gages, the nominal gage resistance of the nonflattened gage is about 195 ohms. After flattening, gage resistance drops below 170 ohms. The gages receive a heat treatment at 1050° F for 2 hours and the gage resistance increases to about 200 to 210 ohms. The bonded resistance of the gage when applied with all-FSA usually falls again to below 200 ohms. Exposure to temperature again causes an upward shift in resistance and a change in gage factors. Changes in gage resistance have been observed with the Candidate 1 (composite-ceramic) applications, but these usually are small.

The level of the postapplication heat treatments selected is dictated by the hardware limitations. Those that were selected were 830° F for 2 hours for use not to exceed 800° F; and a 1050° F 2 hour treatment for stage temperatures not exceeding 1000° F. For higher temperature use, the heat treatment required if any, would be determined by tests.

830° F Heat Treat

Two gages of each candidate were applied to sensitivity beams of U-700. Each beam was installed in the High Temperature Gage Factor Facility (Section 3.0) and heat treated for 2 hours at 830° F. The gages were then cycled between room temperature and 800° F at 1000 microinches/inch peak-to-peak. Figure 73 shows the average gage factor at temperatures to 800° F. Included is the resistance change in ohms caused by the 2-hour soak and the zero offset. While successive temperature cycles caused sensibly no shifts in resistance, there was a slight upward shift in gage factor indicating a soak time of 2 hours was marginally acceptable.

1050° F Heat Treat

The beams were then treated at 1050° F for 2 hours and again tested at 1000 microinches/inch on successive cycles to 1000° F. Figure 74 shows the average results of gage factor and resistance from the gages. As can be seen, the effect of heat treatment at the higher temperature has caused the gage factor to rotate significantly. Variations of resistance and gage factor on successive cycles were considered insignificant even after a 10 to 15 minute dwell time at each temperature to obtain data.

1200° F Heat Treat

The beams were heat treated at 1200° F and tested at 1000 microinches/inch over the temperature range from room temperatures to either 1200° or 1500° F. More data were collected at the 1200° F point because it covers the range of current compressors. Table 13 shows the mean and standard deviations of the candidates and the number of data points included. Test data from fatigue tests have been included.

The average gage factors are plotted in Figure 75. The gage factors of the composite-ceramic gage starts out slightly lower than the FSA gage and diverges rapidly above 1000° F, well above the recommended maximum use temperature discussed in Section 3.2.1 Task 1. It was also observed during testing that a downward shift in gage factor and gage resistance occurred after successive exposures to 1500° F. This contributes to the large standard

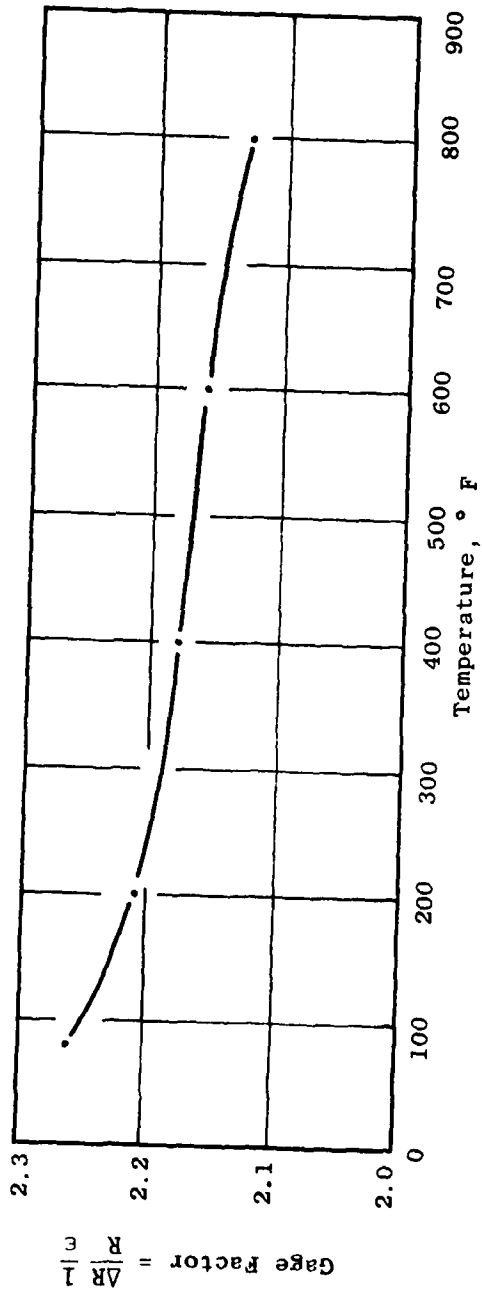
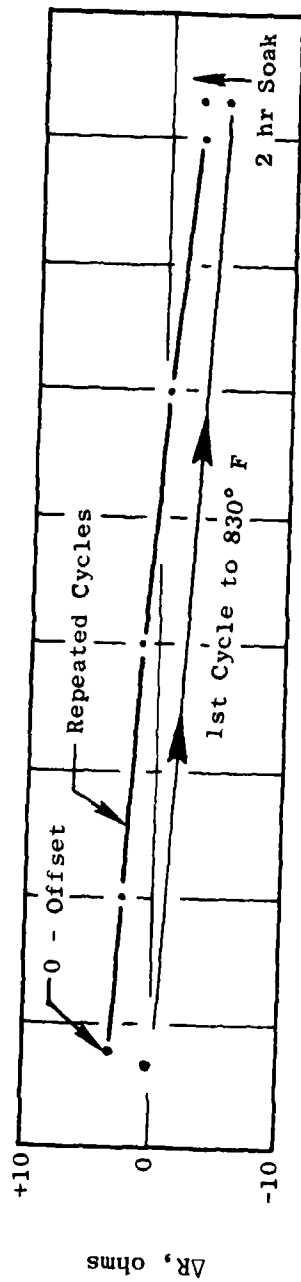


Figure 73. Average Gage Factor and Resistance Versus Temperature 830° F Postheat Treat Candidates 1 and 2.

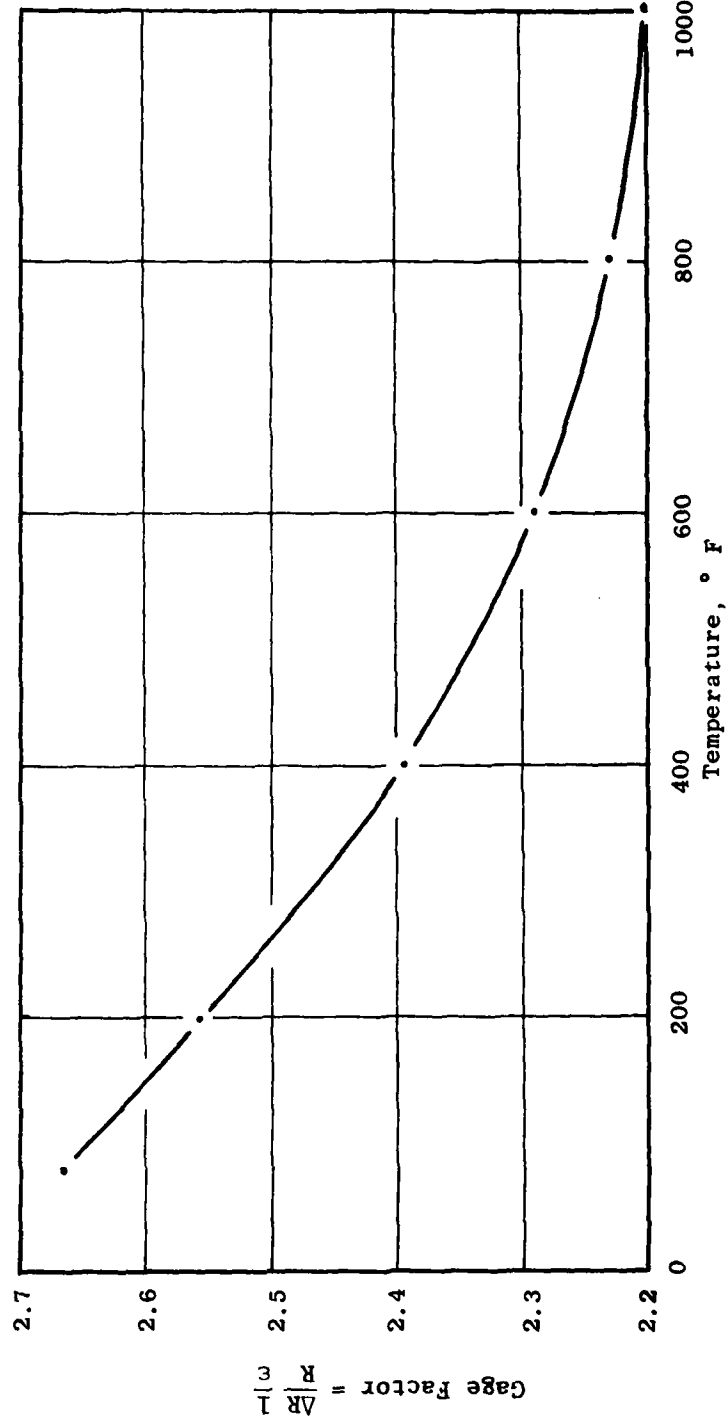
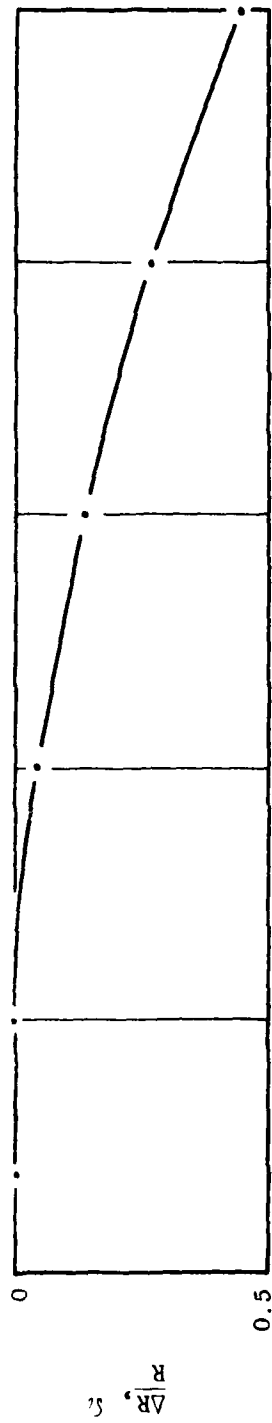


Figure 74. Average Gage Factor and Resistance Versus Temperature
1050° F Heat Treat Candidates 1 and 2.

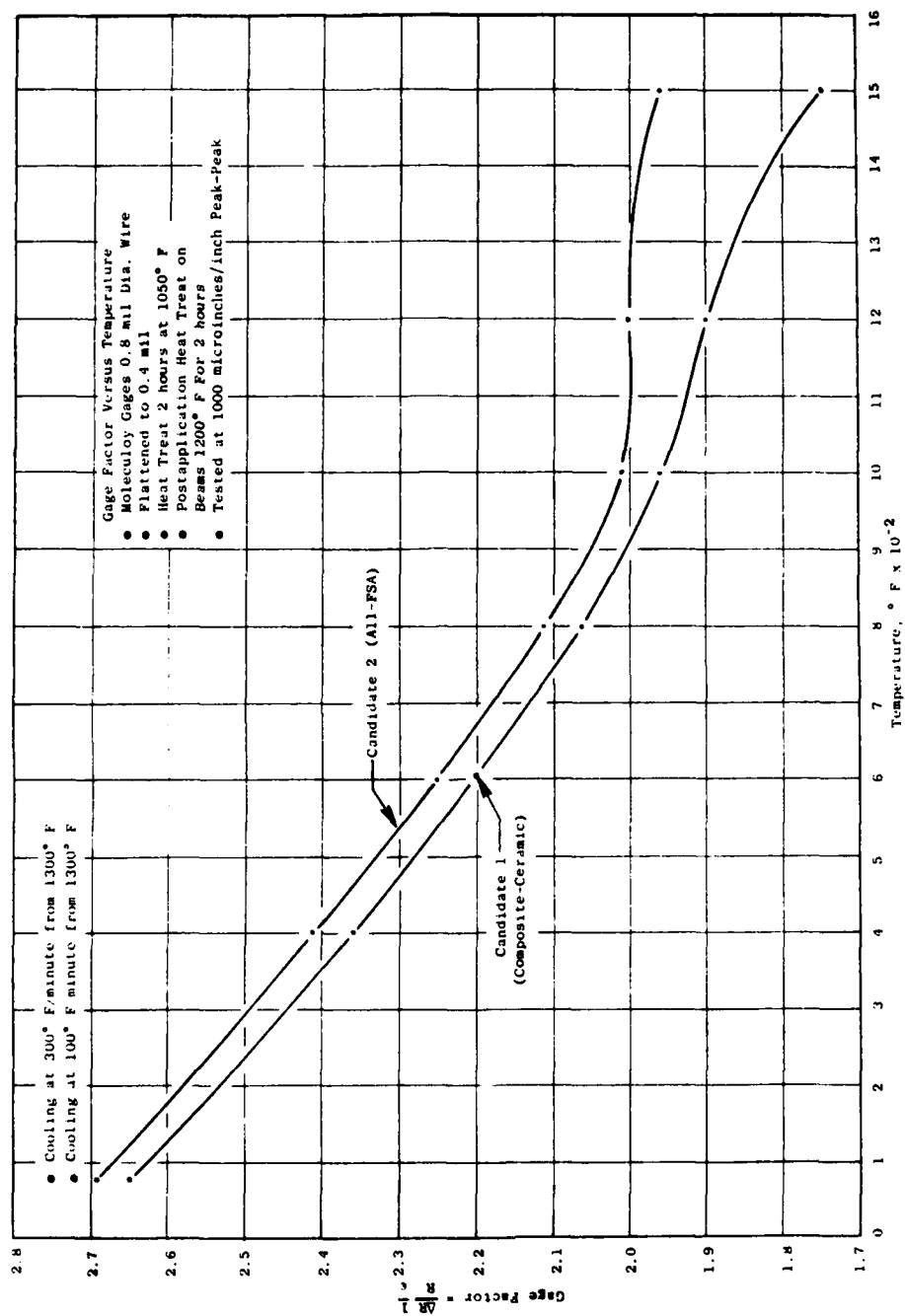


Figure 75. Comparison of Average Gage Factor for Two Candidate Gages.

Table 13. Average Gage Factor and Standard Deviations From 10 Gages Tested.

Test Temp., ° F	Candidate 1			Candidate 2		
	Mean	SD	No. Points	Mean	SD	No. Points
80	2.65	0.10	45	2.69	0.04	30
400	2.36	0.08	10	2.41	0.08	10
600	2.22	0.10	20	2.25	0.08	12
800	2.06	0.08	10	2.11	0.08	10
1000	1.96	0.07	46	2.01	0.05	22
1200	1.90	0.10	66	2.00	0.04	61
1500	1.75	0.03	36	1.96	0.08	8

deviations in the table, but the major part is from starting gage factor differences which were believed to be associated with differences in resistance of the hand-wound gages. If initial gage factor data could somehow be normalized using gage resistance, the large deviations might be reduced.

To investigate this possibility, the data from three successive cycles of two all-FSA gages that were tested from 80° to 1500° F were selected. The gages had been heat treated 2 hours at 1050° F. The initial gage factors were 2.71 and 2.61 with resistance values of 198.4 and 203.0 ohms, respectively. A gage normalizing function was determined. It was found that multiplying average gage factor of these two gages by the function (Average Resistance/Gage Resistance)² would very nearly determine the test gage factor of the different gages at temperature.

$$GF_{AVG} = \frac{2.71 + 2.61}{2} = 2.66$$

and $R_{AVG} = 200.7$ ohms

For the two gages, the calculated normalizing functions were 1.0233 (198.4-ohm gage) and 0.9775 (203-ohm gage). Multiplying the average gage factor of 2.66 produces individual gage factors of 2.72 and 2.60, respectively. Moreover, the downward shift after each cycle can also be corrected using the ratios of resistances at the start of each cycle. The ratio is the resistance at the start of a cycle divided by the resistance at the start of the first cycle.

Table 14 (Page 133) shows the original data and the values determined by normalizing and adjusting gage factor based on resistance ratios. The normalizing function used to correct the Cycle 1 average gage factor to individual gages provides excellent agreement with tested values. The correlation of actual values of gage factor with those determined by resistance ratios is not quite as good, but the average error of both gages of Cycles 2 and 3 is only 1.06% with a standard deviation of 0.78%.

The data from a second pair of FSA applied gages that were tested from room temperature to 1200° F on the same beam were analyzed for normalizing using the same function. The gage factors were 2.71 and 2.76 with gage resistances of 209 and 207.9 ohms, respectively. Using the normalizing functions operating on average gage factor (2.735) produced individual gage factors of 2.72 and 2.75. However, combining the two sets of data just analyzed, normalizing could not be achieved with the four gages. This suggests that normalizing can be accomplished only on gages exposed to the same temperatures and, perhaps, in the same way. Although it was not determined, it is believed, based on the stability of gage factor from room temperature to 1000° F, that normalizing the gage factors after a postapplication heat treat of 1050° F using final resistance measurements, that gage factors would repeat regardless of the temperature range of exposure up to a maximum temperature of 1000° F.

In Figure 75, the effect of varying cooling rates on room temperature gage factor for the all-FSA gage is shown. These cooling rates, which certainly do not approach those that could exist in an engine, were achieved by forced-convection cooling using air. The change in room temperature gage factor for the 100° F/minute rate for the gage tested was 2.72-2.66/2.66 or 2.3%; however, gage resistance changed by 195.4-204/204 or -4%. At the 300° F rate, the changes are 3.4% and -5.5%.

2.2.2.2 Effects of Long Term Exposure

The effect of long term exposure on gage factor was obtained from gages that were being tested for fatigue strength. Plots of the gage factors are shown in Figure 76 for 16 test hours at 1200° F and for 9 hours at 1500° F.

Table 14. Gage Normalizing and Cycle Correction Based on Starting Resistances.

	Temp., ° F	Gage 1			Gage 2			GF Avg. X	Norm. Funct.
		R Ω	GF Act	GF Norm	R Ω	GF Act	GF Norm		
Cycle 1	80	198.4	2.71	2.72	203.0	2.61	2.60	2.66	Gage 1
	200	199.4	2.60	2.59	204.0	2.47	2.47	2.53	1.0233
	400	200.0	2.45	2.45	204.6	2.32	2.34	2.39	
	600	200.2	2.29	2.28	204.8	2.17	2.18	2.23	Gage 2
	800	200.2	2.16	2.15	204.8	2.03	2.05	2.10	0.9775
	1000	200.2	2.08	2.07	204.6	1.95	1.97	2.02	
	1200	197.9	2.09	2.08	202.0	1.97	1.98	2.03	
	1400	194.2	2.09	2.10	197.8	2.01	2.00	2.05	
	1500	191.3	2.05	2.06	194.8	1.96	1.96	2.01	
Ratio =		$\frac{195.9}{198.4}$	X	$\frac{200.3}{203}$	X				
Cycle 2	80	195.9	2.66	2.69	200.3	2.56	2.57		
	200	196.6	2.58	2.56	201.1	2.45	2.44		
	400	197.4	2.43	2.42	201.8	2.29	2.31		
	600	197.7	2.28	2.25	202.2	2.14	2.15		
	800	197.7	2.15	2.12	202.2	2.02	2.02		
	1000	198.4	2.08	2.04	202.9	1.93	1.94		
	1200	196.9	2.08	2.05	201.2	1.94	1.95		
	1400	192.9	2.09	2.07	198.8	1.96	1.97		
	1500	190.0	2.05	2.03	193.8	1.94	1.93		
Ratio =		$\frac{195.5}{198.4}$	X Cycle 1	$\frac{200.0}{203.0}$	X Cycle 1				
Cycle 3	80	195.5	2.63	2.68	200.0	2.53	2.56		
	200	196.3	2.56	2.55	200.8	2.42	2.43		
	400	197.0	2.42	2.41	201.5	2.27	2.31		
	600	197.3	2.26	2.25	201.7	2.10	2.15		
	800	197.4	2.14	2.12	201.9	1.99	2.02		
	1000	198.3	2.04	2.04	202.9	1.90	1.94		
	1200	196.8	2.03	2.05	201.1	1.90	1.95		
	1400	192.8	2.04	2.07	196.6	1.91	1.97		
	1500	190.1	2.03	2.03	193.7	1.89	1.93		
Cycles 2 and 3		Avg. Error = 0.0106 or 1.06%							
Summary:		SD = 0.0078 or 0.78%							

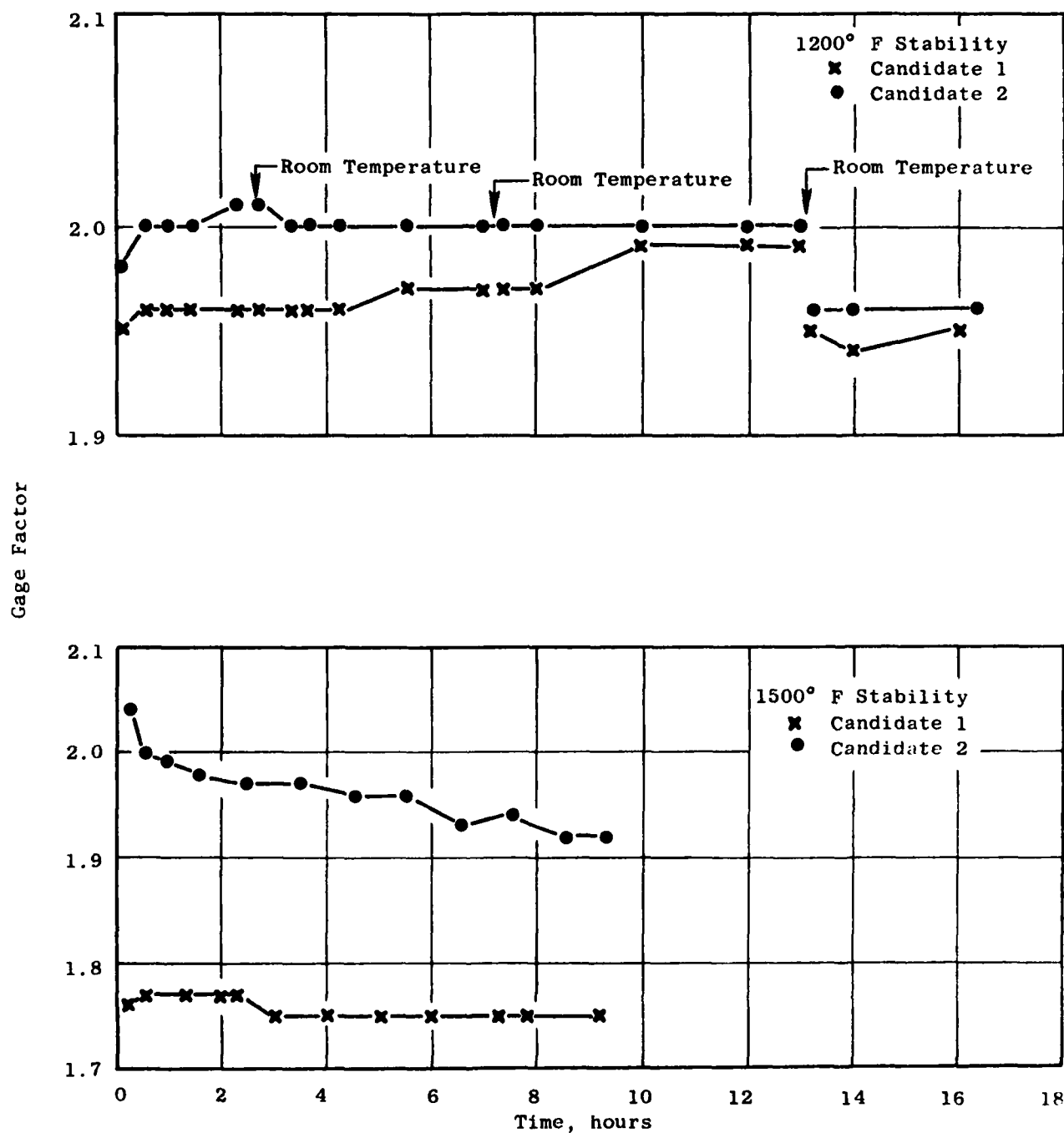


Figure 76. Long Term Stability at 1200° F and 1500° F for Candidates 1 and 2.

The change in gage factor of both candidates at the 1200° F level after 13 hours, when the beam was returned to room temperature to postmortem a failed gage, is believed to be from reinstallation into the Fatigue Test Machine. The gradual increase in the gage factor of the composite-ceramic structure is no doubt real. It cannot be explained at this time. At the 1500° F test level, the rate of change of gage factor is about 0.5% per hour of exposure for Candidate 2. This could be oxidation. The gage factor of the composite gage remained essentially constant. This ties in with oxidation studies in Phase I that Denex 2 cement provides better protection of the Moleculoy wire at both the 1200° and 1500° F temperature level (Tables 3 and 4).

2.2.2.3 Conclusions and Recommendations

To achieve maximum accuracy, all gages should be normalized regardless of the heat treat cycle used. Although untried for gages heat treated at 830° and 1050° F (for use to 1000° F), it is believed the estimated normalizing function will apply. If it is not possible to measure gage resistance after heat treating, the spread in starting gage factor for the composite gage could be as great 12% while for the FSA gage it would be 5%. Some of this difference in the composite gage may be caused by variations in gage bonding using ceramic cement. A proposed technique of measuring gage resistance after heat treat is to complete both applications on the blade without removing the tape strip over the interface ribbon. Remove the tape and heat treat at the prescribed temperature (830°, 1050° or 1200° F). After the part cools, measure gage resistances at the ribbon. Then, mask the part and flame-spray alumina over the tape ribbons. This can be done for both structures. The lead splice and leads can then be applied to the gage.

Recommended heat treat time is 4 to 6 hours for 830° F. This is based on slight upward shifts in gage factor after a 2-hour soak. The heat treat time for both a 1050° and 1200° F soak is 2 hours; although, at the 1200° F level, less than 1 hour should stabilize the gage.

Gages tested to 1500° F should be corrected for gage resistance shifts. The long term drift in gage factor determined for one all-FSA gage was 0.5% per hour but more testing would be required to establish statistical data that could be used with some confidence.

From an accuracy viewpoint, in the absence of normalizing the gage factor, it is concluded the all-FSA is the better gage over the complete range to 1300° or 1400° F where gage oxidation would become a factor; most compressors do not exceed 1230° F.

2.2.3 Task 3 - Effect of Applications on Small Blades

The application of high temperature strain gages using flame-spray alumina or composite-ceramic techniques to a compressor airfoil influences its elastic response to aeromechanical forces. The effect of such instrumentation upon the measurement obtained may be significant.

The effect arises from two separate mechanisms. First, on an instrumented airfoil, the foil and strain gage application participate as a total load bearing structure. The application introduces an effective change in section modulus, a change in overall internal damping, or of other combinations. Second, the application of the gage changes the effective shape of the airfoil and increases the surface roughness, such that turning effects of the flowing air and boundary layers on the airfoil are somewhat modified. Thus, the aerodynamic inputs to the instrumented airfoil must be expected to display certain differences from those experienced by an uninstrumented airfoil.

The effect of the first mechanism, that is, the change in mechanical properties of an airfoil promoted by gage applications, can be tested in the laboratory. The effect of airflow differences on the response of the instrumented airfoil cannot be determined in the laboratory because it is difficult, if not impossible, to meaningfully duplicate the flow conditions existing in an operating engine.

The purpose of this task, therefore, was to determine the differences between the mechanical response of small airfoils when equipped with the two different candidate gage structures. Only the fundamental mode of vibration was considered.

2.2.3.1 Testing and Test Results

There were two different tests conducted to compare the differences of the candidate gage structures on fundamental frequency, strain distribution,

and damping. The first was to compare damping effects; the second, to determine strain distribution changes. Frequency changes between uninstrumented and instrumented blades were obtained in both tests.

Damping Studies

In these studies to determine damping differences between an uninstrumented and instrumented blade, it is important that no extraneous variation in damping be introduced between the two tests. Such variations can be caused by the fixturing used to support the blade, the clamping force that holds the blade in the fixture, and even the equipment used to excite the fundamental frequency of the blade.

The technique that was recommended for these tests was to braze the blade to a steel block having at least 600 times the mass of the blade. The dovetail of the blades was reworked so that the braze line would be at the center of the pressure face of the dovetail as shown in Figure 77.

The blade configurations selected for the damping tests were:

- F101 Stage 6 Titanium
- F101 Stage 9 Inco 718
- J85 Stage 6 Titanium
- J85 Stage 9 Inconel
- J85 Stage 9 Titanium.

Two each of these blade designs were reworked and brazed to the steel blocks. The blocks were sized to have 600 times the weight of the heaviest reworked blade. F101 Stage 9 weighed 5.87 grams and all blocks weighed about 3520 grams or about 7.75 pounds.

Each of the blades was subjected to damping tests before instrumenting. Figure 78 shows the electromagnet drive system and recording schematic. A small magnetic shim was cemented to the tip of each titanium blade in order to couple the blade and magnet. The position of the magnet, the distance from the shim, the location of the crystal pickup, and the ammeter output to obtain

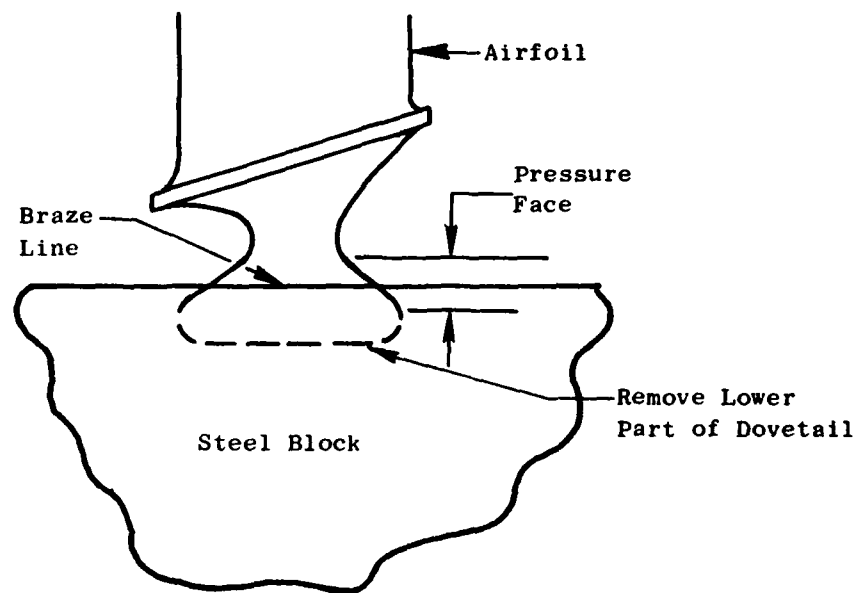


Figure 77. Typical Dovetail Rework Prior to Brazing.

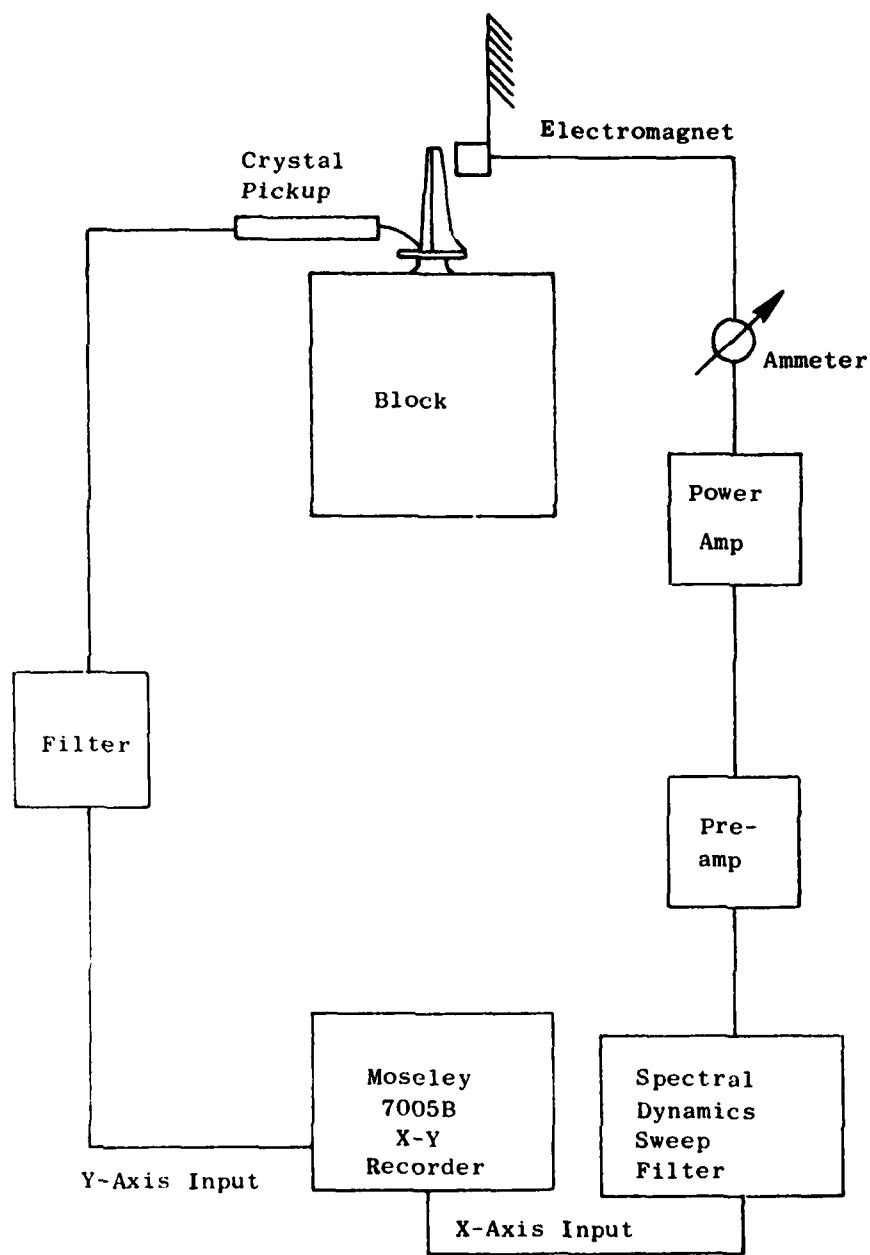
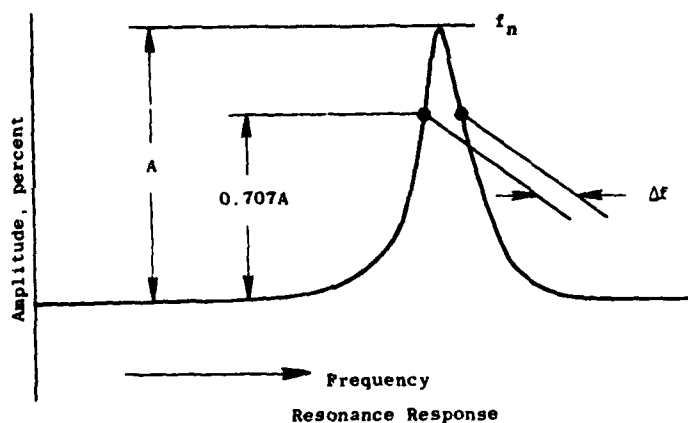


Figure 78. System for Obtaining Resonance Diagram of Blades
Electromagnetic Drive.

good response were recorded for each blade. These measurements were duplicated for tests of the instrumented blade. The bandwidth of the spectral dynamics filter was adjusted to 2 Hz. The sweep rate is variable and was adjusted to 0.2 Hz per second near resonance. A typical resonance diagram is shown in Figure 79.

The percent damping was obtained from this resonance diagram by the following method (Reference 30).



The Equation Used Is

$$\% \text{ Damping} = \frac{\pi \Delta f / f_n}{\sqrt{1 - (\Delta f / f_n)^2}} \times 100$$

Where Δf = Frequency Range at the 1/2 Power Point

f_n = Blade Frequency

After baseline data were accumulated for each blade, the airfoils were equipped with the candidate applications. The gages were not included. All other preparation steps and materials of applications were used. Odd numbered blocks of each pair of blades were equipped with the all-FSA structure. Even numbered blocks received composite-ceramic applications. Figures 80 and 81 are photographs of the instrumented blades mounted on steel blocks. The areas of application on each type of airfoil are very nearly equal for the two candidates.

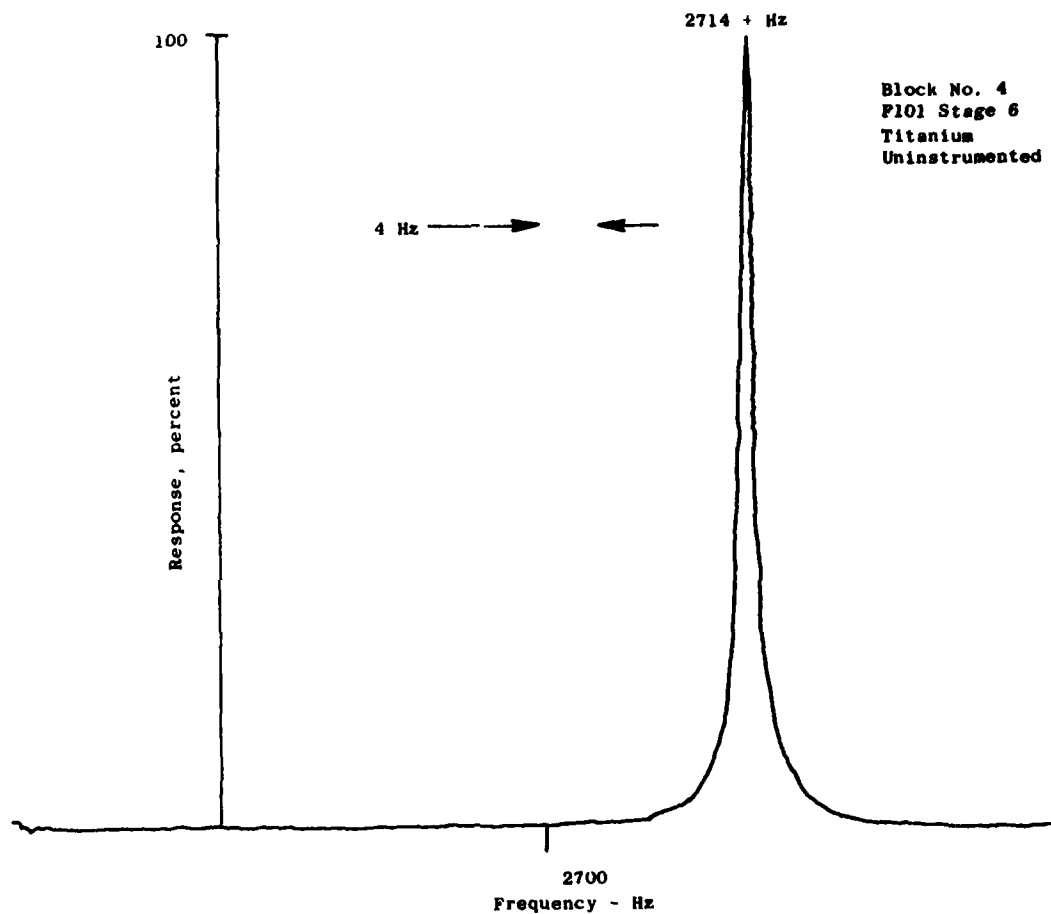


Figure 79. Typical Resonance Diagram for an Uninstrumented Blade.



NOTE: From right to left the blades are FI01 Stage 9, FI01 Stage 6, J85 Stage 6, J85 Stage 9 Inconel, and Stage 9 titanium.

Figure 80. Blocks Contain Blades and Gage Applications for Damping Studies.



Block 5
All-FSA

Block 6
Composite-Ceramic

Figure 81. J85 Stage 6 Blade Mounted on Blocks for Damping Tests.

Typical resonance diagrams of the uninstrumented and instrumented blades are shown in Figures 82 and 83. Notice in Figure 83 the nonlinear response of the all-FSA structure which was characteristic of most blades that were equipped with this structure.

Table 15 (Page 147) is a summary of the damping and frequency difference between the uninstrumented and instrumented blades.

Strain Distribution Studies

Three different blade designs were selected for these studies: F101 Stage 6 (Ti 6-2-4-2) and Stage 9 (Inco 718) rotor blades; and an A 286 blade from Stage 8 of the CF6-50 compressor. Two blades of each design were used: one for Candidate 1 applications, the other for Candidate 2. The test approach was similar to that used in the damping studies. First, the blades would be equipped with up to four foil gages and tested in the fundamental vibratory mode to obtain the relative response of the gages. After establishing the benchmark, the blades would be instrumented at one of the foil gage locations with a candidate strain gage and retested for relative response. The "before" and "after" responses would then be compared to determine the effect of the candidate gage on strain distribution.

The strain gage maps and the table of percent relative strain from the original strain distribution tests were obtained for each blade design. A typical map is shown in Figure 84. From the map and table, the engine gage location and orientation were selected on the convex side of the airfoil. Two reference gage locations on the concave side were selected. The criteria used to select the gage locations were (1) the gage must have a response of at least 30% of the engine gage response, and (2) the difference in relative strain of two successive gages on the map must be less than 10%. For example, on the map of the Stage 6 blade, Figure 84, the relative strain of Gage 7 is 42% of the engine gage location and it is 45% at Gage 8 in the first flexural mode of vibration. Thus, Gage 8 location would provide adequate response and also reduce the need for extremely precise positioning. A third reference gage was added which generally is not a location used in strain distribution mapping. Its location and orientation were on the concave side of the foil exactly opposite the engine gage location. It was assigned gage location 100.

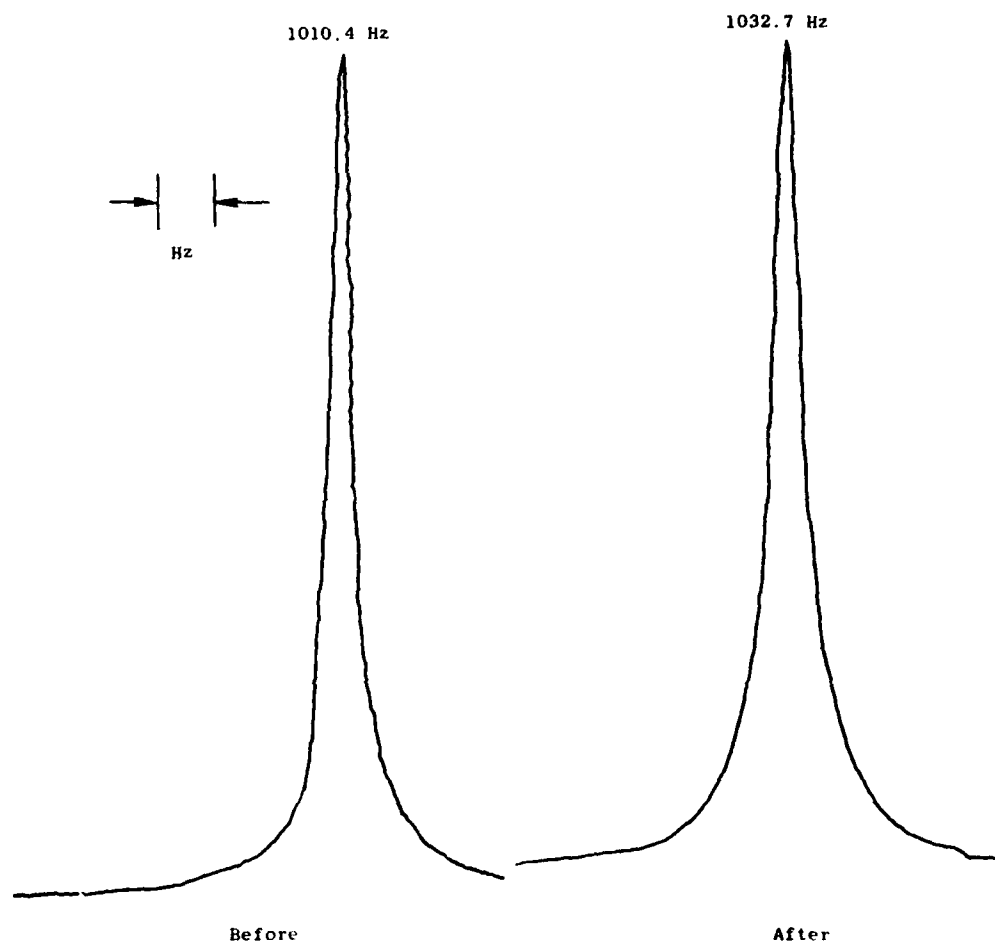


Figure 82. Resonance Diagrams - J85 Stage 6 Titanium Blade, Block 6, Before and After Instrumenting Candidate 1 - Composite-Ceramic.

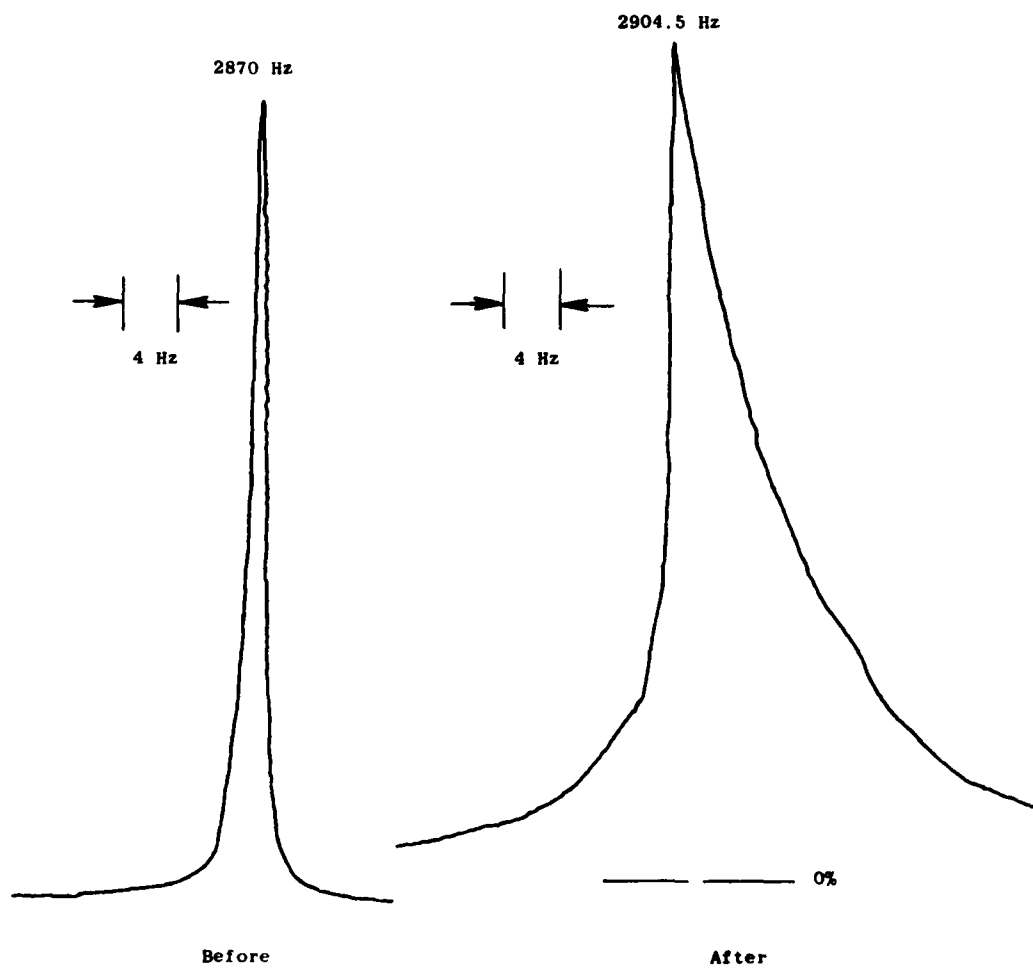
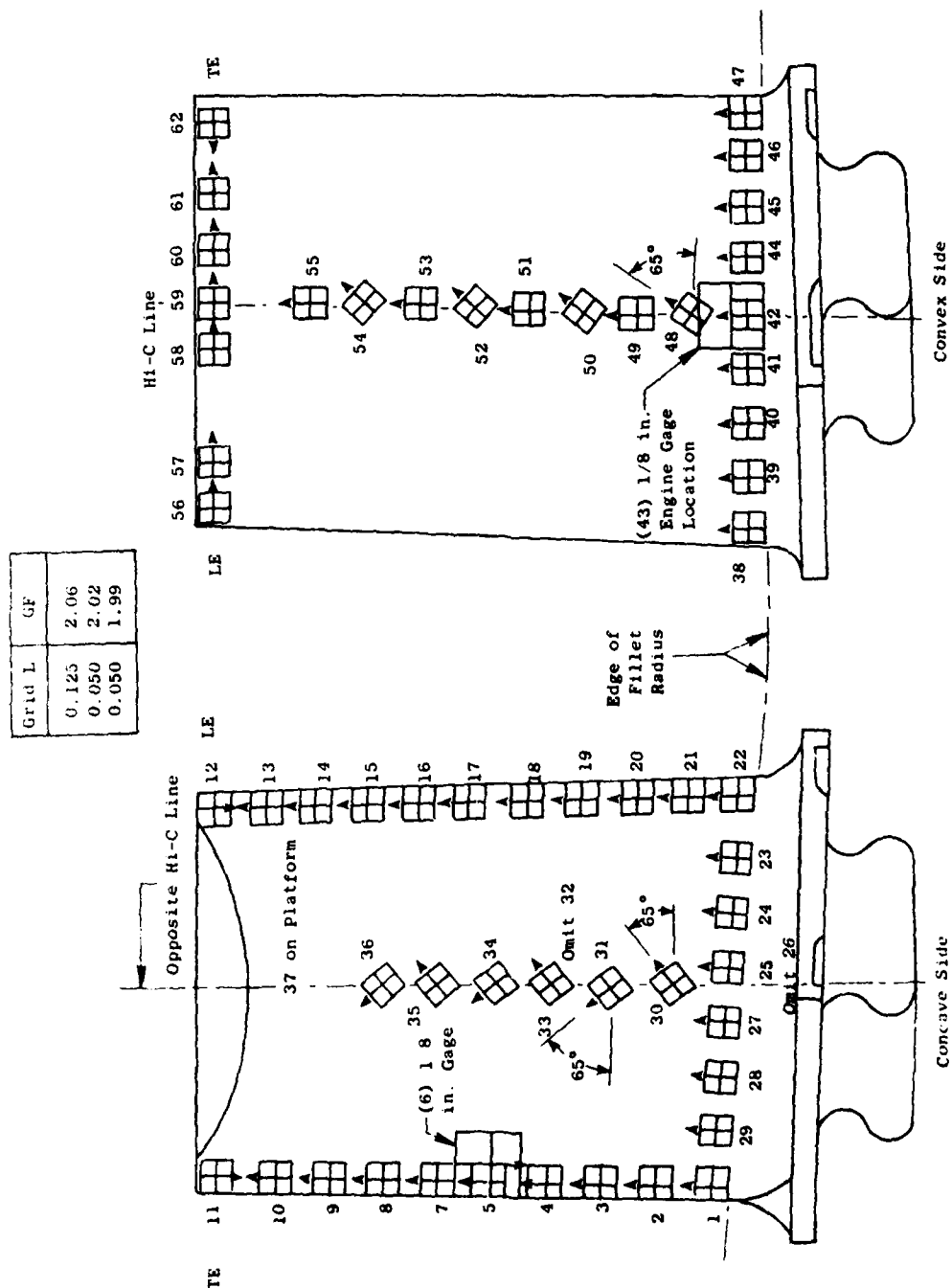


Figure 83. Resonance Diagrams - F101 Stage 6 Titanium Blade, Block 3, Before and After Instrumenting Candidate 2 - All-FSA.

Table 15. Summary of Before and After Instrumenting on Damping and Frequency of blades.

Blade Type	Block No.	Material	Gage Application	Bare Blade		Instrumented		Damp Ratio After/Bare	Δ Frequency % of Bare
				Fn, Hz	% DB	Fn, Hz	% DA		
F101 Stg. 6	4	Titanium	Composite FSA	2714	0.069	2838	0.155	2.25	SNL
	3			2870	0.070	2904	0.398	5.69	NL
F101 Stg. 9	2	Inco 718	Composite FSA	3402	0.13	3630	0.173	1.33	SNL
	1			3294	0.095	3389	0.341	3.59	NL
J85-21 Stg. 6	6	Titanium	Composite FSA	1010	0.0933	1032	0.128	1.37	L
	5			1027	0.0275	1035	0.076	2.76	NL
J85-21 Stg. 9	8	Titanium	Composite FSA	1739	0.108	1757	0.161	1.49	L
	7			1702	0.175	1715	0.311	1.78	L
J85-13 Stg. 8	10	Inco 718	Composite FSA	1701	0.133	1717	0.156	1.17	L
	9			1794	0.166	1799	0.192	1.16	NL

NL - Nonlinear Response SNL - Slightly Nonlinear Response L - Linear Response



1. All Gages Spaced 0.10 in.
2. Gages Can Either Be 0.050 SB or 0.050 AH Unless Indicated
3. Leads are to 5 ft Long of 36 Gage Copper Wire

Figure 84. Strain Gage Map, Typical Stage 6 Rotor Blade.

All blades were instrumented at the selected gage locations with foil gages applied with Eastman 910 contract cement. The centerlines of these gages were scribed on the surface of the blades with a brass awl. This would assure proper positioning when the blade was equipped with candidate gages. Gage 100 and the engine gage were 1/8-inch grids. The grid length of the other reference gages were 1/16 inch. Leads were 36-gage standard copper insulated with teflon.

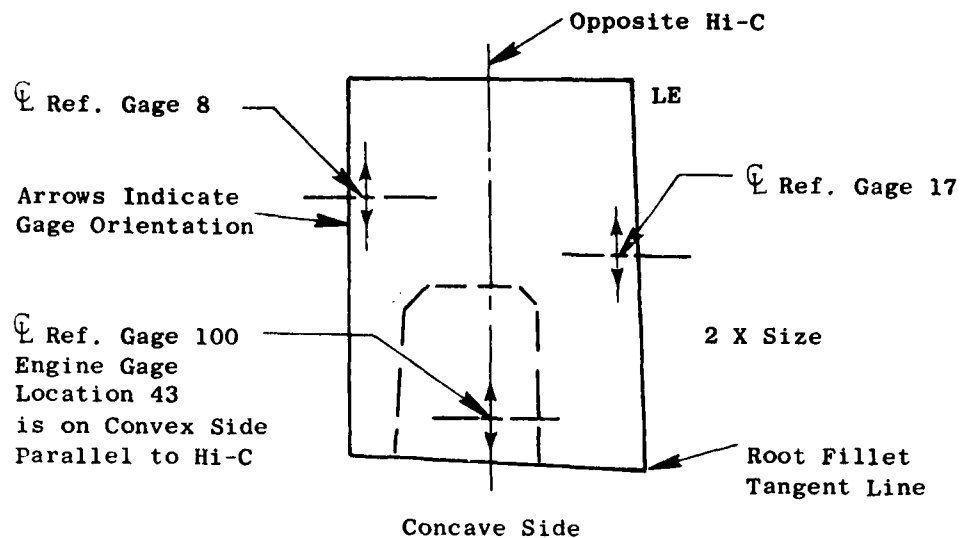
The six blades were calibrated with the standard fixturing and clamping torques used in the original strain distribution studies. A magnetic drive similar to Figure 84 was used to vibrate the blade at its resonant frequency. The first flexural frequency and indicated strain from each gage were measured. Strains were converted to percent of strain of the gage at the engine location.

After this baseline calibration, the foil gages were stripped from the blade and a Candidate 1 or 2 gage system was applied at the engine gage location on the convex side of the airfoil. It was the intent that the gage configurations on each of the two blades of a design would cover the same area. There were minor differences which are shown with the test data in later figures along with gage application thicknesses. Three new foil gages were re-applied to the concave side at the scribed centerlines. The blade was re-tested as before.

The "before" and "after" test data are summarized in Figures 85, 86, and 87. The relative size of the gage application to the size of the blade is shown in the figures.

2.2.3.2 Discussion of Results

The internal or material damping of a blade design is thought to range from about 0.015% to 0.040%. As can be seen from the summary of the damping tests in Table 15 (Page 147), the bare blade damping of the mounted blades on the blocks is much greater with a generally increasing trend as blade size decreases. Except for one case, there is significant spread between the damping of two blades of the same configuration. Both effects, the high damping and the

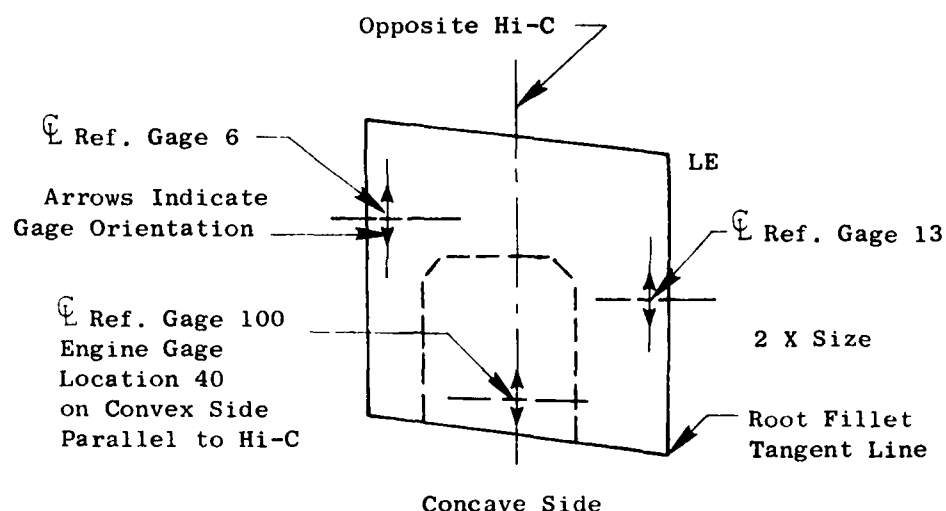


BEFORE and AFTER in the following data summary refers to the application of the candidate gage.

Gage Number	Blade S/N 98 Candidate 1			Blade S/N 614 Candidate 2		
	Relative Strain, %			Relative Strain, %		
	Before	After	%Δ	Before	After	%Δ
8	52	50	-4	59	66	+12
17	62	60	-3	62	69	+11
43*	-100	-100	0	-100	-100	0
100	90	82	-9	76	77	+1
Freq. Hz	2685	2855	6.3	2706	2854	5.4
App. Thickness, Mils		14	-		15	-
% Blade Area		23	-		21	-

* Gage 43 is the Engine Gage Location. The Minus (-) Sign Indicates the Gage Strain is Out of Phase.

Figure 85. Test Data - Effect of Candidate Gages on Strain Distribution, F101 Stage 6 Titanium Blades.

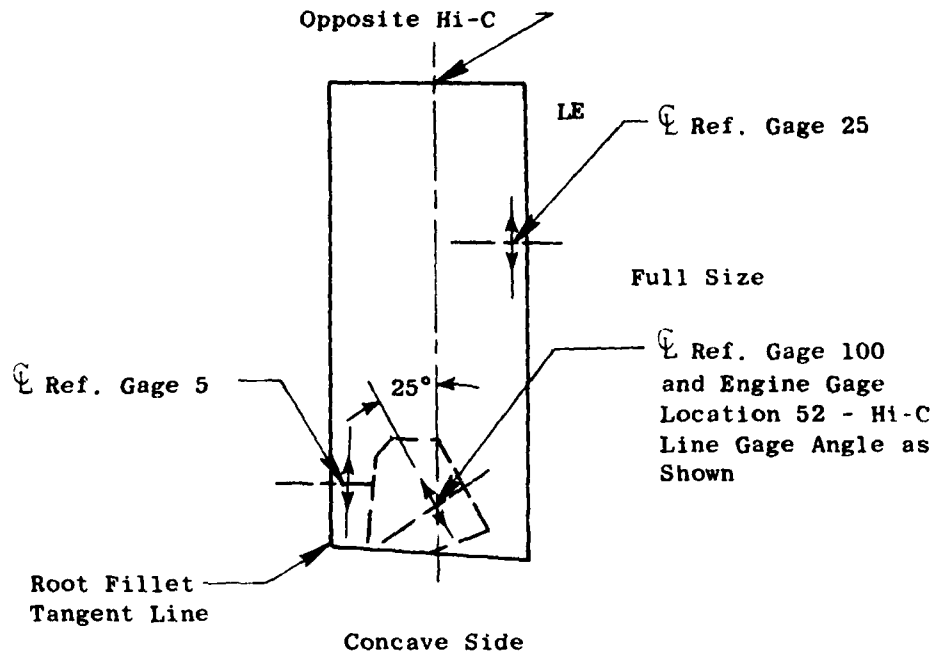


BEFORE and AFTER in the following data summary refers to the application of the candidate gage.

Gage Number	Blade S/N 60 Candidate 1			Blade S/N 64 Candidate 2		
	Relative Strain, %			Relative Strain, %		
	Before	After	% Δ	Before	After	% Δ
6	41	33	-17	35	41	+17
13	46	43	-7	43	43	0
40*	-100	-100	0	-100	-100	0
100	83	78	-6	78	76	-3
Freq. Hz	3256	3466	6.4	3201	3385	5.7
App. Thickness, Mils		12	-	-	17	-
% Blade Area		30	-	-	32	-

* Gage 40 is Engine Gage Location. The Minus (-) Sign Indicates Gage Strain is Out of Phase.

Figure 86. Test Data - Effect of Candidate Gages on Strain Distribution, F101 Stage 9 Inconel 718 Blades.



BEFORE and AFTER in the following data summary refers to the application of the candidate gage.

Gage Number	Blade S/N 361 Candidate 1			Blade S/N 362 Candidate 2		
	Relative Strain, %			Relative Strain, %		
	Before	After	%Δ	Before	After	%Δ
5	112	106	-5	112	104	-7
25	65	64	-2	73	69	-5
52*	-100	-100	0	-100	-100	0
100	58	62	+7	65	58	-11
Freq. Hz	662	673	1.7	650	664	1.2
App. Thickness, Mils		13	-	-	16	-
% of Blade Area		13	-	-	9	-

* Gage 52 is the Engine Gage Location. The Minus (-) Sign Indicates the Gage Strain is Out of Phase.

Figure 87. Test Data - Effect of Candidate Gages on Strain Distribution, CF6-50L Stage 8 A 286 Blades.

spread, can only be from the amount of braze material used to fasten the blades to the block. Because of these, the data cannot be used to determine the absolute damping changes or frequency changes introduced by the application of the candidate gage systems. It should be possible, however, to establish trends and even compare the relative damping of the applications.

The relative damping (R) is defined as the ratio of the change in damping of the blade containing the all-FSA (Candidate 2) structures to the change caused by the composite-ceramic structure (Candidate 1), or

$$R = \frac{\Delta D_2}{\Delta D_1} = \frac{(\%D_{A2} - \%D_{B2})}{(\%D_{A1} - \%D_{B2})}$$

where Damping Before (D_B) and Damping After (D_A) are obtained from Table 15. Since it is believed that the effect of the applications on the characteristics of a blade is related to the area of the application compared with the area of the airfoil, there should be fair correlation of R with % area which is $100 \times \frac{\text{Application Area}}{\text{Airfoil Area}}$.

In Figure 88, the ratio R is plotted against the average area of the applications in percent of airfoil area. (The areas were obtained from measurements from the photographs in Figures 80 and 81.)

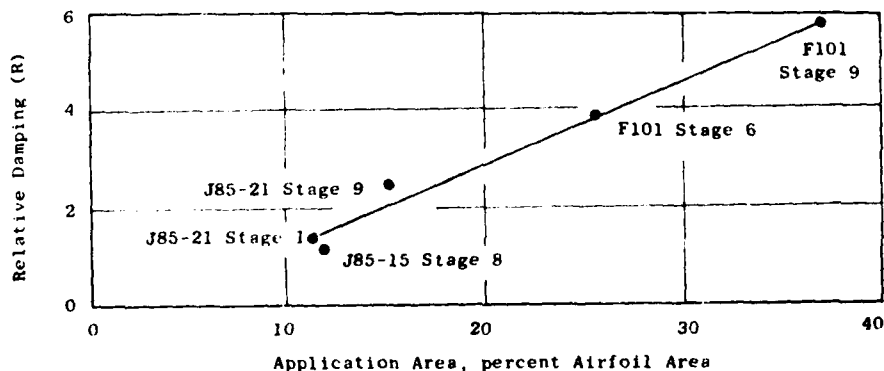


Figure 88. Relative Damping of Candidate Applications with Airfoil Size.

The close agreement between relative damping and percent of airfoil area taken up by the application indicates that the modulus of elasticity of the blade material has little to do with the amount of damping introduced by the gages.

As far as the effects of the applications on blade frequency from the damping tests, the only thing that can be said is that the composite structure introduces more stiffness which causes a greater frequency change than the all-FSA application.

The most unexpected result from testing to determine the effects of instrumentation applications on small blade airfoils was the shape of the resonance diagram of blades instrumented with Candidate 2 applications as shown in Figure 82. J.P. Den Hartog in Reference 31 describes the characteristic as nonlinear damping for a spring in which the stiffness decreases with amplitude. This is depicted in the following sketches:

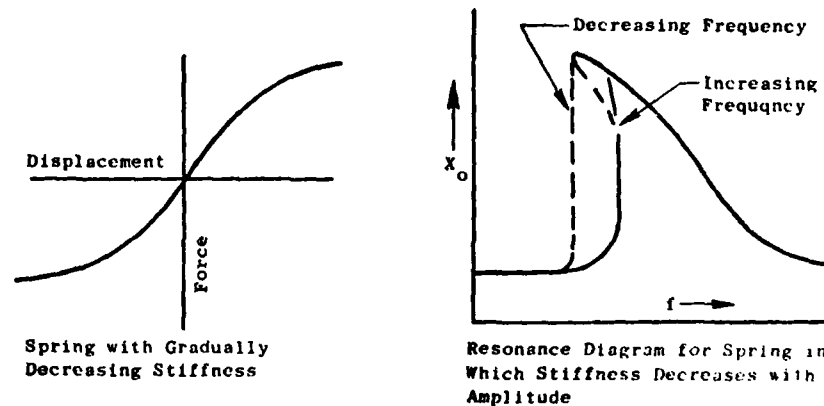


Figure 89 shows the resonance diagrams of the F101 Stage 9 blade equipped with the all-FSA application on increasing and decreasing frequency sweeps. No difference in percent of response is observed because of the method of adjusting the response span (Y-axis) for each sweep. There is a change of resonant frequency, however, and also a broadening of the response curve at frequencies greater than indicated resonance. A detailed description of this nonlinear response may be had in Reference 31.

It is not known why the all-FSA structure imposes this nonlinear, soft-spring damping upon the combined vibrating system, nor is it known why the J85-21 Stage 9 application (Table 15) exhibited linear response. It could be that the high initial damping of the bare blade, silver soldered to Block 7, either masks or overcomes the nonlinear damping characteristics.

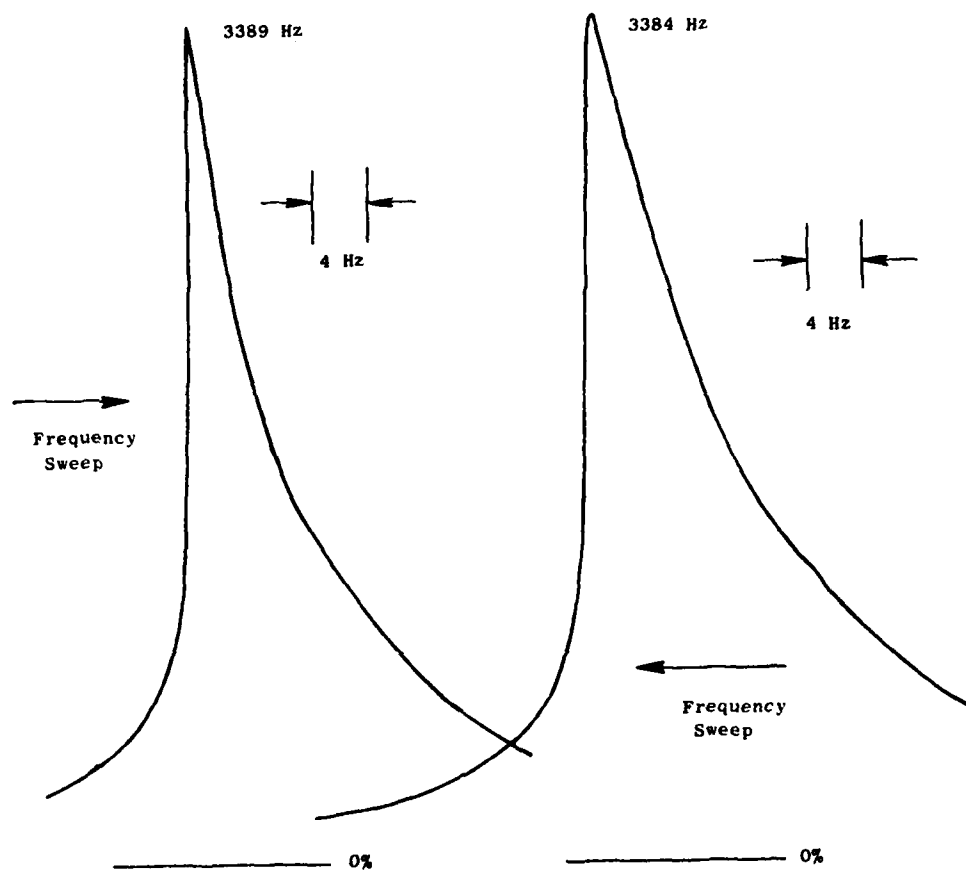


Figure 89. Resonance Diagrams on Increasing and Decreasing Frequency Sweeps, F101 Stage 9 Inconel 718 Blade, Block 1 With Candidate 2, All-FSA.

The test data shown in Figures 85, 86, and 87 can be treated in a number of different ways. In Table 16, it has been normalized using the calibration gage that exhibits the least change between "before" and "after" tests rather than normalizing the engine gage location as shown.

Table 16. Relative Strain Normalized with the Indicated Calibration Gage.

Blade Type	Gage No.	Relative Strain, %					
		Candidate 1			Candidate 2		
		Before	After	%Δ	Before	After	%Δ
F101 Stage 6	8	100	100	0	100	100	0
	17	119	120	---	105	105	0
	43*	-192	-200	+4	-169	-152	-9
	100	173	164	-5	129	117	-9
F101 Stage 9	6	89	77	-13	81	95	+17
	13	100	100	0	100	100	0
	40*	-217	-232	+7	-233	-233	0
	100	180	181	---	181	177	-2
CF6 Stage 8	5	172	165	-4	153	151	-1
	25	100	100	0	100	100	0
	52*	-154	-156	+1	-137	-145	+6
	100	89	97	+9	89	84	-6

*Engine Gage Location

Considering that the gage factor of candidate gages has an uncertainty of 5%, and allowing for some gage mislocation as well as uncertainty in reference gage factors and inaccuracies of equipment, the data are too close to conclude that one candidate gage application would be preferred over the other insofar as causing less disturbance to strain distribution. Considerably more data would be required to quantitatively establish differences between the two application techniques.

From a trend standpoint using both the test data figures and Table 16, it appears that the composite structure-blade combination tends to reduce the amplitude of the dynamic deflection or move the nodal line toward the blade tip. On the other hand, at least insofar as the Stage 6 and 9 F101 blades,

the strain distribution would indicate the participating blade-FSA application seems to increase the deflection amplitude from the fillet to the blade tip. Since the relative size of the applications are practically the same and the method of routing the leads off the airfoil are very similar for a particular foil, it is difficult to envision why this would be so unless it is tied into the soft-spring, nonlinear damping discussed before. As one would expect, the change in strain distribution appears dependent upon the gage application area relative to the airfoil size.

2.2.3.3 Conclusions

The data from these tests, although inconclusive determining absolute effects, can be used to qualitatively relate the effects of the two different candidates on the mechanical response of small blades. The Candidate 1 gage introduces more stiffness and causes a greater increase in frequency between the instrumented and uninstrumented blade than Candidate 2. The significant nonlinear damping introduced by the Candidate 2 structure over that of Candidate 1 would make it less desirable on small blades where the application area would not be small relative to the blade area. In the absence of absolute damping data, it is not possible to establish what is "small."

One would expect from the above, that on an operating compressor, blades containing the different applications would be excited at different frequencies and that the higher damped, all-FSA gage would respond over a broader frequency band.

2.2.4 Task 4 - Effect of High Rotational Speed on Application Integrity

The purpose of this task was to evaluate the mechanical reliability of the gage systems under actual compressor rotor conditions prior to the demonstration of system reliability to be conducted in Phase III.

Inasmuch as the Candidate 2 gage application system is very similar to standard applications (its mechanical performance is well-known) used in the Aircraft Engine Business Group of the General Electric Company, it was not expected that this testing would affect the mechanical integrity of the structure. However, the composite-ceramic gage application could suffer top coat loss if the bond between the flame-sprayed alumina and the Denex 2 fine-ground cement was not sufficient to overcome the centrifugal loads at high rotational

speeds. Such failures had occurred to composite-ceramic (H cement was used) applications on an F101 engine in 1974. The cause of those failures has since been determined to be the Barrier H waterproofing applied to the completed gage applications. To prevent a recurrence of top coat loss, the waterproofing of the composite-ceramic gages was changed to a light spray of fast-drying Krylon (a crystal clear acrylic) for this mechanical integrity test.

In the rotational testing of the application integrity of the gage systems, it is not necessary that gage signals be recorded. Visual inspection of applications for loss of alumina and measurements of gage circuit continuity after test is all that is required to determine the need for design and/or process change considerations.

2.2.4.1 Application Integrity Testing - F101 Engine Applications

F101 Engine 470-021/4 was approved for a piggyback demonstration. Four compressor rotor blades from Stages 3 and 9 were instrumented with gages applied using composite-ceramic techniques. Krylon was used to waterproof the gages. Four blades from Stage 8 received the all-FSA gage application waterproofed with Barrier H. Gage location (SD3 gage only), routing, and splice instructions are shown in Figures 90 and 91.

One blade from each stage was tested in the Hot-Shake Vibration Facility as discussed in Task 1, Fatigue Strength Testing, of this phase. The remaining nine blades were installed in the compressor rotor. One gage of Stage 8 and Stage 9 was routed through the rotor and connected to telemetry dynamic strain modules (Acurex Corp., Model 215-H). These gage-signals were recorded during test.

Figure 92 shows lead routing through the compressor spool of the engine.

Test Conditions and Results

The purpose of the test of F101 engine 470-021/4 was to determine the aeromechanical characteristics of the high and low pressure compressor blading

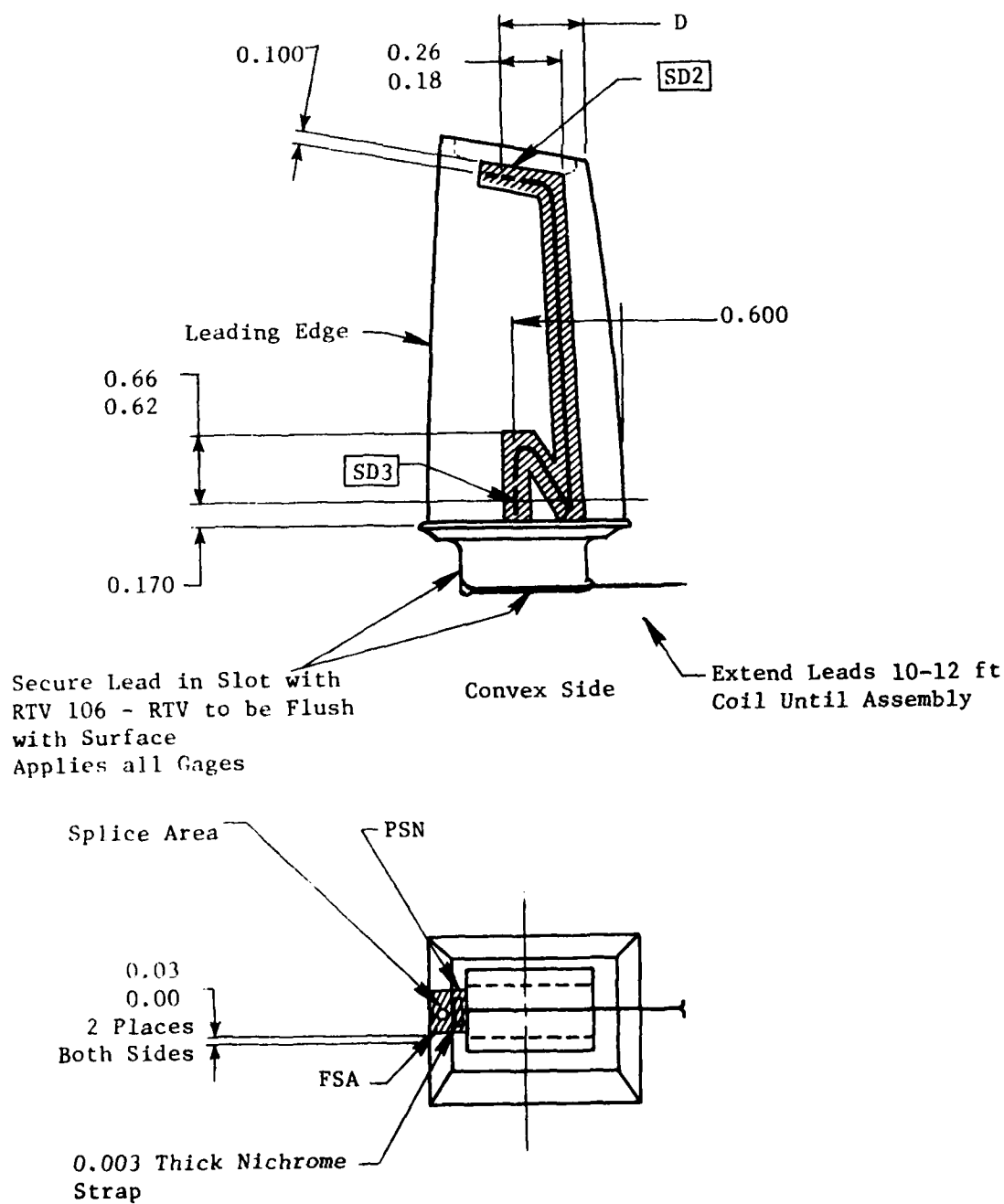


Figure 90. F101 Stage 3 Blade Instrumentation Location and Routing Instructions (Part of GE Drawing 4013246-884).

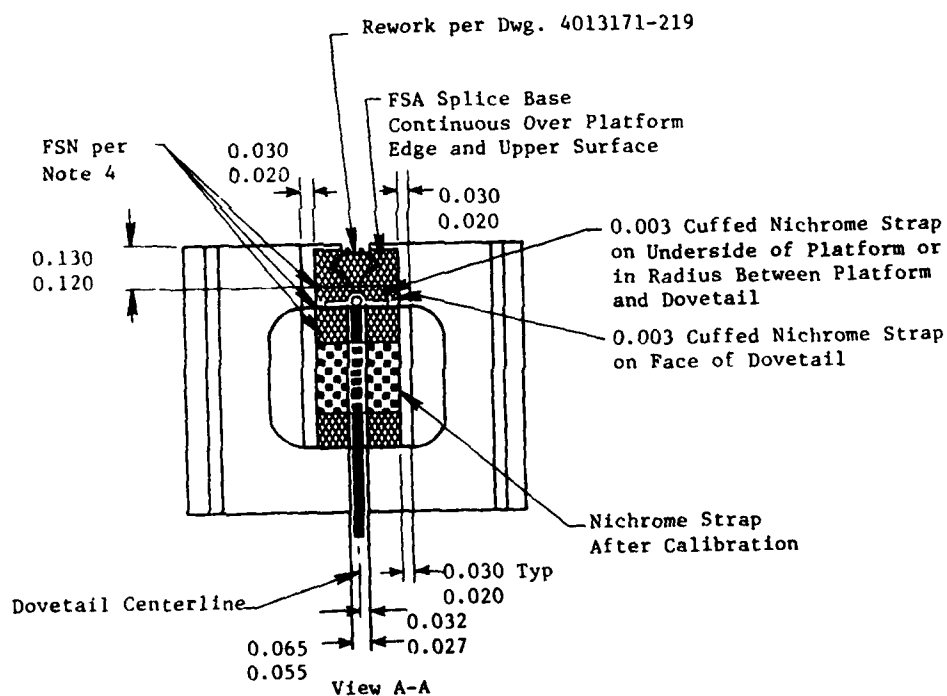
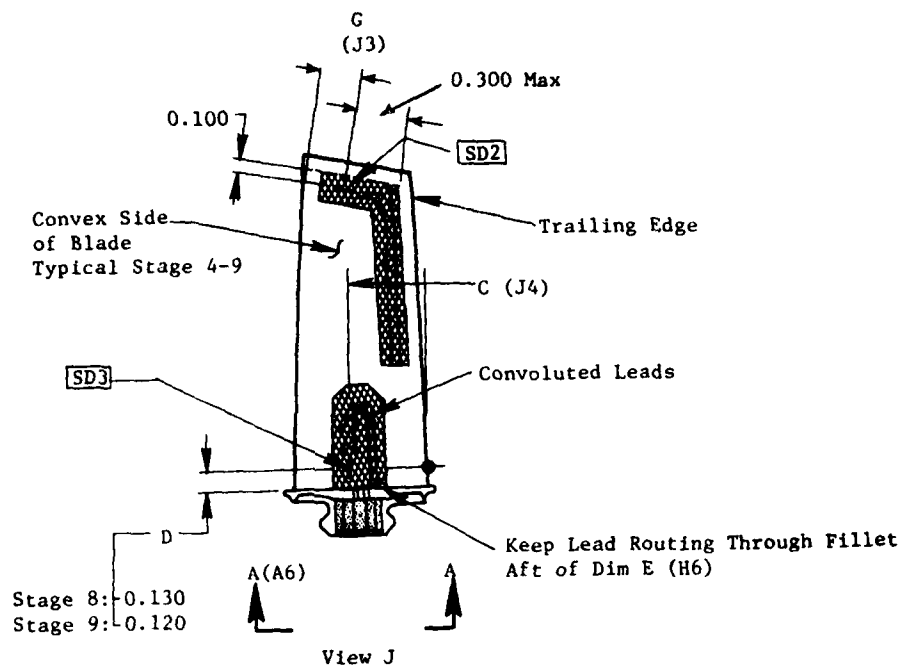


Figure 91. F101 Stage 8 and 9 Blade Instrumentation Location and Routing (Part of GE Drawing 4013246-677).

(CED configuration) over a wide range of engine operations. The test was conducted in the J-2 propulsion engine test cell of the AEDC engine test facility at Tullahoma, Tennessee. The total running time was 54:42 hours. The conditions of maximum compressor blade response and approximate temperatures encountered during the testing of stages containing the candidate strain gages are shown in Table 17. The maximum centrifugal loads exceeded 54,000 gravitational units.

Table 17. Maximum Conditions of Blade Response and Temperature During Testing of F101 Engine 470-021/4.

Stage	Blade Mtl.	Cand. Gage	Limit, %*	Temp. ° F	Strain microinches/inch DA
3	Ti8-1-1	1	21	590	900
8	Inco 718	2	18	1070	410
9	Inco 718	1	21	1170	500

*The limiting strengths (100% limits) are based on the minus 3σ material properties tabulated in General Electric's Materials Redbook.

The Stage 8 blade all-FSA gage returned data throughout the total test time. The composite-ceramic gage circuit on Stage 9 indicated failure at 44:25 hours. Two GE standard applications (FSA application with Karma gage and capacitive discharge interface weld) were both failed by 30:45 hours; one showed signs of erratic operation prior to 6:00 hours.

Visual examination of the blades in the rotor, after disassembly into components, showed no loss of flame-sprayed alumina from any of the structures. After the rotor was disassembled, only the Stage 3 blades were delivered for posttest inspection.

Gage resistance measurements of the blades were made from the Pt-10Ni leads at the edge of the blade platform.

The measurements were:

<u>Blade S/N</u>	<u>Resistance Ω^*</u>
08726	204
08735	204
09042	206

*Bonded gage reading normally range between 190 and 200 ohms. This does not include the PT-IONi leads.

Figure 93 is photographs of the gages at a magnification of 5. The view is looking down the blade airfoil to show as much as possible of the application on the platform. The dark material shown on the alumina is reddish-brown and is assumed to be iron oxide from the J2 test cell.

2.2.4.2 Application Integrity Test - J85 Engine Applications

J85-21, engine 221-010/11A, was approved for a second piggyback demonstration of application integrity. Eight Stage 8 compressor rotor blades were instrumented - four with composite-ceramic, and four with all-FSA gage systems. These gages were not routed through the rotor. Three Stage 9 blades were to be included; two of these would be connected to the slip ring for data. One of each candidate gage application was applied for readout; the third blade received a composite-ceramic application.

Figure 94 shows the routing instructions provided with the Stage 9 blades - about a 50% "guaranteed-failure" technique. An attempt to have the technique revised to give the gage system a better chance of survival was unsuccessful. The applications were completed as requested. The composite-ceramic gage assigned to the slip ring did not survive the assembly cycle.

Test Conditions and Results

J85, engine 221-010/11A, was tested in Cell A1 at the GE facility in Evendale, Ohio. The purpose of the test was to investigate stresses of the third and fifth stage rotor blades at altitude conditions as well as sea-level



S/N 08726



S/N 08735



S/N 09042

Figure 93. Stage 3 Blade Composite-Ceramic Applications - After Test on F101 Engine 470-021/4.

J85-21-010-11A

Stage 9 Rotor Instructions

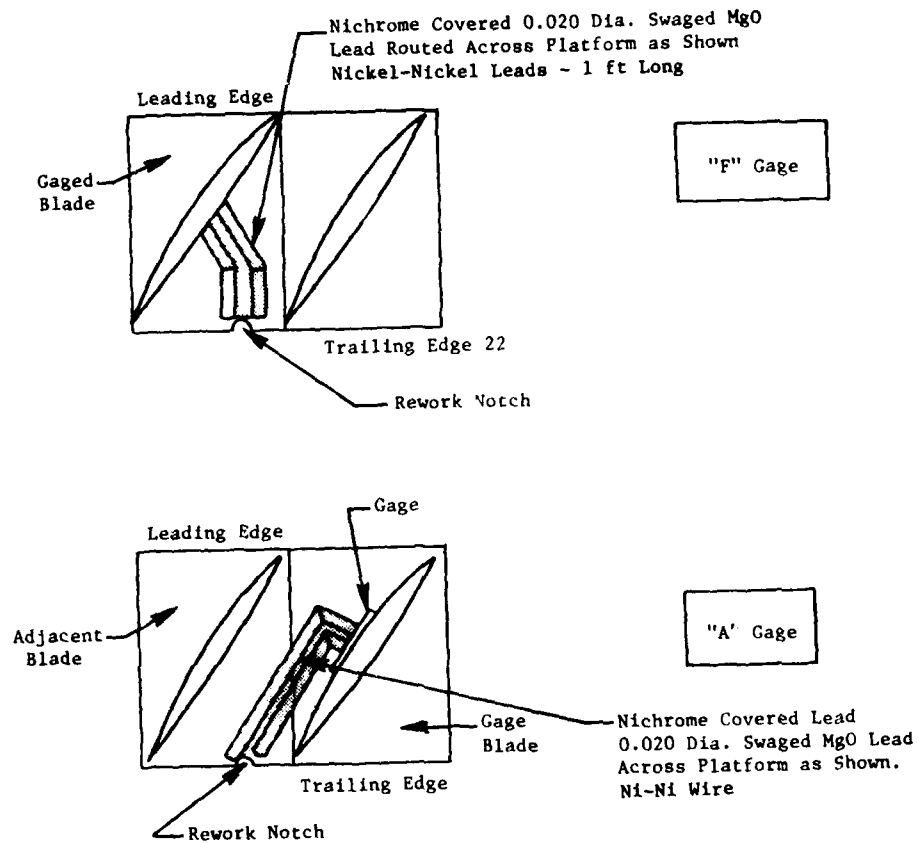


Figure 94. Gage Routing Instructions.

static inlet. The test time in Cell A1 was 37:06 hours during which data were recorded from all operable gages. It was then tested at GE-Lynn facility for 1:25 hours but not gage data were recorded.

The conditions of maximum stress, temperature and g-loads encountered during the test were:

Stage 8: 15,000 psi; 770° F, 54,000 g

Stage 9: 22,000 p .; 880° F, 54,000 g

The only Stage 9 all-FSA gage (Candidate 2) that survived the assembly cycle also survived the 38:31 hours of engine test. Four conventional or standard applications applied to the ninth stage had failed prior to the 24th test hour.

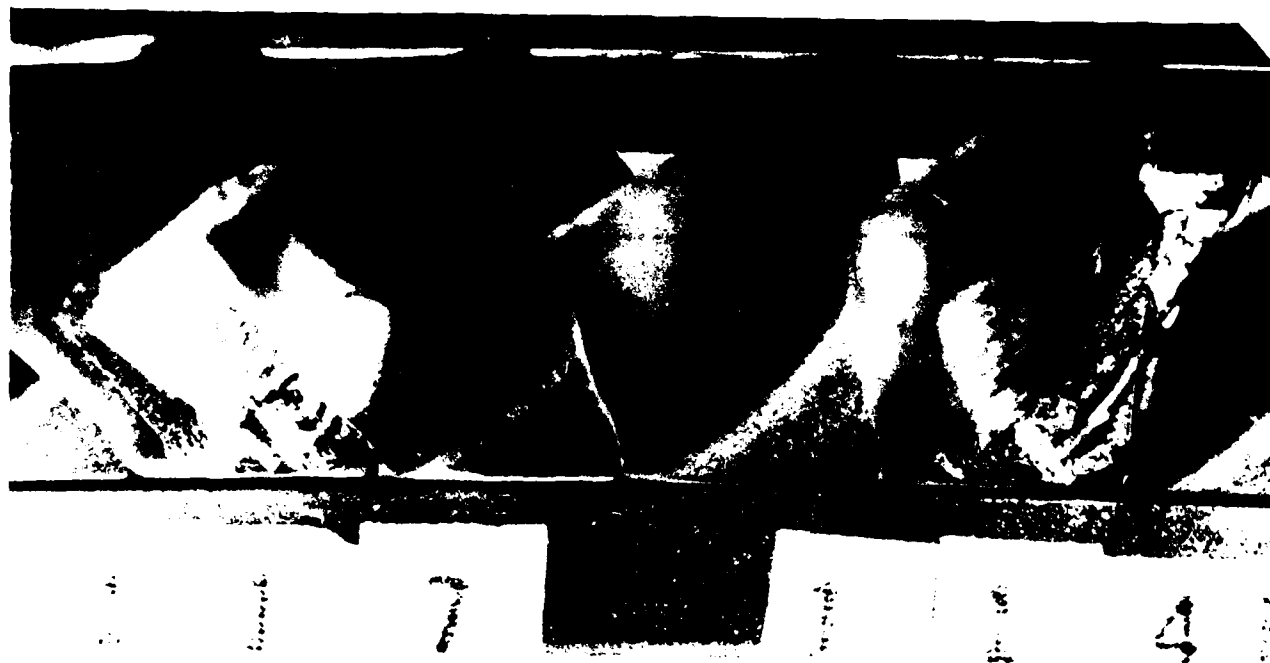
Figure 95 shows the conditions of the gage applications after the stator case was removed. Gage 114, the surviving gage, had a piece of nichrome missing from the top of the platform.

Figure 96 shows Stage 9 blades after removal from the rotor. The lead of Gage 114 was pulled off during removal of the blades from the rotor. There is no unexplained loss of alumina from the structures.

Figure 97 and 98 are photographs of Stage 8 rotor blades containing Candidate 1 gages (map locations 6, 15, 45 and 97) and Candidate 2 gages (map locations 38, 64, 73 and 87). Neither gage system shows any evidence of structure loss, although there does appear to be some slight erosion on the leading edge of the alumina top coat on all applications.

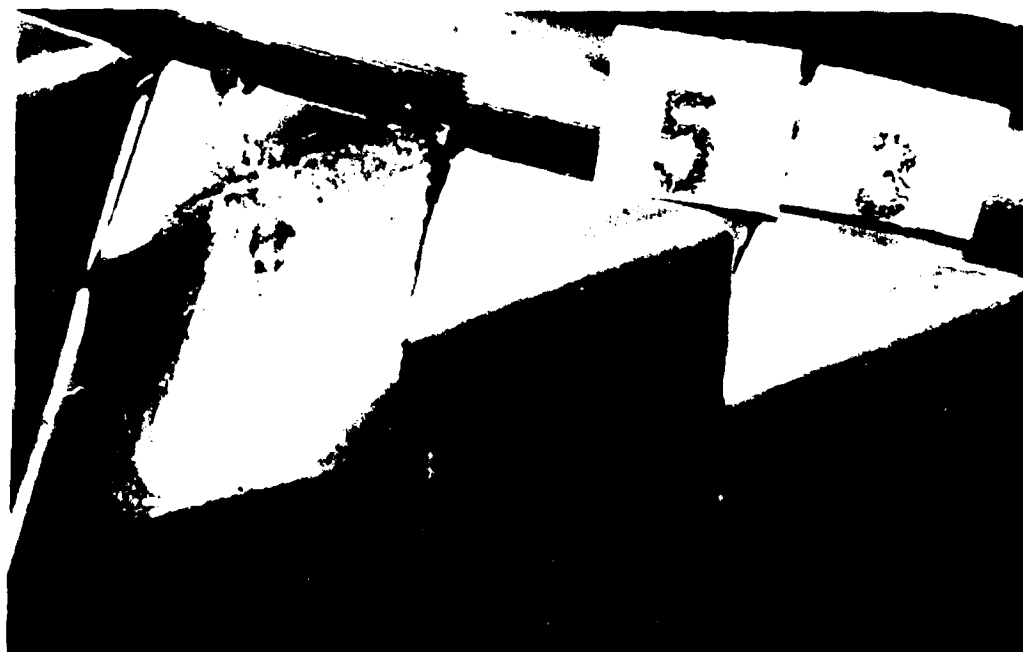
A typical splice of the intermediate leads (Pt-10Ni) to the chromel-alumel primary lead is shown in Figure 99. Some of the applications suffered the loss of the nichrome strap that holds the lead to the bottom of the blade dovetail. The composite-ceramic gage on the blade at map location 97 did not contain the strap. Continuity measurements from the ends of the leads indicated the gage was open. The alumel lead was broken at the splice. Continuity was registered across the two wires at the splice.

The results of postmortem inspection of all blades are tabulated in Table 18 (Page 172).



Failed During
Assembly

Candidate 2
Survived Test



Candidate 2
Lead Thrown
Off During
Test

Figure 95. Stage 9 Candidate Gages After Test and Before
Removal of Nichrome.

J85-21 Engine 221-010-11A

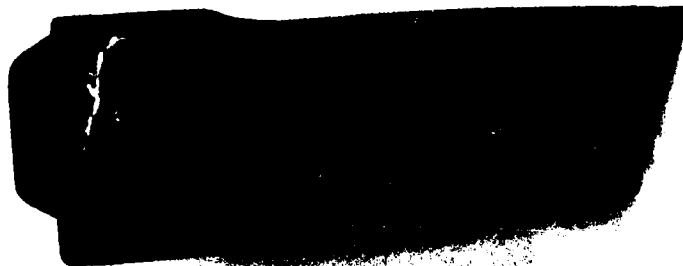
Stage 9R Blades



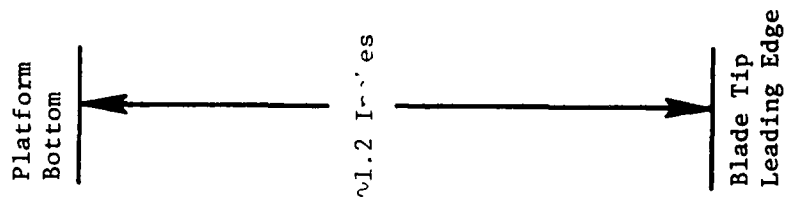
53



114



117

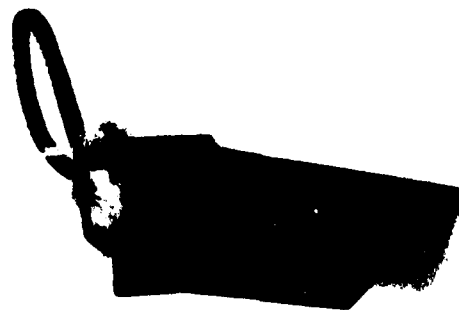


Map Locations

Figure 96. Stage 9 Blades After Removal From Rotor.

J85-21 Engine 221-010-11A

Stage 8R Blades



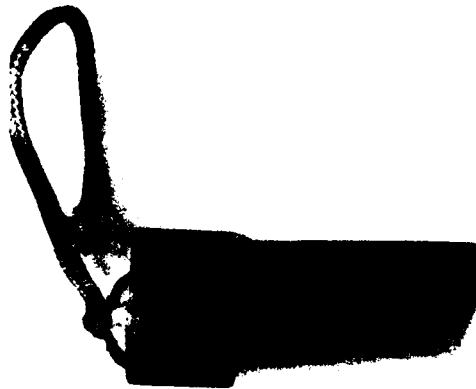
6



15



38



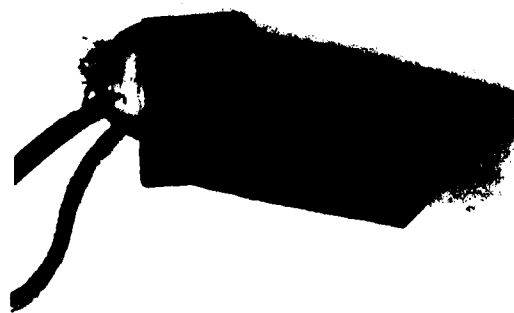
45

Map Locations

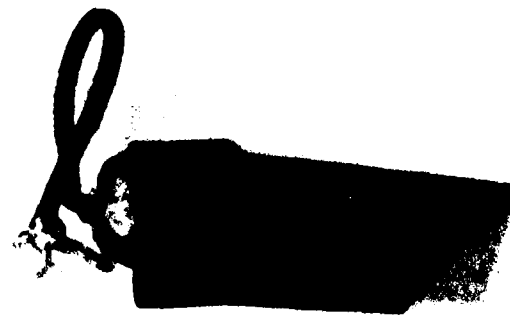
Figure 97. Stage 8 Blades After Removal From Engine.

J85-21 Engine 221-010-11A

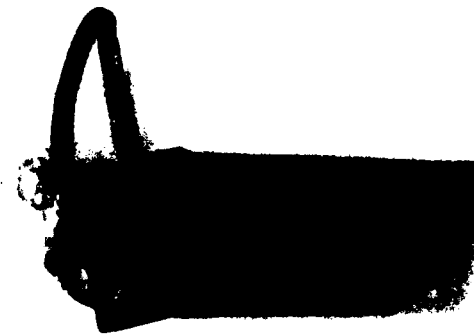
Stage 8R Blades



64



73



87



97

Map Location

Figure 98. Stage 8 Blades After Removal From Engine.

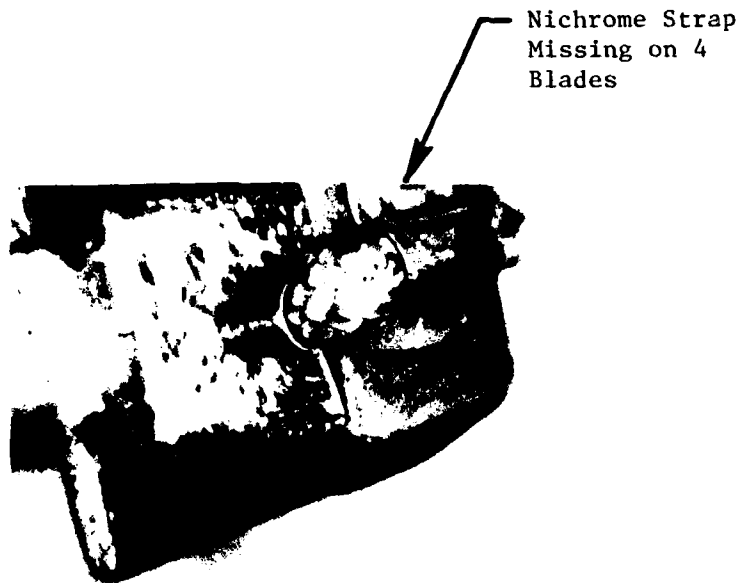


Figure 99. Typical Splice on Dovetail Post of Stage 8 Rotor Blades.

Table 18. Postmortem Results of Stage 8 and 9 Rotor Blades After 38:31 Hours on J85-21 Engine 221-010/11A.

<u>Stage</u>	<u>Map Location</u>	<u>Candidate</u>	<u>Res. Ω^*</u>	<u>Posttest Inspection Comments</u>
8	6	1	210	No Faults
	15	1	217	No Faults
	38	2	210	Missing Strap
	45	1	215	No Faults
	64	2	201	No Faults
	73	2	205	Missing Strap
	87	2	Open	Missing Strap Dovetail Open in Grid
	97	1	Open	Missing Strap Alumel Open at Splice R at Splice 213 Ω .
9	53	1	Open	0.020 Dia. Swaged Lead Gone. Pulled Part of Gage Leadout. Alumina Missing.
	114	2	201	Res. Meas. From Leadwires at Root Fillet Survived Test.
	117	1	203	Visually Intact. Res. Meas. From Leadwires at Root Fillet.

*Bonded gage resistances normally range between 190 and 200 ohms. This does not include the Pt-10Ni leads which are included in the above measurements.

2.2.4.3 Conclusions From Integrity Tests

From the F101 and J85 test results, there appears no real difference in the mechanical reliability of the two candidate strain gage systems. Neither system suffered from structure loss on the airfoil. The loss of the nichrome straps from the J85 Stage 8 dovetail was caused by improper welding techniques. Stage 9 failures could have been prevented by routing gage leads to the side of the dovetail where the splice to primary leads would be in shear.

The fact that the candidate gages that were connected to slip ring or telemetry channels survived test conditions longer than standard gages indicates they are more reliable.

2.3 PHASE III - DEMONSTRATING THE RELIABILITY OF THE TWO CANDIDATE SYSTEMS

It is necessary to test the candidate strain gage systems in the environment of an operating compressor in order to determine their relative reliability. However, it is prohibitive, from a cost standpoint, to conduct a special test to demonstrate strain gage integrity by itself. The approach selected was to "piggyback" this demonstration on an engine scheduled for a compressor rotor stress investigation.

Of course, there are a number of constraints imposed by the piggyback approach. One is the test time and operating conditions depend upon the primary mission of the engine. Another, the number of A-developing sensors approved will depend upon the confidence of the Aeromechanical Engineer in the running-reliability of the new sensors. Obviously, to instill such confidence requires demonstration of running reliability on a limited number of sensors initially.

The results of piggyback testing on F101 Engine 470-021 and J85-21 Engine 221-010, already discussed in Task 4 of Phase II, helped to increase that confidence. But it was not until testing of CF6-50 Engine 455-511 that full conviction was gained regarding the reliability superiority of the all-FSA Moleculoy gage system compared to the standard all-FSA Karma gage system.

On that test, one Candidate 2 (all-FSA) gage was applied to one of each blade from Stages 1 through 7, 9 through 11, 13 and 14. A composite-ceramic gage was applied to a Stage 12 A 286 blade. These gages were routed to the slip ring along with 31 standard applications. After 30 hours of testing, a check was made during reprogramming of the slip ring. At that time, all the candidate gages had survived on the airfoil. The composite-ceramic gage on Stage 12 was the only survivor out of the four gages connected to the slip ring. As a result of the test, the Moleculoy gage, ultrasonic welding of the ribbon to the grid, and the Pt-10Ni intermediate leads were accepted as standard replacing Karma, capacitive-discharge welding, and Chromel P leads.

2.3.1 Reliability Demonstration Engine

With the adoption of the gage materials and processes into the Instrument Shop Unit, the confidence level of the Aeromechanical Engineer became moot. A compressor test survey on CF6-6 Engine 451-000/1 was conducted utilizing both Candidate 1 and Candidate 2 strain gage systems. The purpose of this test was to evaluate aeromechanical performance of two new blade designs of the HPCR Stage 9 blades and to study the affect of the response of Stage 1 and 7 blades to stator closure schedules. The engine was tested in the core mode in the Altitude Test Cell 43 at AEBG-Evendale. A 100-channel Polyscientific slip ring that is freon-oil cooled was used to transfer the rotating signals on the engine. The basic ring is shown in Figure 100 and the assembly in Figure 101.

2.3.1.1 Instrumenting the Engine

The strain gage instrumentation requirements established for the engine were as follows:

- Stage 1 - Four blades for engine test
One for Hot Shake Facility integrity verification
- Stage 7 - Four blades for engine test
One verification blade
- Stage 9 - Seven blades of each design for engine test;
Total - 14 blades
One of each design for verification tests.

Table 19 (Page 177) shows the instrumentation requirements, gage numbers, types of application, etc. that were used to instrument the blades.

Figure 102 shows the locations of the gages applied to Stage 7 and 9 blades.

The candidate gages were applied using the developed procedures and materials described in Section 4.0, Gage Fabrication and Application Details. After applications of the engine gages, all blades were calibrated against a foil gage that was selected from the strain distribution gage map. These calibrations provide corrections to blade operating limits and indicated strain.

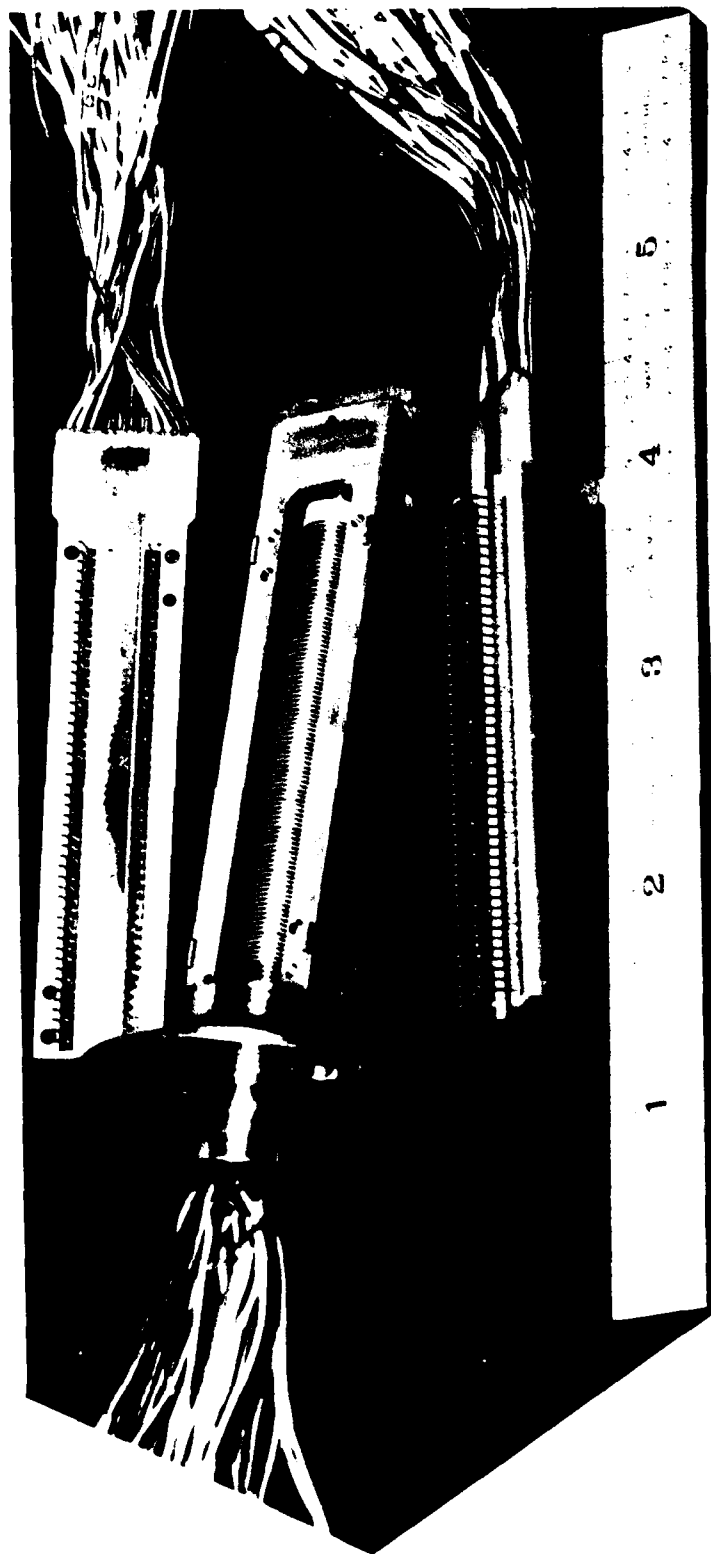


Figure 100. Basic Polyscientific Slip Ring.

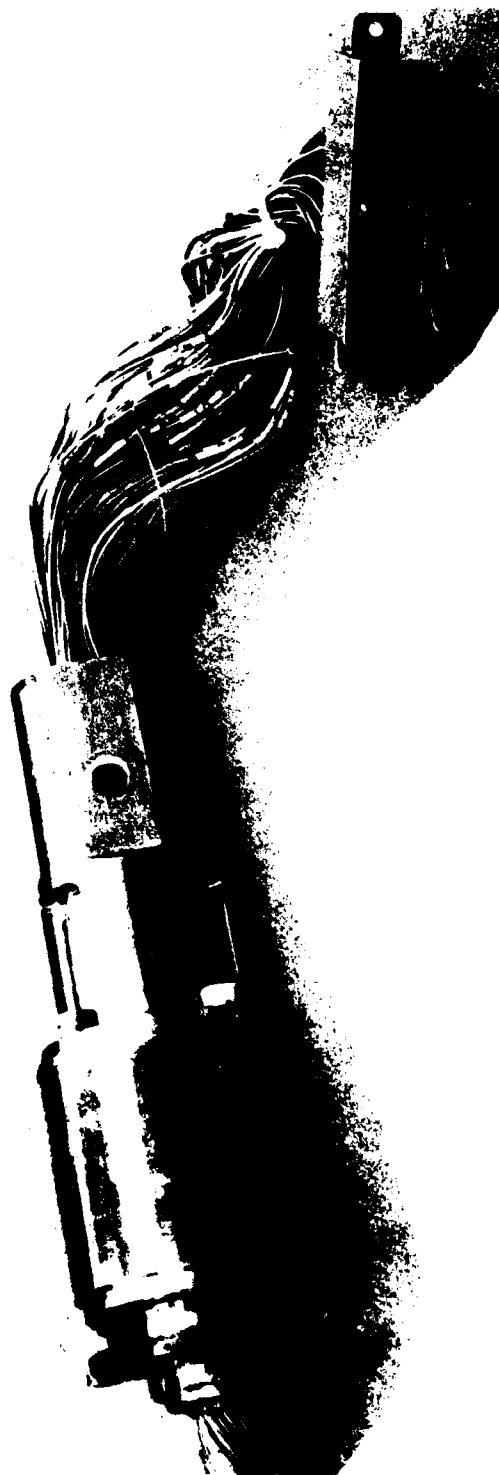


Figure 101. 100 Point Slip Ring Assembly.

Table 19. Instrumentation Requirements for CF6-6 Engine 451-000/1.

Item No.	Blade or Angular	Instrumentation Dwg. No.	Rework Dwg. No.	SD No.	Part No.	Stage No.	Zip Tag		Serial No.	Application Type
							No.	No.		
KD2A03	1	4013283-160P01		2	K159P05	1	1	01	01	Comp
KD2A04	9	P02		2	K	1	2	02	02	FSA
KD2A05	18	P01		2	K	1	3	03	03	Comp
KD2A06	27	P02		2	K	1	4	04	04	FSA
KD2M10	3	4013283-159P01	4013283-164	3	K137P05	7	5	08	08	Comp
KD2M11	28	P02		3	K	7	6	07	07	FSA
KD2M12	37	P01		3	K	7	7	10	10	Comp
KD2M13	46	P02		3	K	7	8	09	09	FSA
KD2Q32	7	P01		2	K908P04	9	9	F	F	Comp
KD2Q33	11	P02		2	K908P01	9	10	B	B	FSA
KD2Q34	19	P01		2	K908P01	9	11	C	C	Comp
KD2Q35	25	P02		2	K908P04	9	12	E	E	FSA
KD2Q36	33	P01		2	K908P04	9	13	1 (18)	1 (18)	Comp
KD2Q37	40	P02		2	K908P01	9	14	3 (15)	3 (15)	FSA
KD2Q38	22	P01		2	K908P01	9	15	5 (17)	5 (17)	FSA
KD2Q39	14	P02		2	K908P04	9	16	4 (16)	4 (16)	Comp
KD2Q40	53	P01		1	K907P01	9	17	6 (12)	6 (12)	Comp
KD2Q41	55	P02		1	K907P01	9	18	2 (11)	2 (11)	FSA
KD2Q42	58	P01		4	K907P01	9	19	J	J	Comp
KD2Q43	60	P02		4	K907P01	9	20	K	K	FSA
KD2Q44	44	P01		4	K907P01	9	21	9 (14)	9 (14)	Comp
KD2Q45	47	P02		4	K907P01	9	22	8 (13)	8 (13)	FSA

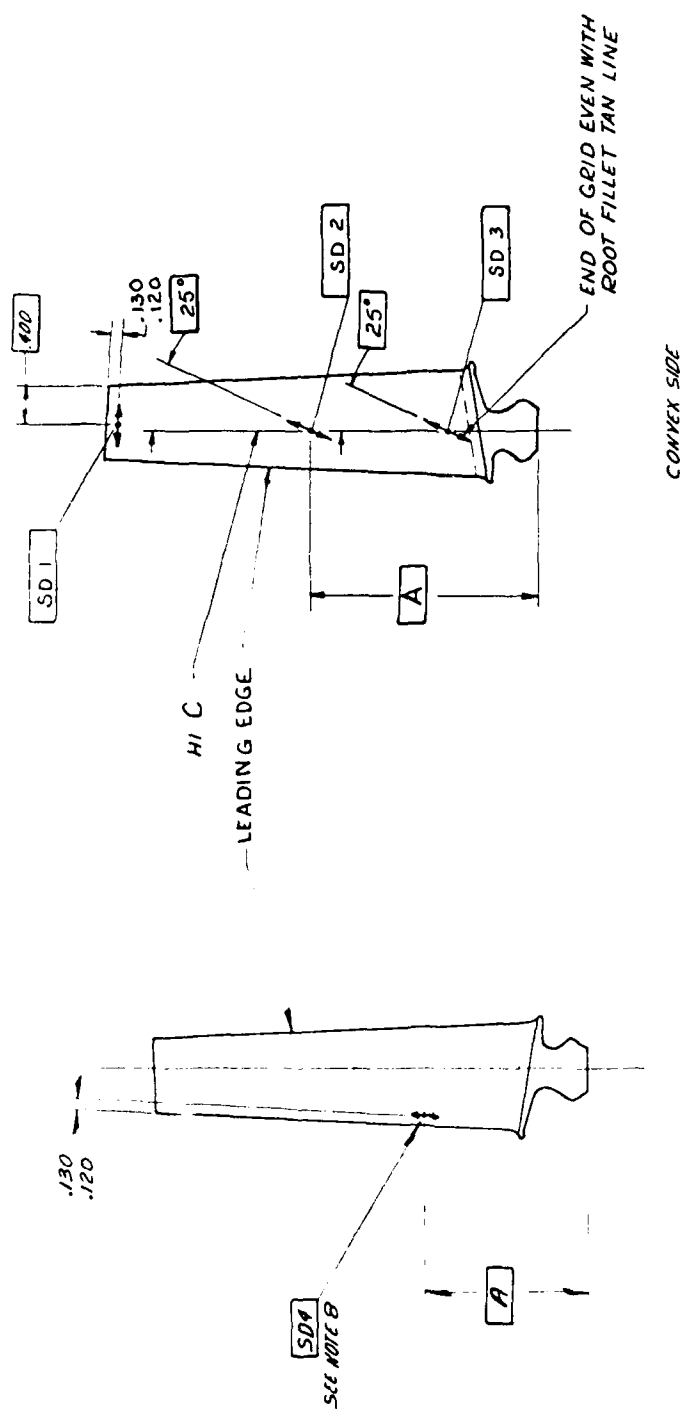


Figure 102. Stage 7 and 9 Blade Gage Locations.

AD-A101 713

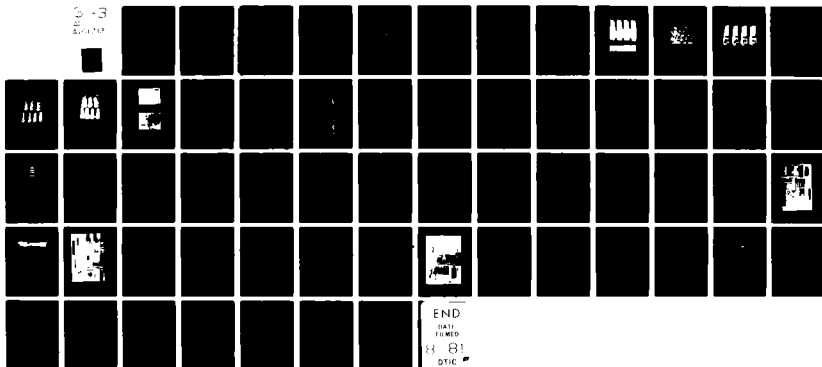
GENERAL ELECTRIC CO CINCINNATI OH AIRCRAFT ENGINE BU--ETC F/G 14/2
HIGH TEMPERATURE STRAIN GAGE SYSTEM FOR APPLICATION TO TURBINE --ETC(U)
JAN 81 R A WEISE, J H FOSTER F33615-76-C-2075
R80AE6388

UNCLASSIFIED

AFWAL-TR-80-2126

NL

Fig. 13
R80AE6388



The calibrated blades were installed and routed through the compressor spool as shown in Figure 103. The rework, lead-routing off the blade, and lead tie-down are standard techniques used in most compressor rotor instrumentation application designs at AEBG-Evendale. Critical Assembly procedures or details are identified on the drawing.

2.3.1.2 Engine Testing

CF6-6 Engine 451-000/1 was tested in Cell 43 from mid-April to early May 1980. The maximum speed tested was 10,080 rpm. The temperatures at the stages were 180° F at Stage 1, 520° F at Stage 7, and 640° F at Stage 9. The blades are titanium.

The total test time on the engine was 54:40 hours. A severe stall occurred in the 13th test hour on a decel from 8940 rpm. Testing was interrupted in the 28th test hour to change Stage 7 blades.

2.3.1.3 Test Results

Prior to the start of the test, two all-FSA gages (A04 and Q45) were inoperative. A composite-ceramic gage indicated intermittent and was considered failed at about 8:50 test hours; however, the gage returned some data during the stall that occurred 4 hours later.

The maximum stress before and after the stall were: Stage 1, 30,000 psi double amplitude, about 12,000 psi double amplitude on Stage 7, and 20,000 psi double amplitude on Stage 9.

The stall-induced stress on Stage 7 caused the loss of three gages. The gage that survived the stall (M11) indicated a stress of 130 ksi double amplitude or about 8400 microinches/inch p-p, as shown in Figure 104. Figures 105 and 106 show stresses before during and after the stall on Stage 9 blades.

During the replacement of Stage 7 blades, the applications on Stages 1 and 9 were visually inspected. All structures appeared mechanically sound; that is, no loss of alumina was observed. The Stage 7 rotor shroud was heavily rubbed. Stage 7 applications, obtained later had lost some of the structures, both composite and all-FSA.

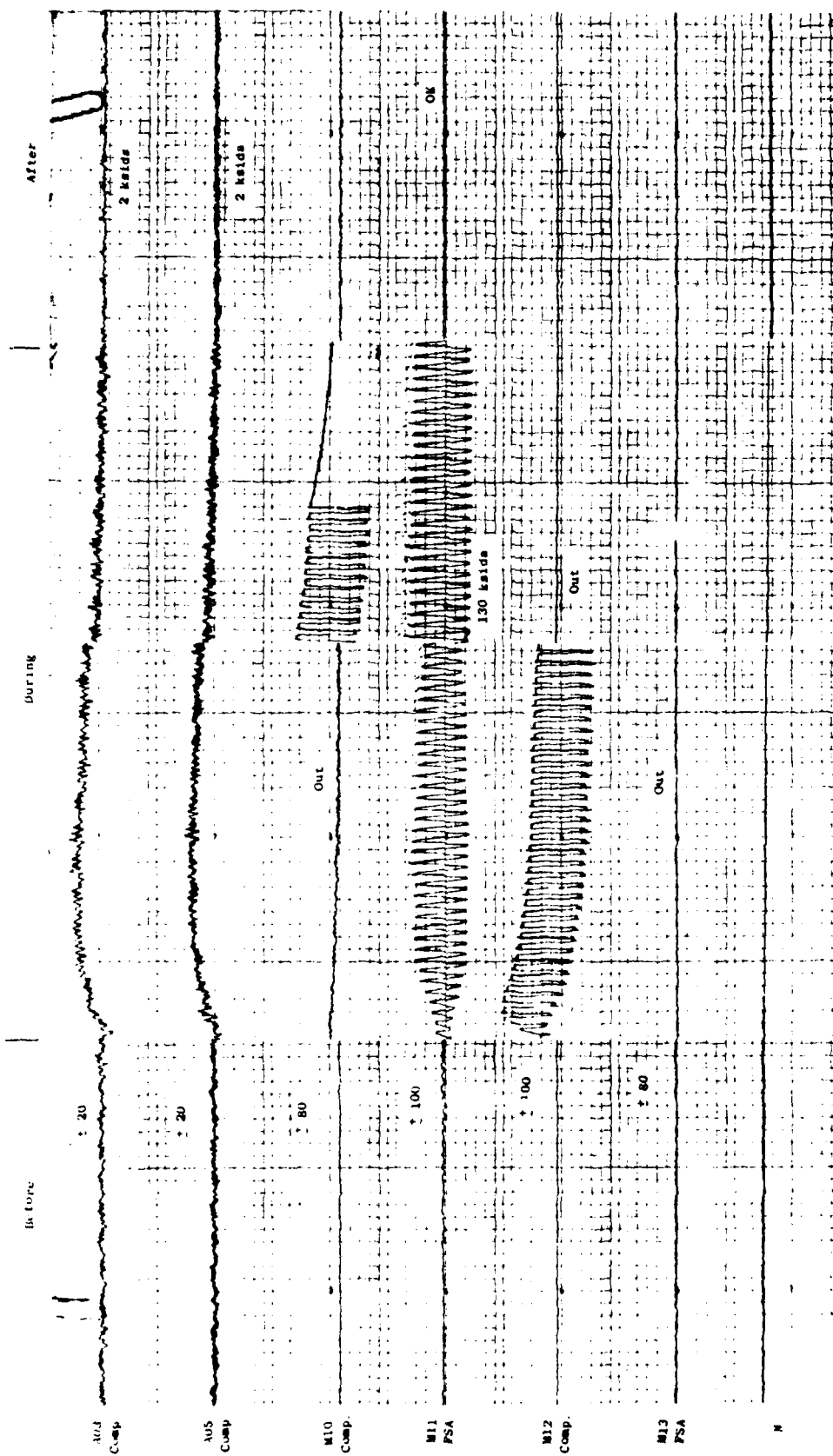


Figure 104. Stage 1 and 7 Strain Gage Signals Before, During, and After Stall.

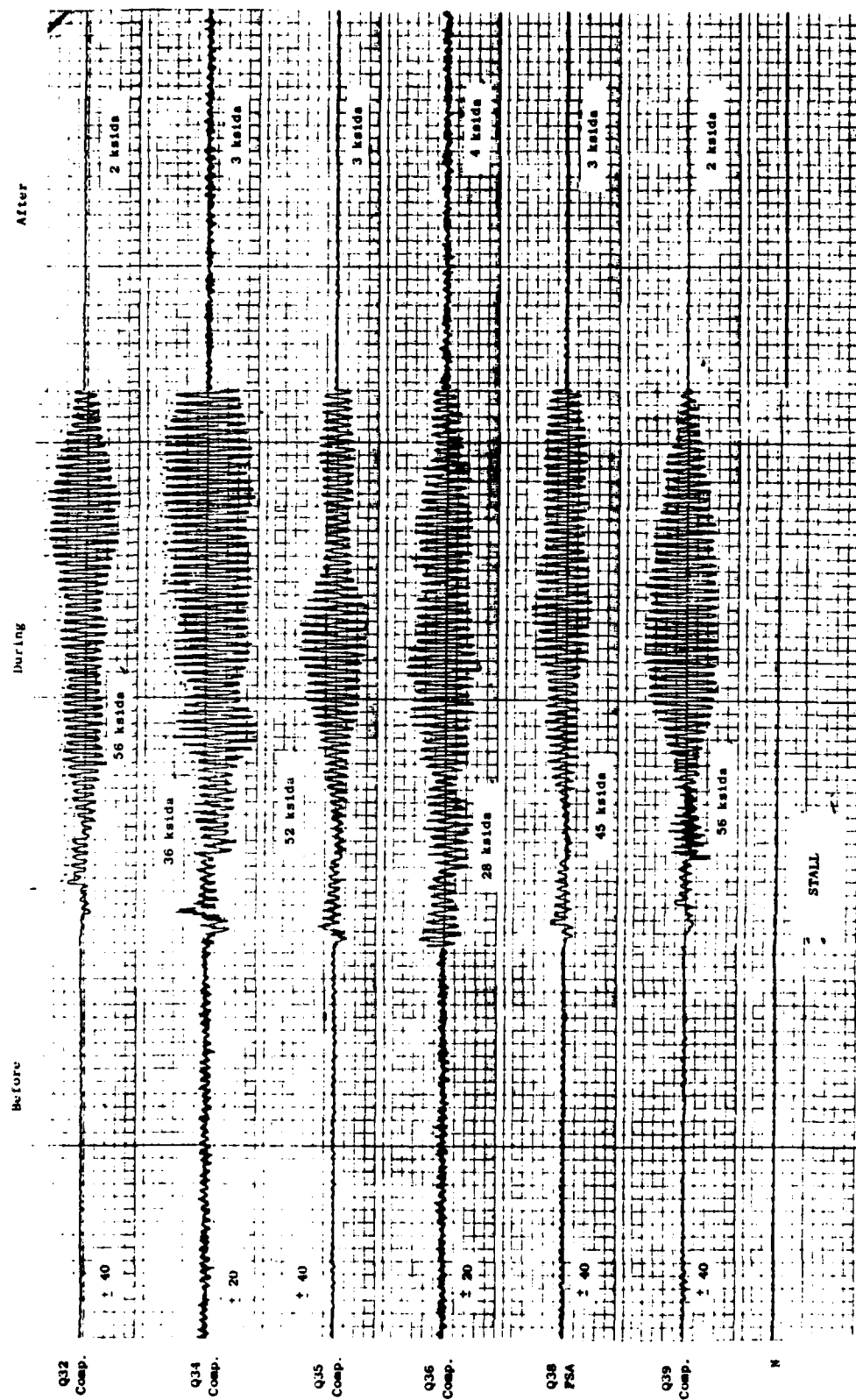


Figure 105. Stage 9 Strain Gage Signals Before, During, and After Stall.

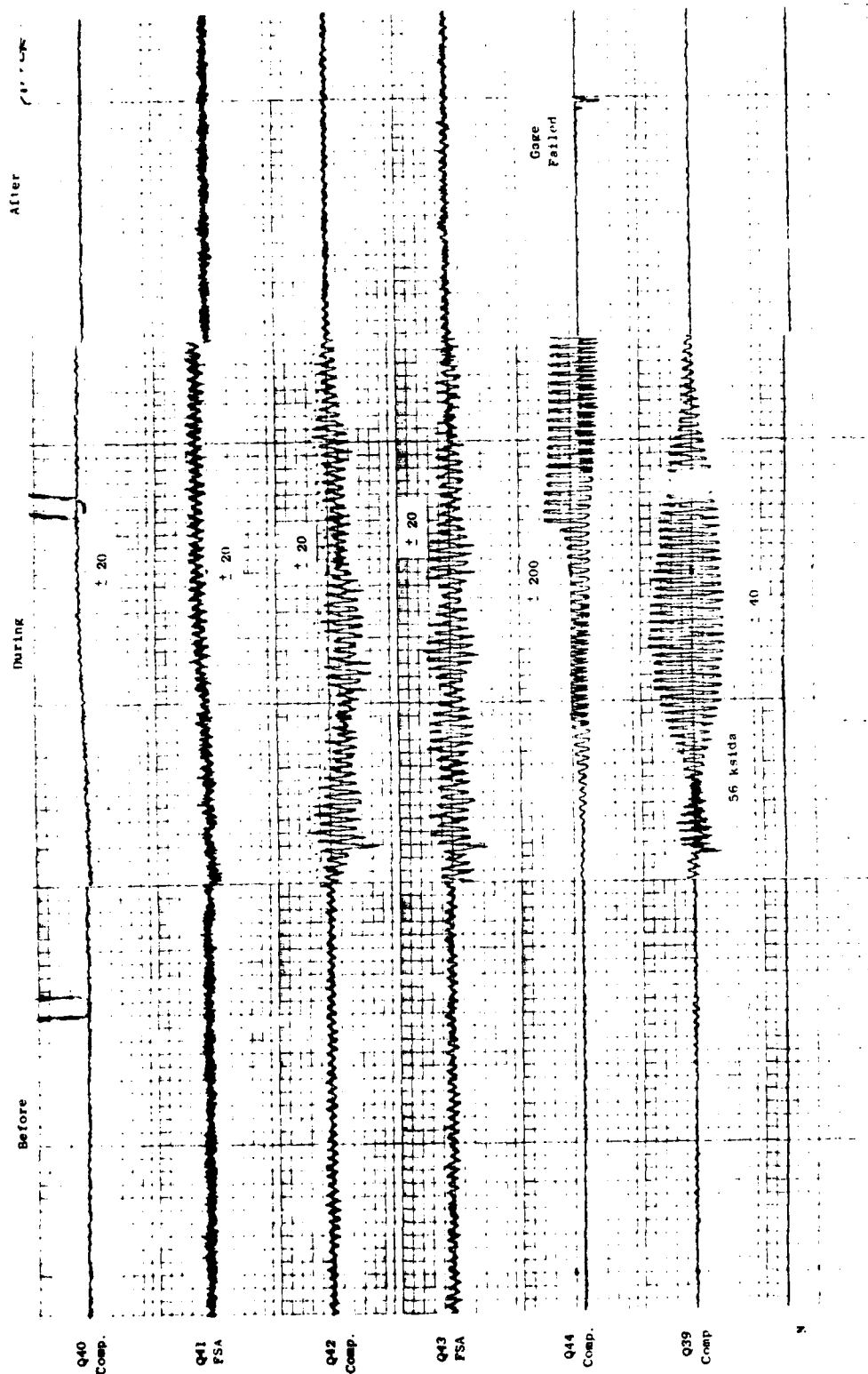


Figure 106. Stage 9 Strain Gage Signals Before, During and After Stall.

Gages remaining at the end of testing:

<u>Stage</u>	<u>Candidate 1</u>	<u>Candidate 2</u>
	<u>Composite-Ceramic</u>	<u>All-FSA</u>
1	1 (A03)	0
7	0 (2 Failed at Stall)	1* (1 Failed at Stall)
9	4	2

*Removed after 28th test hour.

Figure 107 compares the reliability of the two gage systems. Reliability is defined as the ratio of average sensor life and engine test hours.

2.3.1.4 Posttest Inspection

Stage 1 Blades. Resistance measurements of the four blades (Figure 108) showed the gages were continuous. This frequently occurs even though the gage circuit has been identified as faulty on test. Occasionally, a gage will return acceptable signals below some part speed but indicate "noisy" or "open" above it. In order to conduct a postmortem without abrading away the complete top coat, the blade is strained in bending to force the failed circuit to register "open". Attempts to open circuit A04, A05, and A06 were unsuccessful. Gage A04 (all-FSA) was soaked in a solution of hot caustic soda for about 36 hours. Figure 109 shows the remaining structure at 20 magnification. The broken filament is the result of damage during abrading to find the failure because resistance was still continuous after the soak. The postmortem was terminated on these blades.

Stage 7 Blades. These blades were removed in the 28th test hour. The condition of the applications after removal is shown in Figure 110. S/N 08 and 10 contain composite gages and S/N 7 and 10 have all-FSA applications.

Both candidates suffered alumina loss. The areas that show up white are where pieces of alumina were removed after test during inspection of the blades for failures. Blade S/N 07 (Ident. M11) was operating when removed from the

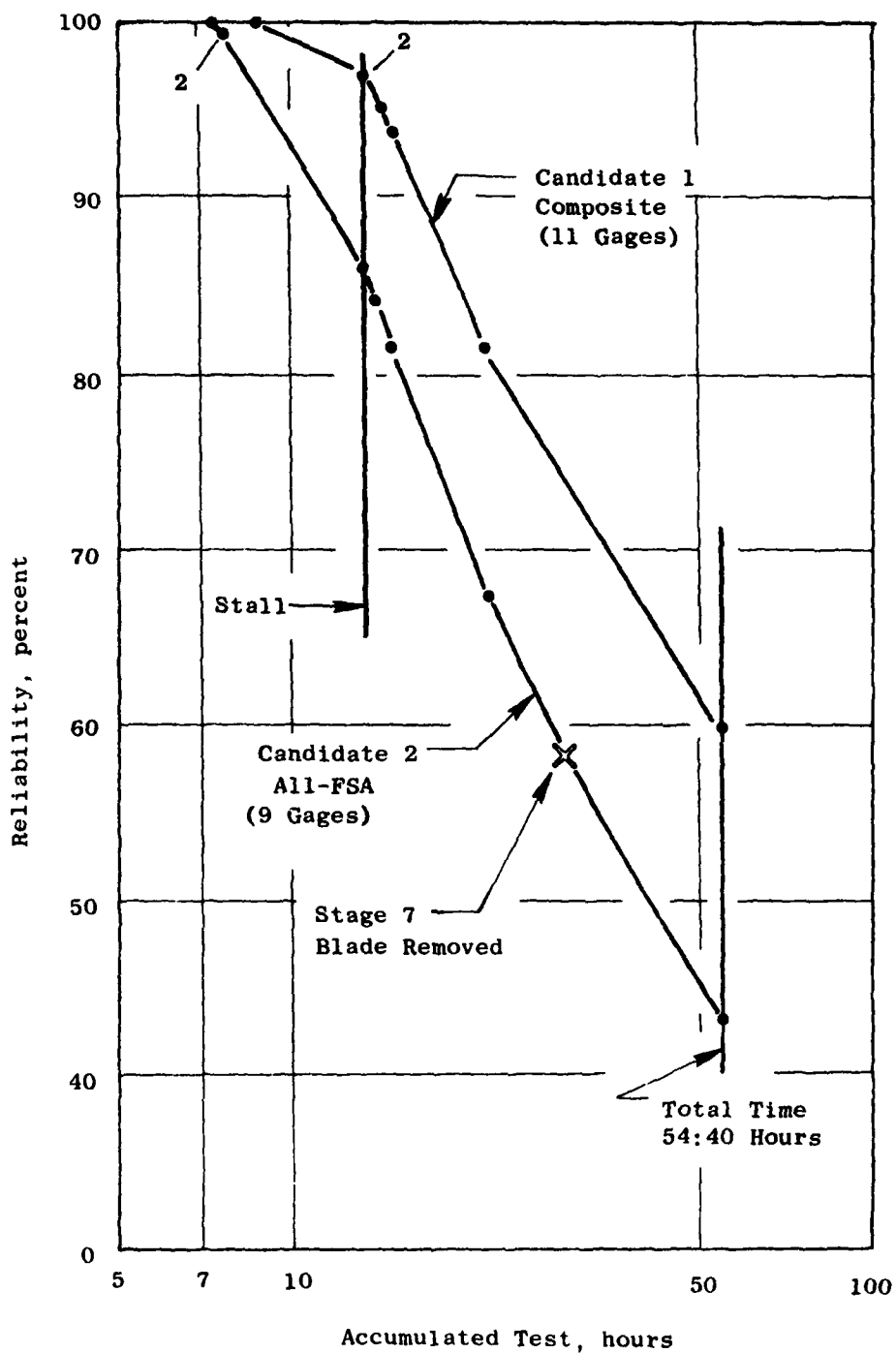


Figure 107. Candidate Strain Gage Reliability Chart, CF6-6 Core Engine 451-000/1.



Figure 108. Stage 7 Blades After 54:40 Hours of Testing.

Broken
Filament

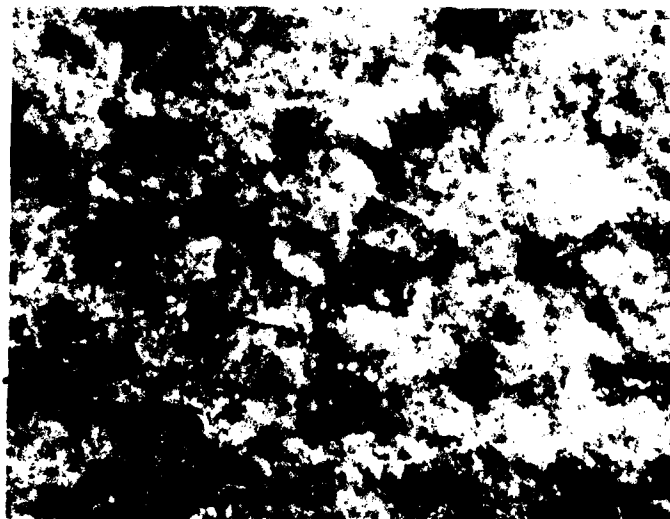


Figure 109. Gage A04 (All-FSA) After
36 Hours in Hot Caustic
Soda.

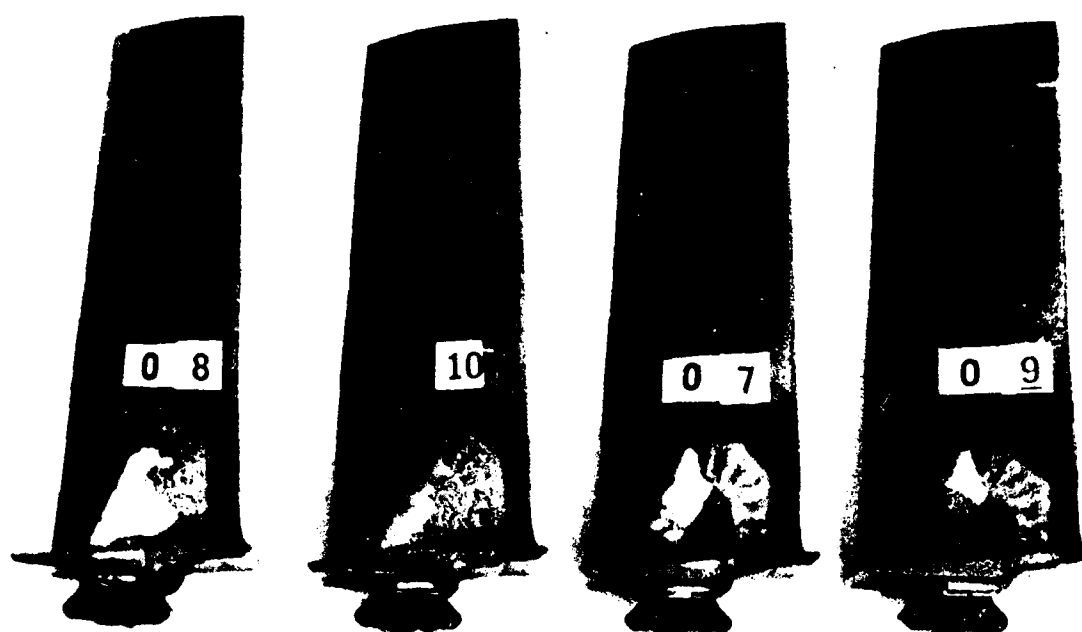


Figure 110. Stage 7 Blades After 28 Hours of Testing.

engine. The loss of the top coat on S/N 10 appears more from erosion than mechanical damage that would be caused by high compressive stress during rubs when the compressor stalled. No postmortem was conducted on these blades.

Stage 9 Blades. All blades with operating gages were dynamically calibrated after test. A failed application (Q39) was replaced by a foil gage. Figures 111 and 112 show the composite-ceramic and the all-FSA gages as delivered from calibration.

The blades containing gage applications on the concave side of the airfoil at the trailing edge (S/N 13 and 14) lost some of the top coat FSA. This is believed to be caused by erosive particles from the Stage 7 rub during stall.

Continuity measurements of resistance except for S/N 13 and 14 indicated the gage circuits were complete. The blades with gages that indicated problems during test were strained to open-circuit the systems. No significant change in resistance was observed. No postmortem was conducted.

S/N 13 and 14 were postmortemed using the usual technique and abrading away the top layers. Figure 113 shows the failure locations in the end loop and grid.

2.3.1.5 Discussion of Engine Testing

Although the test hours were less than desired and most of the gage failures are attributed to damage incurred during stall, the test is considered successful in that the composite-ceramic structure had higher reliability as shown in Figure 107. This was expected going into the test based on fatigue strength estimates discussed in Phase II, Section 3.2.1, and on expected stage temperatures. The losses in both structures were high; but considering the stresses during stall, this could be expected.

The constraint of locating the gages in this piggyback test on Stages 1, 7, and 9 prevented verifying bench test data that shows the reliability of the all-FSA gage application to be greater at temperatures above about 700° F.

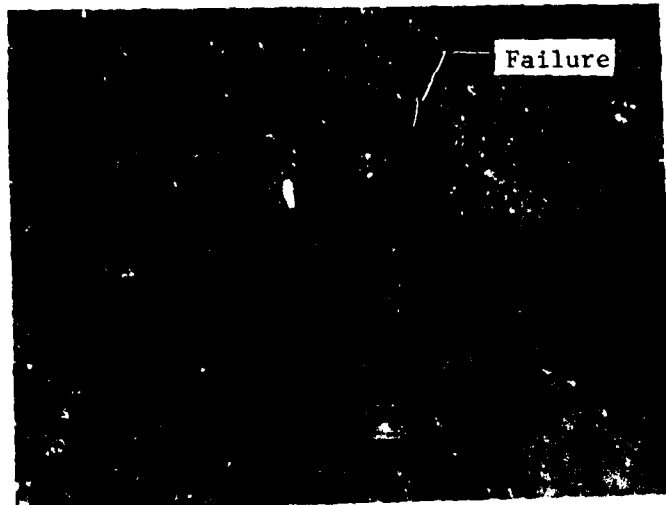
The posttest inspection results do not indicate the need for systems redesign or materials changes. If anything, they point toward a need for an improvement in postmortem techniques.



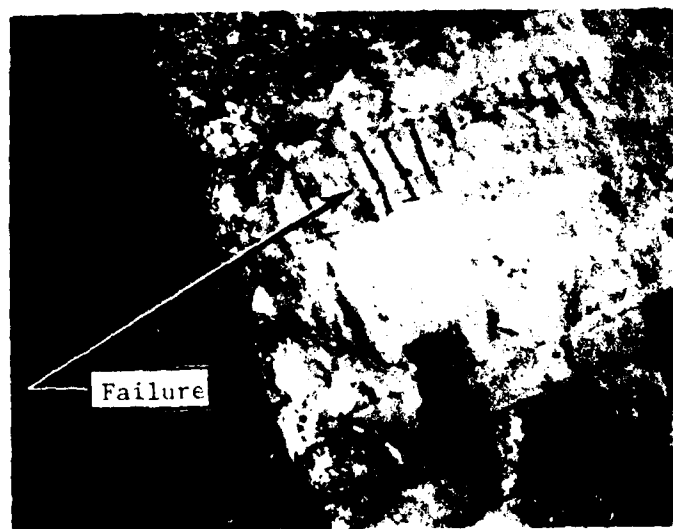
Figure 111. Stage 9 Blades Containing Composite-Ceramic Applications (Except for S/N 16, the Blades Containing Calibration Gages Were Operating at the End of the Test).



Figure 112. Stage 9 Blades Containing All-FSA Gage Applications (S/N K and S/N 17 Gage Applications Were Operating at the End of the Test).



S/N 13 - All-FSA



S/N 14 - Composite

Figure 113. Failure Sites of Stage 9 Applications (S/N 13 and S/N 14).

2.3.2 Selecting the Most Promising Candidate

It is not possible to select from the reliability chart in Figure 107 the better candidate for covering the temperature range to 1500° F. Again, this test indicated the reliability of the composite-ceramic gate is better at the temperatures of the stages instrumented than the all-FSA.

The only recommendation that can be offered must be based on fatigue test results as well as the results from the reliability demonstration. It is to apply the Candidate 1 gage system for stages operating at below 700° F; for temperatures above 700° F, the Candidate 2 structure is preferred.

3.0 GAGE FABRICATION AND APPLICATION DETAILS

In this section, the details required to fabricate and apply strain gages with either of the selected application techniques will be presented. Although the application designs have changed little (Figure 114), process steps and materials are significantly modified from those presented in the Phase I Report issued late 1977. This is especially true for the composite-ceramic structure. Table 20 tabulates the materials and processes of the two applications.

Also presented will be lead routing techniques and designs used at AEG-Evendale to cross the span between the blade and the disk. These methods have proved successful on development test engines.

Where necessary, the equipment used in this program will be identified as to manufacturer and model, although for the most part, appliers of high temperature strain gages have their own preferences. Fixtures designed and built by GE for this program will be detailed. For others, there are sufficient details provided for easy reproduction, if desired.

3.1 STRAIN GAGE FABRICATON

3.1.1 Material

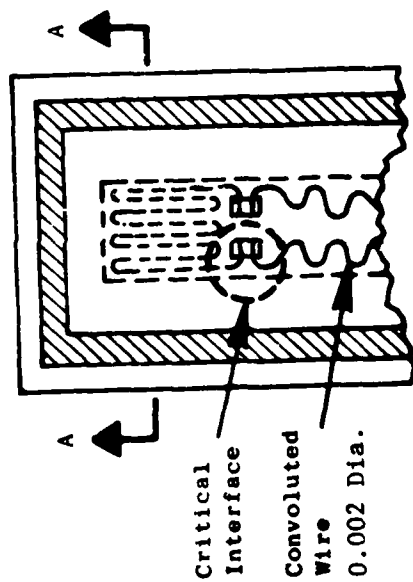
The gage is made from Moleculoy, manufactured by Molecu-Wire Corp., Wall Township, New Jersey. It is 75Ni 20Cr 4.5Al alloy and has a diameter of 0.008 inch or 0.8 mil. It is bright annealed.

Splice-ribbon material is annealed Karma alloy that is 0.001-inch thick and 0.015-inch wide (1 x 15 mils). The wire may be obtained from Driver-Harris Company.

The intermediate leads are Pt-10Ni. It is 0.002-inch diameter. Sigmund Cohn Corp., Mount Vernon, N.Y., is the supplier.

3.1.2 Strain Gage Details

Figure 115 provides the fabrication and dimensional details of the gage. All fabrication equipment of processes are identified by the drawing. The



Typical Structure

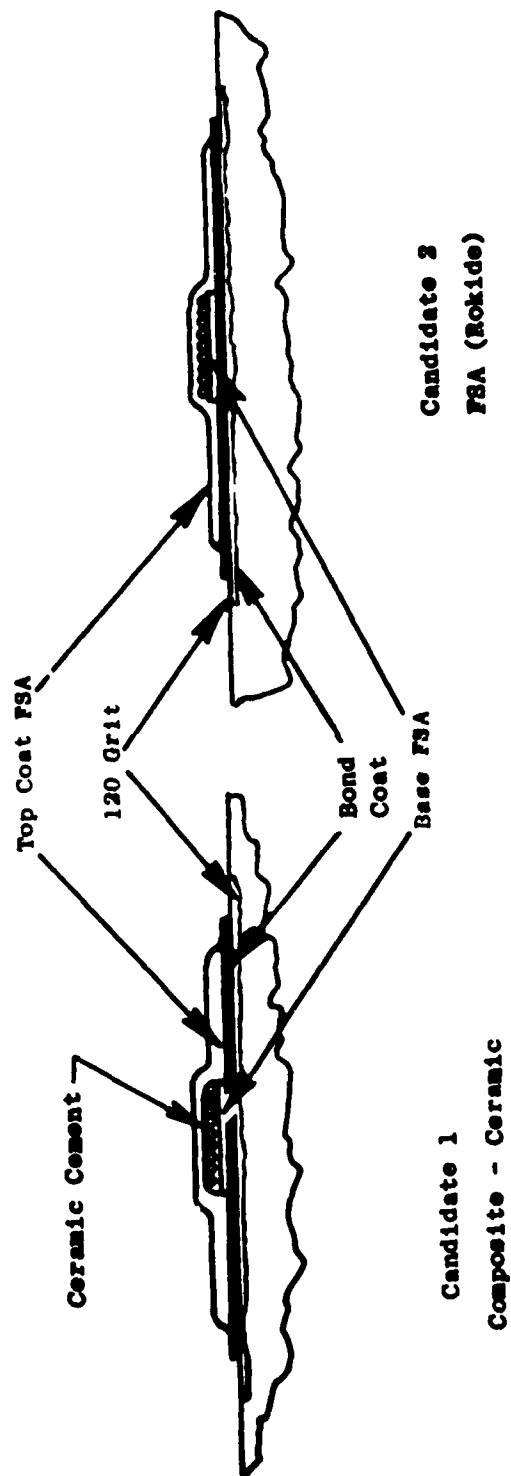


Figure 114. Application Designs.

Table 20. Gage Application Materials and Processes.

<u>Gage System Element</u>	<u>Composite-Ceramic</u>	<u>All-FSA</u>
• Surface Prep	Norton Dynablast 120 Grit	Norton Dynablast 120 Grit
• Adhesion Layer	Flame-Sprayed or Plasma-Sprayed Metco 450	Flame-Sprayed or Plasma-Sprayed Metco 450
• Insulating Layer	Al ₂ O ₃ - 1/4-inch Rod Gun	Al ₂ O ₃ - 1/4-inch Rod Gun
• Gage	Molecularoy, 0.8 mil Dia., Flat to 0.4 mil, Heat Treat 1050° F, 2 hours	Molecularoy, 0.8 mil Dia., Flat to 0.4 mil, Heat Treat 1050° F, 2 hours
• Leads	2-mil Pt-10Ni	2-mil Pt-10Ni
• Lead Attachment	Grid-to-Ribbon; Ultrasonic Weld Ribbon-to-2 mil Convolute Lead Capacitance Discharge Weld	Grid-to-Ribbon; Ultrasonic Weld Ribbon-to-2 mil Convolute Lead Capacitance Discharge Weld
• Gage Attachment	Denex 2 Fine Ground	Al ₂ O ₃ 1/4-inch Rod Gun
• Top Coat	Al ₂ O ₃ 1/4-inch Rod Gun	Al ₂ O ₃ 1/4-inch Rod Gun

gage is wound on a loom, removed, and pressed or flattened to 0.004 inch to 0.00045 inch. The gage flattening blocks are shown in Figure 116.

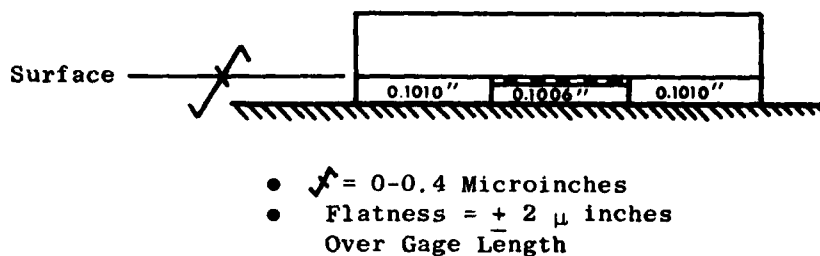


Figure 116. Gage Flattening Block.

The bottom gage blocks are available from Do-All Corp. They are jo-blocks. The upper block is made from a Carboloy tool bit that is 0.20-inch thick and 1-inch diameter. It is specially treated to have the finish and flatness specified in Figure 116. The hydraulic press utilizes a Blackhawk Jack that has a piston area of 1.864 square inches. The flattening force may be greater than that used in the GE system but should not be less. Using this method of flattening will provide uniform gages that are about 0.42 mil thick. Periodic inspection of the surface of the center jo-block is recommended. The blocks, even at a hardness of $R_c = 65$, become sufficiently deformed which mar the gages and cause stress risers and short life. Greater block hardness is preferred.

3.1.3 Gage Annealing

After the flattened gages have been equipped with the ultrasonically-welded ribbon leads, the assembly is heat-treated (Configuration G04 in Figure 115). The heat-treat enhances gage performance by:

1. Increasing the fatigue strength of the gage alloy
2. Increasing the ultrasonic weld strength by diffusion
3. Stabilizing the gage factor.

The heat-treat temperature that is used is 1050° F. This temperature primarily was selected because of the excellent stability characteristics of gage factor over the temperature range to 1000° F. It also, in combination with the coldwork introduced by flattening to 0.40-0.45 mil, increases the fatigue strength of the alloy.

The gages equipped with ribbon are heat treated on a platan which is a piece of quartz 4 inches x 6 inches x 3/8 inch thick. The gages are placed on the clean platan and are spaced 1/4-inch apart. The grids only are covered with SS White Alumina No. 3 powder that is between 20-50 mils deep.

The platan with gages are placed into a furnace that is set to 1050° F. The temperature is maintained for about 1:45 hours. It is then turned off and allowed to cool with the door closed. Platan temperature is monitored using a thermocouple attached to it. After cooling to about 300° F, the oven door is opened, and the platan is removed when it is cool enough to handle.

Brush the SS White Powder from the gage, remove it from the platan, and dip the gage into MEK to remove particles of powder. Tape the gage onto a paper carrier. Use Scotch 64 tape strip 0.050-inch wide by 0.35 to 0.40 inch long. Place the center of the tape at the center of the ribbon lead. Measure gage resistance with a digital multimeter on the ribbon as close to the ultrasonic weld as possible. Log the resistance on the paper carrier and store it in an appropriate folder. The gages are equipped with Pt-10Ni intermediate leads (to either the G05 or G06 configuration in Figure 115) when the length of the lead has been determined.

3.2 GAGE APPLICATION INSTRUCTIONS

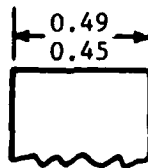
In Phase I, the material selected for the adhesion or bond coat was Metco 443. The selection was based on its oxidation resistance over the temperature range to 1500° F. However, to utilize its self-bond feature which causes maximum adhesion requires the use of plasma-spray equipment. On the other hand, the self-bond feature of Metco 450 is obtained when it is applied with oxy-acetylene flame-spray. The material starts to oxidize (the oxide is green) at about 1300° F with the rate increasing at higher temperatures. However, instrumentation applied on Metco 450 for turbine blade stress tests has shown no evidence of debonding at temperatures between 1400° and 1750° F.

Therefore, it seems advisable to avoid the use of plasma-spray equipment which may not be readily available to change the bond coat from Metco 443 to Metco 450.

The process steps detailed below for the most part are those currently used by the Instrument Shop in AEBG-Evendale to supply Moleculoy gages using Rokide or all-FSA techniques. The composite-ceramic techniques are those that have been developed as a result of this program.

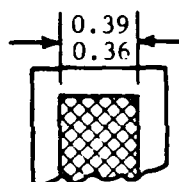
3.2.1 Preparing for the Gage Application

1. Clean Part. Remove all visible dirt/grease with detergent, ammonia, and hot water. It is recommended that some parts be baked to remove impregnated contamination.
2. Lay Out. Lay out the gage location (brass scribe). Extend the gage location lines to a length beyond the flame-spray area. These lines will be covered with tape and after grit-blasting and spraying can be transposed again to gage area. The gage is to be located within ± 0.015 inch and $\pm 1^\circ$ of requested dimensions.
3. Mask for Grit-Blast. Mask around the area to be blasted using Scotch 470 tape (only approved tape) to include all areas which will be in the direct overspray of the grit. The sketch below is the application width dimension for grit-blast:



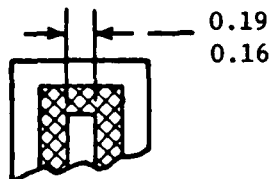
4. Grit-Blast. Small parts shall be blasted in the small Trinco Blast Cabinet, larger parts in the walk-in grit-blast room. New 120-grit aluminum oxide is to be used one time only. Do not reclaim grit and use for this operation again. Adjust the blasting pressure 30 to 50 psi, depending on the parts to be blasted. Higher pressures than 50 psi are not permitted. Nozzle distance shall be 4 to 6 inches and held at 45° angle to the surface being blasted. Nozzle speed should be about 1 inch per second.

5. Check Blast. Using a 3X magnification or greater, compare the blasted surface with the "accept" or "reject" sample specimen. This sample specimen shall be kept in the gage room cabinet.
6. Clean Blasted Area. After the grit-blast, clean the grit-blasted area with neutralizer. Follow by washing with distilled water and blot with clean tissue. Inspect the tissue for contaminants; if any exist, reclean, and inspect. Do not remove Scotch 470 tape. An alternate technique may be used. It is to blow off the surface with clean air. Use 470 tape adhesive side and blot blasted area. Repeat with clean adhesive until tape comes up clean.
7. Mask for Flame Spray. Add additional tape (Scotch 470) around application area to achieve flame-spray dimensions (see sketch below). Apply a coat of Turcoform 537 liquid mask over tape and dry.



To the skilled operator, Turcoform 537 over the edge of the tape is not required. For the beginner, it does prevent overheating the tape and the chance of contaminating the bond coat.

8. Metco 450 Bond Coat. Apply the bond coat with either the plasma-spray unit or the Metco thermospray unit using the Metco 5D spray gun. The coating thickness should be 1 to 3 mils.
9. Clean Metco Bond Coat. Using clean MEK and brush, clean the Metco and any tape residue around the application area. Special precaution must be taken to ensure no surface contamination is imposed on to the flame-spray from time of final cleaning until FSA application. Do not touch spray with fingers and do not leave part exposed when not being worked.
10. Mask for Rokide. Mask the Rokide application area using Mystic 7402 aluminum tape; see dimensions in sketch below. All exposed areas of the part except the application area must be masked to protect against overspray.



11. Rokide Base Coat. Spray application area with 2 to 3 mils of Rokide. Spray distance shall be 6 to 8 inches.

The alumina rod that is recommended because of the erosion resistance of the sprayed material is 1/4-inch diameter. It is purchased from BLH as BLH-H ceramic rod. At GE, it is applied with a Mogul R-3 coating gun.

12. Inspect the FSA Base Coat. Visually inspect the base coat at magnification 5. Large clods or blobs of the material should be removed from the gage area by abrading it with a piece of BLH-H rod. It is not necessary to remove the clods from the lead path area unless they are unusually large.

The above process steps apply to both the composite-ceramic and the all-FSA applications techniques. The remaining process steps are different for the two techniques.

3.2.2 Composite-Ceramic Application

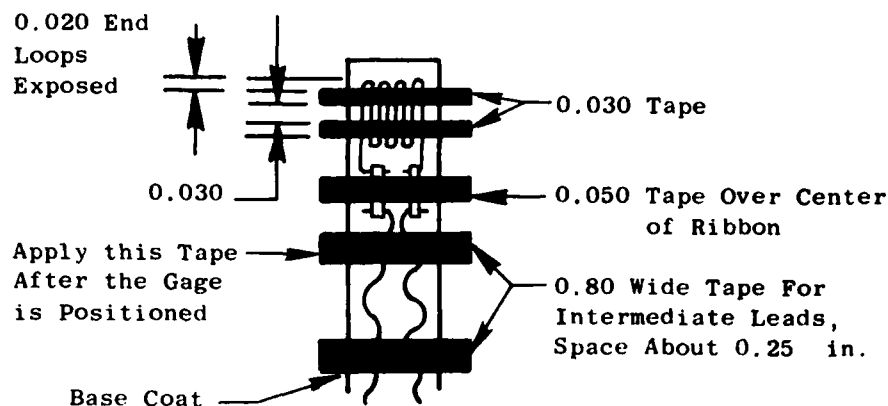
In the developed application, the Denex 2 cement used is ground or pulverized for at least 50 hours beyond the grind of the standard product. The cement is thinned with 1 part distilled water to 4 parts cement by weight.

1. Priming the Al_2O_3 Base Coat. Before removing the 7402 tape used to mask the part for the application of the FSA base coat, apply a thin coat of well-stirred Denex 2 cement using a Kodak No. 2 sable hair brush (or equivalent). Brush the material to be sure it wets the surface of the Al_2O_3 . Remove the excess cement with a cotton swab dipped in distilled water. The coat should be very thin and smooth. Air dry 15 minutes and remove the Mystic Tape. Heat the part slowly 170° to 180° F for 30 to 40 minutes to remove moisture. Use a heat lamp. Heat in an oven at 212° F for 30 minutes followed by 1 hour at 390° F. Remove from the oven and allow to cool.

2. Lay Out. Transpose the grid location lines from the Metco 450 bond coat to the base coat primed with Denex with a sharp tungsten scribe and a clean straight edge. The scribe line should be very lightly marked.
3. Applying the Gage. In the original Phase I Report, the technique specified did not use small tape strips on the gage, because it was believed that Denex could be applied without distorting the gage. This was not the case because the Denex did not wet the surface of the primed base coat. Repeated brushing to spread the cement over the gage caused its distortion. Tape strips, as with the Rokide technique, were used. A subsequent development was to etch the primed surface with aluminum phosphate. This treatment allowed the top coat of cement to spread evenly over the base coat; however, the use of the tape strips still continued.

Recently, since the completion of applications for the demonstration of reliability on the CF6-6 engine, it was shown that a complete gage application can be completed without using the usual tape strips on the gage/grid. Since gages applied using this technique have never been tested, both the method used in the development (old) and the new technique will be presented here.

- a. First, on the base coat of FSA that has been primed with a thin coat of Denex, place a small amount of aluminum phosphate and scrub it in the surface with the No. 2 sable hair brush. Initially, the liquid will puddle until the surface becomes etched where upon the material will spread evenly. Blot the excess liquid from the surface of the basecoat. Dry thoroughly or the tape will not adhere to it. A heat lamp may be used to accelerate drying.
- b. Remove the gage, equipped with proper length leads, from the protective folder. Lift the gage off the paper holder using the 0.050-inch tape strip that secures it. Carefully position the gage over the layout lines. Fasten the tape.
- c. First, place a piece of 0.080-inch wide tape on the intermediate leads just below the ribbon leads and fasten to the part. Then, place a strip of Scotch 64 Tape precut to 0.030 inch wide by 0.35 to 0.40 inch long on the gage grid 0.02 inch from the end loops. It is necessary to dip these strips into alcohol to remove the static charge which will attract and distort the grid. Shake to remove excess alcohol; but while the strip is still moist, press it into position. Place a plastic flap over the grid ribbons and gently roll the plastic to secure the strips.



- d. Thoroughly mix the Denex and apply a very thin coat of cement to the exposed areas. The cement is to be barely sufficient to cover the grid and leads. Do not allow the cement to run onto the Metco bond coat. Should this become a problem prior to starting the gage application procedure, the Metco 450 should be covered with tape.
 - e. Allow the cement to air dry for 30 minutes. Heat the part slowly 170° to 180° F in an oven and soak for 30 to 40 minutes. While the part is still warm, very carefully remove the tape strips by pulling the edge of the tape back over itself at 45° to the length of the tape. Remove any other tape, place the part into an oven, and heat to 212° F. Hold for 30 minutes and then raise the oven temperature to 390° F. Hold for 1 hour and remove and cool the part.
 - f. Apply a coat of thin, well-stirred cement into the areas exposed by removal of tape but not at the ribbon leads. There should be no tape residue and the areas may be easily filled. Again, the thickness of cement should be just sufficient to cover the grid and leads.
 - g. Air dry for 30 minutes. Heat 170° to 180° F for 30 to 40 minutes.
- Cure 1/2 hour at 212° F
 Cure 1 hour at 390° F
 Cure 1 hour at 480° F
 Cure 1 hour at 660° F

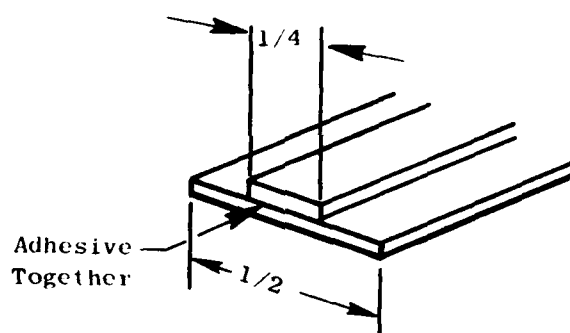
Measure the bonded gage resistance at the still-exposed ribbon leads and log. It is not necessary to apply cement on these leads.

The above steps apply to the new procedure except Step C is modified. In this new procedure, the two strips of tape are not applied onto the gage grid.

New Procedure (Step C)

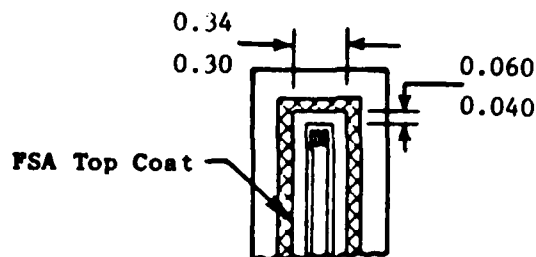
Fasten the gage onto the base coat with the strip over the ribbons. Position and fasten the leads as discussed in Step C. If the gage is flat against the base coat, place a small drop of well-stirred cement in the center of the grid. Carefully spread it with a sable hair brush, brushing it from the tape strip on the ribbon toward the end of the gage. Experience will dictate the size of the drop of cement. Be sure all strands are covered.

If the gage is not flat, prepare a narrow strip of tape in the following manner:



Place the adhesive side of the tapes together. Cut a width of the tape 0.030 to 0.035 inch wide and place onto the gage with the exposed edges of adhesive down. The center of the narrow strip is placed over the gage and gently pressed to adhere to the Metco 450. The gage, now held flat to the base coat, may be covered with cement. The tape should be positioned to just cover the outer grid end-loops. Work the cement near this suppressor strip with the brush. It will flow under the strip and cover the gage with sufficient cement. Cure as in Step E and complete the remaining steps.

Top Coat - Using Mystic 7402 aluminum tape, mask the entire blade and around the gage application to the dimensions shown in the sketch below. There should be a border of Metco 443 on all sides of the cement of approximately 0.062 inch. Cover gage legs in the splice area with tape.



Primary Lead Splice - Follow process steps under 4.2.5.

3.2.3 All-FSA Application

After preparing for the gage application as outlined in Section 4.2.1, the all-FSA or Rokide process is completed using the following procedures:

1. Lay Out. Remove the tape around the base coat of Rokide leaving the second mask of tape with gage location lines exposed. Transpose the gage location lines using the tungsten scribe and straightedge onto the Rokide spray. Mark very lightly.
2. Applying the Gage. Cut strips of Scotch 64 tape. Strips are to be 0.030 inch wide to hold the grid. For the leads, the tape is 0.080 inch wide.

Secure a 0.050-inch wide strip of tape to the ribbon leads 0.02 inch below the gage grid. Lift gage off paper-holder with this tape and locate the grid on layout lines. Fasten grid to Al_2O_3 base coat with the tape. Pick up precut strip of 0.03-inch wide tape with tweezers, dip in alcohol, shake and while still moist, place the strip on the gage grid 0.02 inch below top loops of the grid (top of tape edge from top loops). Place second strip on grid 0.02 inch above bottom loops. Using curved tweezers, press ends of tape to secure. Place plastic flap over grid and gently roll the plastic with finger to secure tapes. In a similar manner, fasten ribbon

and leads to base coat with 0.080-inch wide strips positioned so there is 0.200 to 0.250 inch space between strips. Place strips of tape over the ends of the strips used to hold gage and leads in place. These should be large to hold the small strips during sprays.

3. Spray First Coat. Visually check using 3X magnification or greater in the spray area prior to spraying the first coat of FSA for loose tape, distorted grid and leads, and raised leads.

Spray first gage coat of Rokide 2 to 4 mils thick. Spray the gage application holding the gun 90° to the part surface and moving gun parallel. Move the arm slowly and do not angle the gun nor pivot the wrist with a sweeping or fanning motion. This is important to avoid blowing the tapes loose and flowing the Rokide under the gage and ribbon legs. Spray distance shall be 8 to 10 inches.

4. Check Gage. Visually inspect first coat, FSA (5X or greater):

- Thickness 0.002 to 0.004 inch
- Coverage of complete sensor area.

5. Prepare for Final Spray. Remove the tape holding the tape strips. Remove the tape strips from the gage grid and ribbon legs. Accomplish this by folding the end of the tape strips back over itself and pulling the strip at a right angle to the principle direction of tape.

Remove the second tape mask around application area leaving the first tape mask. Visually check (5X or greater) the installation for:

- Excessive tape residue (remove if possible using new tape strips)
- Leads are down against surface
- Possible damage caused by first coat.

Check gage for continuity and ground.

6. Final Spray. Spray the final coat over gage installation 3 to 5 mils thick. The total thickness of the gage application shall not exceed 15 mils. Spray distance is 6 to 8 inches.
7. Measurements. Measure the bonded gage resistance where the first applied tape was removed below the gage grid. Record in Strain Gage Reliability Log. Mask application and cover leads with flame-spray alumina.

8. Inspect. Measure gage resistance at the primary splice area to assure continuity. Resistance to ground must be better than 40 megohms.
9. Primary Lead Splice. Follow process steps under Section 4.2.5.

3.2.4 Postapplication Heat Treat

Prior to the attachment of the primary leads to the Pt-10Ni intermediate leads, the application is to be heat treated. This heat treat is necessary to stabilize gage factor as discussed in Section 3.2.2, Task 2 Gage Sensitivity. One heat-treat temperature cannot be used for all blade materials. For blades that will be exposed to temperature less than 800° F, the heat treat temperature will be 830° F for 4 to 6 hours. For operating temperatures of 1000° F or less, treat the blades at 1050° F. A 1200° F heat-treat temperature is to be used for blades that will operate between 1000° and 1500° F. The heat-treat time for these temperatures is 2 hours.

The gage factors that will be used with these gages are shown in Figures 73, 74, and 75.

3.2.5 Splice to Primary Leads

The primary lead wire, that is used at AEG-Evendale and is standard for compressor rotor applications, is purchased from the Thermo Electric Co., Saddlebrook, New Jersey. It is 28-gage chromel versus alumel wire in a duplex insulation of carded asbestos. The overall cover is tightly woven glass.

1. Using Mystic 7402 tape, mask the gage application. Remove tape covering gage leads in splice area.
2. Strip 3/8 inch of the outer and inner insulation from EAG30K lead wire that has been cut to the proper length.
3. Flatten each of the wires using duckbill pliers or equivalent to one-half of original diameter. Cut flattened wire to 1/8 inch length from insulation.
4. Nichrome weld lead wire in place extending the bare flattened portion onto the Rokide base coat. The nichrome strap and the insulated portion of the flex lead wire must extend to the edge of the Rokide. Make certain there is no insulation in the splice area.

5. Gently radius the ends of 2-mil Pt-10Ni convoluted wire leads on top of the flattened leads at a right angle to flex wires and weld using a Unitek welder and a copper backup spade. Splice must be flat on surface for spray application. Use tape strips as required.
6. Cover splice with Rokide spray. Use 6 to 8 inch spray distance. Keep buildup to a minimum.
7. Remove all tape. Measure and record gage plus lead continuity resistance and resistance to ground.

3.3 LEAD ROUTING DESIGN

3.3.1 Design Philosophy

The design of rotor instrumentation at AEG-Evendale for new engines is a combined effort of the Aeromechanical Engineer, the Component Design Engineer, and the Instrumentation Designer. This team effort was necessitated in the 1968-1969 time period because of steadily declining reliability of strain gage instrumentation on advanced engines. Prior to the formation of the team, hardware rework was dictated by the Design Engineer with little or no consideration for the instrumentation except that it was there and holes had to be provided for lead routing into the inside of the spool. Often, the rework provided required a portion of the primary lead and splice to intermediate leads to be on the outside of the spool where, even though covered with nichrome, they were exposed to the hostile forces of centrifugal load and high velocity airflow. This was a predominant failure site. An instrumentation system on the blade was designed to prevent the application of leads and splices on surfaces where they would be exposed to these forces.

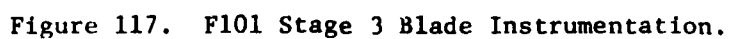
The new, reliable design that was adopted as standard practice was to locate all splices and primary leads under the blade platform where they would be either loaded in compression or shear. This also placed the requirement that the primary leads that would be routed through the spool would be applied on the bench, not after the blade was assembled into the spool, as occasionally was the case with previous designs. Using the new standard design, the Instrumentation Engineer and Component Designer defined rework slots, holes, routing schemes through the spool, compressor assembly sequence, and acceptable application materials and processes that would maintain both engine hardware and instrumentation integrity.

The team of the Aeromechanical Engineer and Instrumentation Engineer establishes "engine" gage locations and routine routing path of intermediate leads on the airfoil. Good instrumentation practice has always decreed that judicious consideration of bench test data for nodal patterns and vibratory strain distributions be exercised to select two or three engine gage locations, on a given airfoil, so as to provide satisfactory sensitivity to all airfoil modes expected to display significant response. An important consideration in the selection is the determination of gage locations in areas of modest vibratory strain gradient so that small variations in gage placement will not introduce prohibitive error in engine test data. Similarly, reference or calibration gages are selected from the bench test data for each of the engine gage locations. The routing paths are defined using the strain distribution data. They are selected to least affect the engine gage and the reference gage locations with consideration for low vibratory strain response at the airfoil fillet-crossing to platform.

The influence of the engine gage on the structural properties of the blade is determined from dynamic testing in the laboratory for the modes expected in the engine test. This calibration against the reference gage is an involved procedure but is necessary to relate the response of the instrumented to the uninstrumented airfoil. Such calibrations are factored into the calculations of the endurance limits/stress limits during test for the modes affected. They also serve as quality control of the applied sensor. Significant deviations of the ratio of engine gage to reference gage readings necessitate re-instrumenting of the blade.

3.3.2 Typical Application and Routing Designs

Figures 117, 118, and 119 show typical blade strain gage applications and lead wire routing designs under the blade platform. These along with Figures 92 and 103 which show typical strain gage instrumentation lead-routing and assembly instructions for the F101 and CF6-6 engines provide adequate description of the materials, processes, and the techniques of routing the primary leads off the blade dovetail to the disk. For blades that are circumferentially loaded into the dovetail slot, the instrumented blade is positioned 3 or 4 blades away from the leadout hole into the inside of the spool. The holes are filled with H cement and nichrome covered on the ID of the spool.



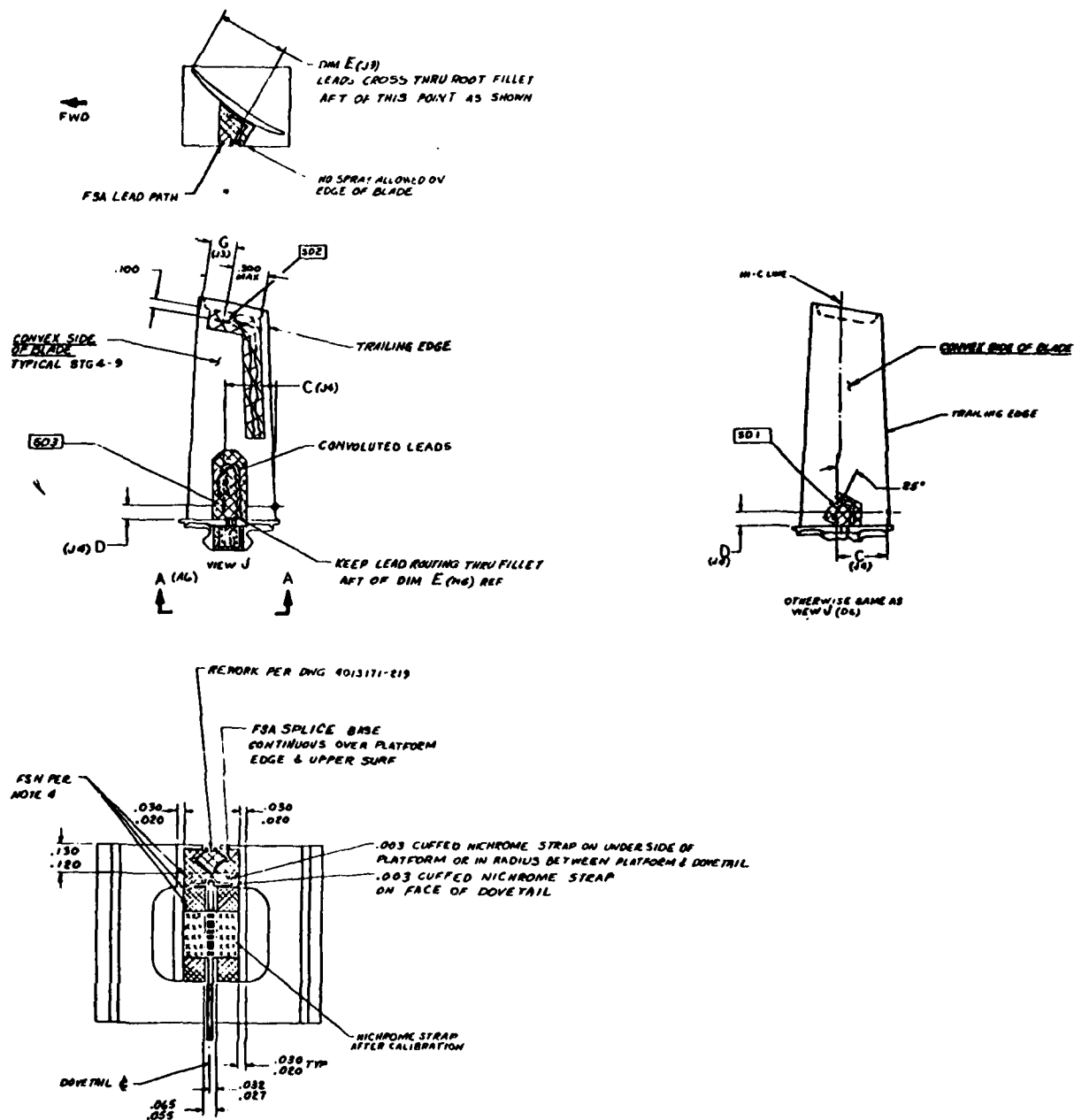


Figure 118. F101 Stage 4-9 Compressor Rotor Instrumentation.

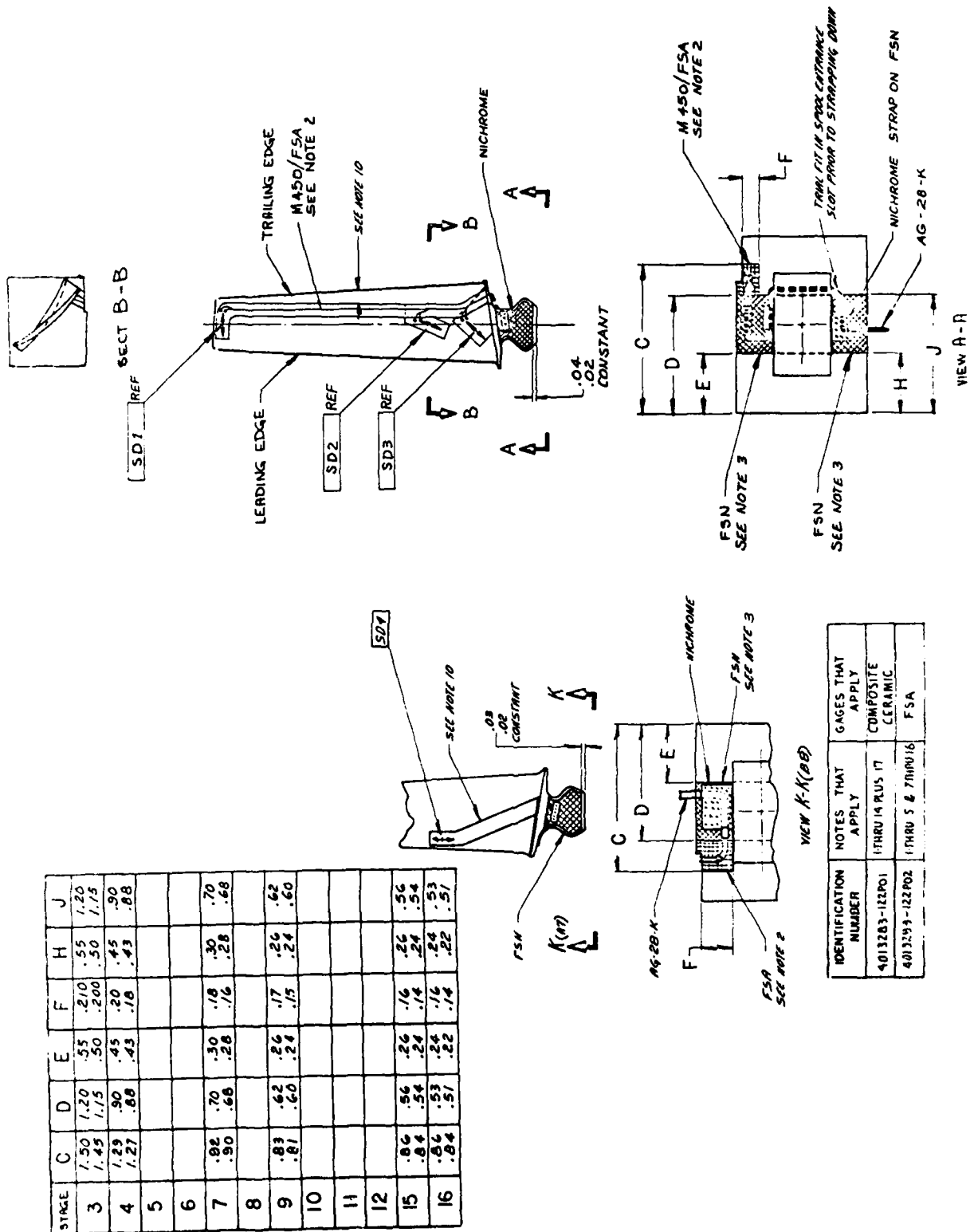


Figure 119. CF6 Compressor Rotor Instrumentation.

The lead in the circumferential dovetail slot is not nichrome-strapped to the spool; rather, it is free and is supported during rotation by the bottom of the blade dovetails between the instrumented blade and the lead-through hole.

Occasionally, for some blade stages that have axial dovetails, and may contain a large gap between the bottom of the blade dovetail and disk, the technique that is preferred, especially if the blade is loose in the slot, is to cross the span to the disk at the pressure face of the dovetail. This is shown in Figure 120.

3.4 SUMMARY

The techniques, materials, and processes developed in this program have been adopted as standard for high temperature strain gage applications. For the most part, the all-FSA or Rokide structure is preferred because the techniques are well-known and the time of application less than for the composite-ceramic method. Primarily, this is so because of the cure cycle of the Denex 2 cement.

Within the last year, the all-FSA structure has been used at temperatures beyond those investigated in this program with dramatic results. Thirty-one of these new gage systems were applied to Stages 1 and 2 of a low pressure turbine of an advanced F101-type engine. The maximum temperature of Stage 1 was 1625° F and 1400° F at Stage 2. Maximum stress observed was 15,000 psi double amplitude. At the end of 33 hours of testing, the reliability, based on numbers of gages, was over 93%; 29 gages were still operating.

Routing designs on blades and through the spool parts are those that have been used for years. Although the designs require significant rework to engine hardware, the reliability of the instrumentation has justified the expenditure. As a matter of fact, for some first-of-a kind hardware, the rework for instrumentation is included in the Manufacturing drawing to reduce turnaround time.

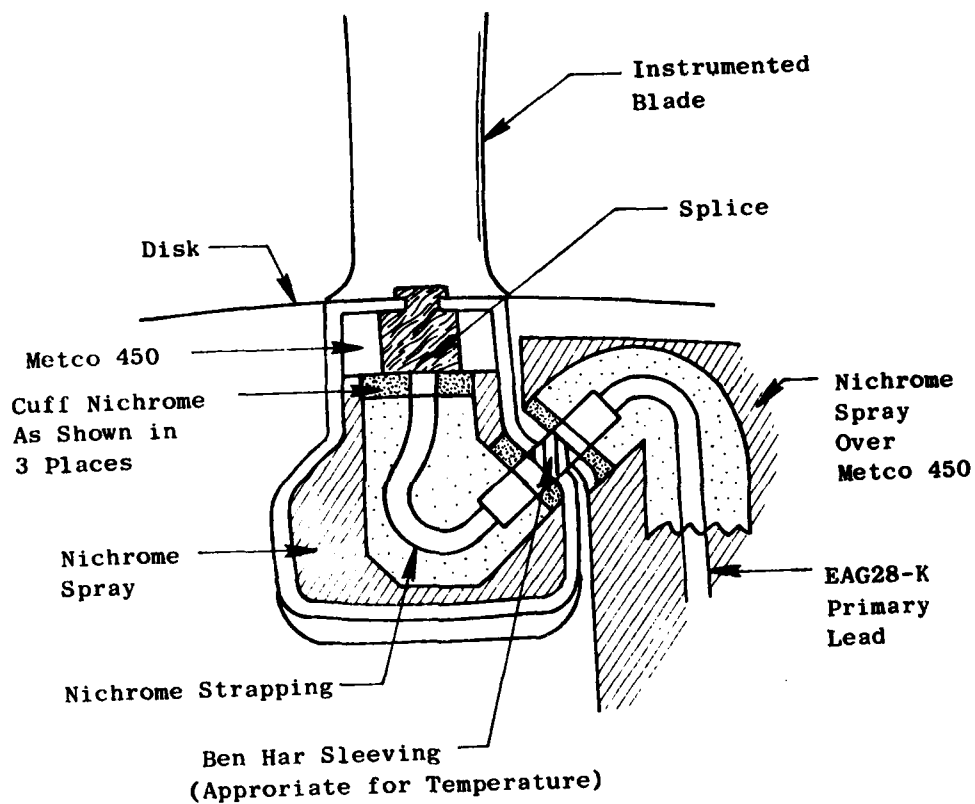


Figure 120. Routing Across Pressure Face.

4.0 TEST EQUIPMENT

The laboratory equipment described in this section was used throughout Phases I and II of the program.

4.1 HIGH TEMPERATURE STRAIN GAGE EVALUATION FACILITY (Figure 121)

4.1.1 General Description

The facility is used to evaluate the performance of dynamic and steady-state strain gages, application materials, and application designs. It is capable of providing gage factor, gage resistance, insulation resistance, and fatigue strength information at temperatures to about 2000° F. Gages undergoing test are excited in a potentiometric circuit by constant current. The gages are applied to beams that are designed to produce a constant stress along the gage test section.

The instrumented beam is mounted as a cantilever in a Krouse Fatigue Test Machine. The free end of the beam is deflected by a motor-driven cam through an arm, the length of which is adjustable and determines the magnitude of the dynamic strain. Static strain is set by shims between the beam free end and the connecting arm bearing plate that is bolted to the beam. Adjustments of static and dynamic strain are verified by a precision low temperature strain gage applied to the beam in the gage section. The Krouse Machine operates at a constant frequency of 30 Hz.

4.1.2 High Temperature Gage Factor Facility

In this facility, the instrumented sensitivity beam, Figure 122, is installed into modified water-cooled mounting jaws of the Krouse machine. Heat is supplied to the beam from a 15 kw Lepel Induction Heater. Figure 123 shows the beam enclosed by the induction heater coil. Sliding water-cooled suppressor plates are mounted at each end of the coil on a rack and pinion to maintain uniform temperature along the beam test section by changing the inductive field. These plates also protect the mounting jaws and the cam-connecting arm-bearing plate bolted to the beam for overtemperature. The distance

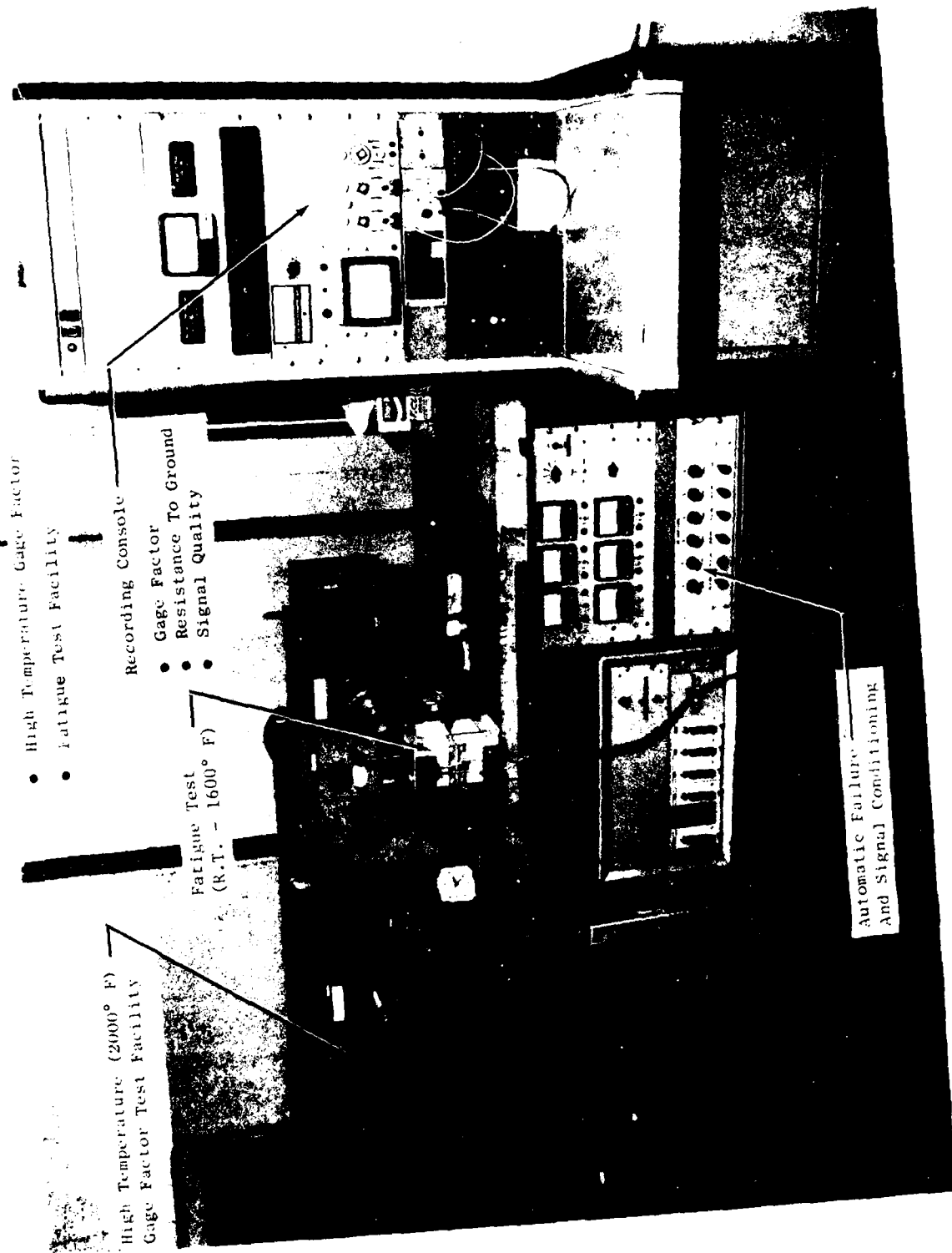
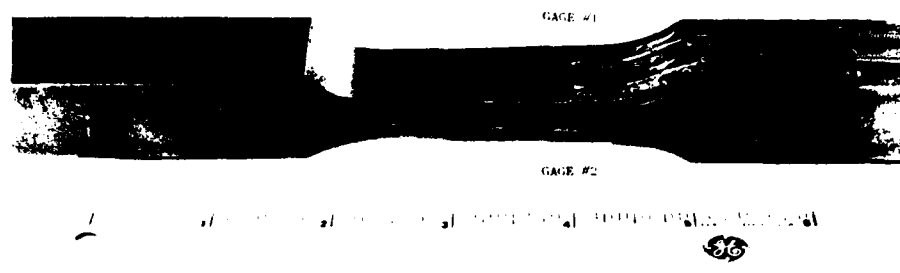


Figure 121. High Temperature Strain Gage Evaluation Facility.



Typical Instrumented Beam

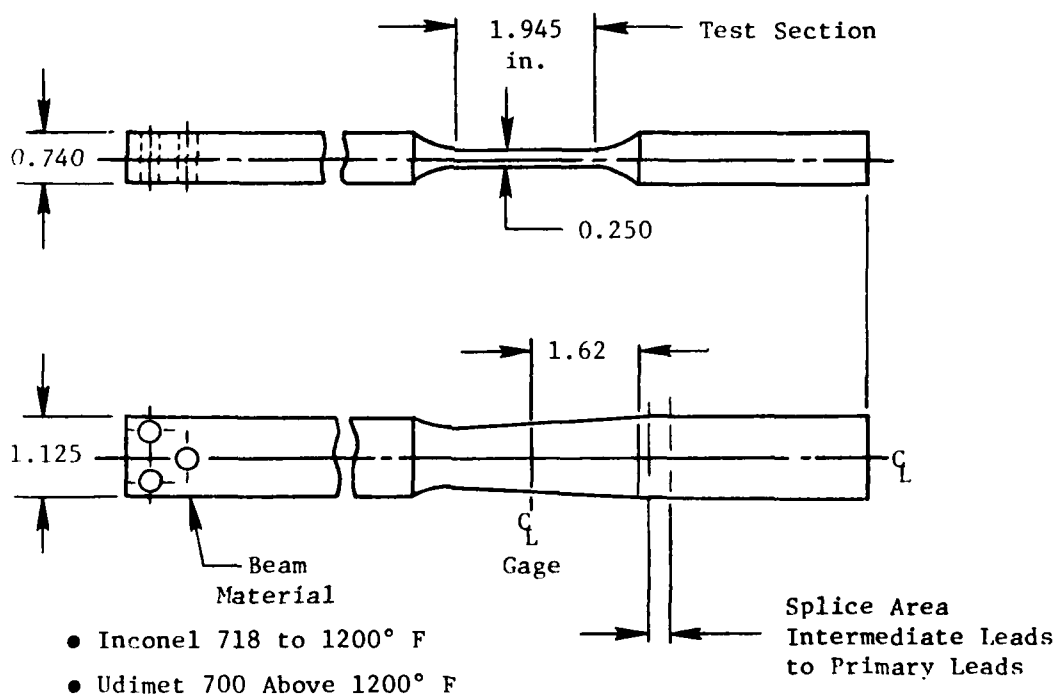


Figure 122. Sensitivity Beam.

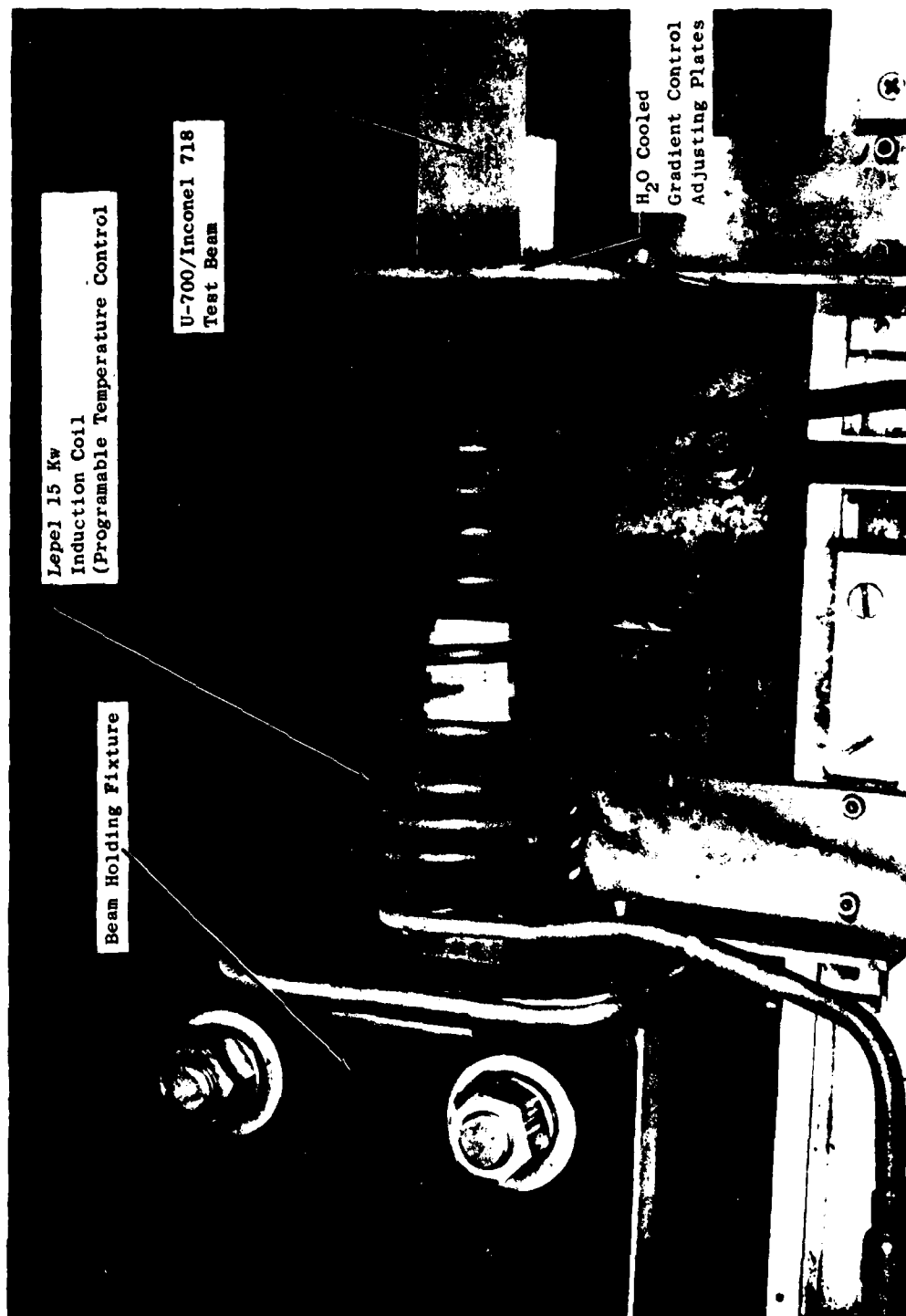


Figure 123. High Temperature Cage Factor Test Fixture.

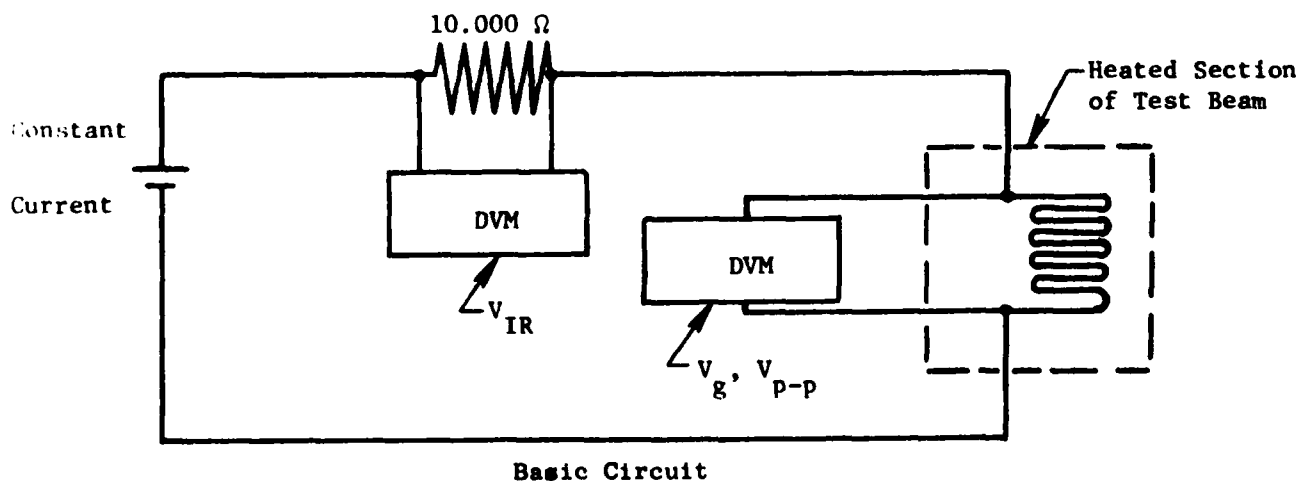
between the suppressor plates is decreased with increasing temperature. The temperature profile along the test beam is shown on Figure 124. A thermocouple applied to the test section near the strain gages is used to record temperature on a strip-chart recorder.

The test section of the beam will accommodate four gages (two per side) along with the thermocouple and a precision strain gage. For high temperature work, the deflection of the beam, as measured by a dial indicator accurate to 0.0001 inch, is calibrated against the indicated strain from the precision strain gage. Thus, after the beam has been exposed to temperature sufficiently high to destroy the calibration gage, the strain gage can be changed to a new value using beam deflection only. Strain gages to be evaluated for sensitivity are equipped with four leads - two on each gage leg. This permits the determination of gage factor without errors that can be caused by the lead wire.

Test Measurements and Calculations

Measurements obtained in this facility are those required to calculate gage factor. The gage power supply, measurement circuits, test switches, and auxiliary wiring are shown in Figure 125.

The basic measurement circuit is a four-wire constant current system shown in the following sketch:



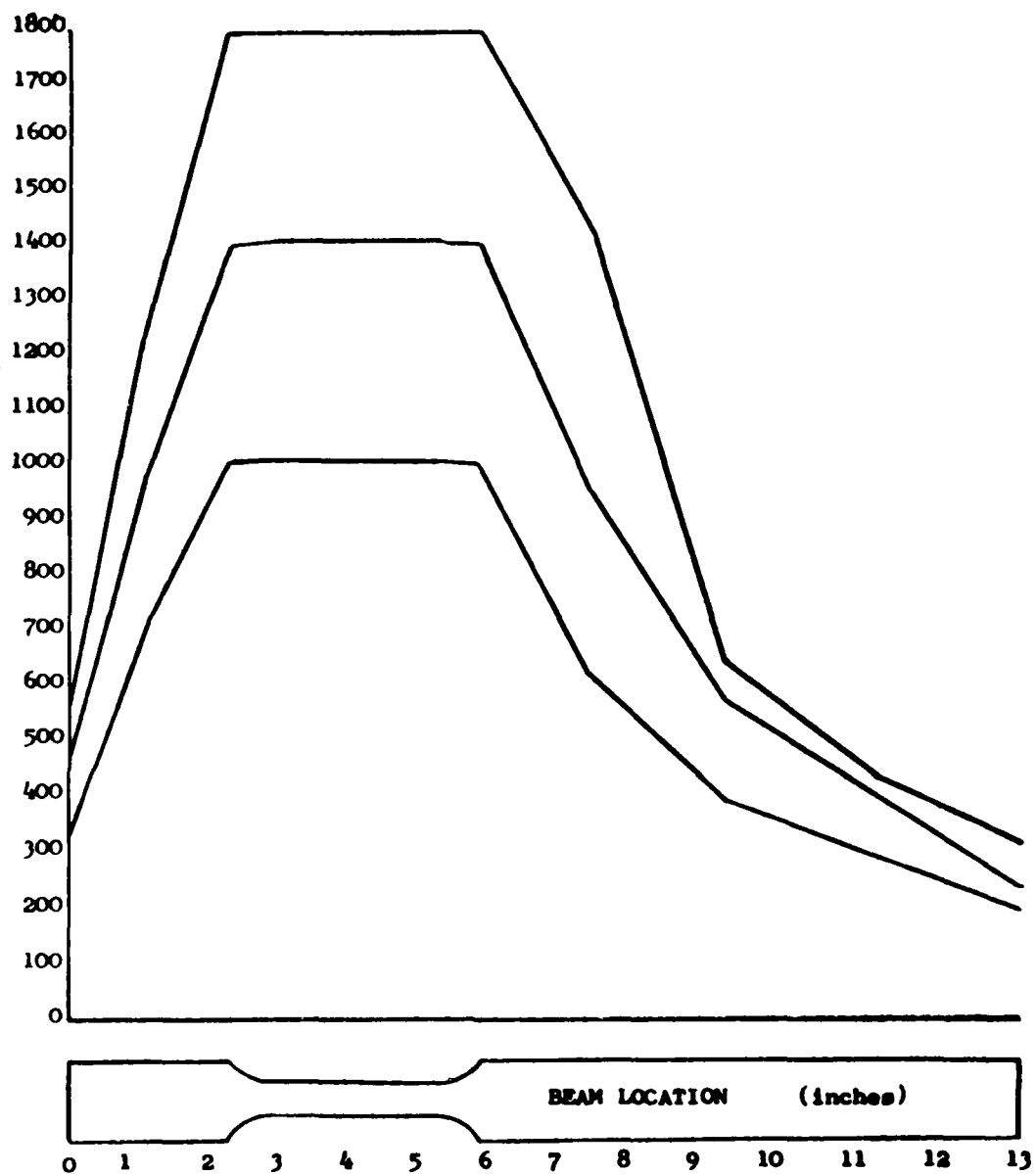


Figure 124. Temperature Profile with Suppressor Plates in Position.

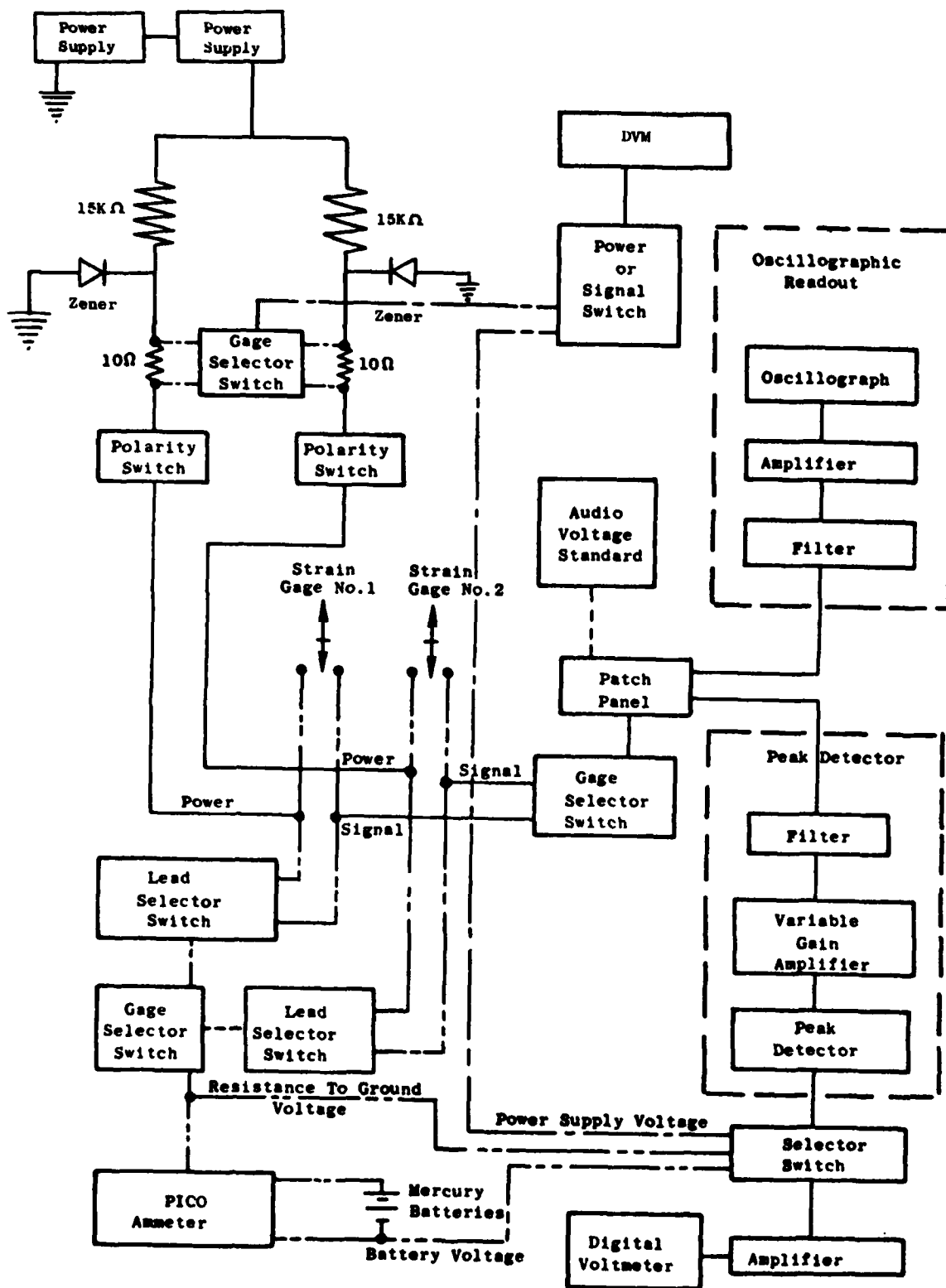


Figure 125. Schematic of Test Wiring Diagram.

where V_{IR} = voltage drop across a precision resistor in series with the gage

V_{p-p} = dynamic voltage, at a set dynamic strain level, is measured by a detector circuit. The magnitude of the difference between plus and minus peaks of the filtered gage signal. (System noise, consisting of 60 Hz and RF from the Lepel Heater, is removed by a narrow band-pass filter.)

V_g = gage voltage is measured with a DVM that is insensitive to the low voltage ac (V_{p-p}) signals from the strain gage.

From the measured values of V_{IR} , V_{p-p} , V_g , and strain (deflection), gage factor is determined:

$$GF = \frac{\Delta R}{R} \cdot \frac{1}{\epsilon}$$

$$\text{but } \Delta R = \frac{V_{p-p}}{V_{IR}/10.000} \text{ and } R = \frac{V_g}{V_{IR}/10.000}$$

$$\text{where } \frac{V_{IR}}{10.000} = I_g = \text{gage current}$$

$$\text{Therefore, } GF = \frac{V_{p-p}}{V_g} \cdot \frac{1}{\epsilon}$$

Gage factor (GF) and gage resistance (R) changes with temperature and/or strain are plotted from these calculated data. GF and R drift at temperature with time obviously may also be obtained in this facility.

The insulation resistance of the materials of application (flame-sprayed alumina, ceramic cements) is used in the analysis of gage system performance. This resistance-to-ground (R_{INS}) is obtained by measuring the current flow (I_{PA}) through the gage adhesive with a picoammeter. Power is supplied from four mercury batteries at 5.4 volts. The adhesive resistance generally is high enough to keep the battery at the open circuit voltage; however, during high temperature testing, battery voltage is checked frequently. Readings are obtained with reversed excitation polarity and averaged. Resistance-to-ground is calculated from

$$R_{INS} = \frac{5.4 \text{ Volts}}{I_{PA}}$$

Figure 124 also shows the temperature variation in the beam test section is essentially zero. However, there is an uncontrolled temperature drop from the test section to the ends of the beam. This will cause an increase in the modulus of the beam material which causes a change in the strain-tip deflection calibration that was obtained at room temperature. Much of this error has been removed by calculation based upon the temperature gradients (Figure 124) and modulus of elasticity versus temperature curves for the beam material.

Accuracy

The system inaccuracy from all error sources in the Gage Factor Facility are:

- GF error using DVM ±1.7%
- Gage resistance error ±0.1%
- Resistance-to-ground error between
15 KΩ to 1.5 MΩ +5%

4.1.3 Strain Gage Fatigue Test Facility

As with the Gage Factor Facility, this facility also includes a Krouse Fatigue Test Machine. Gages undergoing fatigue tests are connected to signal conditioning circuits that automatically turn the machine off if either a gage circuit fails or the signal amplitude varies by 15%. The broad tolerance is necessary to avoid occasional noise "spikes" from causing premature shutdown. The number of cycles to shutdown of the facility is registered on a mechanical counter. Failed gages are inspected or postmortemed to determine the cause of failure. Heat is supplied to the test beam containing the gage(s) undergoing test by a split-shell, muffle-type furnace manufactured by Fatigue Dynamics, Incorporated (Figure 126). Although the furnace is capable of 1600° F, steep temperature gradients along the beam length limits its use to under 1000° F for fatigue tests. For fatigue tests above 1000° F, gages are tested on sensitivity beams (Figure 122) using the Lepel induction furnace as the heat source.

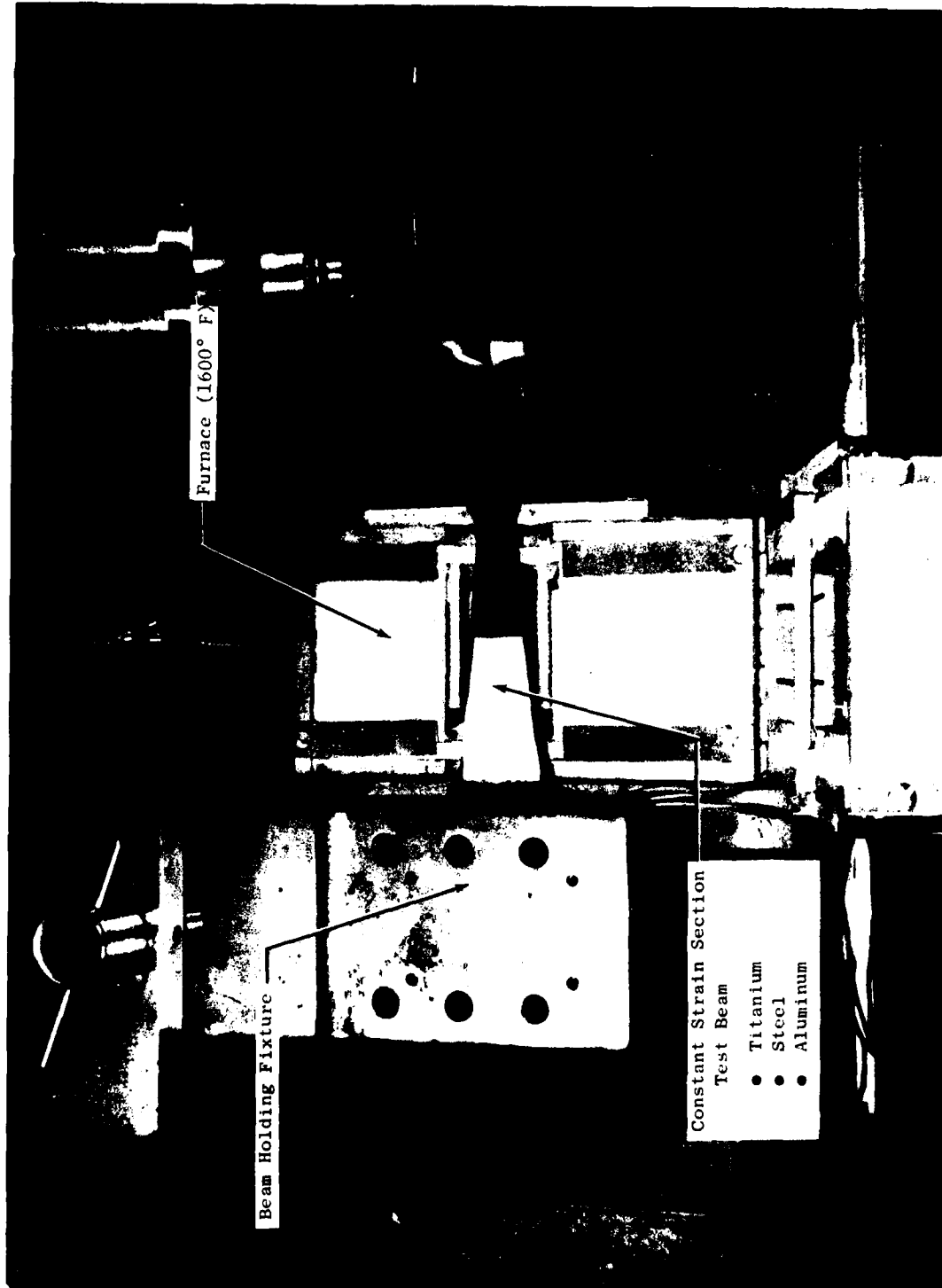


Figure 126. Fatigue Test Fixture.

The constant-stress beam design, Figure 127, is used for fatigue tests to 1000° F. This beam is large enough to accommodate the application of six gages (three on each side) for fatigue testing to about 500° F. Above that temperature, the temperature gradient along the beam dictates that gages be located at the same axial position along the beam and only two gages per beam side are applied (Figure 128). The sensitivity beam that is used for fatigue tests above 1000° F will accommodate four gages, two per side.

Tests may be conducted with or without a mean load, as discussed earlier. When a mean load is used, generally only one side of the beam is instrumented.

Strain gage systems undergoing fatigue testing are periodically monitored for gage factor, gage resistance, resistance-to-ground, and waveform. This is to assure that the gage is accurate throughout its test life. Gages that exhibit changes, e.g., supersensitivity or a decaying gage factor, are considered failed when the change is observed.

4.2 EROSION TEST FACILITY

The erosion test facility comprises a test fixture that holds a grit blast nozzle at a 30° angle to a test specimen that contains up to six strain gage applications (see Figure 129). Number 120-grit is discharged from the nozzle at a pressure of 90 psig. Each of the applications undergoes the erosion test separately; the remainder of the applications on the test specimens is protected from the effects of the grit. In the test, the time to open the strain gage contained in the application is recorded. The average time for the number of applications undergoing test is compared with the average time of other applications. These qualitative data are used only as an indicator of the relative erosion resistance of applications at room temperature.

4.3 HOT SHAKE FACILITY

The hot shake facility, shown schematically in Figure 130, is used primarily to establish the fatigue strength of gages when applied to jet engine compressor blading. It provides a couple of advantages over testing on flat beams. First, because blade fundamental frequencies are generally high, 10⁶

- Beam Material to 700° F = Ti-6Al-4V
- Beam Material to 1000° F = Inconel 718

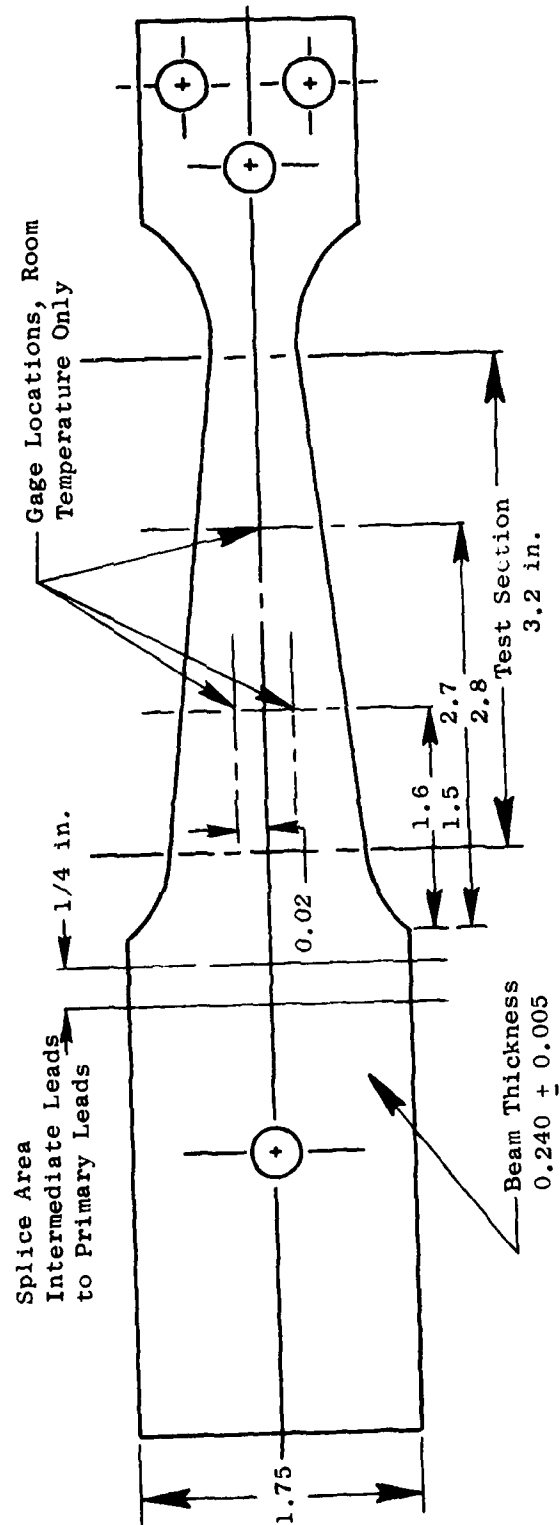


Figure 127. Strain Gage Fatigue Test Beam.

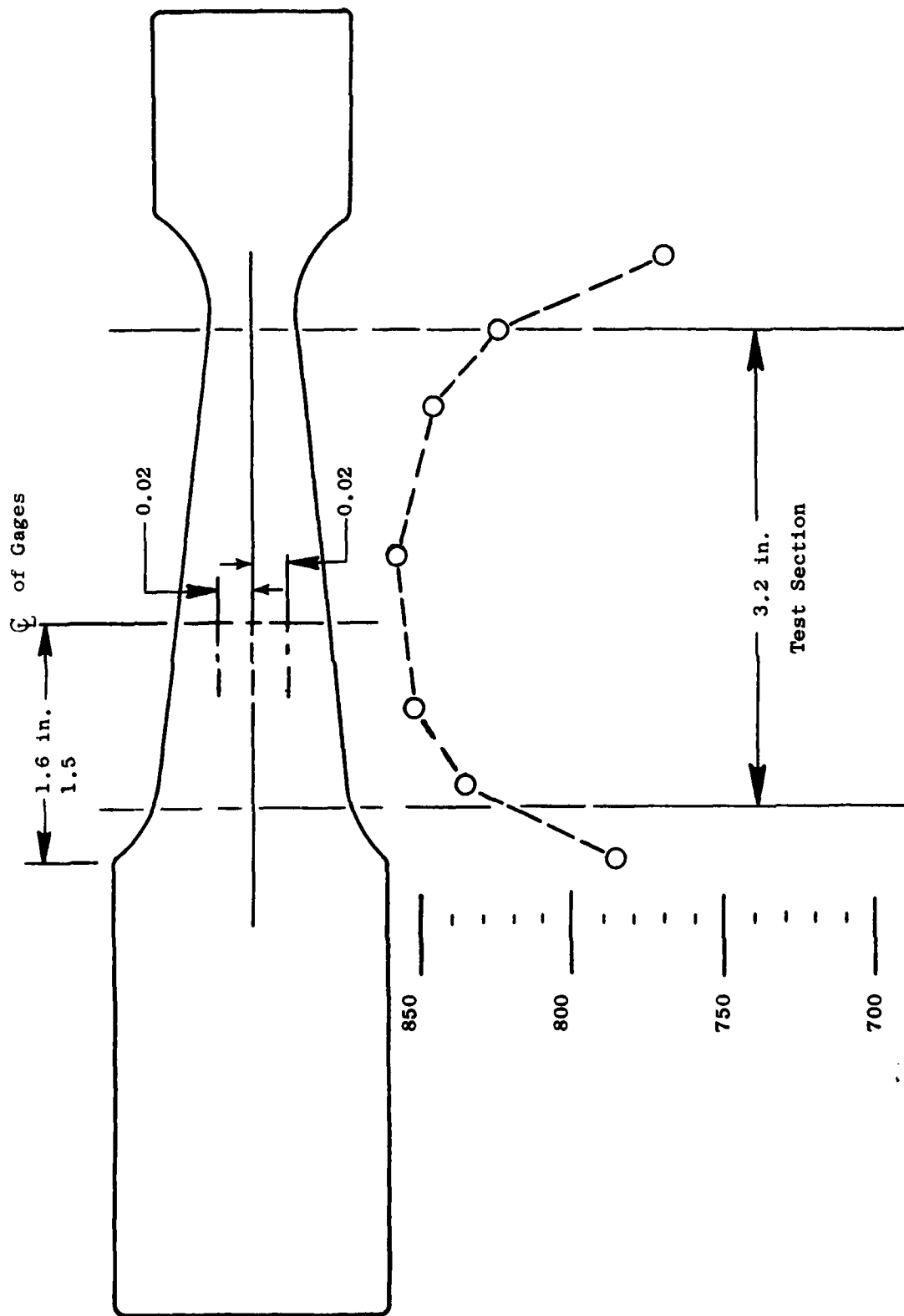


Figure 128. Strain Gage Locations and Temperature Profile for 850° F Fatigue Tests.

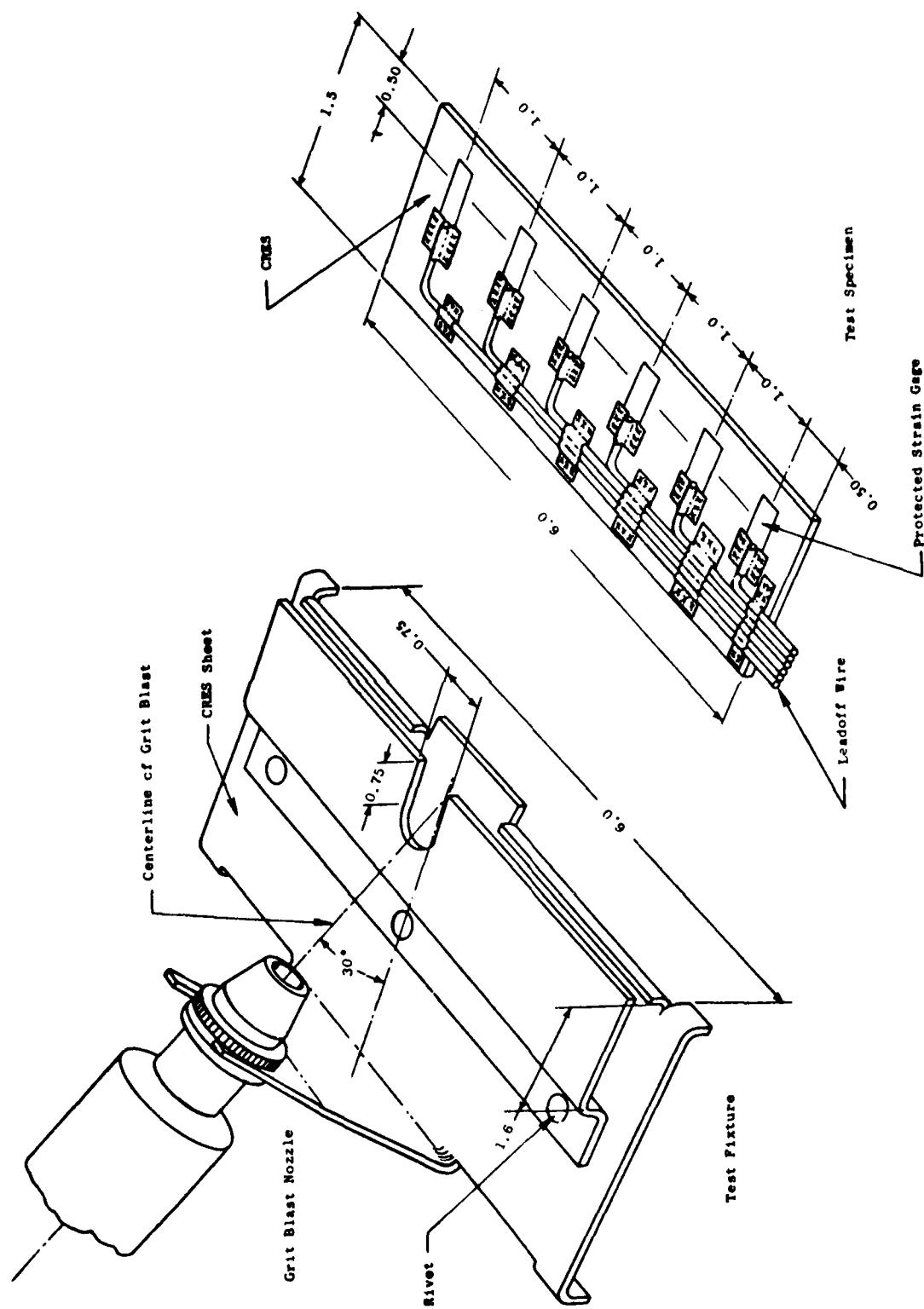


Figure 129. Erosion Test Facility - Grit Blast Nozzle.

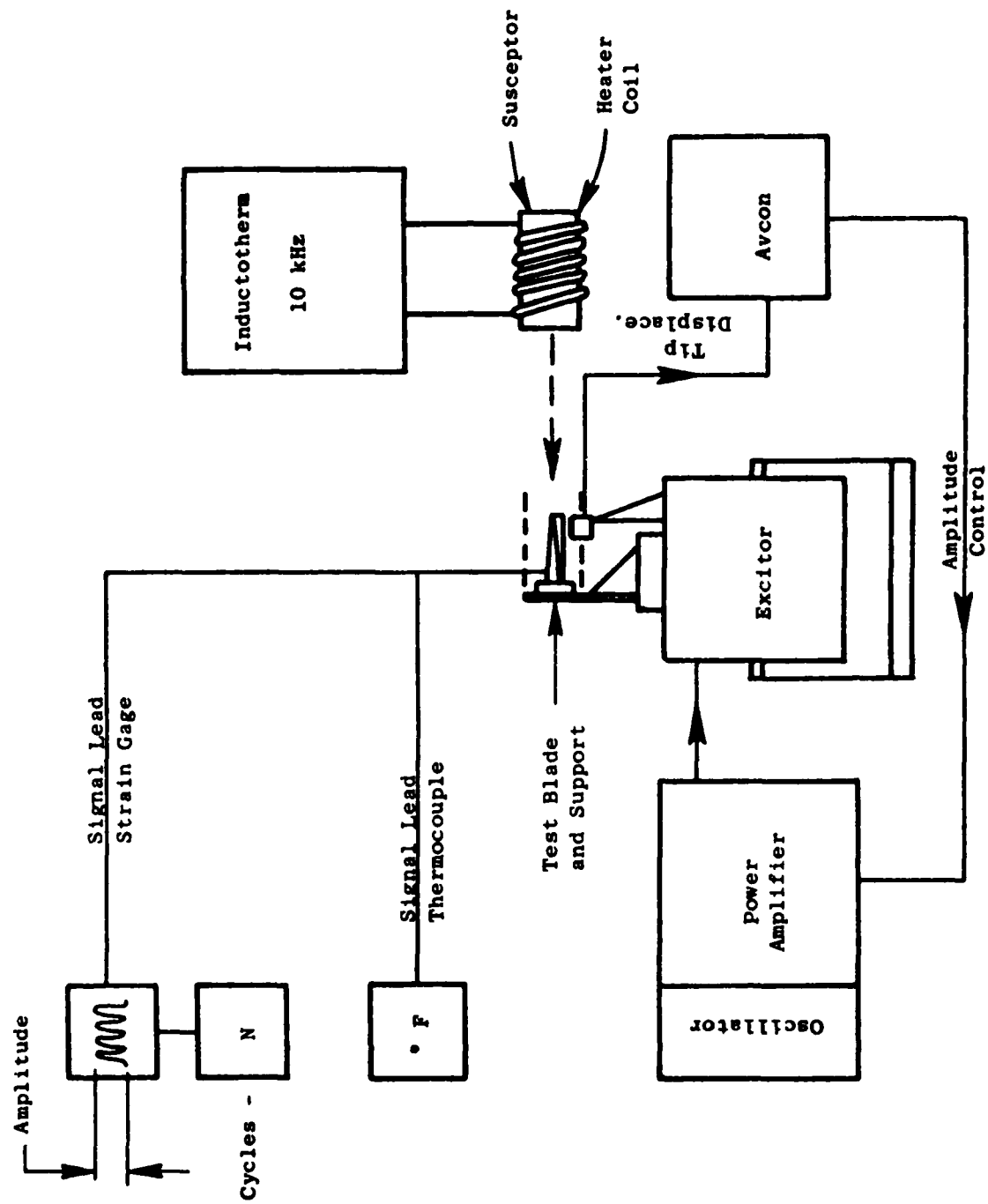


Figure 130. Hot Shake Facility Schematic.

or 10^7 cycles can be accumulated in a short time compared with that in the 30-Hz Krouse Fatigue Test Machine. Second, it factors complexity of application (curved surfaces, lead routing through fillets) into the fatigue strength and, therefore, provides more realistic strain gage life estimates.

REFERENCES

1. THER ENG P60 M 09-00-73
Khatuntsev, E.A.
"Increasing the Accuracy and Reliability of Measurement of Axial Forces of Turbines with Strain Gauges"

To increase the accuracy, it is advisable to use a system with separate measurement of the force in static and dynamic modes of operation of the turbine and with summing of the readings of the strain gages in the dynamic mode.
2. 6th INTERNATIONAL METAL SPRAYING OFFICE 9-14-70
Kayser, Harald
"Group D/Group D(1)"

The influence of the thermal penetration factor on interface temperature and adhesion bond strength in hot spraying.
3. MAT SC ENG 3-24-70
Davidge, Roger W. and Evans, Anthony G.
"The Strength of Ceramics"

For structural or engineering applications, ceramics must compete with both metallic and organic materials. The competition is in terms of desirable mechanical properties, such as strength and toughness, other properties, such as density and stability in the operating environment, and, of great importance, cost. A choice between materials must be made therefore on the basis of relative costs per unit property required.
4. EXP MECH P31N M 10-00-69
Willis, D.L.
"Strain Gages in High-G Environments"

Author outlines some of the basic physical problems involved and describes the techniques that have provided successful operation in environments of 250,000 g.
5. NASA CR-66775 03-00-69
Bean, W.T.
"Research Program to Develop Alloys for up to 1200° F Strain Gages"

Three nickel-base, one iron-base and one cobalt-base superalloys were tested. Numerous precious-metal alloys of platinum were selected for evaluation. N69-22187

6. GE 68-SL-346

12-02-68

Fox, H.M.

"Metallurgical Investigation of PT-W Strain Gages"

Based upon limited studies, it is concluded that the most probable cause of the electrical-resistance instability in PT-W strain gage alloys is a strain/temperature induced coherent precipitation.

7. BR J AP PH P1743

M 12-00-68

Bertodo, R.

"Precious Metal Alloys for High-Temperature Resistance Strain Gauges"

It is concluded that the apparently anomalous behavior of some samples of PT-W is associated with the metallurgical state of the alloy. On the basis of preliminary test results, an alloy of PT, PD and MO is shown to be superior to PT-W for steady strain element manufacture.

8. BR J AP PH VOL14-P79

12-00-68

Easterlin, K.E.

"High Temperature Resistance Strain Gauges"

At present, all high temperature strain gages for use at temperatures above 250° C are made from nickel-chromium alloys usually in the region of 25% chromium. Such alloys have the desirable properties of high resistance to corrosion, high electrical resistivity, and low temperature coefficient of resistance. Experiments have been carried out that confirm the unsuitability of these gages for temperatures above 340° C because of order-disorder phenomena. It is shown that satisfactory gages can be made using alloys based on platinum, containing small percentages of tungsten. Such gages have been tested successfully at temperatures up to 800° C.

9. ASM TRANSACTIONS P730

6-26-68

McCoy, H.E. Jr. and McElroy, D.L.

"Electrical Resistivity Anomaly in Nickel-Base Alloys"

The electrical resistivity of eight commercial nickel-base alloys containing iron, chromium, and molybdenum was measured to 1000° C. Alloys with more than 50 wt % Ni showed a rapid increase in resistivity between 400° and 600° C and a decreasing resistivity from about 600° to 1000° C. For these alloys, the resistivity of alloys with less than 50 wt % Ni increased with temperature with a slope decrease between 400° and 600° C. The effects of annealing and cold working were relatively minor for these alloys. The resistivity variations observed do not seem to show a unique dependence on any one alloying constituent although there is a weak correlation with the total nickel content. Electron microscope results indicate that these changes may be associated with short-range order.

10. RUSTON and HORNSBY, LTD., LONDON, ENGLAND P37 3-20-68
Bertodo, R.
"Platinum Metal Alloys for the Measurement of Strains at High Temperature"

Much work has been carried out over the years in an attempt to develop a gage for the measurement of steady strains up to 1000° C. Essentially, satisfactory elements exist for use up to 300° C; over the range 300° C to 1000° C, alloys of platinum and tungsten were shown to be marginally acceptable in 1963.

11. ASD FDL TDR 65-54 04-00-64
Sokolowski, B.A.
"A Full Bridge Type Strain Gage for Use at Elevated Temperatures"

A full bridge strain gage and installation techniques have been developed which permit the determination of static and dynamic strains above 1200° F. AD 465437

12. PROC INSTN MEC ENGINRS P1 8-23-63
Bertodo, R.
"Resistance Strain Gauges for the Measurement of Steady Strains at High Temperatures"

The paper reviews the principal aspects of an investigation carried out between 1958 and 1962 in order to develop a wire resistance strain gage for the measurement of steady stresses in stationary and rotating turbo-jet components operating at temperatures up to 600° C in oxidizing atmospheres.

The characteristics of a number of alloys are reviewed and the behavior of long unbonded wires drawn from nickel-chromium, iron-chromium-aluminum, and platinum-tungsten alloys is discussed in detail. The effect of such factors as annealing, ordering and oxidation of the alloy's lattice on the resistance-temperature characteristics of the wire is considered. On the basis of such findings three alloys are selected for test in the form of flat grid strain gages. The results obtained from a large number of such gages over periods of time in excess of 200 hours are presented.

13. BRISTOL R-EDR-349 03-11-63
Bertodo, R.J.
"The Measurement of Steady Strains at Elevated Temperatures, Part 5 - The Characteristics of Strain Gauges Manufactured from Stabilized Karma Wire"

The present investigation examines the short and long term behavior of wire resistance strain gages manufactured from Karma wire stabilized in accordance with the recommendations of EDR 324.

14. BRISTOL R-EDR-361 03-11-63
Bertodo, R.J.
"The Measurement of Steady Strains at Elevated Temperature, Part 6 - The Use of FeCrAl Alloys for Temperatures up to 650° C"
- The report discusses the characteristics of iron-chromium-aluminum alloys in relation to the measurement of steady strains at elevated temperatures.
15. BRISTOL EDR-378 03-00-63
Bertodo, R.J.
"The Measurement of Steady Strains at Elevated Temperatures, Part 7 - Precious Metal Alloy Wires for Use up to 650° C"
- It is concluded that an alloy of 9.5% tungsten-platinum is marginally acceptable. The gage factor of some alloys may be increased significantly by utilizing factors likely to affect the lattice parameters.
16. BRISTOL R-EDR-324 06-00-61
Bertodo, R.J.
"The Measurement of Steady Strains at Elevated Temperatures, Part 4 - Effect of Heat Treatment on the Temperature/Resistance Characteristics of Ni-Cr, Ni-Cr-Al, and Fe-Cr-Al Alloys"
- The investigation was initiated in order to develop a method of determining steady stresses at temperatures up to at least 650° C in the general environmental conditions likely to be encountered in turbojet aero engines.
17. DEHAVILLAND 03-00-61
Bertodo, R.J.
"The Measurement of Steady Strains at Elevated Temperatures, Part 2 - Oxidation and Cement Interaction Effects on Strain Gauge Filaments Above 300° C"
- The present investigation considers the effect of oxidation and cement interaction upon the stability of wire resistance strain gages developed for the measurement of steady strains at elevated temperatures.
18. DEHAVILLAND EDR-304 01-00-61
Bertodo, R.J.
"The Measurement of Steady Strains at Elevated Temperatures, Part 1 - Measuring Techniques up to 300° C"
- Nichrome wound gages would appear likely to permit measurements to be carried out up to 300° C, but further work appears necessary. A number of temperature compensating circuits are reviewed and their performance is compared.

19. DEHAVILLAND R-273 11-00-59
Bertodo, R.J.
"Flame Sprayed Oxide Coatings"
- A number of tests were carried out on flame sprayed alumina in order to determine its suitability as bonding medium for wire resistance strain gages.
20. DEHAVILLAND 08-00-59
Bertodo, R.J.
"Vapor Deposited Strain Gauges"
- A vapor deposited gage offers strong possibilities and a number of advantages over comparable wire wound elements. It is recommended that future work be directed towards developing gages of this type.
21. IME PROC P605 M 00-00-59
Bertodo, R.J.
"Development of High-Temperature Strain Gauges"
- Strain gage, operating at 1000° C, accuracy of $\pm 5\%$. Various resistance alloys tested. Effects of metallurgical changes, geometric shape, and long-term exposure. Bonding mediums examined, creep, shear, erosion, and thermal shock.
22. GE 57SE98 09-16-57
Crocker, C. Jr.
"Effect of Strain Gage Thickness on Accuracy of Measured Stress in Blades"
- Tests to obtain quantitative data on accuracy of measured stress in typical small turbine blades vibrating in bending.
23. JORN I MET - VOL. 81 P169 12-00-53
Taylor, A. and Hinton, K.G.
"A Study of Order-Disorder and Precipitation Phenomena in Nickel-Chromium Alloys"
- Electrical resistivity, specific heat, and X-ray measurements have been made on Ni_3Cr and $\text{Ni}_{15}\text{Cr}_4\text{Al}$. It has been shown that both these alloys undergo an order-disorder type of transformation at approximately the same temperature and that an additional high-temperature transformation occurs in the ternary alloys, consistent with the precipitation and the resolution of a second phase.

24. JOURN I MET - VOL 81 P451 12-00-53
Taylor, A. and Floyd, R.W.
"The Consitution of Nickel-Rich Alloys of the Nickel-Chromium-Aluminum System"

The equilibrium relationships in nickel-chromium-aluminum alloys containing more than 50 at % nickel have been studied over the temperature range 750° to 1150° C. It has been shown that the phase fields of the nickel primary solid solution, γ , and the β solid solution based on NiAl both contract as the temperature falls, whereas that of the γ' phase based on Ni₃Al extends. The equilibrium between the γ and β phases which exists from the solidus breaks down at about 1000° C, giving rise to equilibrium between γ and α -chromium by a four-phase reaction: $\beta + \gamma = \alpha + \gamma'$. The ordering of the γ phase is enhanced by the presence of aluminum atoms, and for alloys with more than 10 at % aluminum the ordering temperature is over 1150° C. The equilibrium between the γ and γ' phases is such that over a range of compositions the lattice parameters of the phases are almost identical.

25. RAE TN INSTN-127 06-00-50
Maslen, R.R.
"Strain Sensitivities of Fine Wires"

This note deals with the changes in electrical resistance of fine metallic wires when subjected to strain. The results of tests on a wide range of materials. Both pure metals and alloys are given, and applications to instrumentation in the field of strain gaging and temperature measurement are discussed. AT192820

26. GETM 77-176
Foster, J.H.
"Gage Factor and Resistance Corrections for Karma Wire Gages Used for Dynamic Strain Measurements to 1000° F"

Thermal stabilization schedules were determined that will permit the use of GE Karma strain gages over two temperature ranges - RT to 800° F and RT to 1000° F. Gage errors are less than 3.8% with a 95% confidence that 95% of all applied gages will fall within these limits.

27. PLENUM PRESS, NEW YORK, Vol I 1973
Rozenberg, L.D., Translated from Russian by Word, J.S.
"Physical Principles of Ultrasonic Technology"

28. ST. MARTIN'S PRESS, NEW YORK 1968
Tylecote, R.F.
"The Solid Phase Welding of Metals"

29. Driver Harris FW103
"Fine Size Resistance Wire for Precision Resistors and Potentiometers"

30. General Electric Company 1974
Danforth C. and Brooks, R.
"A Method of Determining Damping in a System.
31. McGraw-Hill Book Co., Inc, MIT, Third Edition 1947
Den Hartog, J.P.
"Mechanical Vibrations"